CYCLIC AND CORROSION BEHAVIOR OF NICKEL TITANIUM SHAPE MEMORY ALLOYS MODIFIED WITH VARIOUS BIOCOMPATIBLE COATINGS

A Dissertation

by

Görkem Muttalip Şimşek

Submitted to the
Graduate School of Sciences and Engineering
In Partial Fulfillment of the Requirements for
the Degree of

Doctor of Philosophy

in the
Department of Mechanical Engineering

Özyeğin University
February 2023

Copyright © 2023 by Görkem Muttalip Şimşek

CYCLIC AND CORROSION BEHAVIOR OF NICKEL TITANIUM SHAPE MEMORY ALLOYS MODIFIED WITH VARIOUS BIOCOMPATIBLE COATINGS

Approved by:

Professor Dr. Güney Güven Yapıcı,
Advisor, Department Head
Department of Mechanical Engineering
Özyeğin University

Assist. Professor Dr. Altuğ Başol
Department of Mechanical Engineering
Özyeğin University

Assist. Professor Dr. Özkan Bebek
Department of Mechanical Engineering
Özyeğin University

Assist. Professor Dr. Hakan Yılmazer
Department Of Metallurgical And Materials Engineering
Yıldız Technical University

Date Approved: 14 February 2023

Assist. Professor Dr. Mehmet Ipekoğlu
Department of Mechanical Engineering
Turkish-German University

To beloved Mustafa Kemal Atatürk...

ABSTRACT

Metallic materials including stainless steels, cobalt-chromium based alloys, commercial titanium, Ti6Al4V, and nickel-titanium (NiTi) shape memory alloys (SMA) have long been considered to be the dominant source of implant materials in the medical industry. Among all, the practical use of NiTi SMAs is fascinating due to their extraordinary behaviors, which are entirely new compared to other conventional metallic materials. However, a major problem associated with the use of NiTi for in-vivo applications is the potential risk of Ni release due to the highly corrosive environment of the human body. There have been many attempts to overcome such difficulties and to understand the corrosion mechanisms for conventional NiTi implant materials during the last decade through simulations or in-vivo and in-vitro experimental studies.

Within this context, the effect of heat treatment parameters on the mechanical properties of NiTi shape memory alloy in wire form is investigated since heat treatment can strongly influence the mechanical properties of shape memory alloys. Detailed experiments were planned and utilized to examine the following properties as a function of heat treatment condition; phase transformation temperature, movement and repeatability, cyclic behavior, corrosion resistance, and biocompatibility. All experimental setups were custom designed and manufactured based on specific test requirements. Corrosion and cyclic experiments were performed in Ringer solution and Simulated Body Fluid (SBF) to better understand the response of NiTi in a human body environment.

Besides heat treatment parameters, the effect of biocompatible layer on the functional behavior of NiTi was also investigated since the method was found highly

promising by several research groups. In this dissertation, CaP and PVA based hydrogel coatings were applied on NiTi SMAs in wire form via the dip coating method. However, bioceramics and biopolymers possess poor mechanical properties that constitutes a drawback. The main contribution of the dissertation is combining the superior mechanical properties of NiTi with the excellent biocompatibility of certain polymers and ceramics to develop a new type of implant for various medical applications. The present work also demonstrates for the first time the effect of NaOH pre-treatment on the wire form HA coated NiTi. These efforts show that deposition of biocompatible layer on metallic surfaces may act as physical or chemical barriers and inhibit the ion release from the surface in a highly corrosive environment. Besides, the influence of biocompatible layer on the cyclic behavior of NiTi was also investigated with CaP and hydrogel coated NiTi samples. Cyclic experiments were performed in different environmental conditions including dry condition, SBF and Ringer's solutions with different frequencies to better understand the NiTi response in a human body environment.

Finally, this dissertation investigates the mathematical modeling of NiTi corrosion mechanisms. Even though the biomaterials were tested in the experiments for corrosion, it is hard to experimentally predict all the situations that can occur in the body. The reasons for incomplete experimental testing include stochastic nature of the corrosion process, the need for long-term data collection, and the different responses of different patients to the same biomaterials. In this manner, mathematical modeling of the corrosion process was structured with selected parameters such as pH, temperature, and difference between potential of the metal and solution by utilizing Cellular Automata (CA) to simulate the corrosion behavior of uncoated and coated NiTi wires. It was concluded that the developed model accurately captures the corrosion progress development in response to changes of different environmental parameters.

ÖZETÇE

Paslanmaz çelik, kobalt-krom alaşımları, titanyum, Ti6Al4V ve Nikel Titanyum (NiTi) şekil hafızalı alaşımlar (ŞHA) gibi metalik malzemeler medikal endüstrisinde uzun süredir implantların ana malzemesi olarak kullanılmaktadır. Bu malzemeler arasında NiTi ŞHA, geleneksel metalik malzemelerle karşılaştırıldıklarında sahip oldukları süper elastiklik ve şekil hafızası gibi eşsiz özellikleri ile dikkat çekmektedir. Ancak bu eşsiz özelliklere rağmen NiTi alaşımların korozif ortamlarda implant üzerinden Ni iyonu salınım riskinin olması, bu malzemelerin özellikle vucüt içi kullanımlarını sınırlamaktadır. Bu önemli problemi aşmak ve NiTi alaşımların korozyon süreçlerini daha iyi anlamak amacıyla deneysel ve modelleme yöntemleriyle birçok çalışma yapılmaktadır. Tez kapsamında yapılan çalışmaların amacı ise bu çözümleri incelemek ve soruna farklı bir mühendislik bakış açısıyla yaklaşarak alternatif çözümler üretmektir.

Bu kapsamda yapılan çalışmalarda öncelikle ısıl işlemlerin NiTi alaşımların mekanik özellikleri üzerindeki etkileri farklı sıcaklık ve zaman parametreleri kullanılarak incelenmiştir. Seçilen parametreler ile uygulanan ısıl işlemlerin NiTi alaşımların faz dönüşüm sıcaklıkları, hareket kabiliyeti, tekrarlanabilirlik, döngüsel davranış, korozyon dayanımı ve biyouyumluluk gibi mekanik özellikler üzerine etkileri detaylı bir deney serisi oluşturularak araştırılmıştır. Yapılan testler için ana gereksinimlere uygun özel düzenekler tasarlanmış ve üretilmiştir. NiTi numunelerin döngüsel davranışları ve korozyon dayanımları incelemek için planlanan testler, alaşımların vücut içinde kullanım durumunu daha doğru modellemek amacıyla yapay vücut sıvıları (SBF ve Ringer) kullanılarak gerçekleştirilmiştir.

Isıl işlem parametreleri haricinde, tel şeklinde NiTi alaşımların üzerinde oluşturulacak biyouyumlu kaplamaların alaşımın fonksiyonel davranışları üzerine etkileri

de incelenmiştir. Bu bağlamda tez kapsamında NiTi tel numuneler kalsiyum fosfat (CaP) bazlı biyoseramik ve polivinil alkol (PVA) bazlı biyopolimerler ile daldırma yöntemi kullanılarak kaplanmıştır. Biyoseramiklerin ve biyopolimerlerin biyouyumlulukları çok yüksek olmasına rağmen tek başına kullanıldıklarında zayıf mekanik özelliklere sahip oldukları bilinmektedir. Bu sebeple tez çalışmasının ana amaçlarından biri NiTi alaşımların üstün mekanik özellikleri ile seramik ve polimerlerin yüksek biyouyumluluklarını birleştirerek vücut içi uygulamalarda kullanılabilecek yeni tip bir implant malzemesi geliştirmektir. Bunlara ek olarak kaplama öncesinde yüzeylere NaOH ile işlem uygulanmasının mekanik özelliklere ve kaplama kalitesine olan etkiler de araştırılmıştır. NiTi üzerine yapılan biyouyumlu kaplamaların alaşımın döngüsel davranışına etkileri de incelenmiştir. Bu testler kuru ortamda, YVS ve Ringer solüsyonu içinde farklı frekanslar kullanılarak gerçekleştirilmiştir.

Son olarak, tez kapsamında NiTi alaşımların korozyon mekanizması matematiksel modelleme yöntemleri ile incelenmiştir. Literatür kapsamında yapılan araştırmaların birçoğu biyomalzemelerin korozyon dirençlerini test ortamlarında incelemeye yönelse de vücut içinde meydana gelecek tüm durumları deneysel olarak tahmin etmek korozyon sürecinin uzun vadeli veri toplama ihtiyacı ve farklı hastaların aynı biyomalzemelere farklı tepkiler vermesi gibi sebeplerden ötürü mümkün değildir. Tez kapsamında yapılan çalışmalar bu tip güçlüklerin hesaplamalı modelleme yöntemleri kullanılarak aşılabileceğini göstermektedir. Korozyon sürecini modellemek için oluşturulan sayısal yöntem parametrik olarak kurgulandığı ve girdilere çok hızlı yanıt vererek kolayca değişebilecek kabiliyete sahip olduğu için deneysel çalışmalara kıyasla zaman ve veri miktarı açısından çeşitli avantajlar sağlamaktadır. Bu bağlamda tez çalışmaları kapsamında NiTi alaşımların kaplama yapılmadan önceki ve biyomalzemeler ile kaplı yüzeylerinin korozyon süreçleri CA yöntemi kullanılarak oluşturulan sayısal modelleme yöntemi ile incelenmiş ve geliştirilen modelin farklı çevresel koşullarda korozyon gelişimini doğru şekilde simüle ettiği sonucuna varılmıştır.

ACKNOWLEDGEMENTS

First and foremost, I would like to thank my advisor Dr. Güney Güven Yapıcı for his guidance and for giving me the opportunity to join the MEMFIS research group at Özyeğin University. Sincere thanks to Dr. Özkan Bebek and Dr. Mehmet Ipekoğlu for their feedback and guidance to improve my work. Special thanks to Dr. Nihal Engin Vrana for his precious guidance. I would like to thank Dr. Garrett McGuinness for his kind hospitality at Dublin City University and Dr. Julien Barthes for his support. I would also like to thank all those with who I have collaborated and cooperated in Özyeğin University; Ali Husseinzade, Ali Vahidyeganeh, Onur Bilgin, Orhun Tugay, Seyed Vahid Sajadifar and Ulaş Yıldırım for their friendship and technical support was much appreciated. Additionally, a big thanks to Barış Balcı, Gizem Bakır, Mehmet Can Yıldırım, and Yiğit Kaan Sayınbaş for their precious help and support. I always enjoyed working and having fun with you.

I am also thankful to all members of the fellowship of the ring; Berkan Öztürk, Doğaç Callak, Elif Cebecioğlu, Meltem Yürekli, Merve Mert, Oğuz Can Sarıçayır, Sabri Orçun Orhan (my Sam), Serhat Gül, Şeyma Kahraman and mostly Işıl Külah who has always been there for me unconditionally. More importantly, I am forever indebted and must thank my parents, Düriye and Osman Şimşek. Especially to my sister Sinem Şimşek, whose support and magical ways of encouragement always propelled me to follow my dreams and persevere in the face of difficulties that I came across in life. Without their specific and special skills, I would not have been able to destroy the ring successfully. Dear Gollum, it is all yours now!!

Finally, I would like to acknowledge the support from The Scientific and Technological Research Council of Turkey (TÜBİTAK) within project no: 113S096.

TABLE OF CONTENTS

DEDICATION . . . . . **iii**

ABSTRACT . . . . . **iv**

ÖZETÇE . . . . . **vi**

ACKNOWLEDGEMENTS . . . . . **viii**

LIST OF TABLES . . . . . **xii**

LIST OF FIGURES . . . . . **xiv**

I INTRODUCTION **3**

1.1 Basics of Shape Memory Alloys 3

1.2 Fundamentals Characteristics of NiTi Shape Memory Alloys 8

1.3 Applications of NiTi Shape Memory Alloys 14

1.4 Critical Requirements for NiTi for Biomedical Applications 23

1.4.1 Biocompatibility 23

1.4.1.1 Chemical surface treatments 27

1.4.1.2 Ceramic based coating 29

1.4.1.3 Polymer based coating 38

1.4.2 Corrosion Properties 46

1.4.2.1 Corrosion Mechanisms of NiTi shape memory alloys 47

1.4.2.2 Mathematical Modeling of corrosion 57

1.4.3 Cyclic Behavior 62

1.5 Motivation 67

II MATERIALS AND METHODS **69**

2.1 Materials Selection 69

2.1.1 Selection of NiTi 69

2.1.2 Materials for biocompatible coatings 70

2.2 Experimental Procedures 71

2.2.1 Heat treatment of NiTi wire . . . 71
2.2.2 Functional characterization of NiTi wire . . . 72
2.2.2.1 Measuring phase transformation temperatures of NiTi 73
2.2.2.2 Actuation and cyclic behavior of uncoated and coated NiTi . . . 74
2.2.3 Biocompatible coating procedure . . . 78
2.2.3.1 Biomimetic coating . . . 79
2.2.3.2 Dip coating . . . 80
2.2.3.3 Hydrogel coating . . . 83
2.2.4 Surface Characterization . . . 86
2.2.4.1 Heat treated NiTi samples . . . 87
2.2.4.2 CaP based coated NiTi samples . . . 87
2.2.4.3 Hydrogel coated NiTi samples . . . 87
2.2.4.4 Contact angle measurement . . . 88
2.2.4.5 Hardness measurement . . . 88
2.2.5 Corrosion behavior . . . 88
2.2.5.1 Mathematical modeling of corrosion . . . 89
2.2.6 Cytotoxicity experiments . . . 94
2.3 Research Equipment . . . 95
III RESULTS AND DISCUSSION . . . 99
3.1 Effects of Heat Treatment on the Functional Behavior of NiTi Shape Memory Alloy . . . 99
3.1.1 Determining transformation temperatures . . . 100
3.1.2 Displacement and repeatability experiments . . . 102
3.1.3 Force experiments . . . 107
3.1.4 Cyclic experiments . . . 109
3.1.5 Investigation on the hardness of NiTi . . . 114
3.1.6 Corrosion properties . . . 115
3.1.7 Investigation on surface characteristics . . . 129

3.2 Effect of biocompatible coating on the functional behavior of NiTi Shape Memory Alloy 132

3.2.1 CaP coated NiTi Shape Memory Alloy 132

3.2.1.1 Effect of Coating Method on the Surface Characteristics of NiTi Shape Memory Alloy 132

3.2.1.2 Evaluation of NaOH pre-treatment on the surface characteristics of CaP coated NiTi alloy 147

3.2.2 Hydrogel coated NiTi Shape Memory Alloy 159

3.3 Effect of biocompatible coating on the mathematical modeling of corrosion 179

IV CONCLUSIONS 182

REFERENCES 187

VITA 207

LIST OF TABLES

1 Mechanical properties of NiTi shape memory alloy for different phases [6] . . . 7

2 The general properties of hydroxyapatite . . . 30

3 Ca/P ratio of NiTi substrates after immersing into SBF solution for different duration [86] . . . 36

4 General properties of PVA [94] . . . 39

5 Elements in the human body [143] . . . 48

6 Potential adverse reactions caused by the releasing of metal ions [145] 49

7 Activity and required cycles for implanted hip prosthesis . . . 65

8 Selected reagents for simulated body fluid . . . 70

9 Selected reagents for depositing biocompatible layer on NiTi . . . 71

10 The planned heat treatment conditions . . . 72

11 Reagents for preparing 1000 ml of simulated body fluid (SBF) [60] . . . 77

12 Ringer physiological solution . . . 77

13 Selected parameters for depositing CaP based biocompatible layer on NiTi . . . 81

14 Sample naming convention based on NaOH surface treatment and HA coating conditions . . . 83

15 Transformation temperatures of heat treated NiTi samples measured by DSC . . . 100

16 Total material loss after potentiodynamic test . . . 116

17 Selected parameters for corrosion modeling . . . 120

18 Relation between mean corrosion and percentage of corrosion . . . 128

19 Average contact angle values of heat treated NiTi samples . . . 129

20 Average contact angle values of CaP coated NiTi samples . . . 141

21 Corrosion rate values of the NiTi samples as a function of coating method 145

22 Total material loss as a function of coating method . . . 146

23 Contact angle measurements . . . 153

24 Total material loss of NaOH treated NiTi after electrochemical measurements 157

25 Selection of ideal amounts of PVA and gelatin 160

26 Results of preparation steps 160

27 Total material loss of hydrogel coated NiTi after electrochemical measurements 175

LIST OF FIGURES

1 Diagrammatic representation of shape memory effect [4] 4

2 Diagrammatic representation of one and two shape memory effect . . 5

3 Stress strain curve of superelastic behavior of shape memory alloys [1] 5

4 Phase transformation between martensite and austenite [5] 6

5 Phase diagram of shape memory alloys as a function of stress and temperature [7] 7

6 Phase diagram of NiTi shape memory alloys [18] 9

7 Previous studies shows the relation between transformation temperature and NiTi composition [14] 9

8 Effect of Ni content on the A_f temperature of NiTi alloy [19] 10

9 Effect of heat treatment parameters on hardness of cold roled NiTi alloy [15] 11

10 Tensile curves of NiTi alloy treated with different temperatures [23] . 12

11 Microstructure evaluation of Ti-52Ni for different duration: (a) 15 min; (b) 1h; (c)100h; (d) 1000h [26] 13

12 Applications of NiTi shape memory alloys [6] 14

13 Stress-strain behavior of common living tissue and NiTi shape memory alloys [34] 15

14 Potential shape memory alloys applications in human body 16

15 Comparison of the mechanical properties of (a) conventional metallic materials and NiTi in wire shape; (b) stainless steel and NiTi in coil spring shape [43] 17

16 The use of Homer mammalok to identify breast cancer [44] 18

17 Cardiovascular applications of NiTi: (a) Simon filter [46], (b) origmai stents and (c) self expanding stents [47] 18

18 NiTi shape memory implants for healing bone fracture: (a) NiTi staples; (b) Medullary nails; (c) NiTi plates [49] 19

19 The use of NiTi SMA in scoliosis correction treatment: (a) proposed design; (b) after implementation for 6 months [9] 20

20 Designed active catheter systems: (a) kidney operations; (b) surgical applications [53] 21

21 Active guide wire system: (a) movement capability; (b) measured surface temperatures in air and water condition [54] 22

22 Implementation of NiTi (a) 3 days; (b) 9 weeks [56] 25

23 Comparision of three conventional metallic biomaterial as a function of: (a) total bone mineral density of the ossicles; (b) amount of cartilage as an area proportional to the ossicle area; (c) amount of new bone as an area proportional to the ossicle area [57] 26

24 SEM images of (a) uncoated; (b) coated at 400^oC; (c) coated at 600^oC; (d) coated at 600^oC with higher magnification [64] 28

25 SEM images of stent surfaces; (a) after laser cut, (b) after etching for 220 seconds [66] 28

26 Auger analysis of NiTi plate sample surfaces (a) polished and heat treated, (b) polished, chemically etched, boiled in water, and heat treated [67] 29

27 SEM images of HA coated surfaces via electrophoretic deposition method [75] 31

28 SEM images of HaP coated NiTi surfaces via sol-gel deposition at 5000x magnification [76] 32

29 SEM images of (a) as received NiTi; (b) coated NiTi; (c) as received NiTi; (d) coated NiTi [78] 33

30 Apatite layer on 600^oC heat treated NiTi surfaces before and after immersion into SBF solution: (a) before immersion; (b) after 3 days; (c) after 14 days [82] 34

31 Apatite layer on NiTi surfaces after being immersed into SBF solution for different duration: (a) 1 day; (b) 3 days; (c) 5 days at 5000x magnification [83] 35

32 SEM images of (a) titanium sample; (b) NiTi sample after scratch test at 500x magnification [85] 36

33 Steps of dip coating method [87] 37

34 Mechanical experiments on investigation mechanical stability of CaP layer [90] 38

35 Relation between dissolution time and PVA concentration[97] 40

36 Mechanical properties of hydrogel as a function of composition ratio (a) compression strength; (b) degradation rate; (c) swelling rate [129] 43

37 SEM images of hydrogel membrane (a) before drug release; (b) after drug release [92] 43

38 SEM images of chitosan/gelatin/PVA based hydrogel (a) 50 x; (b) 300x; (c) 500x [132] 44

39 Hydrogel coated implant for orthopedic applications [135] 45

40 Comparison of corrosion behaviors of commercial metallic implant materials [147] 49

41 SEM images of the NiTi substrate after potentiostatic test in (a) NaCl solution at 640x magnification ; (b) Ringer solution at 1000x magnification [153] 50

42 Polarization curves of the NiTi SMA in (a) 0.5M H2SO4 solution; (b) 0.2M NaCl solution; (c) borate buffer solution [154] 51

43 Polarization curves of NiTi for different pH values [155] 52

44 SEM images of the NiTi substrate (a) anodized; (b) anodized and annealed NiTi; (c) Ni release of bare, anodized and anodized and annealed substrate for different periods [157] 53

45 Thickness of the oxide layer on the grounded and polished NiTi surfaces after boiling water [160] 54

46 AFM images of NiTi surfaces (a) polished NiTi; (b) after chemical treatment; (c) after chemical treatment and annealing; (d) after chemical treatment, annealing, and passivation [162] 55

47 AFM images of NiTi surfaces (a)A_f=-3^oC control; (b) A_f=-3^oC oxygen implanted [163] 56

48 A Ni release from different NiTi orthodontic archwires [164] 56

49 (a) Computational intelligence methods; (b) corrosion damage identification process and corrosion damage quantification process [167] . . 58

50 (a) a square-shaped neighborhood: Moore, (b) Neumann [168] 59

51 Effect of pH on corrosion [173] 60

52 The pitting initiation and growth simulation with different time steps [174] 61

53 Developed computational approach in three dimensions and the results of the simulation at different cycles; (a) 70 cycles, (b) 85 cycles, (c) 100 cycles and (d) 115 cycles [174] 62

54 Failure of implants and their causes [175] 63

55 The illustration of the complex interactions between the implant surface and the body environment [182] 64
56 Complex interactions between the implant surface and body environment [183] 65
57 SEM images of the NiTi substrate (a-b) as-received; (c-d) laser-welded after the bending rotation fatigue test in Hanks' solution [184] 66
58 Custom made holder for shape setting process 72
59 Determining transformation temperatures with tangent method [187] 74
60 Experimental setup for displacement and bending angle measurement (a) side view; (b) top view [188] 75
61 Three-dimensional depiction of force setup [188] 75
62 Three-dimensional depiction of force setup [188] 76
63 The experimental setup for the cyclic response tests in corrosive medium 78
64 The types of coating for the dissertation 79
65 Manufactured holder for biomimetic method 80
66 Dip coating setup with dipping apparatus: (a) preparation process; (b) coating process 82
67 Different amounts of agents of hydrogel suspension 84
68 Different preparation parameters for hydrogel suspension 85
69 Design of teflon sample holder for potentiodynamic corrosion experiments 89
70 Flowchart of the corrosion modeling [193] 90
71 Area of image denoting Moore neighborhood 92
72 Furnace for heat treatment 96
73 Differential scanning calorimetry (DSC) to measure phase transformation temperatures 96
74 DAQ systems and power supply 97
75 Magnetic stirrer and analytic balance 97
76 Experimental setup for electrochemical corrosion measurements . . . 98
77 Equipment for surface characterization (a) confocal microscope; (b) digital microscope; (c) scanning electron microscope (SEM) 98

78 DSC heating and cooling curves: the austenite and martensite transformation temperatures of NiTi samples treated at 520^{o}C for 30 minutes 101

79 Temperature-displacement graph to determine austenite transformations temperatures 101

80 The displacement behavior of NiTi samples for the constant duration (a) 30 minutes and (b) 60 minutes 103

81 The displacement behavior of heat treated NiTi samples for different conditions (a) 460^{o}C for 30 and 60 minutes; (b) 520^{o}C for 30 and 60 minutes 104

82 The repeatability behavior of heat treated NiTi samples for different conditions 105

83 Repeatability of heat treated NiTi samples: 460^{o}C (above) and 520^{o}C (below) for 30 min. 106

84 Repeatability of 520^{o}C for 30 minute treated NiTi samples 107

85 Actuation forces of NiTi as a function of heat treatment conditions . 108

86 Force-temperature relation for the sample treated at 520^{o}C for 30 minutes 109

87 Response of the proportional controller (a)before and (b)after tuning 110

88 Response of (a) PI; (b) PD; (c) PID with different K_p, K_i, and K_d values; (d) PID with different K_p, K_i, and K_d values controllers . . . 111

89 Effect of heat treatment on the total number of cycles before failure in different conditions (a) dry; (b) simulated body fluids, (c) Ringer solution 113

90 Effect of testing medium on the total number of cycles before failure in (a) dry; (b) simulated body fluids, (c) Ringer solution 114

91 The variation of the hardness of NiTi samples as a function of heat treatment parameters 115

92 Potentiodynamic polarization curves of the heat-treated samples at 460^{o}C, 520^{o}C, 600^{o}C (a) 30 min and (b) 60 min, and the results of corrosion experiments 117

93 Surface morphology of heat treated at 520^{o}C for 30 min. NiTi sample 118

94 SEM surface micrographs of NiTi treated at 520^{o}C for 30 min. (a) before and (b) after potentiodynamic polarization experiment 119

95 Effect of corrosion on the total number of cycles of the sample treated 520^{o}C for 30 min. 120

96 Relation between mean corrosion and pH of as-received NiTi sample . 121

97 Relation of mean corrosion and temperature as-received NiTi sample 122

98 Relation of mean corrosion and concentration of the reaction species as-received NiTi sample 123

99 Relation between mean corrosion and diffusivity of the reaction species as-received NiTi sample 124

100 Relation between mean corrosion and charge of the reaction species as-received NiTi sample 124

101 Electrochemical curves of NiTi samples for different temperature and pH values 126

102 Corrosion state S(u,t) at time steps t=0, 1, 2, 3, 4, 5 respectively . . 127

103 Optical micrographs of NiTi samples with different heat treatment parameters (a) 460^{o}C for 30 min; (b) 520^{o}C for 30 min; (c) 600^{o}C for 30 min; (d) 460^{o}C for 60 min; (e) 520^{o}C for 60 min; (d) 600^{o}C for 60 min 130

104 SEM images of NiTi samples: (a)as-received NiTi; (b)heat treated sample at 520^{o}C for 30 min 131

105 Initial experiments with optical microscopy at 20x magnification (a) as-received NiTi; (b) 24 h; (c) 48 h and (d) half immersion for 48 h . 133

106 Total weight change as a function of immersion periods 134

107 Optical image of initial experiments on dip coating method at 20x of as-received NiTi 134

108 SEM images of (a) NiTi wire sample prior to any form of coating, (b) calcium phosphate tribasic coating on NiTi wire sample after dip coating and subsequent sintering, (c) biomimetic calcium phosphate coating on NiTi wire sample after 24 h, and (d) biomimetic calcium phosphate coating on NiTi wire sample after 48 h 135

109 The thickness of the coatings on NiTi (a) biomimetic method (24h); (b) biomimetic method (48h); (c) dip coating method 136

110 Confocal analysis of CaP coated NiTi via dip coating method (a) true color view of the image; (b) pseudo color view of the coated surface . 137

111 SEM micrograph of CaP coated NiTi surface with different parameters via dip coating method (a) as-received; (b) sample 1; (c) sample 2; (d) sample 3; (e) sample 4; (f) sample 5; (g) sample 6; (h) sample 7 . . . 138

112 Weight change of the CaP coated NiTi samples as a function of different coating parameters 139

113 SEM image of CaP coated NiTi surface with dip coating method . . . 140

114 Elemental analysis of NiTi samples after bending test 142

115 Cyclic behavior of uncoated NiTi and CaP coated NiTi (a) dry condition; (b) SBF solution; (c) Ringer solution 143

116 Fracture surface of CaP coated NiTi tested in dry condition at 4 Hz . 144

117 Cytotoxicity analyses of as received and CaP coated NiTi 146

118 SEM micrographs of NiTi samples with different surface conditions; (a) as-received, (b) heat treated and CaP coated, (c) 0.5NaOH treated and CaP coated, (d) 1NaOH treated and CaP coated, (e) 4NaOH treated and CaP coated 148

119 XPS measurements of Ni elements for the following samples (a) C; (b) 0.5NaOH-C; (c) 1NaOH-C; (d) 4NaOH-C 149

120 XPS measurements of Ti elements for the following samples (a) C; (b) 0.5NaOH-C; (c) 1NaOH-C; (d) 4NaOH-C 150

121 XPS measurements of Ca elements for the following samples (a) C; (b) 0.5NaOH-C; (c) 1NaOH-C; (d) 4NaOH-C 151

122 Ca/Ni and Ni/Ti ratio of NaOH treated samples with selected conditions152

123 Images of contact angle measurements; (a) as-received, (b) C, (c) 0.5NaOH-C, (d) 1NaOH-C 153

124 Cyclic behavior of untreated and NaOH treated NiTi samples (a) dry condition; (b) SBF solution; (c) Ringer solution 155

125 Fracture surface of the sample that treated with NaOH prior to bioceramic coating in dry condition at 4 Hz 156

126 Polarization curves of NiTi samples with different surface conditions . 156

127 SEM micrographs of NiTi samples following corrosion experiments in different magnifications (a) sample C; (b) sample 0.5NaOH-C; (c) sample C (higher magnification); (d) sample 0.5NaOH-C (higher magnification) 157

128 Cell viability test results of as-received, C and 0.5NaOH-C NiTi samples158

129 Surface images of the NiTi substrate; (a) and (c) before, (b) and (d) after coating with a hydrogel layer 161

130 OM images (a) RGB images of hydrogel coated NiTi samples; (b) converted grayscale images of hydrogel coated NiTi samples 162

131 After immersing NiTi samples in SBF solution: (a) 7 days; (b) 14 days; and (c) 28 days 163

132 SEM image of hydrogel coating on the NiTi surface 164

133 Confocal images of hydrogel coated surface (a) pseudo color view; (b) true color view of the image; (c) 3D view of the surface 165

134 Confocal images of hydrogel coated NiTi (a) pseudo color view of the surface; (b) true color view of the image; (c) 3D view of the surface; (d) SEM images of hydrogel coated NiTi 166

135 Elemental analyses of hydrogel coated NiTi sample for selected elements 167

136 Hardness measurement: (a) experimental results of uncoated NiTi and hydrogel-coated NiTi; (b) hydrogel coated surface after hardness test 168

137 Contact angle of water droplets on uncoated and hydrogel-coated NiTi surfaces with the respective variation in contact angles 169

138 Bending behavior of uncoated and hydrogel-coated NiTi samples . . . 170

139 Hydrogel coated NiTi sample after cyclic experiment in dry condition (a) 500 cycle; (b)1000 cycle 171

140 Cyclic behavior of hydrogel coated NiTi sample in (a) dry condition; (b) SBF solution; (c) Ringer solution at different frequencies 172

141 Fracture surface of hydrogel coated NiTi sample that tested in dry condition at 4 Hz 173

142 Potentiodynamic polarization curves of uncoated NiTi and hydrogel coated NiTi at 37^{o}C 174

143 Corroded surface of hydrogel coated NiTi sample after corrosion experiment (a) color-map analysis; (b)digital microscope image at magnification of 105x 175

144 Viability of Balb/3T3 cells estimated after 24 h of contact with different materials 176

145 A DAPI/F-Actin stainings performed on Balb/3T3 cells after 7 days of culture on uncoated and hydrogel-coated samples (top) and confocal microscopy 3D reconstructions (bottom) scale bar = 100 m; b Balb/3T3 cells after direct (top) and indirect (bottom) cytotoxicity tests (magnification 10X) 177

146 Relation between mean corrosion and potential difference 180

147 Evolution of black and white pixels as a function of step 181

PUBLICATIONS AND PRESENTATIONS

Publications

- G.M. Simsek, G.G. Yapici, Y.K. Sayinbas, M. Uysal, “Effect of Heat Treatment Parameters on the Corrosion Fatigue of NiTi Shape Memory Alloys”, Journal of Applied Physics, August 2019.

- G.M. Simsek, M. Ipekoglu, G.G. Yapici, “ Effect of Coating Method on the Surface Characteristics of NiTi Shape Memory Alloy”, Materials Science Forum, November 2020.

- G.M. Simsek, M. Ipekoglu, G.G. Yapici, “Effect of NaOH treatment on the corrosion behavior of hydroxyapatite coated NiTi wire”, Applied Physics A, July 2020.

- G.M. Simsek, G.G. Yapici, “Influence of heat treatment parameters on the functional behavior of a shape memory wire actuator”, Materials Science Forum, April 2020.

- G.M. Simsek, J.Barthes, C. Muller et al., "PVA/gelatin-based hydrogel coating of nickel-titanium alloy for improved tissue-implant interface", Appl. Phys. A 127, 387, 2021.

- T. Sustersic, G.M. Simsek, G.G. Yapici, M. Nikolic, R. Vulovic, N.Filipovic, N.E. Vrana, "An In-Silico Corrosion Model for Biomedical Applications for Coupling With In-Vitro Biocompatibility Tests for Estimation of Long-Term Effects", Frontiers in Bioengineering and Biotechnology, 9, 2021.

Oral and Poster Presentations

- G.M. Simsek, A.V. Yeganeh, S. Jabeen, G.G. Yapici, O. Bebek, "Characterization of a Smart joint for Biomedical Applications" Frontiers in Materials Processing Applications, Research and Technology, FiMPART, Hyderabad, India, 2015.

- G.M. Simsek, A.V. Yeganeh, G.G. Yapici, "On the cyclic behavior of a Smart Joint", European Congress and Exhibition on Advanced Materials and Processes, EUROMAT 2017, Thessaloniki, Greece, 2017.

- G.M. Simsek, G.G. Yapici, "CaP based coatings on Nitinol for Improved Corrosion Properties in Biomedical Applications", EUROMAT 2019, Stockholm, Sweeden, 2019.

- G.M. Simsek, G.G. Yapici, "Influence of heat treatment parameters on the functional behavior of a shape memory wire actuator", International Conference on Design, Materials and Manufacturing (ICDMM), Salamanca, Spain, 2019.

- G.M. Simsek, G.G. Yapici, N.E. Vrana, "The Effect of PVA-based Hydrogel Coatings on the Shape Memory Effect of NiTi for Biomedical Applications", 13th International Conference on Advanced Computational Engineering and Experimenting (ACEX), Athens, Greece, 2019.

CHAPTER I

INTRODUCTION

This chapter briefly introduces the basics of shape memory alloys, fundamental characteristics and behavior of NiTi SMAs and their applications in various fields. Following, the most critical requirements of NiTi alloys are briefly introduced in three main subsections as Biocompatibility, Corrosion Resistivity and Cyclic Response, respectively. Finally, the motivation and significance of the dissertation is introduced with main objectives and novelties.

1.1 Basics of Shape Memory Alloys

Shape memory alloys were introduced by Adolf Martens in the 1890s with the discovery of a new phase, called martensite, in steel [1]. In 1932, the shape memory transformation was observed on Au-Cd alloys by Chang and Read [2]. In the following years, researchers recognized unique behaviors in many shape memory alloys, including Nickel and Titanium (Ni-Ti), Silver and Cadmium (Ag-Cd), Gold and Cadmium (Au-Cd), Nickel and Aluminum (Ni-Al), Manganese and Copper (Mn-Cu), Iron and Platinum (Fe-PT), Copper and Zinc (Cu-Zn), and Copper-Aluminum and Nickel (Co-Al-Ni). Shape memory alloys (SMA) have two main extraordinary properties; shape memory effect (SME) and superelasticity (SE) [1, 3]. Shape Memory Effect (SME) defined as the ability to remember the parent phase and to recover above austenite finish temperature as illustrated in Figure 1 [4]. In (a), the single crystal alloy is in the austenite phase and by cooling the austenite phase, it turns into martensite phase without any macroscopic change, called self-accommodation (b). In this stage, the deformed structure changes the microstructure (c) until heating above critical transformation temperature to gain its initial shape (a).

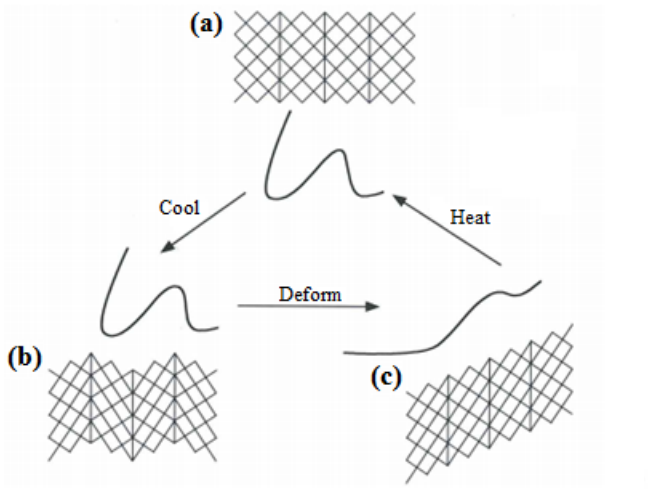


Figure 1: Diagrammatic representation of shape memory effect [4]

Shape memory effect is mainly classified into two groups: one-way shape memory effect and two-way shape memory effect, as represented in Figure 2-a. One-way shape memory alloys tend to remember only a parent phase as a consequence of certain external stimulus such as thermal, magnetic or mechanical loads. The one-way shape memory effect is generally driven by temperature change. Stage (a) refers to the form in the martensite phase. In stage (b), material is deformed below the martensite finish temperature and the returning pre-deformed shape process is induced by heating above austenite start temperature. Parent phase is completely recovered at stage (c). Cooling the specimen below martensite finish temperature does not induce any macroscopic shape change as illustrated in stage (d). In contrast to this, two way shape memory alloys have the ability to retain not only the shape of the parent phase but also the shape at the low-temperature phase as defined in Figure 2-b. The martensitic specimen (a) is severely deformed as shown in stage (b). The specimen changes its shape between (c) and (d) by heating or cooling repeatedly. This thermal cycling leads to the specimen remembering two learned forms for both the austenite and martensite phases. Moreover, cooling of the specimen from high temperatures causes macroscopic shape change as illustrated in stage (d).

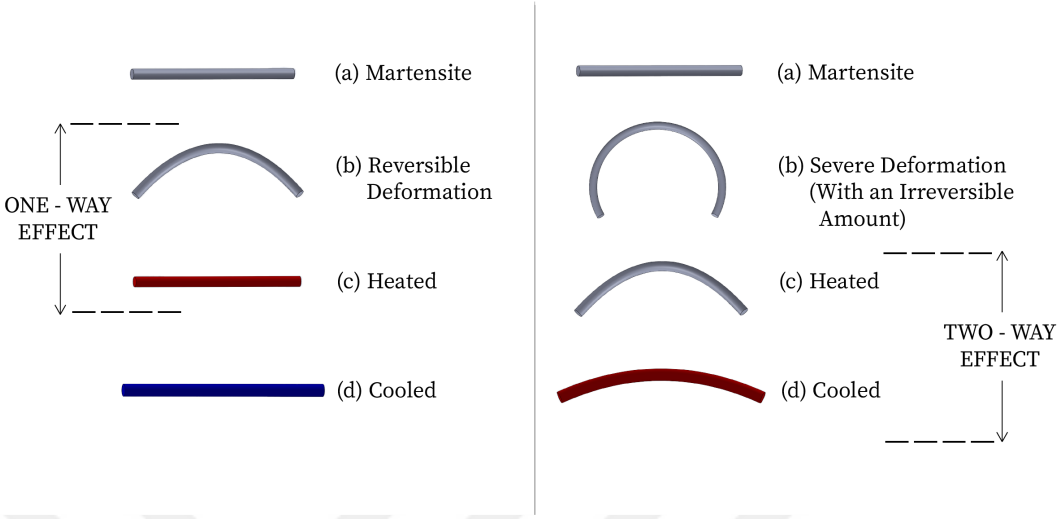


Figure 2: Diagrammatic representation of one and two shape memory effect

Superelasticity, called stress-dependent elastic response, is another distinct characteristic of shape memory alloys. Shape memory alloys can undergo large strain values up to 8% in the parent phase and recover the pre-deformed shape with the removal of the load. Superelasticity is induced by loading and unloading above austenite finish temperature. The stress-strain curve of superelastic behavior of shape memory alloys is shown in Figure 3.

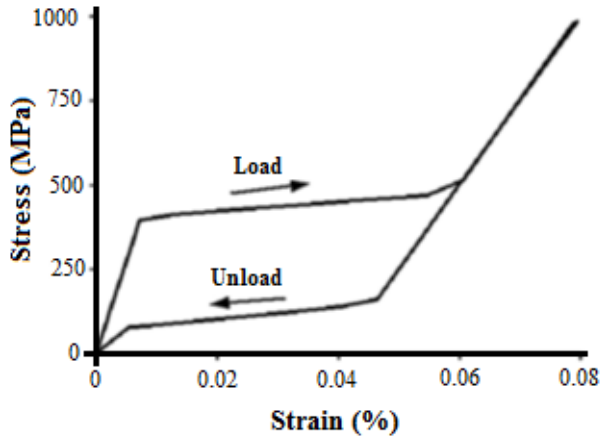


Figure 3: Stress strain curve of superelastic behavior of shape memory alloys [1]

All these extraordinary characteristics are associated with the transformation between austenitic (B2 cubic-parent phase) and martensitic (B19'monoclinic phase) phases [4]. The phase transformation mechanisms of shape memory alloys are illustrated in Figure 4. This diffusionless transformation occurs through low temperature martensite phase to high temperature austenite phase where M_s and M_f represent martensite start and martensite finish temperatures, respectively. Consequently, heating the austenite phase starts at austenite start temperature (A_s) and continues until reaching the austenite finish temperature (A_f).

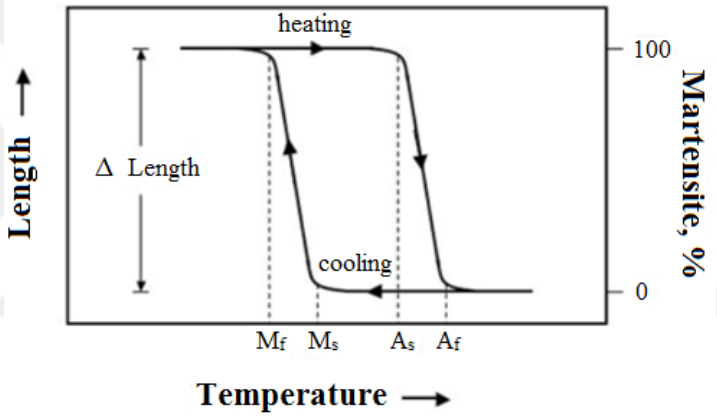


Figure 4: Phase transformation between martensite and austenite [5]

The crystal structure of shape memory alloys differs between austenite and martensite phases. Martensite is the low-temperature phase named after Adolf Martensite, whereas, austenite is the high-temperature phase named after by William Chandler Austen. This phase transformation process consists of B2 type cubic structure (austenite) and B19' type monoclinic structure (martensite). In the range of austenite phase transformation temperature, NiTi crystal structure is body-centered cubic (BCC) and usually appears in B2 type. At a lower temperature, the crystal structure of NiTi alloys changes into a close-packed hexagonal crystal structure and appears in the B19' monoclinic phase. Due to this difference, the mechanical properties of SMA differ between austenite and martensite phases as shown in Table 1 [6].

Table 1: Mechanical properties of NiTi shape memory alloy for different phases [6]

Mechanical Properties	**Austenite**	**Martensite**
Youngs Modulus (GPa)	28-41	75-83
Ultimate Tensile Strength (MPa)	800-1500	103-1100
Elongation to failure	20-50	5-10
Recoverable strain	1-20	8-10

Lagoudas [7] created the phase diagram as shown in Figure 5 to comprehensively separate the shape memory alloys based on transformation field, where A is austenite phase, M_t is twinned martensite, M_d is detwinned martensite, A_{st} is twinned austenite start temperature, A_{ft} is twinned austenite finish temperature, A_{sd} is detwinned austenite start temperature, and A_{fd} is detwinned finish temperature.

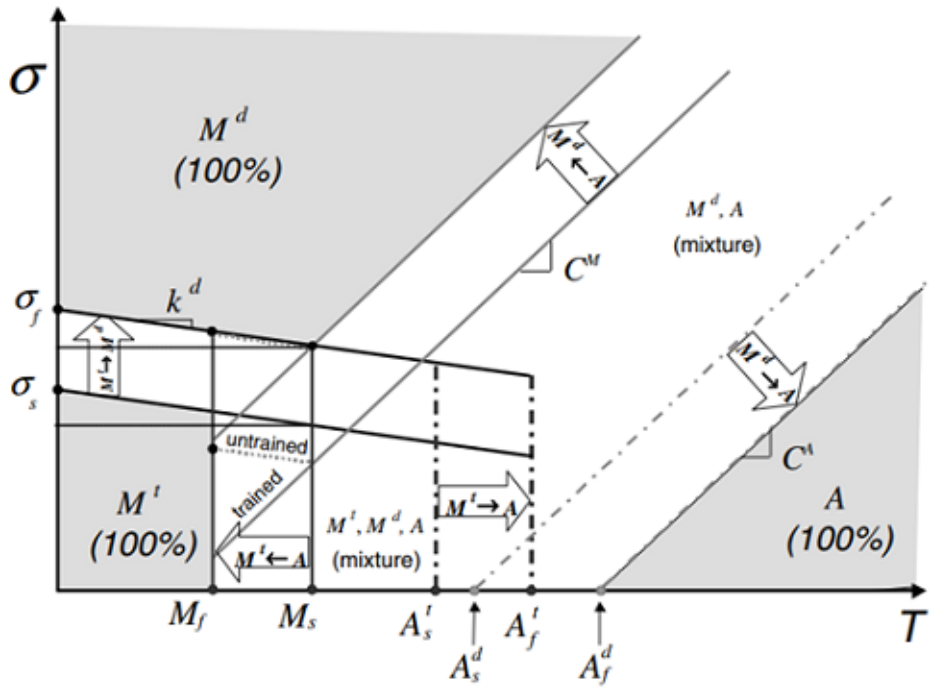


Figure 5: Phase diagram of shape memory alloys as a function of stress and temperature [7]

Among all shape memory alloys, applications of NiTi are continuously growing, ranging from bio-related applications [8, 9] to automotive [10] and aerospace [11] fields due to their high force to mass ratio, great ductility, more recoverable motion, excellent corrosion resistance, stable transformation temperatures, and favorable biocompatibility [12].

1.2 Fundamentals Characteristics of NiTi Shape Memory Alloys

Nickel-Titanium shape memory alloys were discovered by W.F. Buehler in 1961 and named as a combination of Nickel, Titanium and the acronym of the Naval Ordnance Laboratory, Nitinol. Among other SMA, NiTi alloys received a significant interest due to their favorable mechanical properties and reasonable biocompatibility. Several studies have indicated that the mechanical properties of NiTi alloys are highly dependent on the composition of nickel and titanium elements [13, 14] and heat treatment process [15, 16]. It was reported that even 0.1% composition difference of Ni could affect the transformation temperature approximately by 10 K [17]. Phase diagrams are utilized to understand the characteristics of NiTi alloys as a function of mentioned parameters. Otsuka and Massalski have established the phase diagram of NiTi alloys as given in Figure 6 [18].

Many efforts have been conducted to examine the effect of composition on the mechanical properties of NiTi alloys. Khalil-Allafi and Amin-Ahmadi have investigated the effect of chemical composition on enthalpy and entropy changes of martensitic transformations in binary NiTi shape memory alloys [14]. It was reported that with the increase of Ni concentration, the phase transformation temperatures tend to decrease as illustrated in the Figure 7. They also claimed that the rise of Ni atomic content, changing enthalpy, and entropy negatively affected the elastic energy and chemical forces.

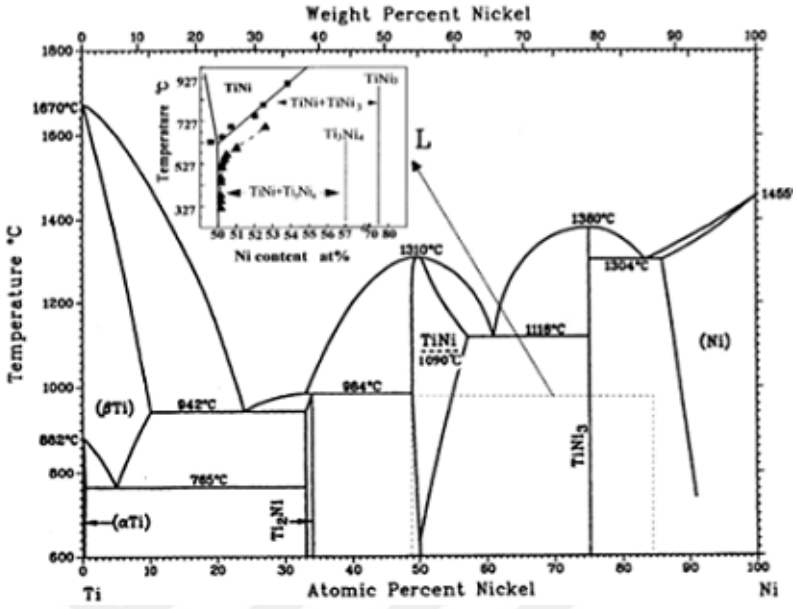


Figure 6: Phase diagram of NiTi shape memory alloys [18]

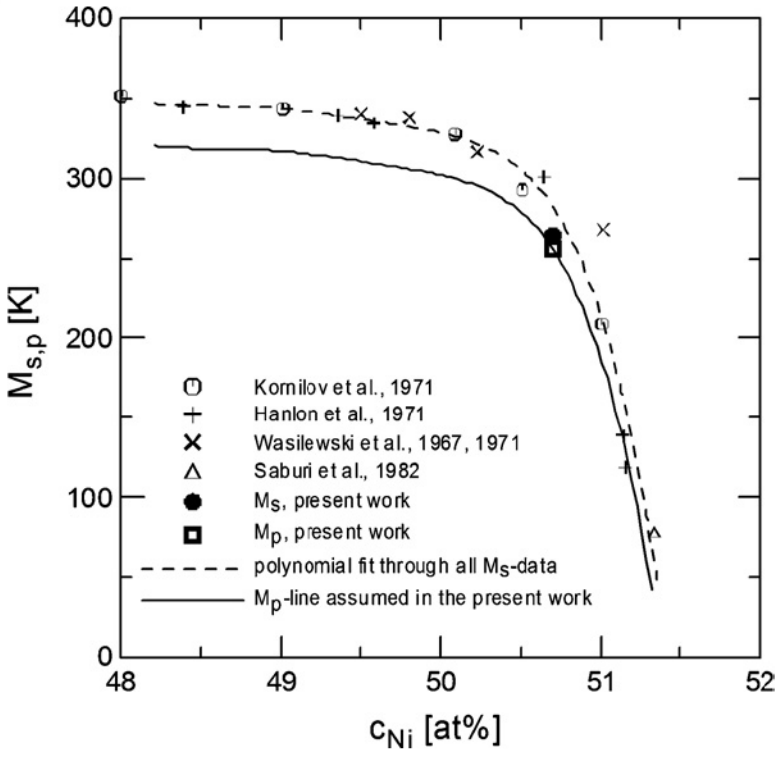


Figure 7: Previous studies shows the relation between transformation temperature and NiTi composition [14]

Similarly, Pelton et al. have also demonstrated the effect of Ni content on the austenite finish temperature as shown in Figure 8 [19]. Austenite finish temperature was nearly constant between 54-55 (wt), while there was a dramatic decrease above 55. They pointed out that the adjustment of the austenite finish temperature may directly affect the performance of NiTi based medical devices.

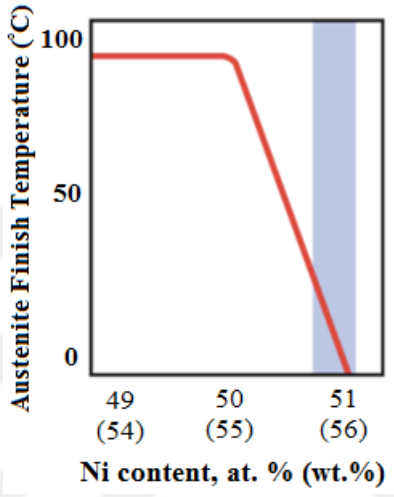


Figure 8: Effect of Ni content on the A_f temperature of NiTi alloy [19]

Much like composition, the effect of heat treatment on the mechanical behavior of NiTi alloys has been investigated by many researchers. Previous studies reported that control of heat treatment parameters is significant for tailoring the transformation behavior, the cyclic behavior, the mechanical behavior, and the pseudoelasticity of SMAs [20, 21]. As mentioned before, Pelton et al. have exhibited the relationship between annealing parameters and the transformation temperatures of NiTi alloy. Temperature parameters for annealing were selected between 300^{o}C and 600^{o}C. Similarly, a study by Mitwally et al. sought to characterise the effect of annealing at temperatures ranging from 400^{o}C to 600^{o}C [22]. It was found that hardness and superplasticity decreased at the temperature range of 400-500^{o}C, which was attributed to dislocation annihilation. However, above 500^{o}C, due to the observation of the recrystallization stage, there is an increase in hardness.

Figure 9 indicates the change of hardness as a function of annealing temperature. Paryab et al. also showed an increase hardness between 400^{o}C and 500^{o}C [15]. However, the hardness tends to decrease with the rise of temperature until 700^{o}C. They reported that the formation of coarse precipitates and phase transformation matrix might also induce the observed drop in hardness.

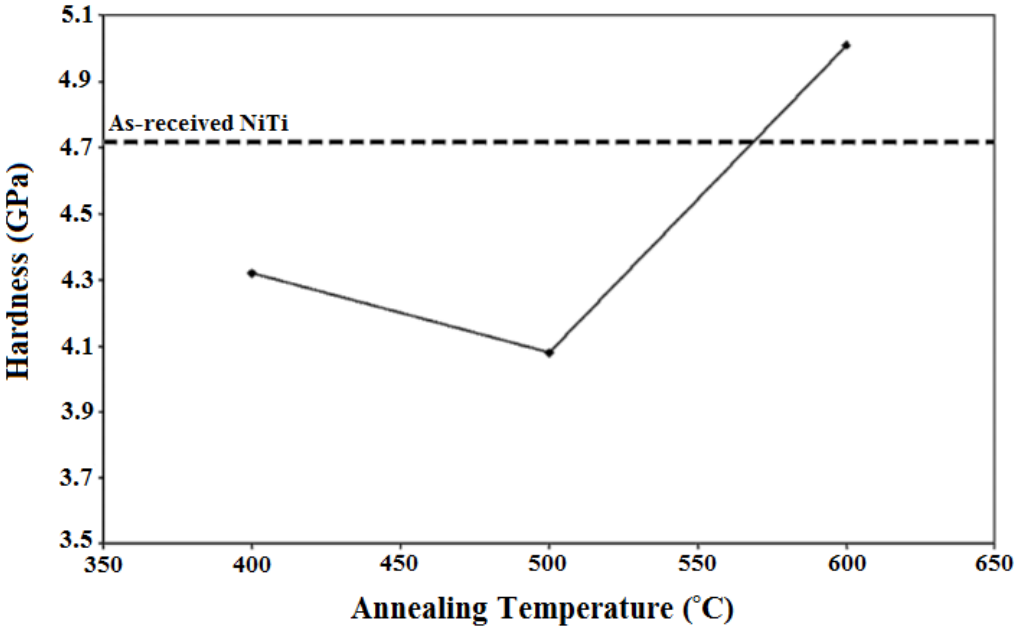


Figure 9: Effect of heat treatment parameters on hardness of cold roled NiTi alloy [15]

Sadiq and colleagues investigated the influence of heat treatment temperature on the recovery stress of Nickel rich shape memory alloy [23]. The heat treatments were obtained with the range of 350^{o}C to 700^{o}C for 30 minutes followed by quenching in ice water. Tensile tests were conducted at room temperature to evaluate the mechanical behavior of Ni-rich SMA as a function of heat treatment temperature. Initial findings were showed that ductility of NiTi SMA was directly related to heat treatment temperature. Figure 10 shows the tensile curves of different heat treated NiTi alloy at room temperature. It was observed that the ultimate strain to failure increases with the rise in the annealing temperature.

Along the same lines, around 600^{o}C, the yield stress and ultimate strength tend to decrease. It is worth noticing that recovery stresses was significantly deteriorated with increasing of heat treatment temperature above 600^{o}C. Due to this reason, it was recommended that the heat treatment temperature should be lower than the critical recrystallization temperature of 600^{o}C.

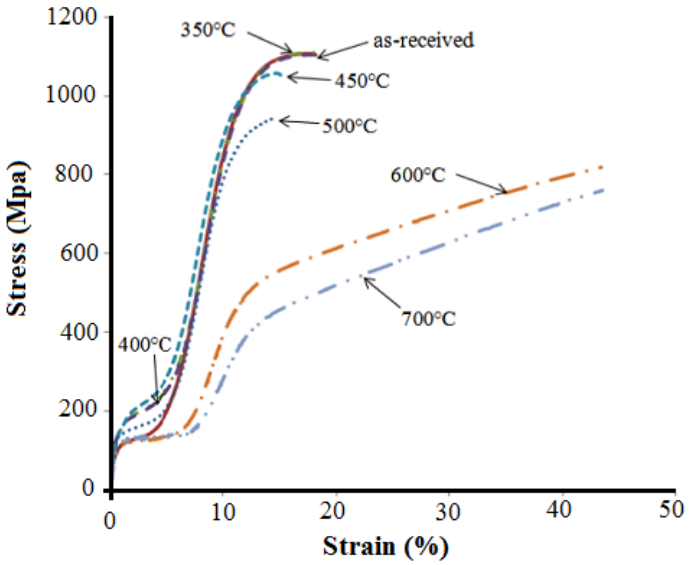


Figure 10: Tensile curves of NiTi alloy treated with different temperatures [23]

Similar to the heat treatment temperature, the effect of annealing duration has been a topic of research interest. In study by Yoon and Yeo, the impact of heat treatment parameters on the phase transformation and thermo-mechanical behavior of Ni-rich NiTi alloys was investigated [24]. It was stated that the duration should be longer than 15 minutes to provide stable phase transformation in samples treated between 400^{o}C to 600^{o}C. Similarly, work on wire form samples grappled with the influence of NiTi alloy's short time heat treatments on the wire form samples' ultimate tensile strength (UTS) and transformation stress (TS) [25]. It was concluded that the strength of NiTi alloy was improved by heat treatment temperature at the 410-460^{o}C range. On the contrary, at 485^{o}C and above, the strength of the wire decreased due to precipitation processes.

Nishida et al. have made a very detailed work series to establish the effect of heat treatment temperature and duration on the microstructural evolution of NiTi [26]. In this study, the microstructural evaluations of shape memory alloys such as the change in grain size, distribution of precipitates or recrystallization, and grain growth have elucidated comprehensively and used as an approach to enlighten the correlation between heat treatment and mechanical properties of NiTi shape memory alloy.

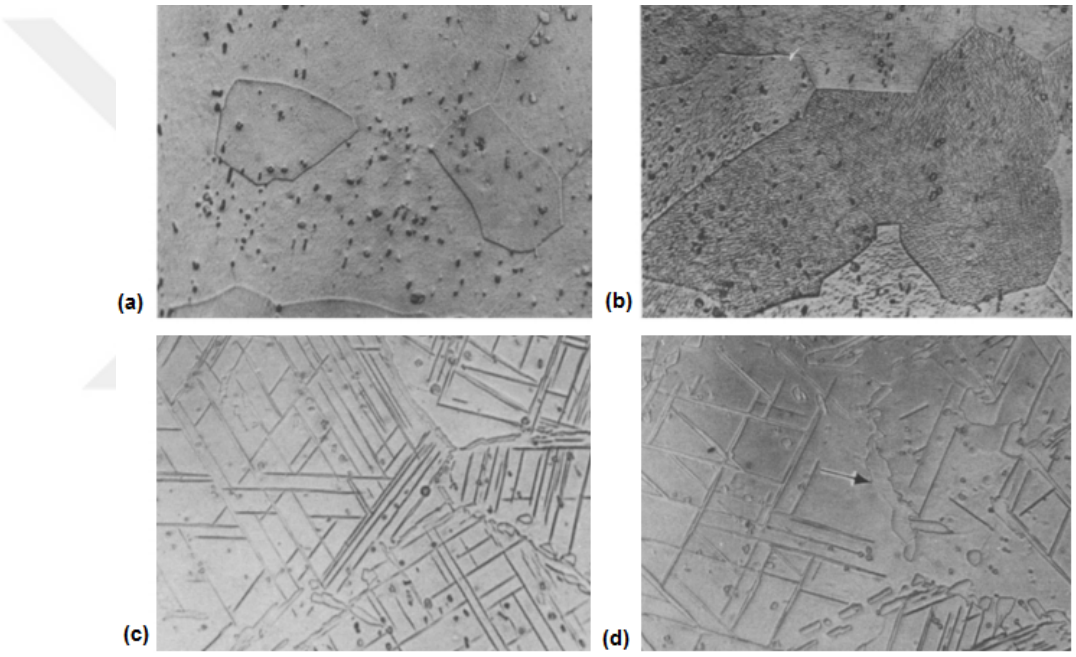


Figure 11: Microstructure evaluation of Ti-52Ni for different duration: (a) 15 min; (b) 1h; (c)100h; (d) 1000h [26]

Figure 11 shows the microstructural evaluations of Ni-rich NiTi alloy treated at 600^{o}C for different duration. For 15 minutes annealing, $Ti_{11}Ni_{14}$ particles were observed. It was found that the rising time leads to growth of the $Ti_{11}Ni_{14}$ particles. After 16 hours of treatment, the Ti_2Ni_3 particles occurred, and their volume expanded with increasing aging time. Moreover, Ti_2Ni_3 particles were observed between some grains as a result of long time treatment, shown in Figure 11 (d).

Tadayyon et al. have also reported that the recrystallization stage leads to the expansion of Ti_2Ni precipitates size, which is attributed to the annealing above 600^{o}C [27]. Characterization of martensitic variants and fine structures were conducted with high resolution electron microscopy [27]. The TEM analyses showed that martensite plates were self-accommodated well for heat treated samples. The particle size of each condition was measured and seen that with the annealing process, the particle size tended to increase, whereas during the solution treatment, the particle size was found to be more uniform.

1.3 Applications of NiTi Shape Memory Alloys

Shape memory alloys are widely used and continually growing in various industries such as automotive [28, 29], aviation [30] and aerospace [7, 31], robotics [32] and biomedical domains [33] as schematized in Figure 12, due to their extraordinary properties. However, given the purpose of the present dissertation, this section will focus on the particular uses of NiTi shape memory alloys in medical applications.

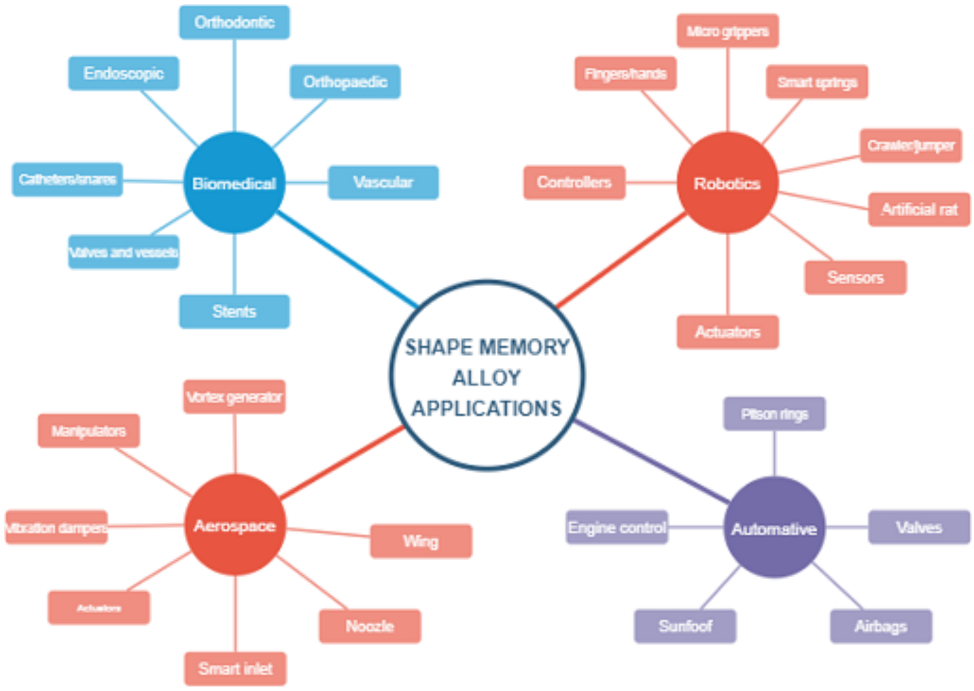


Figure 12: Applications of NiTi shape memory alloys [6]

In the past few years, there is an increasing demand for NiTi SMAs as implant materials and surgical instruments for various in vivo and in vitro biomedical applications due to their unique mechanical properties, moderate corrosion resistance and biocompatibility [6]. Compared to other commercial metallic materials, NiTi contains the most mechanically similar properties to natural human materials as shown in Figure 13 [34].

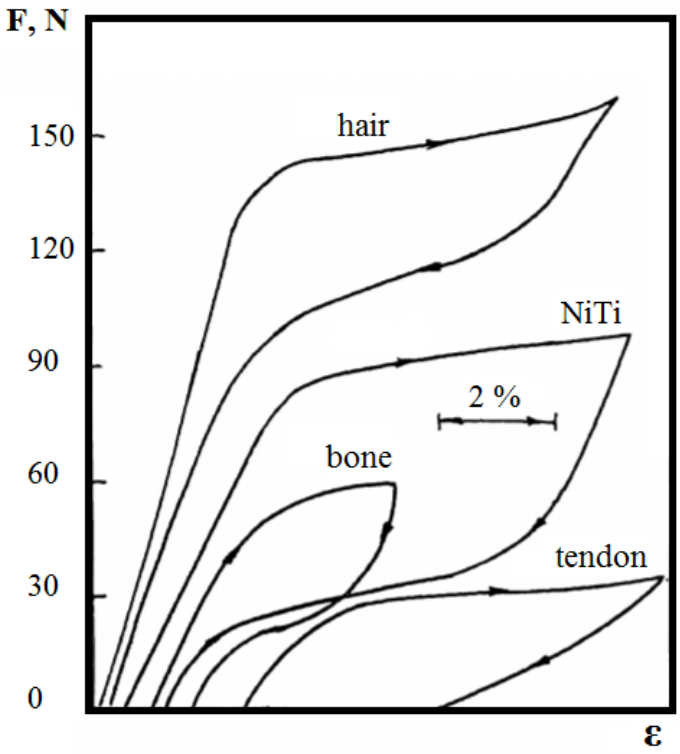


Figure 13: Stress-strain behavior of common living tissue and NiTi shape memory alloys [34]

Figure 14 shows the potential shape memory alloy applications in the human body. Generally, biomedical applications of NiTi shape memory alloys can be classified into two categories. The first category is used as passive substitutes such as bone plates [33], screws, and dental implants since they have excellent mechanical properties and corrosion resistance [35]. The second category is generally used for more active roles such as active catheters [36, 37], stents [38, 39], orthodontic arc wires [40, 41].

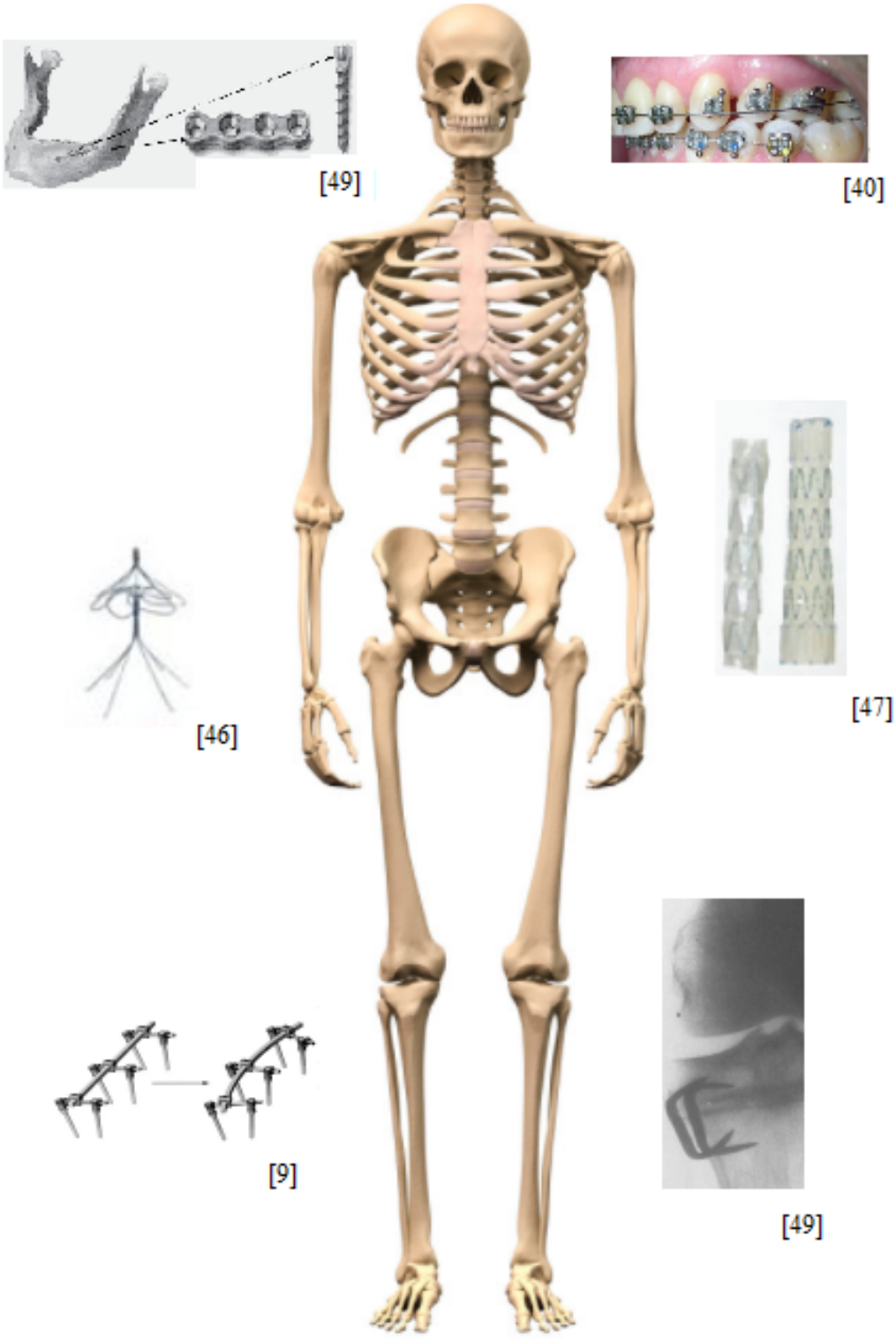


Figure 14: Potential shape memory alloys applications in human body

The first use of NiTi shape memory alloys in the biomedical field appeared as dental treatments in the 1970s, found by Andreasen [8]. As one of the early investigations, Andreasen and Brady focused on the superelastic behavior and shape recovery properties of NiTi alloys for orthodontics. Kapila and Sachdeva further reported that NiTi alloys have the ideal orthodontic wire requirements, which are low stiffness, high formability, and large super elasticity [42]. Sachdeva and Miyazaki compared the mechanical properties of conventional metallic materials in wire and coil spring shapes as given in Figure 15 [43]. These initial studies showed that NiTi alloys showed large correction forces with small sizes and were able to distribute constant forces homogeneously in comparison.

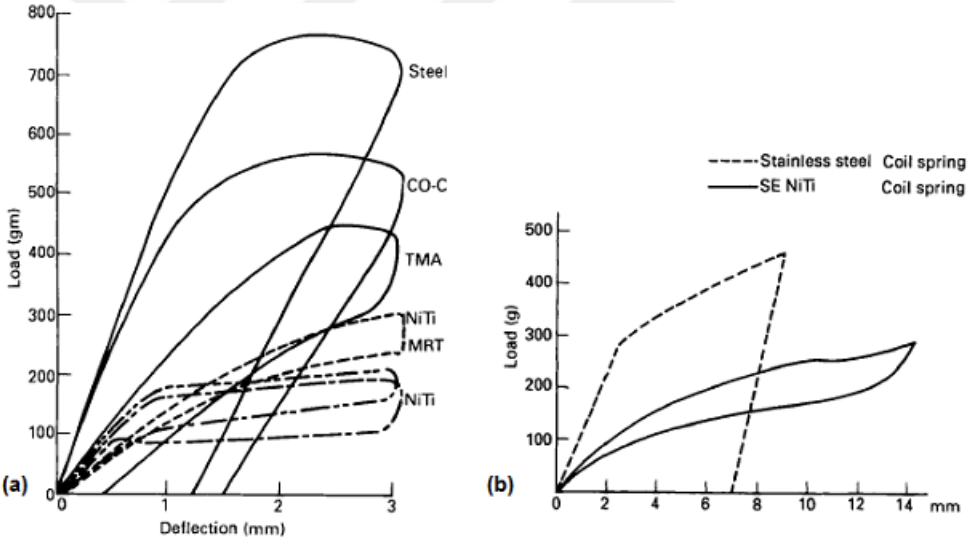


Figure 15: Comparison of the mechanical properties of (a) conventional metallic materials and NiTi in wire shape; (b) stainless steel and NiTi in coil spring shape [43]

O'Leary and colleagues proposed a prototype of homer mammalok to identify breast cancer, which became a guide to remove lesions as displayed in Figure 16 [44]. This device was used in approximately 300,000 cases. The device has the ability to change its position during the operation. The initially straight wire can be thermally activated with body temperature until it reaches the target radius of 9 mm.

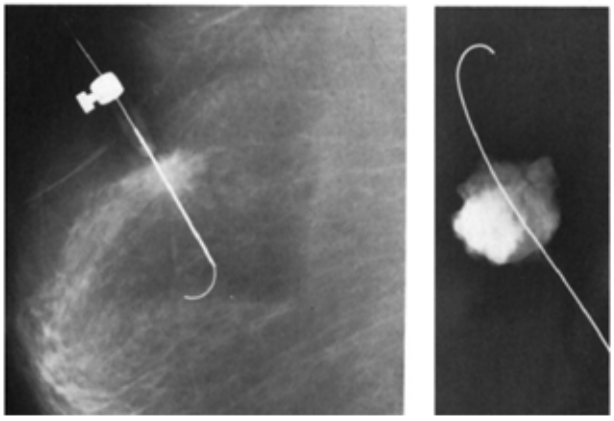


Figure 16: The use of Homer mammalok to identify breast cancer [44]

Cardiovascular applications of NiTi shape memory alloys are extensively investigated and proposed in the field [45]. Figure 17 depicts the most successful and common attempts, including the Simon filter, self-expanding and origami stents that were developed with shape memory alloys for cardiovascular application.

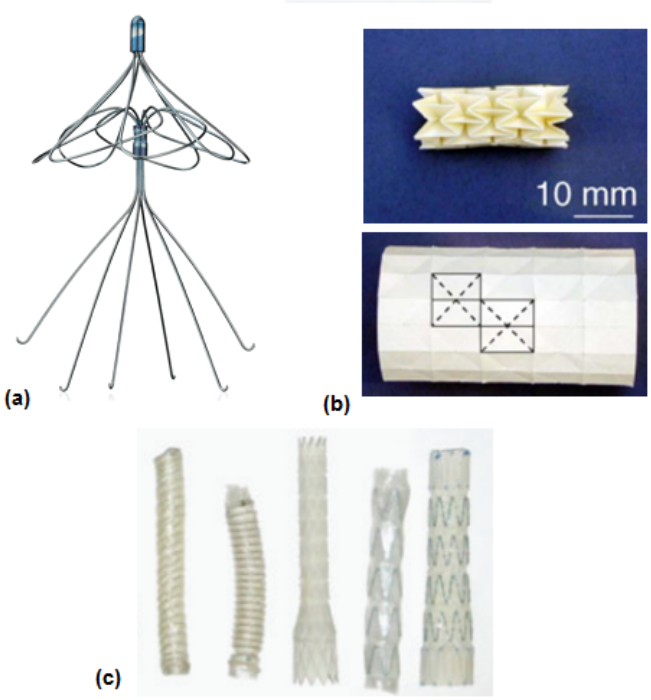


Figure 17: Cardiovascular applications of NiTi: (a) Simon filter [46], (b) origmai stents and (c) self expanding stents [47]

The use of NiTi SMA in orthopedic applications are also widely studied for recovering fractured bones by exerting a constant force since they can be manufactured in different forms such as wire, springs, foil, sheet, tube, and ribbon based on particular application. In recent years, different types of NiTi based orthopedic applications are developed for clinical use owing to their biocompatibility, size advantages, and the combination of shape memory effect and superelasticity properties as shown in Figure 18 [48, 49]. These implants bring significant advantages, including ease of implementation, faster insertion, anti-bending, anti-torsional effects, and patient-friendly response, enhanced implant life-time, and less invasive surgeries.

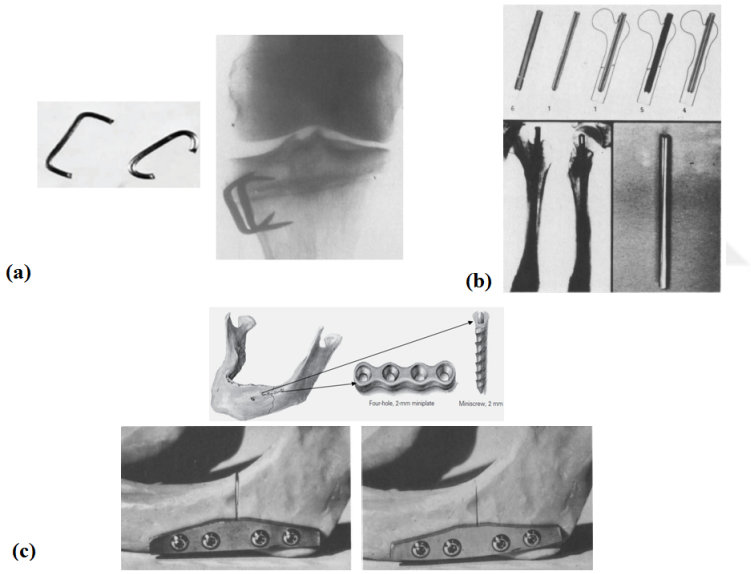


Figure 18: NiTi shape memory implants for healing bone fracture: (a) NiTi staples; (b) Medullary nails; (c) NiTi plates [49]

In their pioneering work, Wever et al. investigated the availability of NiTi shape memory alloy spinal rod for scoliosis correction treatment by using the shape recovery forces as illustrated in Figure 19 (a) [9]. It was reported that the generated bending moment was used for correcting scoliotic spine curves after the implantation process. The preclinical experimental studies proved that the implementation of the device is compatible in the martensitic phase.

Correspondingly, the in-vivo tests were carried out in the spine of immature pigs. The results argued that the spinal correction device was covered entirely with the new tissues after six months, which can be attributed to good integration with surrounding host tissue as shown in Figure 19 (b).

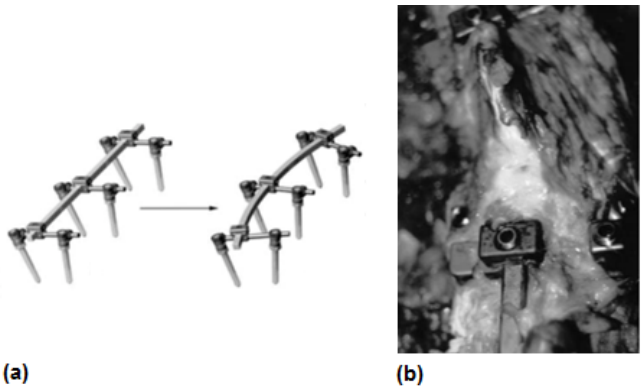


Figure 19: The use of NiTi SMA in scoliosis correction treatment: (a) proposed design; (b) after implementation for 6 months [9]

Minimally invasive techniques have brought about various advancements in interventional medical procedures. Conventional catheter systems have been probed in various medical applications. On the other hand, the operations with conventional catheters require operator experience and skill due to these tools' manual insertion. Like many catheter treatments, there is no feedback on the force applied to the surface. Excessive force may cause damage or rupture of tissue. Also, the operator would face difficulties while monitoring and controlling the catheter tip position. Hence, the development of active catheters with high movement capability is needed to provide reliable catheter placement while decreasing the possibility of injury and amount of pain. Active catheters are medical systems where the shape can be altered autonomously, and thus their orientation can be adjusted without the need of a guide. An active catheter's effectiveness and the procedure's resulting success are directly related to the accuracy of position and orientation.

NiTi SMAs are used to make the catheter system active since their mechanical behavior exhibits shape memory effect and superelasticity. These systems have been developed in order to enhance the medical procedures, improve quality of life tendency, and decrease the surgical operation risk by using controllable steering. In the 1990s, various types of active catheter systems were introduced for biomedical industry. Lim et al. demonstrated a prototype of an active catheter system with multi-link structure that can have 2.8 mm outer diameter and large bending angle [37, 50]. In another work, Maeda et al. developed an active endoscope system which is actuated by shape memory alloy coil springs [51]. In 1998, Peirs and colleques introduced two different designs of shape memory actuated endoscopic tips [52]. Haga et al. proposed three kinds of active catheter systems for ultrasound imaging purposes for kidney operations as shown in Figure 20 a [53]. Two years later, they also introduced a new fabrication method of active catheters that has features like bending and torsional and extending functions for medical applications.

The new system consists of an inner tube, link structures, serially connected joints, and an outer tube, and has a large bending motion as represented in Figure 20 b. Both devices are designed to provide feasibility develop an active instrument for surgical applications.

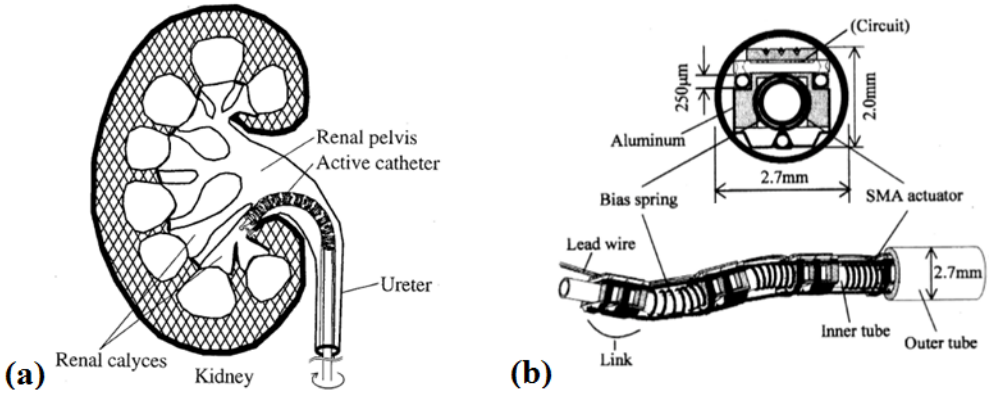


Figure 20: Designed active catheter systems: (a) kidney operations; (b) surgical applications [53]

Similarly, Esashi et al. [54] developed the shape memory actuated active guide wire system that has two main parts; a NiTi SMA actuator and a spring as the outer tube. All actuators were manufactured from a NiTi SMA sheet and are heat treated with selected conditions. The one way treated NiTi alloys tended to actuate in one direction by heating, and during the cooling process, the system went back to its initial shape with coil spring's help as given in Figure 21 a. The bending experiments of active guide wire were performed in air and water, separately. Due to the cooling effect of the water, different current values were used to achieve desired bending angle. The system's surface temperature was increased with air conditioning as shown in Figure 21 b. On the contrary, it was reported that the temperature reached over 41^oC, which is the critical temperature of in-vivo medical applications, in water.

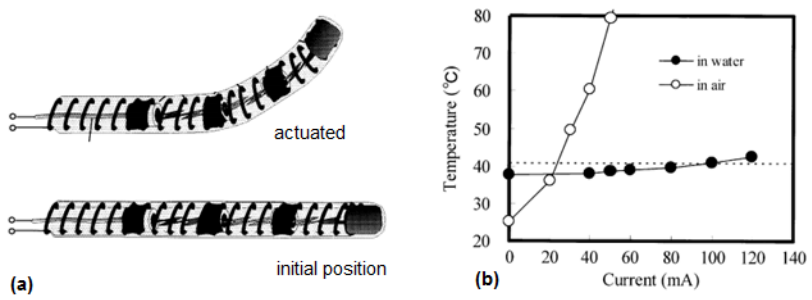


Figure 21: Active guide wire system: (a) movement capability; (b) measured surface temperatures in air and water condition [54]

All these extensive studies proved that NiTi alloys offer great potential and is a valuable implant material in the biomedical field due to their unique mechanical properties such as the shape memory effect, superelasticity, resistance to corrosion, and biocompatibility. Due to these favorable properties, there is a growing interest in NiTi alloys various medical based fields. However, there are still some concerns over the potential adverse reactions for applicability of NiTi in vitro and in vivo at high concentrations.

The aim of this dissertation is mainly based on developing a new NiTi based implantable material by focusing on understanding of critical necessity of NiTi shape memory alloys in biomedical applications. In this manner, the following sections are structured on crucial necessity of NiTi for biomedical applications including biocompatibility, corrosion resistance and cyclic response based on a detailed literature survey.

1.4 Critical Requirements for NiTi for Biomedical Applications

Metallic materials have been used in biomedical applications since the 1940s. Especially Ti and Ti6Al4V are commonly used as implant materials due to their favorable mechanical properties and biocompatible behavior. Nevertheless, metallic implants do not have the ability to integrate with bone tissue in some cases. It was reported that the risk of implant related infections were highly significant after especially spine surgery, trauma fixation, and joint arthroplasty. Several studies have been proposed to investigate implant related infection problems. There are some requirements that appear to be crucial, and are presently being investigated by research groups. This section compiles the fundamentals of requirements for biomedical based application for implantable materials.

1.4.1 Biocompatibility

Over the past decade, metallic materials have been successfully used as implant materials. There is a steadily growing interest in expanding knowledge on implant material's biocompatibility. First, it is important to define "biocompability" term. In some cases, the immune system detects the implant material as foreign and the implant harms the body in an undesirable manner. Biocompatibility may be defined as the ability of a material accepted by the body without any harmful reaction. Another detailed description of this term by William is "the ability of a biomaterial to

perform its desired function with respect to a medical therapy, without eliciting any undesirable local or systemic effects in the recipient or beneficiary of that therapy, but generating the most appropriate beneficial cellular or tissue response in that specific situation, and optimising the clinically relevant performance of that therapy."

The osseointegration and interaction between implant surface and body are highly important factors that affect the implementation success. The interaction between implant material and the host tissue can be narrated under two categories. The first one is "bioinert" and refers to a material that retains its structure after implantation and does not create any harmful effects on the body. If the device or implant is in contact with the blood directly, the selected materials should have blood compatibility, also known as hemocompatibility. The second category is "bioactive" and is defined as the ability of the material that deposits bonds with living tissue in the body [55].

NiTi shape memory alloys have been developed as novel materials that may be a replacement for other conventional metallic materials since they exhibit reasonable biocompatibility, corrosion resistance, and cell culture compatibility. These alloys are passive like titanium and stainless steel with a stable oxide layer. This layer normally acts as a barrier and is very efficient against corrosion in the body. Over the past decade, many aspects of NiTi's biocompatibility have been studied extensively by many groups. Cutright et al. have investigated the tissue response of NiTi wire shape implant material in rats by comparing to the case obtained with stainless steel [56]. Figure 22 (a) shows that there were some inflammatory cells in the implantation at day three. However, the inflammatory cells significantly decreased at the end of ninth week as seen in Figure 22 (b). It was reported that the reaction was minimal for all periods and the healing time was fast for both NiTi and stainless steel implants with comparable histological performance.

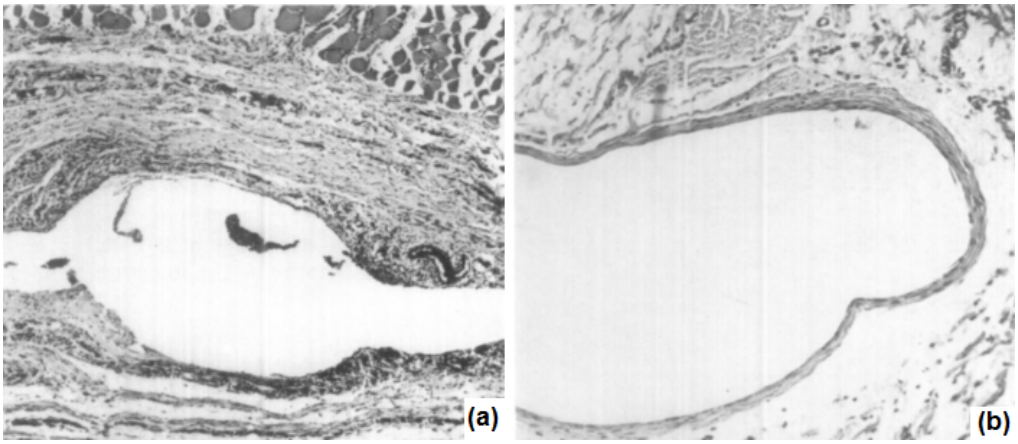


Figure 22: Implementation of NiTi (a) 3 days; (b) 9 weeks [56]

The histological analysis of NiTi and Cr-Co plates was comparatively examined by Castleman [35]. The biocompatibility experiments were utilized through in vivo studies on beagles for different periods from 3 to 17 weeks. It was found that there was no metallic contamination in the tissues and organs after NiTi implant implementation. However, due to the presence of Cr-Co, there was some chromium contamination in the bone tissue. Similarly, Kapanen et al. have investigated the effect of implant material including NiTi, stainless steel, and Ti6Al4V on bone formation by implanting them for eight weeks in 3-month-old rats [57]. Among all samples, NiTi possesses favorable biocompatibility in bone tissue by showing the largest cartilage-new bone area and presenting faster endochondral bone formation, as given in Figure 23.

Trepanier et al. investigated the biological response of NiTi stents with animal testing and reported that between the implementation period of 3 to 12 weeks, NiTi stents exhibit positive biological response [58]. In a similar work, Chrzanowski et al. established a relationship between surface treatment and biocompatibility of NiTi alloy [59]. NiTi substrates were then soaked into different media, including Hank's balanced salt solution, Dulbecco's modified Eagle's medium, and osteogenic for various duration to examine the evolution of bioactivity.

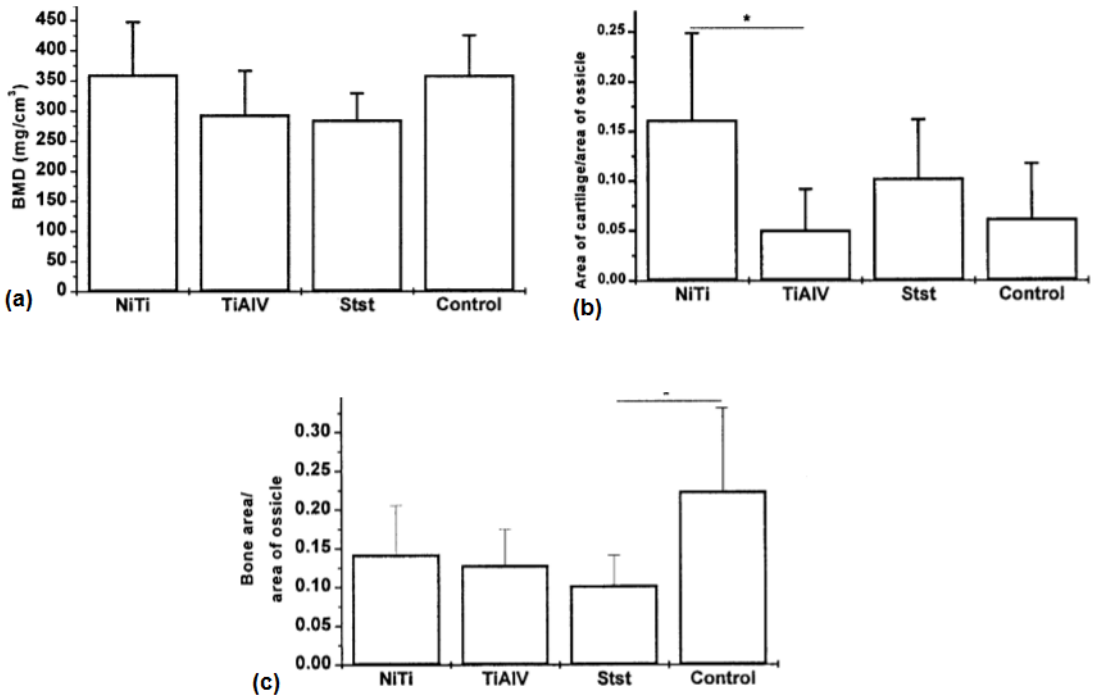


Figure 23: Comparision of three conventional metallic biomaterial as a function of: (a) total bone mineral density of the ossicles; (b) amount of cartilage as an area proportional to the ossicle area; (c) amount of new bone as an area proportional to the ossicle area [57]

Normally, Ni is one of the essential ions in human tissue for biological functionality, at 0.1 ppm. However, there are still some concerns that the potential release of nickel ions from NiTi implant at higher concentrations may cause harmful allergic, toxic, or carcinogenic reactions in vitro and in vivo. The best way to overcome implant related infections and to improve the mechanical contact of the implant with human tissue is to coat the implant material with a biocompatible layer. Among them, chemical surface treatment techniques and bioceramic or polymer based coatings have been utilized with the aim of enhancing biocompatibility and blood compatibility.

1.4.1.1 Chemical surface treatments

Several researchers have utilized the surface treatments on metallic implants and reported that surface treatment of implant material is a significant requirement for biomedical applications that may improve biofunctionalization, biocompatibility of metallic material, and promote its osseointegration to host bone. The common types of surface treatment techniques are heat treatment, acid etching, mechanical polishing, and sandblasting etc. In vivo and in vitro experiments confirm that all these treatment methods showed notable improvements on the surface bioactivity of metallic implant material [60, 61].

Heat treatment is one of the most applicable surface treatment methods for metallic implant materials. Heat treatment of metallic material generally results in the TiO_2 layer formation on its surfaces[62]. TiO_2 layer have proved to be an attractive interface to retard the release of harmful ions within the human body and to increase bonding between implant surface and bone [63]. Yu et al. investigated the influence of titanium oxide coatings on biocompatibility, bioactivity, and mechanical properties of NiTi shape memory alloys [64]. The deposition of TiO_2 coating layer onto NiTi substrates was utilized via thermal treatment method at 400^oC and 600^oC for one hour as shown in Figure 24. The flake-like structure of the oxide layer was observed on the NiTi substrate treated at 600^oC for one hour. The biocompatibility of coated and uncoated NiTi wires was determined with SBF solution incubation for different periods, which resulted in enhanced bioactivity of the sample treated at 600^oC.

On the other hand, Yang et al. have demonstrated the effect of surface modification by chemical and electrochemical etching on the surface of NiTi square blocks. They investigated the effect of etching parameters with SEM, XPS, and the corrosion property with an electrochemical workstation in simulated body fluid. Samples were chemically etched with the solution of HNO_3 and HF for a different duration.

According to the results, the biocompatibility of NiTi blocks was enhanced with both etching methods. However, electrochemical etching was more promotive than chemical etching [65].

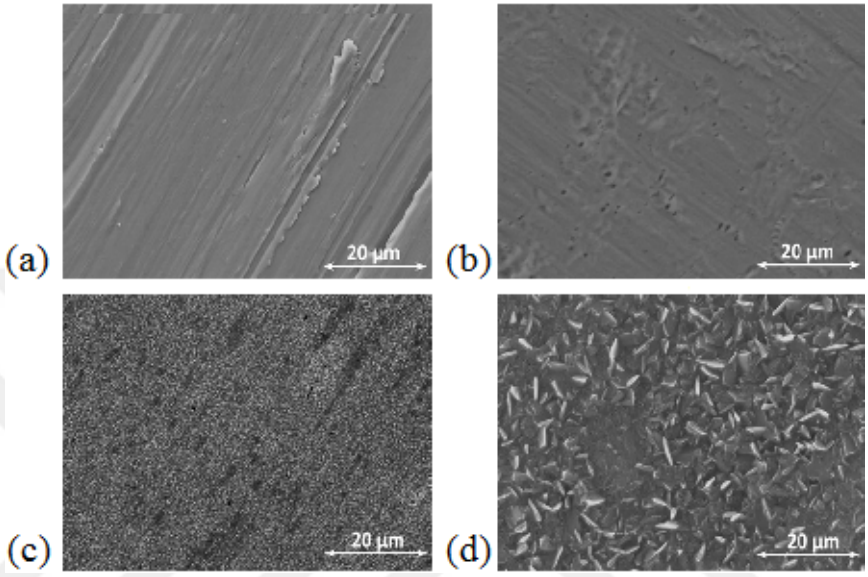


Figure 24: SEM images of (a) uncoated; (b) coated at 400^{o}C; (c) coated at 600^{o}C; (d) coated at 600^{o}C with higher magnification [64]

Katona et al. reported that one of the crucial necessities for cardiovascular stents is surface quality [66]. In their work, surface quality is initiated with a chemical etching process by modifying stents surfaces. Figure 25 shows the effect of etching on the NiTi surface after laser cutting. They concluded that chemical etching was a sufficient method to obtain good surface quality.

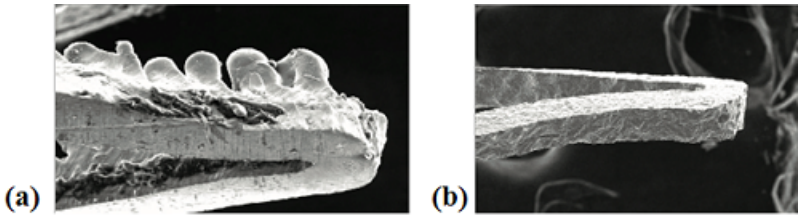


Figure 25: SEM images of stent surfaces; (a) after laser cut, (b) after etching for 220 seconds [66]

Shabalovskaya [67] et al. have reviewed aspects of different surface modification techniques. The correlation between etching time and intensity of ions as a function of different treatments was reported as given in Figure 26. They concluded that mechanical polishing with 600 grit was not suitable for NiTi implantation due to surface heterogeneity. Furthermore, the heat treatment method increased Ni concentration on the surface, which was unsuitable for biomedical applications.

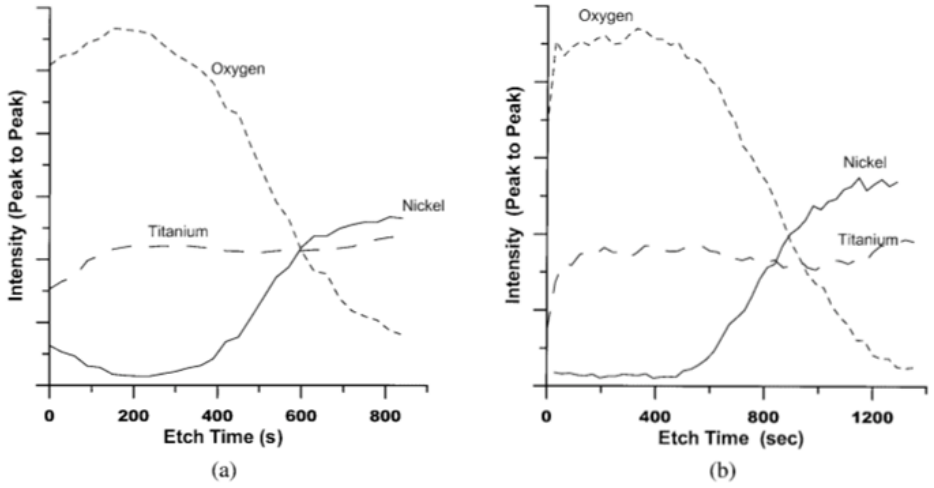


Figure 26: Auger analysis of NiTi plate sample surfaces (a) polished and heat treated, (b) polished, chemically etched, boiled in water, and heat treated [67]

1.4.1.2 Ceramic based coating

This subsection will focus on the influence of bioceramic based coating layer on the biocompatibility and corrosion behavior of NiTi wire-shaped samples. The section mainly contains biomimetic and dip coating approaches to deposit a CaP based layer on the NiTi surface. Bioceramic based coatings represent one of the most prominent approaches in use today in the medical field. This coating strategy is based on a combination of superior mechanical properties of NiTi metal substrate and biocompatibility of the ceramic layer on the surface via different methods including sputtered [68], electrophoretic deposition [69, 70], electrodeposition [71], sol-gel [72], biomimetic, and dip coating techniques.

It's believed that the formation of a bioceramic layer may act as a barrier against bacterial adherence, and mostly resulted in increased biocompatibility and minimized release of harmful ions from the implant surface. Calcium phosphate (Ca-P) based ceramics have been attractive materials in the biomedical field. These ceramics are used to coat metallic implant materials that aim to increase biocompatibility, corrosion resistance, and bonding between live tissue and implant materials. Among these ceramics, hydroxyapatite (HA) shows magnificent similarity with bone and living tissue, and thus is an effective and successful long-term implant fixation widely used for coating metallic materials for biomedical applications. Although hydroxyapatite has excellent biocompatibility, osteoconductivity, and ability to elude drugs [73]; it possesses weak mechanical properties such as brittleness and poor tensile strength as summarized in Table 2 [74].

Table 2: The general properties of hydroxyapatite

Property	**Value**
Lattice parameter	a=9.432, b=6.8810
Bravais Lattice	Hexagonal
Elastic modulus (GPa)	40-117
Bending strength (MPa)	147
Poissson's ratio	0.27
Coefficient of thermal expansion (W/m/K)	13.3x10-6
Density (g/cm^3)	3.156
Thermal conductivity (W/m/K)	0.72

Ozeki et al. [68] investigated the effect of hydroxyapatite, alumina, and titanium sputtered coatings on inhibition of Ni release from NiTi alloy. The coated samples were directly implemented into the animal bone. In the study, NiTi plates were used

as main substrates for the coating process. The immersion test was obtained for the non-coated, Ti-coated, HA-coated, and alumina-coated plates. In the immersion test, these plates were immersed into NaCl solution at 37^oC for one and four to eight weeks to determine the Ni release before in-vivo experiments. The amount of released Ni ions was measured with a microwave induced plasma mass spectrometer. The non-coated and the Ti-coated substrate exhibit the highest and the lowest Ni release respectively. Animal tests demonstrated that coated plates have higher osteocompability compared to the non-coated NiTi plates.

In recent years, researchers made significant progress in the electrophoretic deposition method to form a biocompatible layer on metallic materials for medical application [69, 75]. Karimi et al. have utilized the electrodeposition method for forming HA/Al composite coating on NiTi samples with the aim of improving bioactivity. Similarly, Maleki-Ghaleh and Dudek et al. have proved the performance of electrophoretic deposition method to form hydroxyapatite coatings on the surface of NiTi substrates as shown in Figure 27 [75]. Lastly, Albayrak et al. have investigated the influence of calcination and coating voltage on the HA coating quality on Ti and Ti6Al4V samples via electrophoretic deposition technique [70].

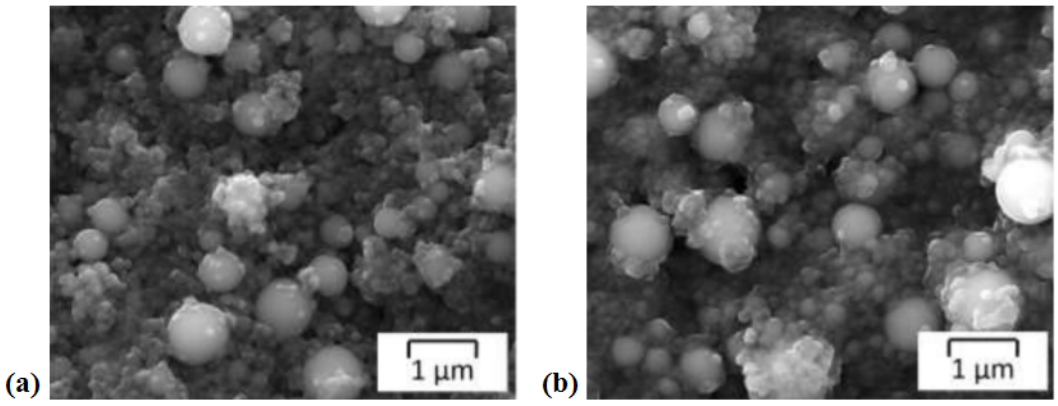


Figure 27: SEM images of HA coated surfaces via electrophoretic deposition method [75]

Yang et al. have exhibited favorable outcomes in the biocompatibility of NiTi alloys by coating the surfaces with SiO_2 via sol-gel method. The effect of coating on the biocompatibility of NiTi alloys was evaluated with in-vivo experiments. For 56 days, the surface morphologies were found nearly the same, whereas the Ni content of the tissue was much lower for the SiO_2 coated surfaces for 112 days post implantation. Katic et al. [76] have compared the efficiency of sol-gel and electrochemically assisted deposition methods on calcium phosphate coating formation on the NiTi surface. The solution for the sol-gel deposition method was prepared with $Ca(EHA)_2$, EHA, and EHP. The formation of a bioceramic layer on NiTi substrate with both methods was proved by SEM results as shown in Figure 28. The conclusion was drawn that the coated NiTi substrates with sol-gel deposition method are more resistive than the NiTi substrates coated by the electrochemically assisted procedure.

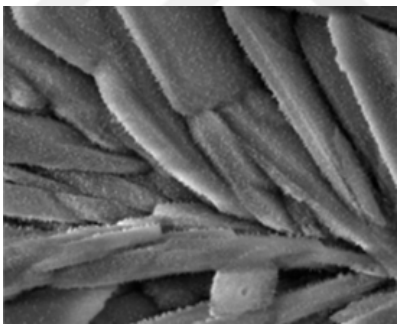


Figure 28: SEM images of HaP coated NiTi surfaces via sol-gel deposition at 5000x magnification [76]

Sun et al. used plasma immersion ion implantation and deposition with magnetron sputtering coating methods together to enhance the bioactivity and biocompatibility of NiTi shape memory alloys [77]. The influence of the coating layer on the transformation temperatures and degradation of the shape memory effect was not significant. Similar to the present dissertation, Dunne et al. [78] recently investigated hydroxyapatite deposition onto wire shaped NiTi alloy via blast process with the aim of developing HA coated stent for a drug delivery system.

Hydroxyapatite and alumina were sprayed on the NiTi wire as shown in Figure 29. The results revealed that the shape memory behavior of NiTi was not changed after the coating process. These extensive literature reviews led us to focus on biomimetic and dip coating methods due to their ease of applicability and simplicity. The essence of these techniques is briefly discussed in the following section, presenting the most significant developments and notable improvements. These subsections explore the fundamental properties of biomimetic and dip coating methods.

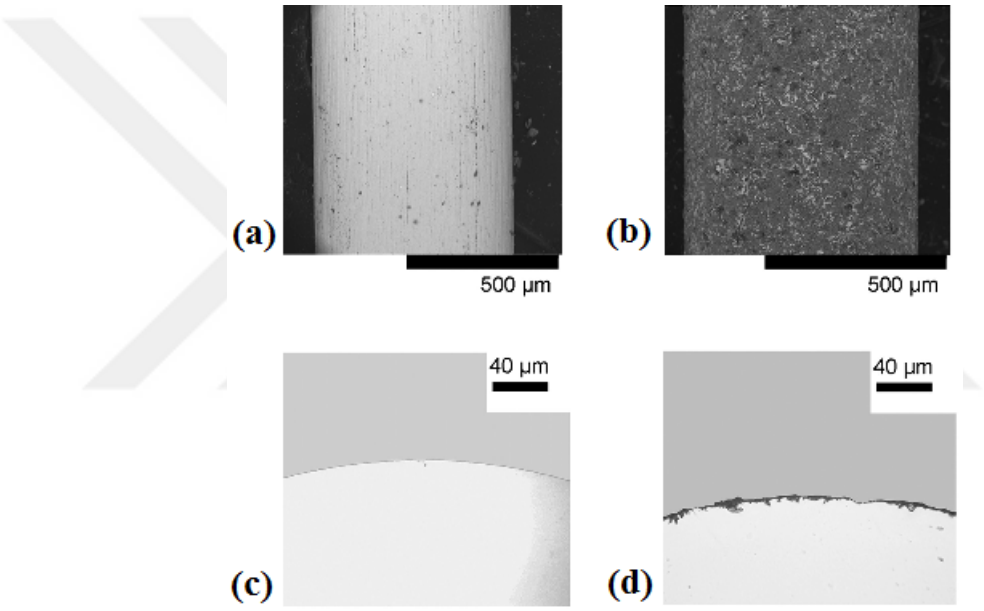


Figure 29: SEM images of (a) as received NiTi; (b) coated NiTi; (c) as received NiTi; (d) coated NiTi [78]

Biomimetic coating is mostly utilized by using simulated body fluid, discovered by Kokubo et al. [79] and commonly used to produce biocompatible layers on the implant material with favorable properties such as low processing temperature, forming bone-like apatite, ability to coat complex shape, high cost-effectiveness, ability to incorporate growth factors, and versatility for potential medical application [80]. However, there are some disadvantages related to the process such as long immersion period requirement and limited applicability [81].

Biomimetic method has been investigated comprehensively by many scientists. Gu et al. have reported successful attempts of biomimetic coating for depositing apatite layer on NiTi plate shape substrates [82]. In their work, NiTi substrates were heat treated at the range between 300^{o}C to 800^{o}C for one hour and were subsequently immersed into SBF solution for different periods at 37^{o}C. Figure 30 shows the SEM images of NiTi samples before and after immersion in SBF for different periods.

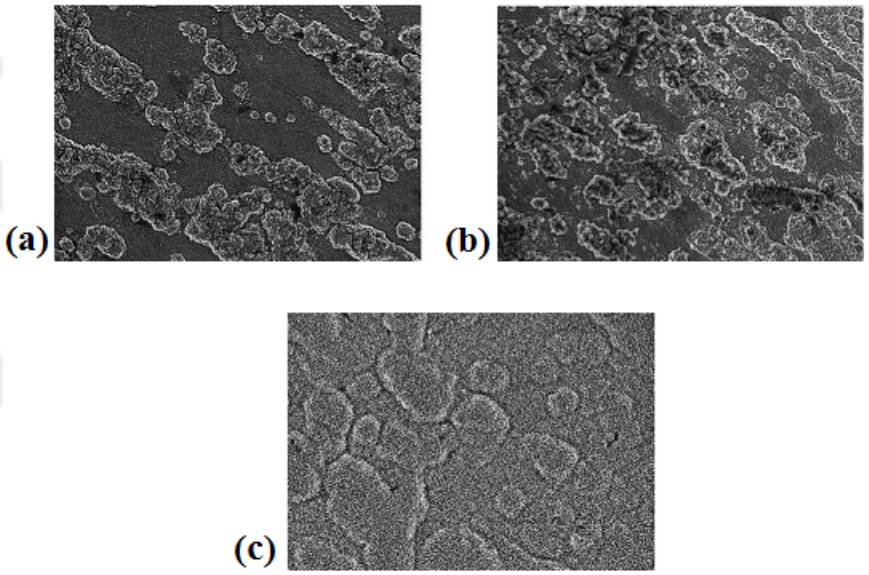


Figure 30: Apatite layer on 600^{o}C heat treated NiTi surfaces before and after immersion into SBF solution: (a) before immersion; (b) after 3 days; (c) after 14 days [82]

Chen et al. [83] have utilized biomimetic method to form an apatite layer on NiTi substrates. Before the coating process, NiTi samples were treated with HNO_3 and subsequently with NaOH solution. The effect of duration on apatite layer deposition was investigated. In conclusion, it was seen that the surface of NiTi block was completely covered at the end of the 5 day experiment as shown in Figure 31. These results consequently agreed with the EDS analyses that reported the Ca and P ratio of 1.596.

In 2004, Chen and colleagues have also investigated bioactivity of NiTi SMA, which is particularly used as bone bonding implant [84]. All substrates were coated with the same procedure mentioned before. It was reported that the nature of osteo-bonding was observed between coated NiTi implant surface and bone after 13 weeks, whereas uncoated NiTi implant presents weak bone implant interface.

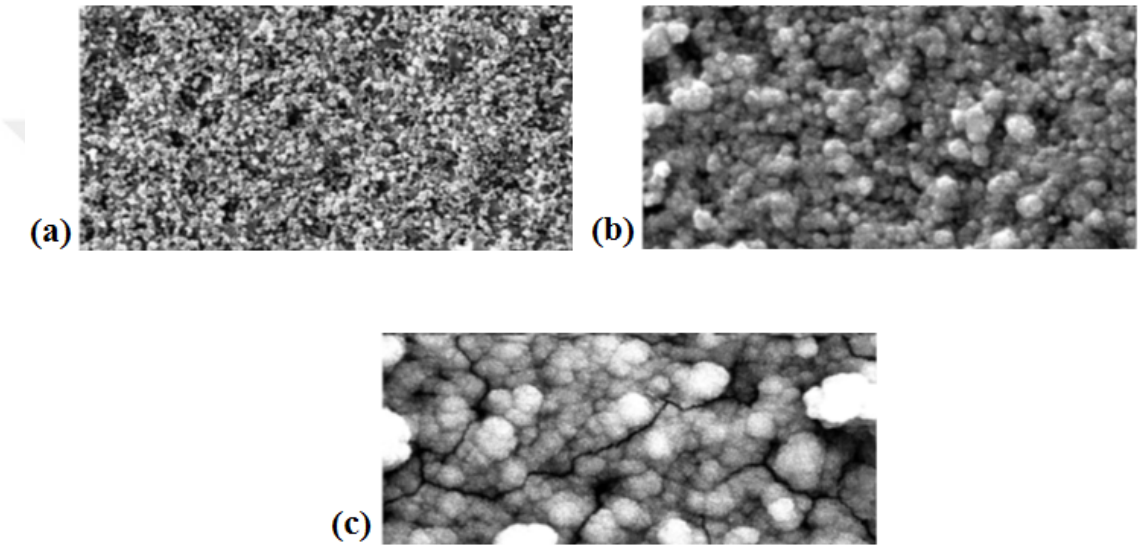


Figure 31: Apatite layer on NiTi surfaces after being immersed into SBF solution for different duration: (a) 1 day; (b) 3 days; (c) 5 days at 5000x magnification [83]

Sun and Wang [85] have compared the mechanical performance of apatite and TiO_2 composite coatings deposited on Ti and NiTi. In order to evaluate the mechanical properties of coating layers, nanoindentation, scratch, and fractional tests were utilized. Figure 32 represents the SEM images of Ti and NiTi surfaces after a scratch test where both coating layers on different substrates showed similar mechanical properties. However, adhesion strength between coating layer and substrate surface was much higher in Ti substrates than in NiTi substrates. Conversely, composite coated NiTi samples presented better wear properties than Ti samples.

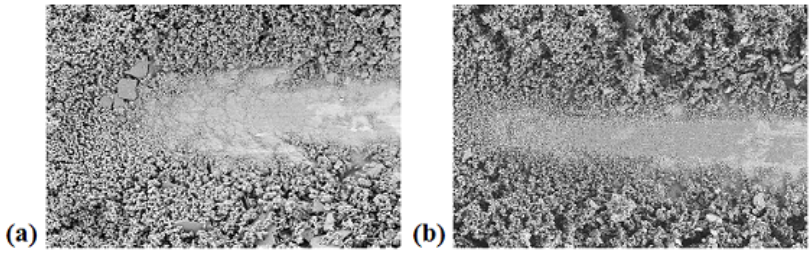


Figure 32: SEM images of (a) titanium sample; (b) NiTi sample after scratch test at 500x magnification [85]

Cai et al. have comprehensively investigated the biomimetic growth of apatite layer on chemically treated NiTi substrates [86]. Prior to coating, samples were chemically treated and some particles were present after 9 hours of immersion on the NiTi surface, whereas the surface was covered after 24 hours and the coating layer became thicker with tiny cracks after 5 days. Table 3 shows the Ca/P ratios as a function of duration. It was reported that the Ca/P ratio reached the closest ratio of hydroxyapatite after 120 hours.

Table 3: Ca/P ratio of NiTi substrates after immersing into SBF solution for different duration [86]

Duration	**Ca**	**P**	**Ca/P**
12	1.86	1.73	1.07
24	5.43	4.63	1.15
72	11.95	8.62	10.15
120	16.20	10.15	1.60

On the other hand, dip coating method is one of the oldest and most common wet coating techniques with its advantages including simple, low cost, minimal equipment requirement, ease of controlling coating thickness, high degree of uniformity, and propriety for multi layer coatings. Brinker and Hurd have comprehensively investigated theoretical fundamentals of the dip coating method [87].

Figure 33 shows the steps of the dip coating method including dipping and immersion, deposition and drainage, and evaporation. Dip coating is simply achieved by dipping the substrate into a bioceramic doped solution where they are fully dissolved under selected conditions. In a pioneering study by Mavis and Tas, Ti6Al4V substrates were coated with a HA layer via dip coating method [88]. After the dipping process, coated Ti6Al4V substrates were calcinated at 840^{o}C to strengthen the bioceramic layer. It was concluded that, according to adhesive-strength tests the bonding strength of the coating layer was sufficient and resistant to the scratch test. The formation of layers also has the potential of enhancing the interaction between layer and implant surface. Similarly, Li et al. have utilized the dipping method to deposit hydroxyapatite layer onto titanium surface [89]. In this work, titanium substrates were immersed in HA solutions seven times. It was seen that the thickness of the coating layer tends to increase with the number of dips and highly depends on solution concentration.

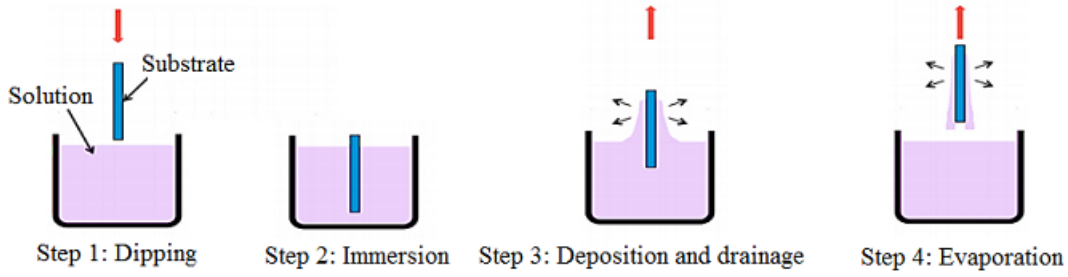


Figure 33: Steps of dip coating method [87]

Moreover, Choi et al. have investigated the mechanical stability of calcium phosphate coating of NiTi SMA [90] deposited via the dipping method. It was reported that the stability of the deposited layer might increase with the second immersing and drying processes. The uncoated and coated wire was bent to examine the mechanical stability of the CaP layer, as shown in Figure 34. It was concluded that the coated layer withstands the bending and did not affect the shape memory properties of NiTi.

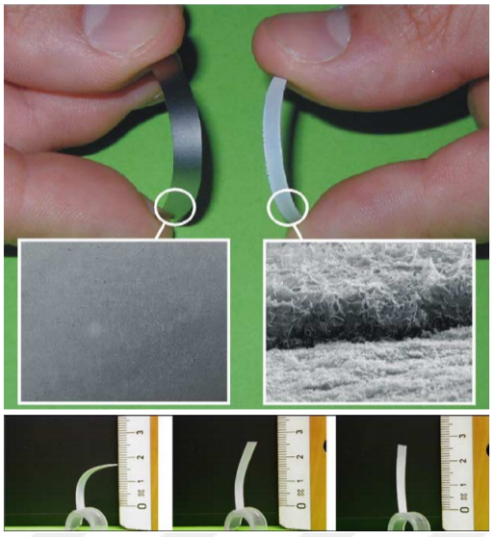


Figure 34: Mechanical experiments on investigation mechanical stability of CaP layer [90]

1.4.1.3 Polymer based coating

In this dissertation, hydrogel is selected as an alternative coating material to used as coating material since ceramic-based materials possess brittleness and low crack resistance that restrict their use, especially in medical applications [91]. However, hydrogels have desirable characteristics including their viscoelastic nature, non-toxicity, high water content, and ability to mimic human tissue which makes them easy to handle during surgery.

The present section focuses on polyvinyl alcohol (PVA) based hydrogels and their applications in the medical industry. The primary aim of the study is to develop an antibiofouling surface on NiTi substrates that can decrease the risk of implant-related infections and prevent undesirable adhesion of bacteria. This is considered by utilizing hydrogels on the NiTi surface to provide a soft and biocompatible interface that does not alter the shape memory effect of NiTi and maintains on the surface after repeated bending. This is, to our knowledge, the first attempt to coat the wire shaped NiTi substrate with PVA based hydrogel biofilm layer.

Polymers are classified as natural and synthetic, based on their fabrication. Natural polymers have the ability of interacting with cells and biocompatibility whereas they possess poor mechanical properties. Most notably among natural polymers, gelatin is an attractive naturally-derived material for biomedical application and has been used extensively in a variety of applications from pharmacology and wound dressing to adhesive and surgical use in the medical fields due to its promising properties such as body compatibility, nontoxicity, nonirritant, and biodegradability. In addition, gelatin is one of the most widely affordable adopted agents to obtain the necessary properties of hydrogel [92].

Synthetic polymers are more stable and controllable than natural polymers due to their configurable composition. PVA is the most convenient and commonly used synthetic polymer and, was discovered by Haehnel and Hermann in 1924 [93]. PVAs are produced by polymerization of vinyl acetate to polyvinyl acetate and are classified as into the group of water soluble polymers. General properties of PVA are given in Table 4 [94].

Table 4: General properties of PVA [94]

Property	**Values**
Density	1.19-1.31 g/cm^3
Melting and boiling point	180-240^{o}C / 228^{o}C
Degradation temperature	180^{o}C

PVA has received more serious attention for medical applications, including wound dressing [95] and drug delivery systems [96] due to their biocompatible, biodegradable, and water soluble behavior. Hence, the potential applications of PVA materials can show differences based on their solubility.

The solubility of PVA highly depends on its molecular weight, degree of polymerization, and degree of hydrolysis. Aina et al. [97] has investigated the solution behavior of PVA in water and reported that at low concentration. The relation between dissolution time and concentration was linear, whereas for higher concentration the behavior was changed dramatically as shown in Figure 35. In light of these results, it can be asserted that PVA has a non-ideal solution behavior in water.

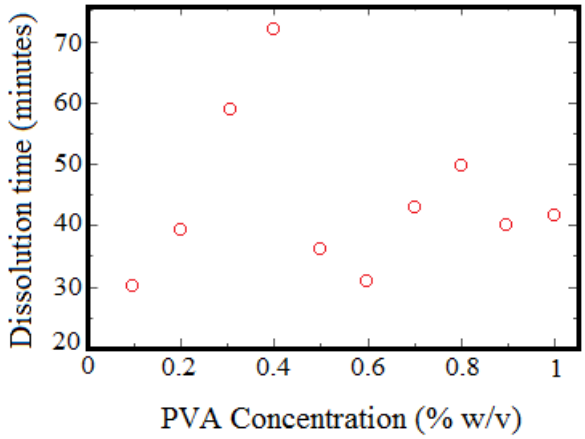


Figure 35: Relation between dissolution time and PVA concentration[97]

Another aspect that must be considered is a combination of natural and synthetic polymers. Both types have their pros and cons; however, it is possible to obtain desired properties by blending natural and synthetic polymers. In order to enhance mechanical properties, PVA could be blended with different additives such as gelatin [98], dextran [99], chitosan and its derivatives [100], alginate [101, 102], and starch [103] to form a hydrogel. It was early established that PVA-based hydrogel can be obtained by combining PVA and gelatin, which promote much better mechanical and biocompatible properties compared to each component. Owing to their excellent properties, hydrogels appear as more promising materials for biomedical applications. Hydrogels have been introduced in 1960 by Wincterle [104] and, increasingly applied in industrial fields mainly the biomedical industry due to their biocompatibility and

hydrophilic character. Hydrogels may be produced in various physical forms including; solid molded, pressed powder matrices, microparticles, coatings, membranes of sheets, encapsulated solids, and liquids [105]. Moreover, they can be fabricated in the form of permanent or chemical hydrogels with respect to their crosslinking networks.

There are three main factors to control the mechanical properties of hydrogels; altering the comonomer composition [106, 107], the density of cross-linking [108, 109] and the environmental conditions [110]. Increasing the amount of physically stronger components can enhance the mechanical strength of the polymer by increasing the stiffness of the backbone polymer. The aforementioned studies showed that the addition of larger cross-linking agents significantly increased not only the mechanical strength but also the glass transition temperature of the networks. Researchers have repeatedly shown that an increase in the strength of the hydrogel may be associated with a rise in its cross-linking density. The addition of different agents is the most common way to increase the cross-linking density in order to control mechanical properties such as strength, dynamic modulus, and glass transition temperature.

The polymerization conditions including reaction time, temperature, and type of the solvent also alter the mechanical properties of hydrogel [110]. A large amount of solvent will reduce the effective cross-link density and mechanical strength. It was previously reported that the freezing and thawing cycle is one of the most effective condition parameters to control the mechanical strength. According to results, cycling the polymer often leads to an increase the Young's modulus significantly [111, 112]. Contrary to PVA, hydrogels are not water soluble but they have the ability to swell in an aqueous solution. The swelling behavior is one of the most promising ways to understand the structure and network of the hydrogels [113]. It is well known that the swelling ratio has a significant effect on the mechanical properties of the hydrogel. There has been many attempts to improve the material strength by reducing the swelling ratio [114, 115].

There is a wide array of potential applications of hydrogels. In particular, they are quite suitable for biomedical applications due to their desirable characteristics including their viscoelastic nature, non-toxicity, high water contact, and ability to mimic human tissue [116]. These biomedical applications may vary from optical lenses and corneal prostheses [117], artificial muscles [118, 119], nerve regeneration [120, 121], tissue replacement [116], bioartificial pancreas [122], spinal prosthesis and repair [123, 124], and medical sensors [125], wound dressing and healing [126] to drug delivery devices [127, 128].

Hydrogels have a combination of enthralling characteristics including biocompatibility, resistance to protein adsorption, and flexibility for medical applications. However, they provide poor mechanical properties. So that many efforts have been conducted to characterize their behavior and mechanical properties and tailor them to meet the requirements of different applications. Nguyen et al. have produced PVA/gelatin hydrogel with different compositions for bone generation applications [129]. Genipin was obtained as a crosslinking agent in PVA/gelatin hydrogel fabrication. The effect of composition on the mechanical properties of hydrogel was investigated and results were summarized in Figure 36. It was found that PVA/gelatin with the ratio of 20:20 samples exhibits the highest strength, lowest swelling rate, and good biocompatibility with improved bone regeneration and the osteogenic activity.

Pal et al. reported that PVA/gelatin hydrogels were super hemocompatible with human blood, which is a required property for biomedical applications such as drug delivery systems or moist wound dressings [130]. Pawde and Deshmukh have investigated the effect of gelatin content on the properties of PVA hydrogel films and showed that the tensile strength of hydrogels increases with the increase in the amount of gelatin [131].

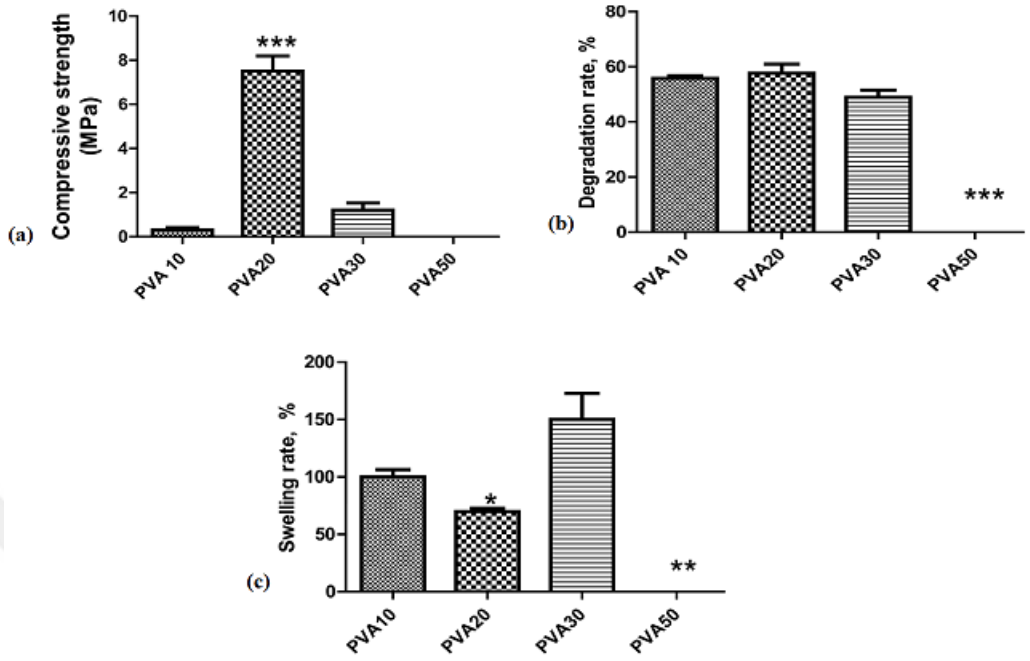


Figure 36: Mechanical properties of hydrogel as a function of composition ratio (a) compression strength; (b) degradation rate; (c) swelling rate [129]

Similarly, Tareq et al. reported the effects of composition on PVA/gelatin-based hydrogel to be used for drug delivery systems [92] and concluded that the produced hydrogel with the ratio of 10:8 PVA to gelatin exhibits satisfactory results compared to others in terms of drug release. All PVA/gelatin hydrogels were found to be nontoxic and biodegradable. SEM images show that there were some protrusions due to degradation after releasing the drug as seen in Figure 37.

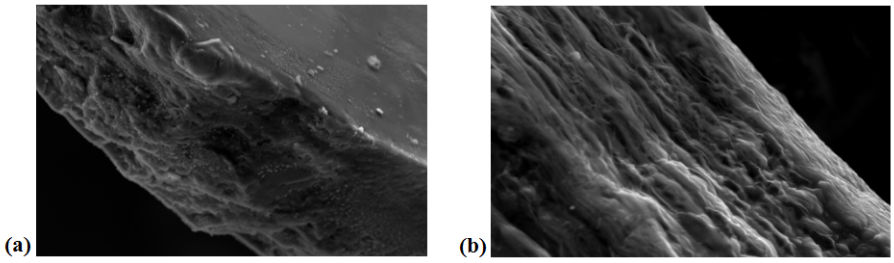


Figure 37: SEM images of hydrogel membrane (a) before drug release; (b) after drug release [92]

Fan et al. synthesized hydrogels by using chitosan, gelatin, and PVA for wound dressing application [132]. The use of chitosan resulted in enhanced tensile strength and hemostatic properties of the hydrogel. Figure 38 presents that all hydrogels have a 3D network structure and uniformly distributed pores on the surfaces. On the other hand, another type of additive in PVA was studied by Vrana et al. [133]. The chitosan was used as the agent to improve the cell attachment performance of the hydrogel. The solution was prepared at a ratio of 9:1 w/w for 2 hours at 60^oC and poured into the mold for the characterization tests. Moreover, they also investigated the effect of freeze/thaw cycle on hydrogel structure and found that the number of the freeze/thaw cycles changes the hydrogel structure critically. Trzaskowski et al. have coated the polyurethane (PU) surface with a polyvinylpyrrolidone (PVP) hydrogel [134] which makes the surface more hydrophilic and hemocompatible.

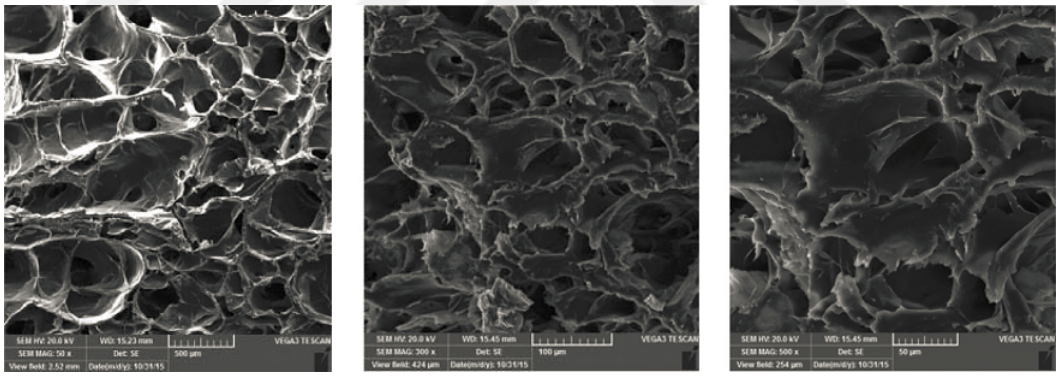


Figure 38: SEM images of chitosan/gelatin/PVA based hydrogel (a) 50 x; (b) 300x; (c) 500x [132]

The effect of hydrogel coating on bacterial colonization was investigated in great detail by Drago et al. [135]. Different types of substrates were coated with hydrogel and antibacterial-loaded hydrogel for orthopedic implants. Biocompatibilities of all samples were quantified via in vivo test on human femurs as shown in Figure 39. The results of in vivo experiments showed that hydrogel coating with antibacterials additives reduced bacterial colonization and the formation of biofilms.

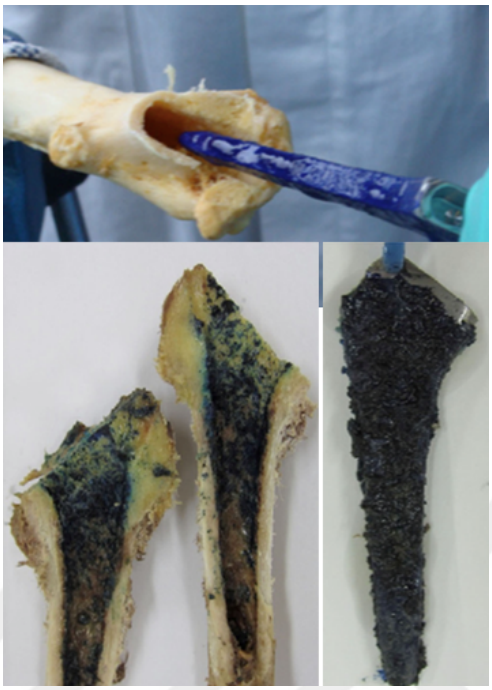


Figure 39: Hydrogel coated implant for orthopedic applications [135]

Zang et al. proposed a method to fabricate hierarchically porous NiTi/hydrogels nanocomposites [136]. NiTi substrates were electrochemically dealloyed in order to obtain a rough surface with the selected condition. Subsequently, dealloyed samples were immersed in the solution that consists of PVA, acrylamide, glutaraldehyde, and vinyl phosphonic acid (VPA). VPA was selected as anchor monomer to improve the binding-interaction between the NiTi surface and hydrogel. It was seen that the adhesive strength between NiTi surface and hydrogel was sufficient, and the coated substrate was showed to have excellent failure resistance of cyclic and twisting tests.

Recently, Chen et al. published two similar studies that investigate the effect of using hydroxyapatite as an additive material in order to fabricate PVA-based hydrogel. In the first study, ultrahigh-molecular-weight polyethylene (UHMWPE) substrates were cross-linked with the PVA/HA hydrogel to examine biotribology behavior and fluid load support [137]. According to the findings, PVA/HA layer has sufficient load-buffering ability.

In the second study, the interaction between PVA, HA, and PAA along with their effect on the mechanical behavior of PVA/HA-PAA hydrogel were examined [138]. PVA-HA/PAA hydrogel was fabricated by freeze and thaw cycle with 16 different combinations. Additionally, the result indicated that the annealing process leads the PVA-HA/PAA hydrogel to be more thermostable and annealed hydrogel presented good strength and mechanical properties.

1.4.2 Corrosion Properties

Stainless steels, cobalt-chromium-based alloys, commercial titanium, Ti6Al4V, and NiTi SMA have long been considered to be the dominant source of implant materials in the medical industry. Among all, the practical uses of NiTi are fascinating due to their extraordinary behaviors, which are entirely new compared to other conventional metallic materials. However, a current problem related to NiTi SMAs is the risk of Ni release from the implant surface due to corrosion. There have been many attempts to overcome these difficulties and to understand the corrosion mechanisms for these conventional NiTi implant materials during the last decade through simulations or in-vivo and in-vitro experimental studies.

In this section, a comprehensive background was provided by reviewing the pioneering studies on corrosion properties of the NiTi shape memory alloys. The experiments that are designed for this study were addressed in detail later in this chapter. Moreover, in this work, the effects of heat treatment and biocompatible coating layers on the corrosion behavior of NiTi were investigated. This chapter also focuses on the implementation of cellular automata (CA) in the computational modeling of the corrosion process in medical implant surfaces. The model consists of two pit initiation and pit growth model, as well as a set of rules that define the change of states through time. The model for conduction adopted in this dissertation is informed by the reviewed literature.

1.4.2.1 Corrosion Mechanisms of NiTi shape memory alloys

Metallic implant materials have to possess some essential properties including biocompatibility, non-toxicity, high corrosion and wear resistance, and osseointegration to be durable and to prevent any harmful defect to the living tissue. Among these properties, corrosion resistance is one of the most crucial features that can directly decrease the lifetime of the implanted material or even lead to its failure. Several methods were proposed to evaluate the corrosion behavior and improve the corrosion resistance of biometallic materials.

Common corrosion experiments are standardized for different cases through the ASTM standards with the numbers of ASTM G61-68 and G5-94, ASTM G71-81, ASTM F746-87, and ASTM F2129-01. Furthermore, two methods are commonly utilized to evaluate the corrosion resistance of metallic materials; measuring the ion release by atomic absorption spectrometry (AAS) [139, 140] and measuring polarization resistance along with passive current density by electrochemical tests [141, 142].

Metals including stainless steel, commercial Ti and its alloys, and cobalt-chromium have long been used as implant materials. These implantable materials face an aggressive environment including blood and other constituents of the body fluids that may trigger the corrosion mechanisms. In order to mimic the body condition, the corrosion behavior of metallic materials has been investigated in body-like mediums including phosphate buffer solution (PBS), simulated body solutions, Hank's solution, NaCl solution, Ringer solution, and artificial saliva at specific pH values between the range of 7,2-7,4 before implementation. These body like media includes similar elements and show properties that are similar to the human body. Elements that exist in the human body are summarized in Table [143]. Prolonging the duration of use under these harsh conditions may result in an ion release from the implant surface especially in the long-term implantation [144].

Table 5: Elements in the human body [143]

Element	Wt %	At %
O	65.0	25.5
C	18.5	9.5
H	9.5	63.0
N	3.3	1.4
Ca	1.5	0.31
P	1.0	0.22
K	0.4	0.06
S	0.3	0.05
Na	0.2	0.3
Cl	0.2	0.03
Mg	0.1	0.01

Aksakal et al. have analyzed and reported the influence of released ions from common implant materials on the human body summarized in Table [145]. For instance, Ti6Al4V exhibits some advantages over other alternative biometallic materials. However, the potential risk of releasing Al and V ions from the Ti6Al4V-based implant surface may lead to negative long term illnesses such as Alzheimer and peripheral neuropathy which make this material inefficient in such cases. The average daily dietary intake of Nickel for humans was calculated to be between 200-300 micrograms/day [146]. The Ni release must be compared with the daily dietary intake because if the amount of nickel ion release is higher than the daily dietary intake, it can cause allergic reactions and harmful health problems like pneumonia, chronic sinusitis, and lung cancer for patients. Thereby, controlling and altering the risks of potential ion release are highly crucial for medical applications.

NiTi alloys have been used for years in various applications including cardiology, neurology, dental and orthopedic applications, interventional radiology, and medical equipment and devices due to their superior properties. Studies reported that NiTi SMA show reasonable corrosion resistance in comparison to commercial metal implant materials such as 316L stainless steel and Ti6Al4V as illustrated in Figure 40 [147].

Table 6: Potential adverse reactions caused by the releasing of metal ions [145]

Metallic biomaterials	Effects of corrosion
Nickel	Affect skin, pneumonia, chronic sinusitis
Cobalt	Anemia B
Chromium	Ulcers and central nervous system disturbances
Aluminum	Epileptic effects and Alzheimer's disease
Vanadium	Toxic in the elementary state

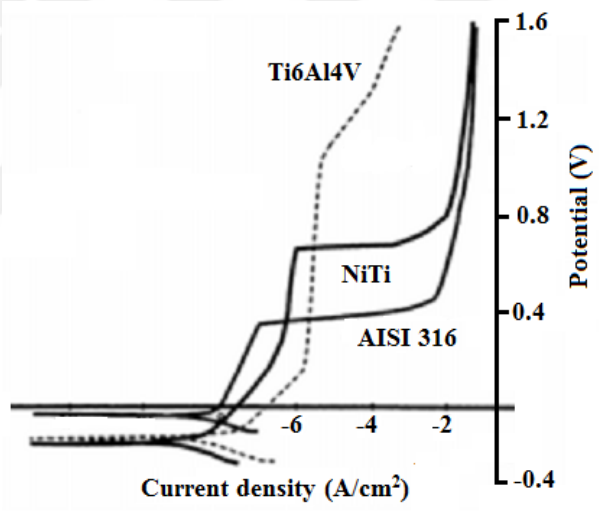


Figure 40: Comparison of corrosion behaviors of commercial metallic implant materials [147]

In recent years, several studies highlighted the susceptible factors to corrosion in the medical field including the surface composition and chemistry, surface roughness, and homogeneity [148, 149]. Hu et al. increased the corrosion resistance of NiTi alloys by forming a nanocrystalline and amorphous structure on the surface via the surface mechanical attrition treatment [150]. Sun et al. reported the effects of porosity on the corrosion behavior of NiTi shape memory alloys [151].

In a pioneering study by Zhang, the corrosion behavior of NiTi coupons was investigated in seven different media, including synthetic saliva, synthetic sweat, Hank's solution, sodium chloride solution, lactic acid, hydrochloric acid, and sodium sulfate acid which simulate the mouth and human body environments at 37^oC for 72 hours [152]. Similarly, the corrosion behavior of NiTi shape memory alloys in Ringer and NaCl solution was investigated [153]. Low pitting corrosion was found only in Ringer solution after potentiostatic test that was affirmed by the SEM analyses as shown in Figure 41. The corrosion test revealed that the corrosion resistance of NiTi in the NaCl solution was more sufficient than Ringer solution. On the other hand, the Ni release in the NaCl was smaller than that of in the Ringer solution, and both values were negligible compared with the daily intake of the Ni ion humans. The biocompatibility tests showed that the number of cells increased with the increasing holding time, and the cell growth rates decreased. The surface of the NiTi sample was completely covered after 9 days.

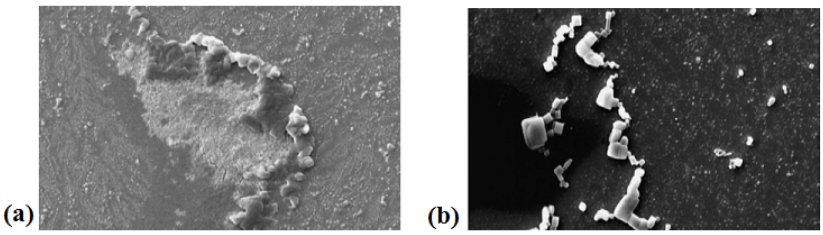


Figure 41: SEM images of the NiTi substrate after potentiostatic test in (a) NaCl solution at 640x magnification ; (b) Ringer solution at 1000x magnification [153]

Jinlong et al. measured the environment's effect on the corrosion behavior of NiTi through electrochemical tests by using different mediums including acid, sodium chloride, and borate buffer solution [154]. The polarization curves of the NiTi substrates in each solution were given in Figure 42. Their results indicate that the corrosion resistance of NiTi substrates were decreased by increasing the passivated potential for all solutions that attributed to thin passive film deposited on the NiTi substrates.

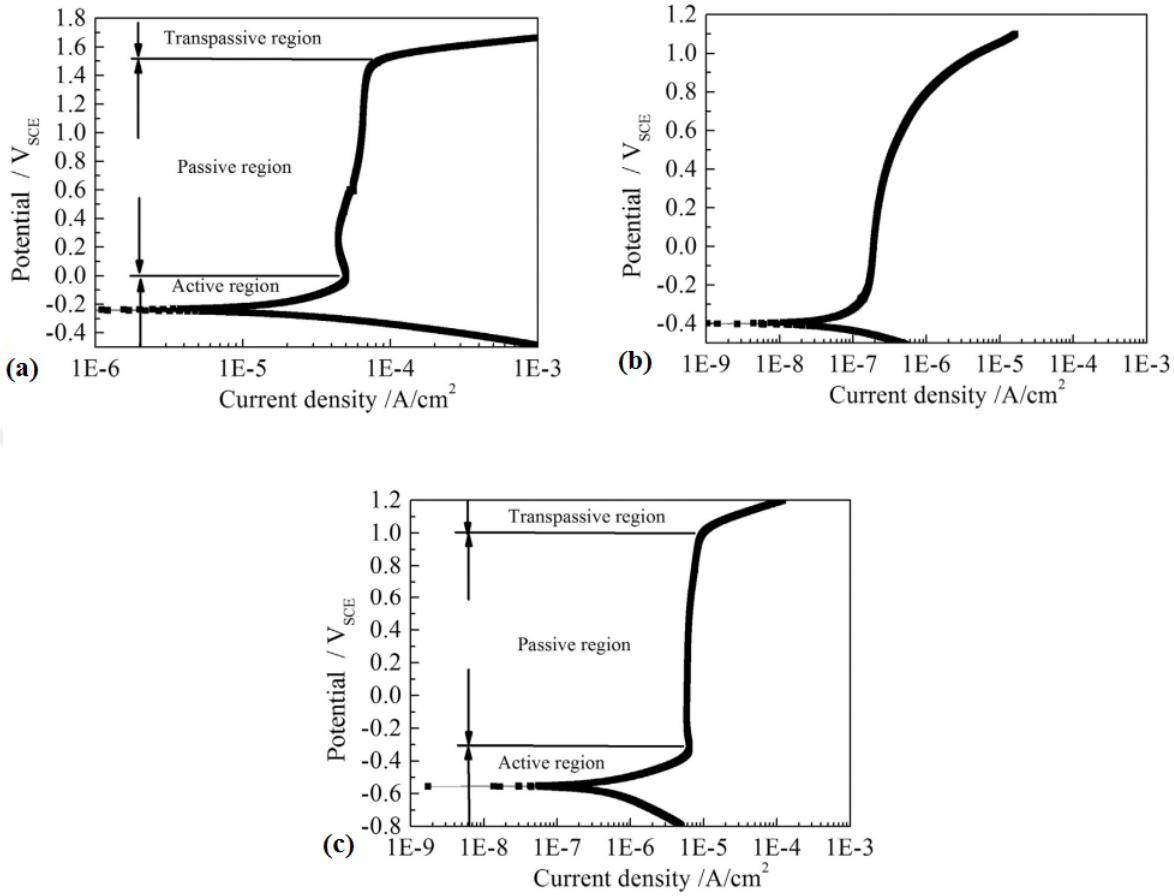


Figure 42: Polarization curves of the NiTi SMA in (a) 0.5M H2SO4 solution; (b) 0.2M NaCl solution; (c) borate buffer solution [154]

Another important factor, pH, was investigated by Figueira et al. [155]. The obtained pH values were selected to simulate the condition that could be resulted in possible inflammatory and allergenic reactions in the human body. However, no differences in corrosion resistance were found as a function of the applied pH range as shown in Figure 43. Results pointed out that the NiTi substrates behave more resistively than Ti and Ti6Al4V. Moreover, the NiTi substrates were highly susceptible to crevice corrosion.

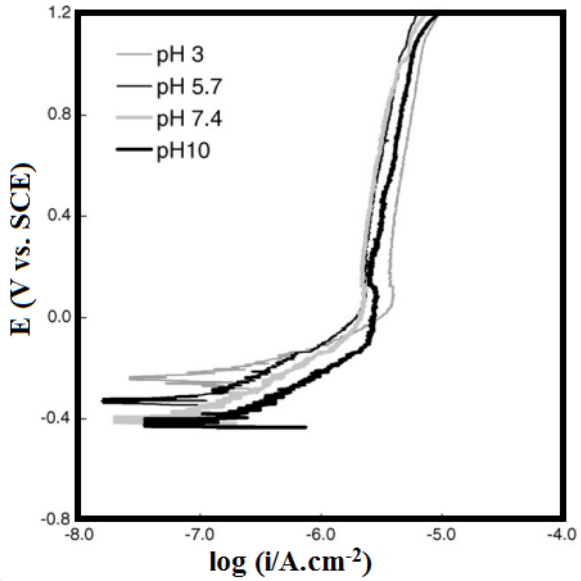


Figure 43: Polarization curves of NiTi for different pH values [155]

Different methods have been proposed to slow down the Ni release from the implant. Heat treatment is one of the simplest and most efficient ways to improve the mechanical properties of NiTi alloys as well as their biocompatibility. The enhanced biocompatibility may be attributed to the formation of an oxidation layer on the surface as a result of the reaction between NiTi and the atmosphere which counts as an intrinsic property. This oxide layer may provide two major advantages; protecting the material's surface from corrosion and increasing the stability, and acting as a physical and chemical barrier to prevent Ni release from the surface [156]. However, it was also reported that the passive layer on the NiTi surface is less protective than that created on Ti6Al4V.

Chembath et al. thoroughly demonstrated the effect of anodization and annealing on corrosion and biocompatibility of the NiTi shape memory alloy [157]. It was reported that the surface of the anodized sample has irregularly distributed pores. However, due to annealing at 400^{o}C, the grain sizes increased within the nodular structure as shown in Figure 44 a and b.

According to biocompatibility test, the amount of Ni release was significantly enhanced by the anodization and annealing processes as clearly seen in Figure 44 c. It was asserted that the anodized and annealed surface exhibited not only better corrosion resistance, but also good bioactivity.

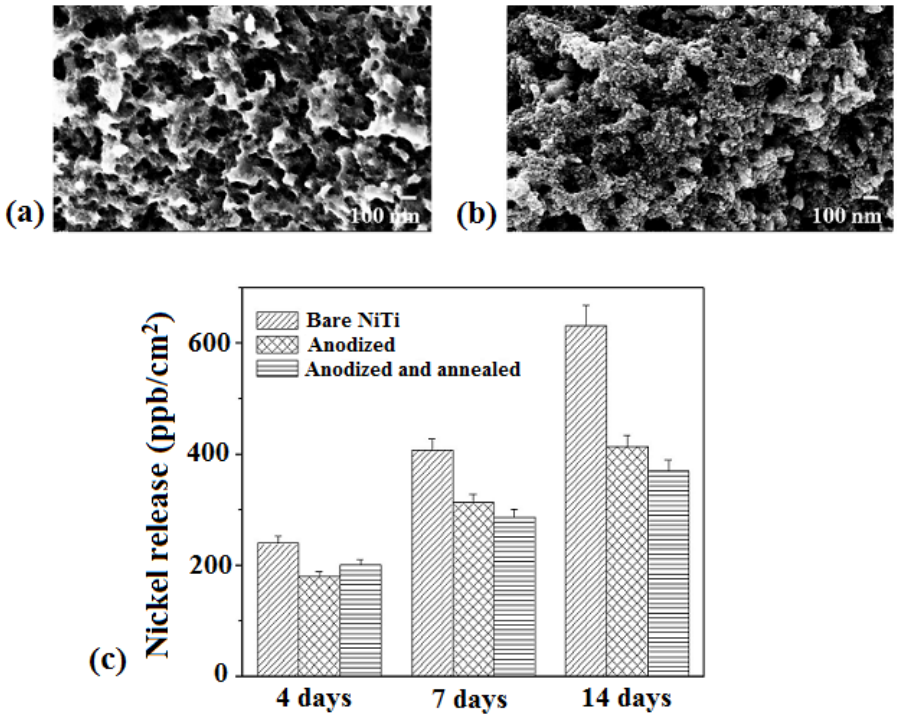


Figure 44: SEM images of the NiTi substrate (a) anodized; (b) anodized and annealed NiTi; (c) Ni release of bare, anodized and anodized and annealed substrate for different periods [157]

Surface modification is another suggested method to decrease the possible leaching of Ni from the implant material. The effect of the thermomechanical treatments on the corrosion behavior of NiTi alloys was established by Vandenkerckhove [158]. It was found that the solution treated sample presented lower corrosion intensity while aging enhanced the corrosion rate of the NiTi substrates. From a different aspect, Starosvetsky has exploited the biocompatibility of titanium nitride coating in order to increase the corrosion resistance of NiTi shape memory alloys [159].

Milosev and Kapun have extensively investigated the corrosion resistance of NiTi shape memory alloys by applying surface preparation and surface treatment methods [160, 161]. In the first study, the effect of the surface preparation methods, including grinding, mechanical polishing, and chemical etching on the corrosion resistance of NiTi substrates, was disclosed. The ground surface has a rough surface with many cracks, pits, and pores that result in localized corrosion while polishing and chemical etching induce improved resistance. Among the different methods, polishing was found more promising for practical applications due to the provision of sufficient corrosion protection.

In other works, boiling water and thermal oxidation methods were utilized by preparing the NiTi surfaces following the procedure outlined in the first study [160]. The thickness of the oxide layer on the grounded and polished NiTi surfaces was measured after boiling water, and the results are given in Figure 45. In general, the authors concluded that for the polished substrate, the evolution of thickness was directly attributed to the corrosion behavior of NiTi. It was also reported that the formation of oxide layers at high temperatures via thermal oxidation enhances the corrosion properties of polished NiTi samples.

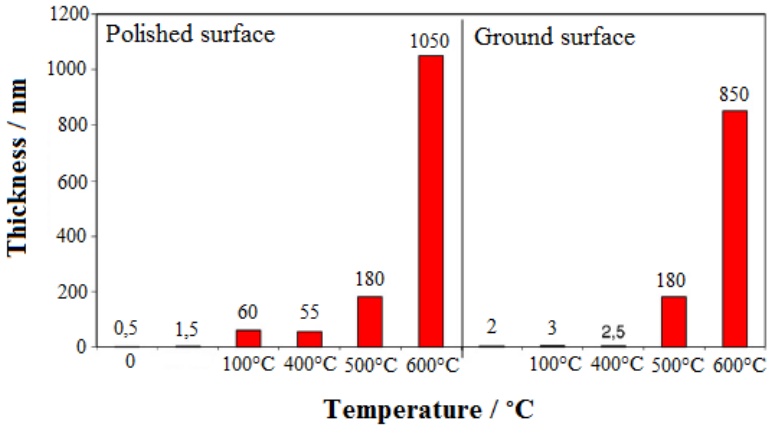


Figure 45: Thickness of the oxide layer on the grounded and polished NiTi surfaces after boiling water [160]

Chembath et al. established that chemical treatment by using acidified ferric chloride solution has reduced the concentration of the Ni ions at the NiTi surface [162]. The relationship between surface roughness and hydroxyapatite growth rate was investigated through different surface treatment methods. The surface roughness was measured with AFM as given in Figure 46. They observed that the increase in surface roughness was associated with faster hydroxyapatite growth which is related to sufficient corrosion resistance and bioactivity with better osseointegration.

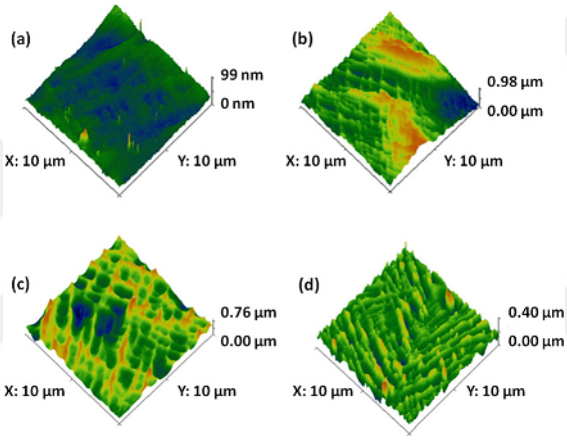


Figure 46: AFM images of NiTi surfaces (a) polished NiTi; (b) after chemical treatment; (c) after chemical treatment and annealing; (d) after chemical treatment, annealing, and passivation [162]

Another surface modification technique, plasma source ion implantation (PSII), was applied by Tan et al. with the aim of enhancing the corrosion resistance of NiTi shape memory alloy [163]. Cyclic potentiodynamic polarization and wear-corrosion measurements were obtained to investigate the effect of PSII and heat treatment on pitting and wear-corrosion resistance in NiTi. These properties were enhanced as a result of the PSII and heat treatment processes. During the wear-track analysis, the total mass loss was measured to evaluate the wear-corrosion resistance. The sample showed less mass loss after PSII compared to the control sample that displayed nobler wear-corrosion resistance as shown in Figure 47.

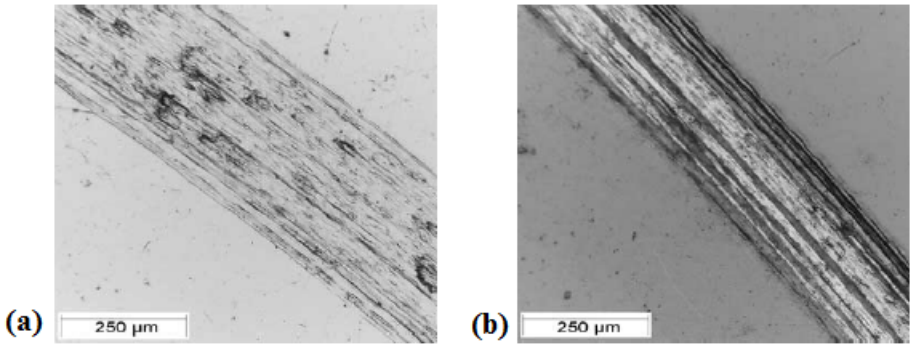


Figure 47: AFM images of NiTi surfaces (a)A_f=-3^oC control; (b) A_f=-3^oC oxygen implanted [163]

Briceno investigated the effect of microstructure on electrochemical corrosion and Ni release in NiTi orthodontic archwires [164]. It was reported that the martensitic phase tends to enhance corrosion resistance which is related to the decrease in Ni release. The Ni release from each orthodontic archwire was measured as a function of immersion time as given in Figure 48.

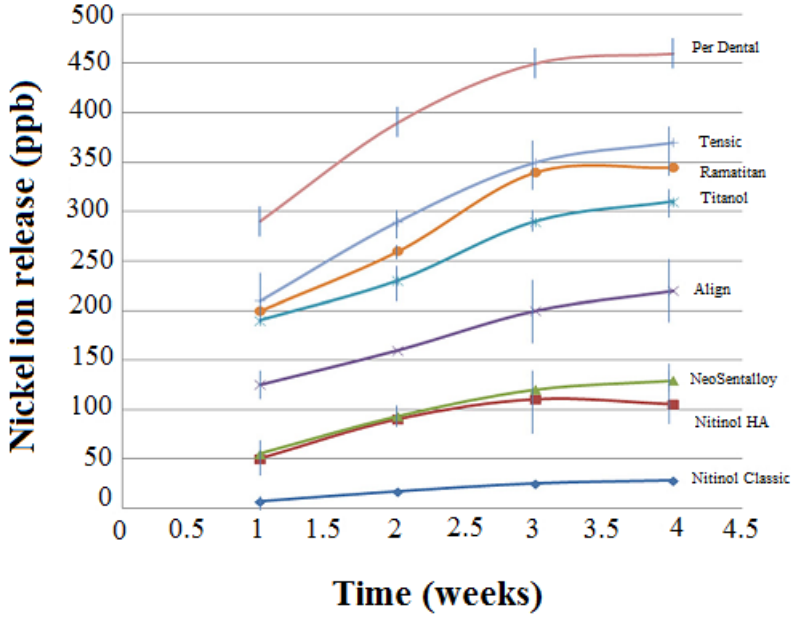


Figure 48: A Ni release from different NiTi orthodontic archwires [164]

The corrosion behavior of NiTi orthodontic wires has been extensively carried out by many groups of researchers since the oral cavity exhibits a highly corrosive environment. In the study of Rondelli and Vicentini, the localized corrosion behavior of NiTi orthodontic wires was investigated in simulated human body fluids [165]. They concluded that the NiTi wires have good resistance to pitting corrosion in artificial saliva and the localized corrosion did not depend on the shape or geometry of the cross-section. In another work by Li, the corrosion behavior of NiTi orthodontic wires was associated with the interaction of fluoride and chloride that are used as dental products [166].

In this dissertation, the corrosion behavior of NiTi shape memory alloys was measured by/through potentiodynamic polarization. The extensive results produced through the measurements allow to understand the effect of heat treatments and biocompatible coatings on the corrosion behavior of NiTi substrates.

1.4.2.2 Mathematical Modeling of corrosion

Predicting corrosion behavior is highly important, especially for medical applications. Different mathematical models were developed to better understand the corrosion mechanisms and potential factors that result in corrosion. The computational intelligence methods, including cellular automata modeling (CA), wavelet-based image processing (WIP), and artificial neural networks (ANN), were developed to predict the corrosion damage assessment as categorized in Figure 49 a [167]. The wavelet-based image processing approach uses the images that are obtained from the nondestructive imaging (NDI) system as an input to simulate the damage assessment. In this approach, the corrosion damage identification and quantification process can be explained in the flowcharts that are given in Figure 49 b. The parameters that are based on material loss and residual strength as well as structural geometry are used for the artificial neural networks approach.

By using these specific parameters, the damage assessment, structural integrity, and corrosion fatigue life can be estimated. This approach is mostly used for estimating the future behavior of a material and is not suitable to elucidate the physics of localized corrosion. The artificial neural network does not contain empirical and deterministic models.

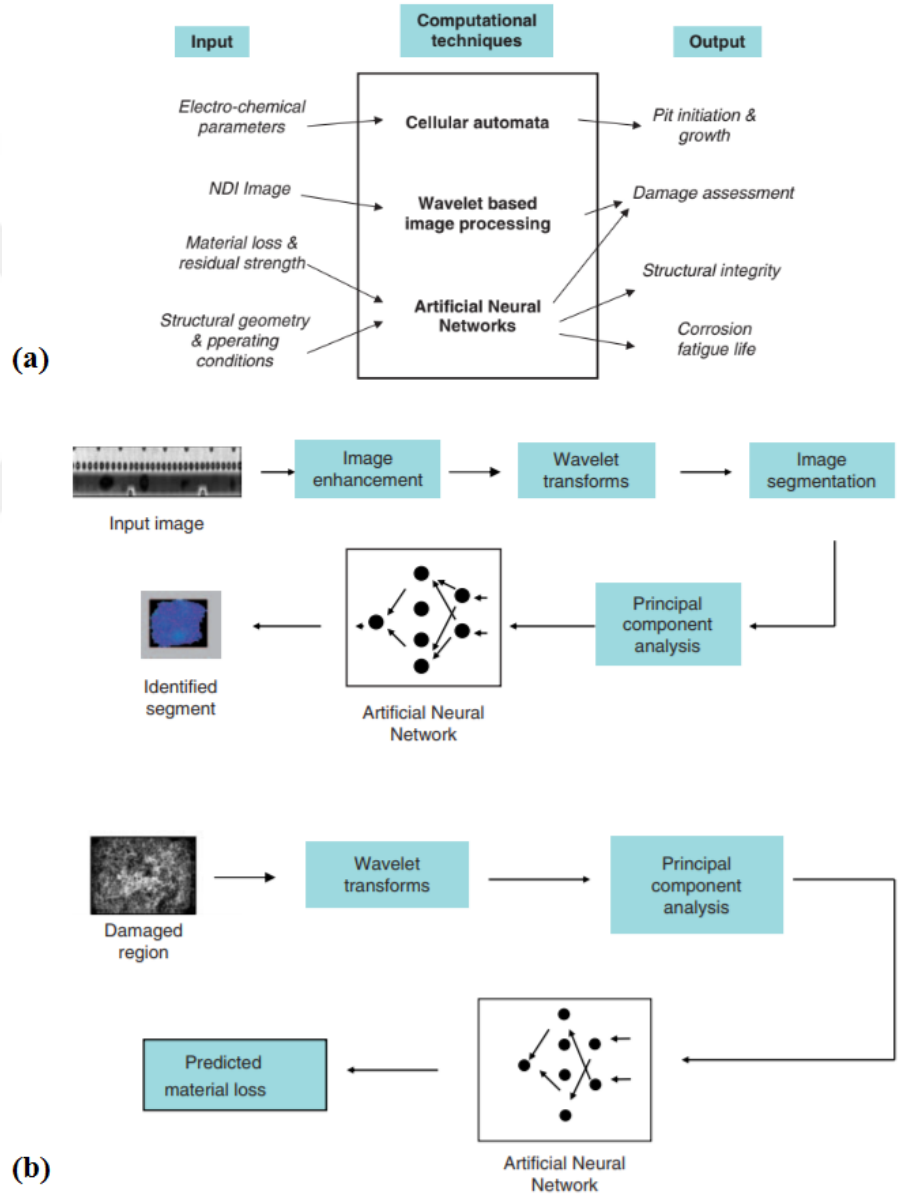


Figure 49: (a) Computational intelligence methods; (b) corrosion damage identification process and corrosion damage quantification process [167]

The cellular automata modeling (CA) approach is highly suitable for modeling complex physical systems [168] and has proved to be a powerful technique for modeling physical and biological systems that use the local rules governing the electrochemical reactions [169]. The cellular automata approach is a type of discrete dynamical model based on electrochemical reactions that need electrochemical parameters such as pH, temperature, and electrolyte concentration, and that has the potential to simulate the pit initiation and growth mechanism. The CA model is very broad and suitable for many cases that are based on physical systems, and it provides a simpler framework compared to other computational approaches. The application of CA models has varied in modeling different cases, including flows of porous media [170], erosion and transport problems [171], or forest fires and turbulence [172].

The first CA model was discovered by Von Neumann [168]. Moore and Neumann are the most common neighboring cell schemes, which consist of a number of squares or cells, as shown in Figure 50. In the Moore neighborhood approach, the interactions between red-like (8 cells) cells.

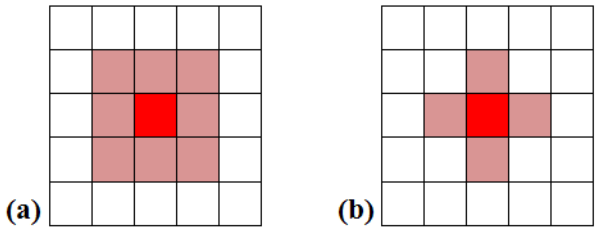


Figure 50: (a) a square-shaped neighborhood: Moore, (b) Neumann [168]

In 2004, the first two-dimensional model was proposed in order to predict the mechanism of pitting corrosion and pitting corrosion growth that is based on the CA approach [173]. The model was based on experimental data and built as feature-based. In this study, the effect of pH, potential difference, and solution concentration were investigated comprehensively. Figure 51 shows the pH effect on the corrosion growth mechanism.

It can be observed from Figure 51 that the corrosion rate increases with low pH values between 2.5 and 3.5 as well as the higher pH values that vary between 9 and 10. The investigation of the effect of the potential difference on the corrosion growth mechanism shows that the corrosion rate increased with the increase of the potential difference. The simulation was run with a constant pH value of 3.5 and a set solution concentration. The effect of the solution concentration was compared within the same simulation at 3.5 pH and 0.5 potential difference. The results showed that the corrosion rate is based on the area and corrosion levels increased as solution concentration rose.

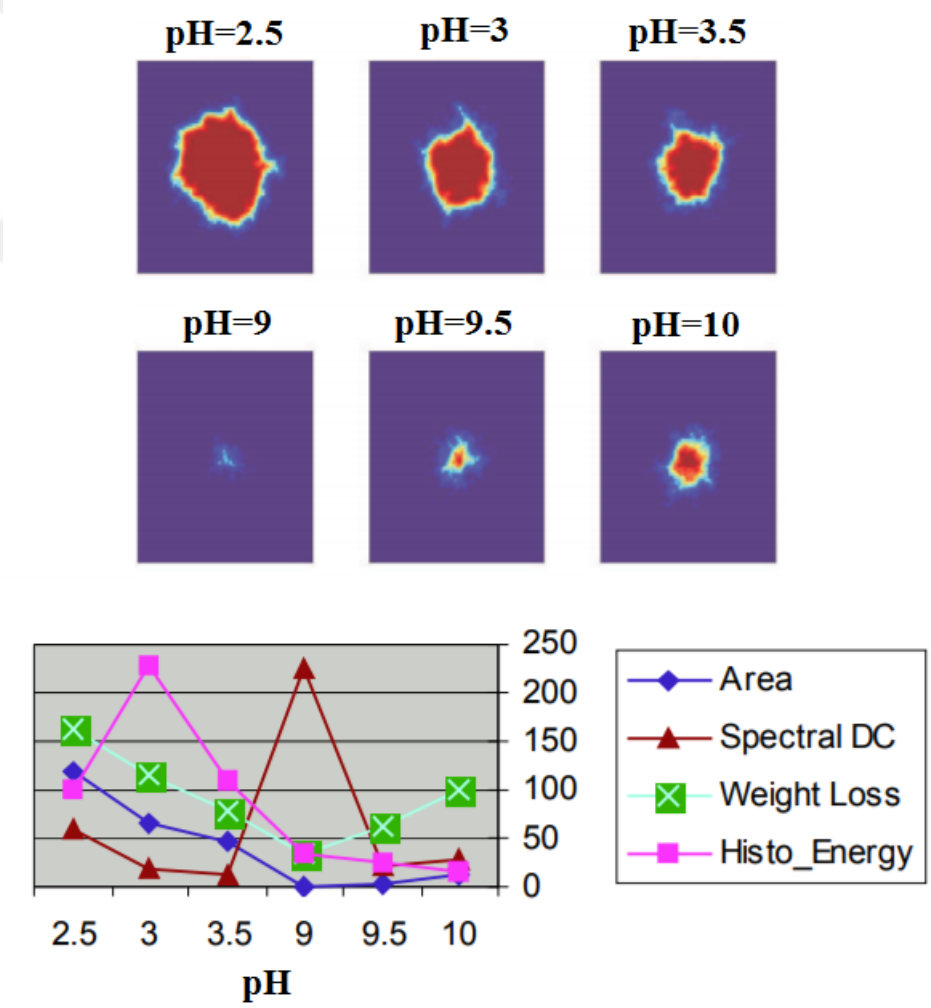


Figure 51: Effect of pH on corrosion [173]

In 2008, the effect of different electrochemical parameters on multi-pit corrosion was simulated [174]. The model was developed in order to predict multi-pit corrosion damage initiation and growth by using the local rules governing the electrochemical reactions. The pitting initiation and growth simulation were investigated at different time steps. As seen from Figure 52, the pit initiation mechanism was started at step 2 and increased step by step.

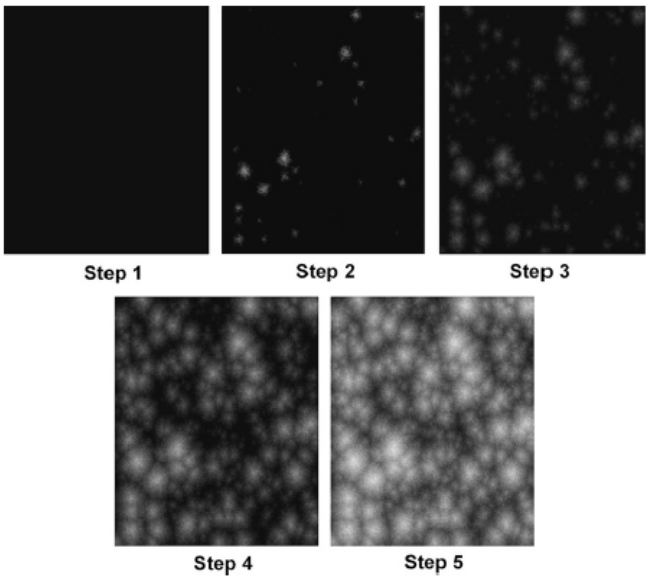


Figure 52: The pitting initiation and growth simulation with different time steps [174]

Consequently, the researchers also developed a three-dimensional model that includes the initiation phase of pitting corrosion. The computational approach is given in Figure 53. The experimental data and corrosion growth model was compared extensively. In this model, they assumed that pit initiation started from the top layer and that pits were metastable. The simulation was run for 150 cycles with selected parameters. It was concluded that with the increase in the number of cycles, the total corroded area increased. The simulation and experimental data were compared and found relatively similar.

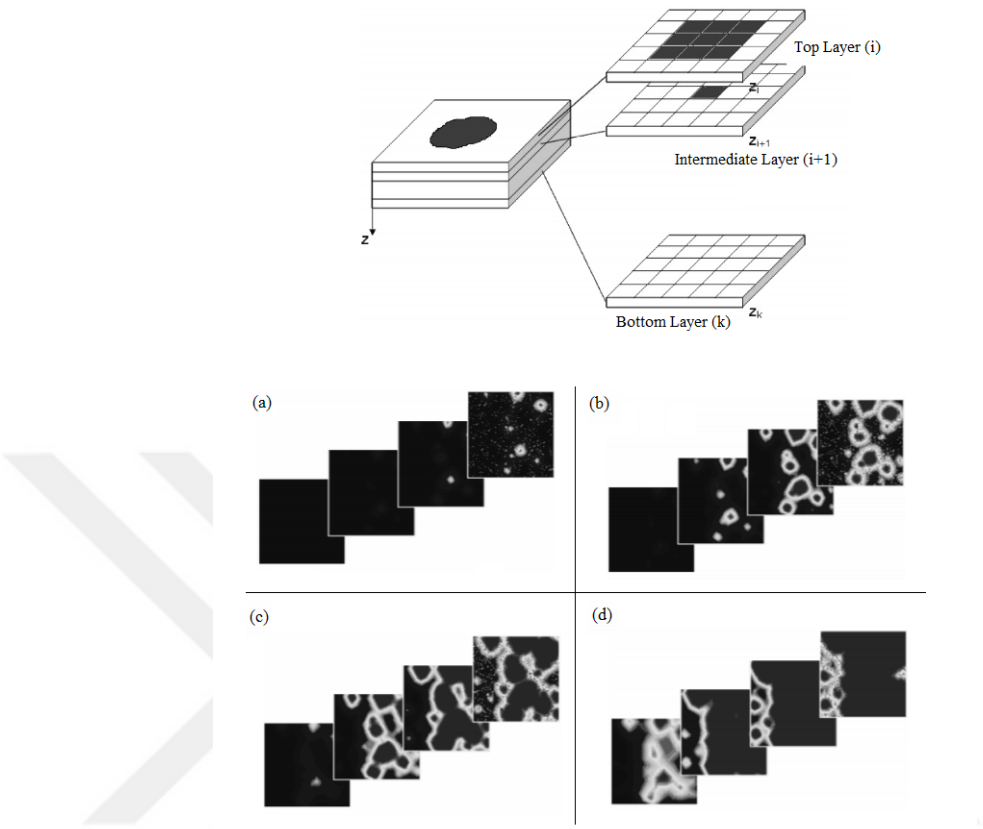


Figure 53: Developed computational approach in three dimensions and the results of the simulation at different cycles; (a) 70 cycles, (b) 85 cycles, (c) 100 cycles and (d) 115 cycles [174]

1.4.3 Cyclic Behavior

Metallic implants are known to be subjected to cyclic loading under thermo-mechanical conditions that may result in a fatigue fracture that places a limit on the practical uses of NiTi. Studies have clarified that corrosion mechanism and fatigue loading are the main sources that lead to the failure of implants as shown in Figure 54 [175]. Corrosion-based failure is a very dangerous process that may result in unpredictable fatigue fracture within the implant and therefore require expensive and dangerous surgical revision.

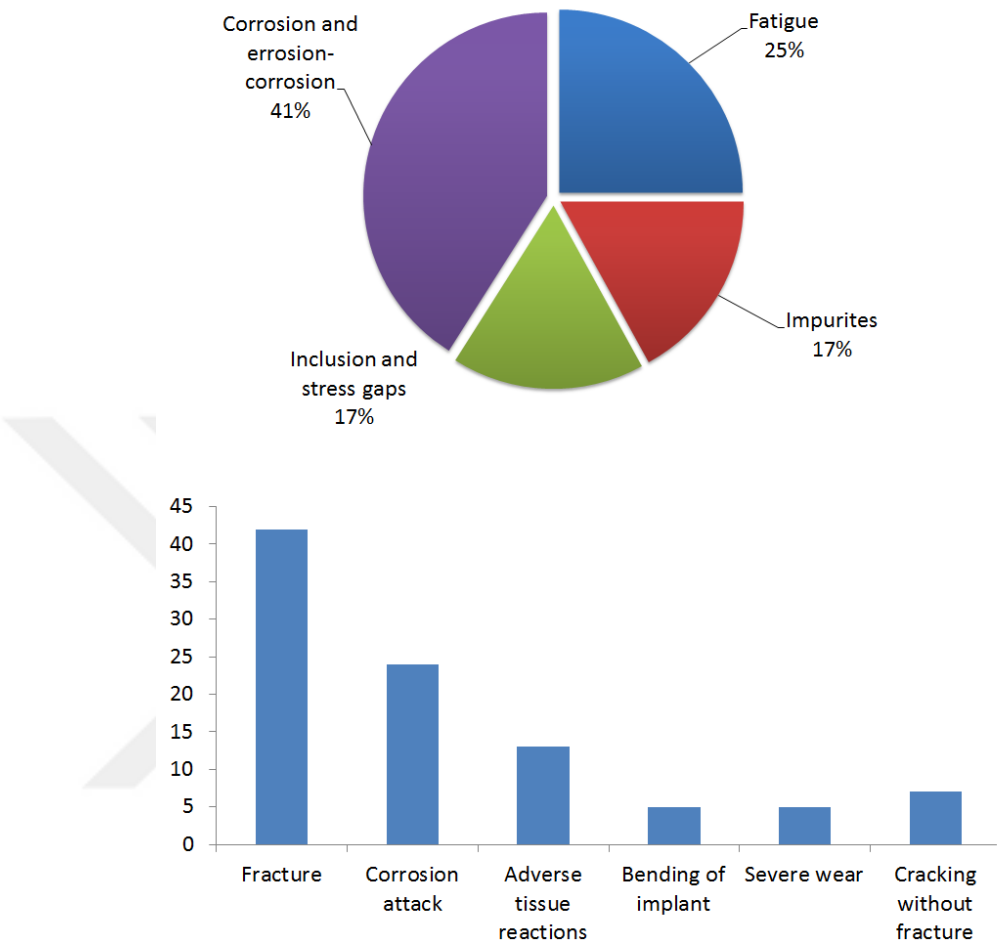


Figure 54: Failure of implants and their causes [175]

It has been extensively reported that the composition of the alloy, thermo-mechanical processing and treatments, and the stress-strain-temperature regime may affect the fatigue life [176]. So far, there are numerous studies on the improvement of the fatigue life of shape memory alloys by controlling physical variables. However, understanding the fatigue behavior of shape memory alloys has remained a challenge since those alloys lead to nonstandard fracture and fatigue responses due to phase transformations. Therefore, current methods for investigating the fatigue of NiTi may be found insufficient in particular with the effect of the corrosive environments.

Various types of corrosion and their correlation with the fatigue life of metallic implants have been investigated. The corrosion type may differ depending on the area/space; for instance, galvanic corrosion mostly occurs in dental implants [177], while crevice corrosion and pitting corrosion occur in temporary implants [178, 179]. Among all, pitting corrosion has been extensively studied due to the integrity of the material affected by this type of corrosion. The initiation of the corrosion pits occurs due to chemical and physical reasons, including inclusions, mechanical damages, dislocations, or second-phase particles. It was well documented that the fatigue life of metallic materials is highly related to corrosion pitting.

Uhlig reported that the corrosion fatigue process mainly consists of two stages. The first stage occurs as a combination of cyclic stress and a corrosive environment that accelerates the pitting and crack formation. The following stage, named the fatigue stage, is controlled by stress concentration effects and physical properties of the metallic material [180]. Combining these two stages results in decreased fatigue strength and mostly a failure of the implants, especially for artificial joints and bone plates [181] as illustrated in Figure 55.

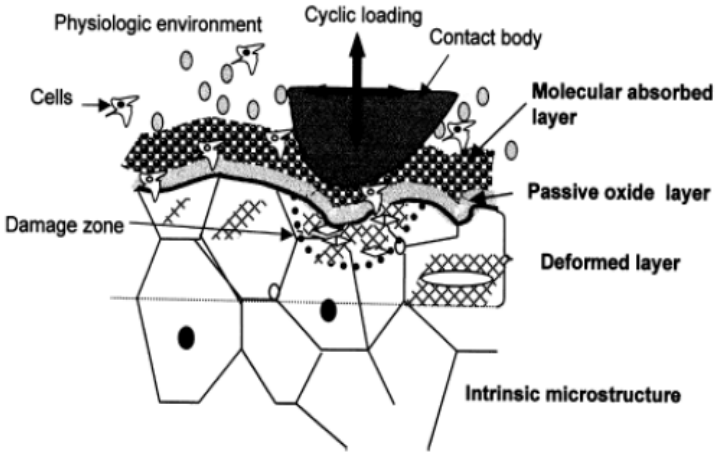


Figure 55: The illustration of the complex interactions between the implant surface and the body environment [182]

The cyclic life of conventional metallic implant materials may still be found insufficient for many applications. Many potential NiTi orthopedic implants such as bone or hip implants, may suffer from fatigue due to cyclic loading. Investigations are being increasingly deployed on the enhancement of the corrosion-based fatigue life of NiTi implant materials. The desirable implant material should be able to withstand a high number of flexing motions without failing. The daily human activities and their mechanical working conditions within the human body were summarized in Table 7.

Table 7: Activity and required cycles for implanted hip prosthesis

Activity	**Approximate Cycles Year^{-1}**
Walking	2.5x10^6
Jogging	6.4x10^5
Ascending Stairs	4.2x10^4
Descending Stairs	3.5x10^4

Pardo et al. [183] have investigated an accelerated methodology for corrosion fatigue for diamond-like carbon-coated CoCrMo alloys in body-like media. The surface of DLC/Si-DLC/CoCrMo was scratched in order to simulate stress. They reported that the interface lifetime performance was affected by pre-damage scratch dimensions, the frequency, and the body-like solution. The SEM analysis showed that the shear band formation had occurred before the crack formation, as given in Figure 56.

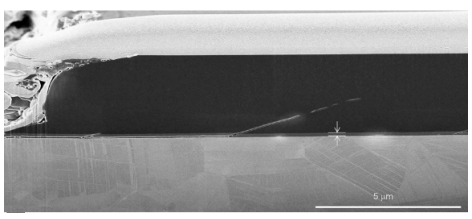


Figure 56: Complex interactions between the implant surface and body environment [183]

Recently, the research done by Chan reported the corrosion fatigue behavior of laser-welded shape memory alloys in a simulated body condition [184]. As received and laser welded NiTi samples were mechanically characterized via bending rotation tests in air and in Hanks' solution. It was found that the fatigue life of the as-received NiTi sample examined in air condition was longer than that examined in Hanks' solution. However, the fatigue life of laser welded NiTi substrates examined in Hanks' solution presented a significant reduction which is attributed to the hydrogen embrittlement. The fracture surfaces that occur in both conditions were observed with SEM as shown in Figure 57. Many microcracks were found on both surfaces. In particular, striations were found on the laser-welded NiTi surfaces.

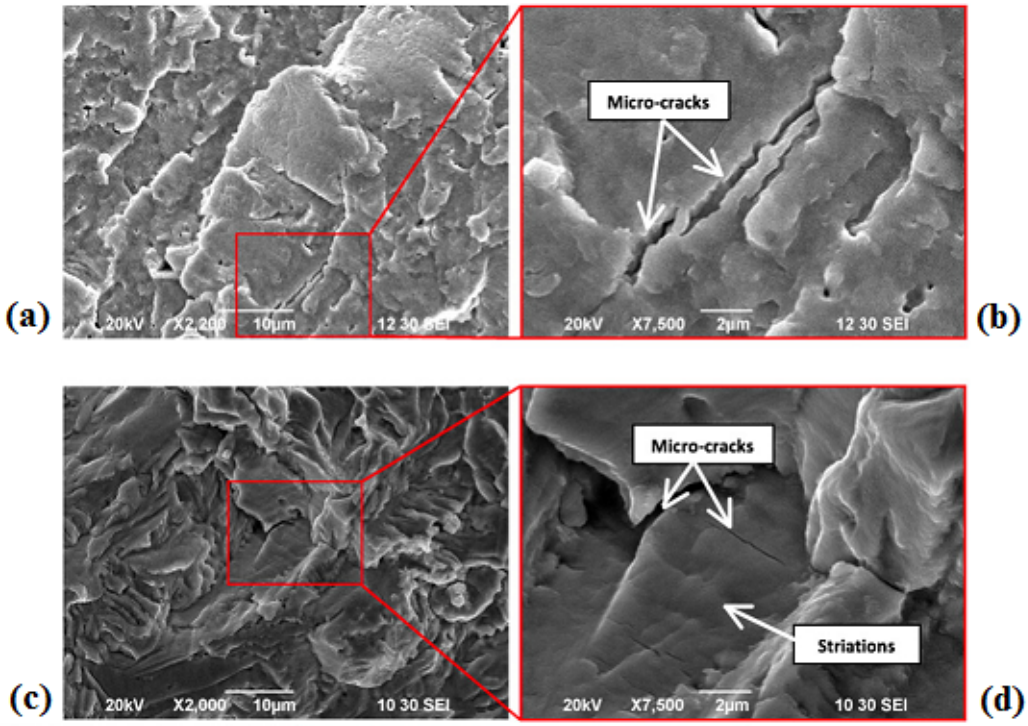


Figure 57: SEM images of the NiTi substrate (a-b) as-received; (c-d) laser-welded after the bending rotation fatigue test in Hanks' solution [184]

1.5 Motivation

Developing shape memory alloy based implantable material for improved properties, including reliable mechanical performance and biological response, requires a comprehensive understanding of the corrosion mechanism and cyclic behavior of the suggested biomaterial. In particular, for NiTi, the major concern is the potential risk of Ni ion release from the implant surface into the body environment that may cause adverse health effects. Successful short-term implementation of NiTi shape memory alloys as implants has been a motivation for the development of long-term applications. This dissertation primarily focused on suggesting a new innovative implant material that has high acceptability by the human body, extremely high corrosion resistance, and sufficient mechanical strength to sustain forces for medical implants. In this manner, the following objectives were established with given novelties:

- Selection of NiTi: NiTi wires with 0.8 mm diameter were selected as substrate material. The utilization of substantially small scale NiTi substrates in wire geometry that are exploited as implant materials with the advantage of a large force-to-mass ratio.

- Biocompatible layer on NiTi wire: Calcium phosphate (Ca-P) based ceramics and PVA based hydrogels were utilized as coating materials. This effort aims to combine the superior mechanical properties of NiTi with the excellent biocompatibility of certain polymers and ceramics to generate a new type of implant for in-vivo medical applications.

    1. CaP coating on NiTi wire: Calcium phosphate (Ca-P) based ceramics have been viewed as attractive materials in the biomedical field. Among these ceramics, hydroxyapatite (HA) is a well known and widely utilized bioceramic for coating metallic materials for biomedical applications due to its high similarity to natural bone and living tissue.

2. Hydrogel coating on NiTi wire: The polyvinyl alcohol (PVA) based hydrogels have desirable characteristics like viscoelasticity, non-toxicity, and the ability to mimic human soft tissue. To the best of knowledge, this is the first time that a study addresses the hydrogel coating of NiTi SMA in wire shape. The novelty is the provision of flexible and soft coating layers on NiTi surfaces to create a composite structure using an aqueous process since the layer must withstand the large strain and the bending movement of the substrate.

- Characterization of uncoated and coated NiTi shape memory alloys: The effect of heat treatment and biocompatible coatings on the functional behavior of NiTi alloys were comprehensively investigated with custom-made functional experimental setups. The characterization studies present two important novelties:

  1. Cyclic experiments of NiTi wire were conducted in Ringer and Simulated Body Fluid. Conditions of cyclic experiments were designated according to daily activities and working conditions within the human body.
  2. Mathematical modeling of the corrosion mechanisms of uncoated and coated NiTi SMAs is studied for the first time in this study. Information and Knowledge gained through surveying the literature were further extended by adding different conditions to investigate the effect of selected parameters.

CHAPTER II

MATERIALS AND METHODS

This chapter is structured into three main sections. The first section presents the process of material selection of NiTi and related materials for biocompatible coating on NiTi surface. Subsequently, all details of the experimental characterization of the functional behavior of uncoated and coated NiTi are given with a comprehensive and theoretical overview in the second section. Additionally, detailed research steps and methods for biocompatible coatings are presented as flow charts. Finally, the research equipment utilized in this dissertation are listed in the last section.

2.1 Materials Selection

NiTi SMAs have great potential in various applications. Since all mechanical properties are directly related to the composition of Ni and Ti, the selection of NiTi SMA is extremely important for particular purposes. This section depicts the material selection process that is affirmed as one of the most crucial steps of experimental studies.

2.1.1 Selection of NiTi

There are several applications SMA in wire geometry that can be utilized as implant materials and components in medical devices because they possess a large force-to-size ratio with a small footprint. This is especially promising with implications in specific medical interventions that require a limited operational area. In this study, the near-equiatomic NiTi wire with 0.8 mm diameter was selected as the substrate material since it is the most promising SMAs regarding applicability for medical applications [185].

2.1.2 Materials for biocompatible coatings

NiTi shape memory alloys have long been recognized as implant material with their unique properties, such as shape memory effect, and superelasticity. However, several studies have shown their limits in medical applications. For instance, there is a risk of Ni ions being released from the NiTi implant surface that result in adverse reactions, damage to the nervous system, eczema, and allergic inflammations [186]. In order to overcome this risk, NiTi SMA implants may be covered by a biocompatible layer as a shield against aggressive body fluids, protecting surrounding body tissues against toxic products, and decreasing the risk of Ni ions diffusing out of the metal. With this aim, two approaches were used to achieve the following objective; CaP based coating and PVA based hydrogel coating.

In this section, detailed information on coatings materials was presented in the given tables. Table 8 shows the reagents for simulated body fluids, that are used in biomimetic coating procedures and corrosion experiments. All items, except HCl, were purchased from Sigma Aldrich.

Table 8: Selected reagents for simulated body fluid

Reagent	**Brand**	**Information**
NaCl	Sigma Aldrich	31434-1KG-R
$NaHCO_3$	Sigma Aldrich	31437-1KG-R
KCl	Sigma Aldrich	12636-1KG
$K_2HPO_43H_2O$	Sigma Aldrich	60349-250G
$MgCl_26H_2O$	Sigma Aldrich	13152-1KG
$CaCl_2$	Sigma Aldrich	12022-1KG
Na_2SO_4	Sigma Aldrich	13464-2.5KG-R
$(CH_2OH)_3CNH_2$	Sigma Aldrich	252859-100G
HCl	Rokim	DNE

On the other hand, Table 9 summarized the reagents that were used to prepare CaP and PVA based hydrogel coating solution.

Table 9: Selected reagents for depositing biocompatible layer on NiTi

Reagent	**Brand**	**Information**
CaP	Alfa Aesar	36731-36-500G
Poly(vinyl alcohol)	Sigma Aldrich	341584-1KG
Gelatin	Sigma Aldrich	G1890-100G

2.2 Experimental Procedures

This section depicts all experimental procedures and methods. The characterization of thermomechanical and functional behavior of NiTi SMA wires is investigated as a function of selected heat treatment conditions. First of all, the transformation temperatures were measured for each condition. Subsequently, mechanical properties of SMA including force, repeatability, and cyclic response experiments were given in detail with related custom made experimental setups. Section 2.2.3 represents biocompatible coating process including biomimetic coating and dip coating methods for both CaP based and PVA based hydrogel coating. Surface characterization and cytotoxicity experiments are described in Sections 2.2.4 and 2.2.5. After all, Section 2.4.6 explains the experiments for evaluating corrosion behavior of NiTi alloys through heat treatments and coating applications. Moreover, development and implementation of mathematical modeling for multi-pit corrosion was described with related equations.

2.2.1 Heat treatment of NiTi wire

The thermomechanical behavior of NiTi wires is characterized by different conditions, to get a better understanding of all unrivaled mechanisms of shape memory alloys.

As mentioned earlier, optimal heat treatment conditions which combine the annealing temperature and the annealing duration have to be planned comprehensively to gain the desired mechanical properties. Based on, a detailed literature survey, heat treatment parameters are selected for this dissertation, given in Table 10. NiTi samples were heat treated with given conditions using a custom made titanium and steel fixtures for the shape setting process as shown in Figure 58.

Table 10: The planned heat treatment conditions

Temperature	**Time (minute)**
460^{o}C	30 and 60 min
520^{o}C	30 and 60 min
600^{o}C	30 and 60 min



Figure 58: Custom made holder for shape setting process

2.2.2 Functional characterization of NiTi wire

A better understanding of the behavior of shape memory alloys is one of the necessary aspects that requires thorough characterization. The following subsections point out all characterization experiments for the presented dissertation.

2.2.2.1 Measuring phase transformation temperatures of NiTi

The phase transformation temperatures (TTRs) are one of the most crucial properties of NiTi shape memory alloys due to their high impact on mechanical properties. TTRs are determined with two different techniques: measuring with differential scanning calorimetry and performing bend and free recovery experiments. Differential scanning calorimetry (DSC) is a powerful and expensive tool for determining phase transformation temperatures of shape memory alloys at zero stress. It relies on the correspondence between heating rate and temperature and investigates the heat flow required to increase the sample temperature. During DSC measurements, two crucibles are placed in the chamber. One empty crucible was used as a reference and a NiTi sample was placed into the other pan at room temperature. Each wire was weighed 25 to 45 mg and placed in an aluminum crucible and sealed tightly. The scanning was carried out from -10 to 200^{o}C at a rate of 10^{o}C/min as suggested in ASTM F2004-05 for shape memory alloys. Liquid nitrogen was utilized as the coolant to reach low temperature for measuring martensitic transformation temperatures. The purge gas (helium) is used at a flow rate of 40 mL/min. The DSC curves were plotted and analyzed using the DSC manufacturer's software. In the bend and free recovery (BFR) test method, the deformation recovered of NiTi sample during the thermal transformation is measured as expressed in ASTM F 2082-16. Compared with the DSC method, the BFR method is quicker and more economic. Moreover, the BFR method is highly suitable for wire, tube, and strip shape substrates. The measurement of the austenitic transformation temperatures is obtained with the tangent method as described in Figure 59 [187]. Temperature and displacement data were collected with DAQ systems with different modules during the experiment. In the presented dissertation, both techniques were performed to measure phase transformation temperatures and compared results were discussed in the following chapter.

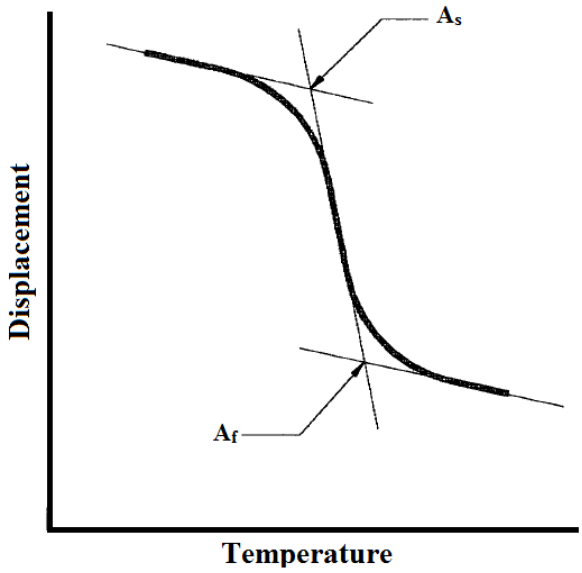


Figure 59: Determining transformation temperatures with tangent method [187]

2.2.2.2 Actuation and cyclic behavior of uncoated and coated NiTi

The measurement of displacement and bending angle were performed with a custom designed experimental setup that consists of encoder, LVDT, a slider, and pulley for LVDT connection as shown in Figure 60 [188]. NiTi samples were fixed from both ends with electrically conductive rotatable links. The fixed end of the sample was connected to the encoder with the free bend stationary pivoting pin. During actuation, the rotation of a stationary pivot is measured using the optical encoder. Test samples were activated by joule heating by using a power supply. Displacement, bending angle, and temperature data were collected and recorded by the data acquisition system (DAQ). A resistive heating method was utilized to activate NiTi samples, as it possesses fast and homogeneous response for characterization experiments.

Shape memory alloys have the ability to exert force to recover their memorized shape [189]. The property of a large force to mass ratio makes SMAs an appropriate candidate for actuators. In this study, the exerted forces of heat treated NiTi samples were measured with the designed and manufactured setup as illustrated in Figure 61.

In the setup, one end of NiTi is fixed with the screw while the other one is connected to the load-cell. The exerted load was measured with perpendicular connection. The temperature of the wire was recorded with a thermocouple and DAQ system. NiTi samples were activated via power supply with constant current.

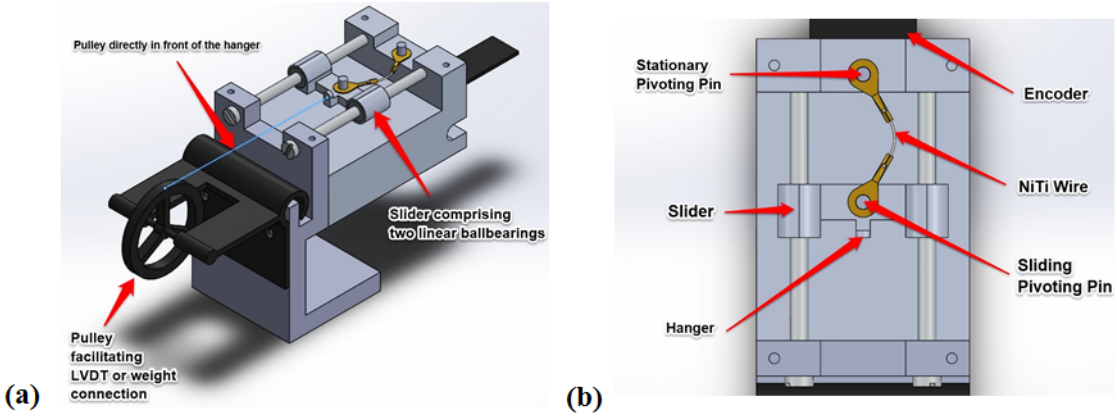


Figure 60: Experimental setup for displacement and bending angle measurement (a) side view; (b) top view [188]

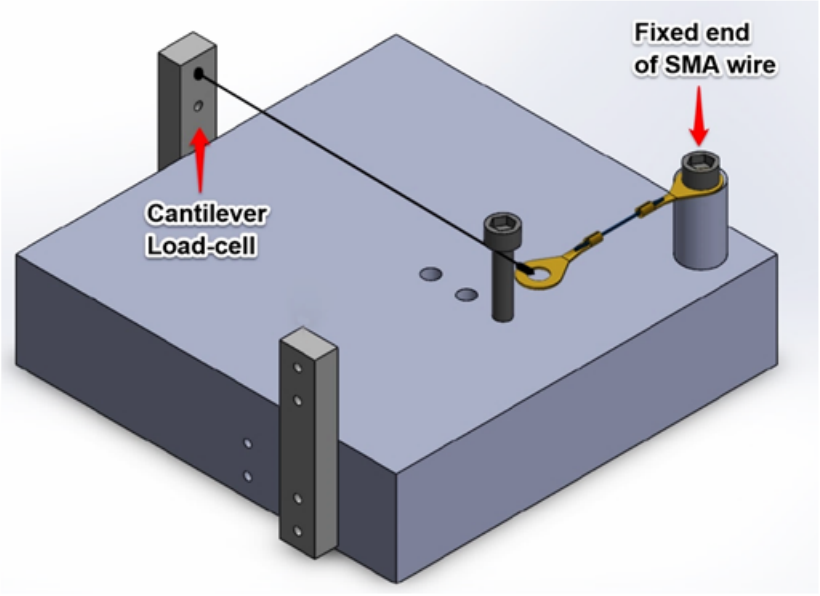


Figure 61: Three-dimensional depiction of force setup [188]

The cyclic behavior is another important feature that affects the use of NiTi shape memory alloys for biomedical applications. In order to examine the cyclic behavior, tests were performed for samples treated at selected treatment conditions in atmospheric conditions. The bending angles of each cycle were measured and recorded with the given setup in Figure 62 [188]. This setup was improved with higher control and more effective movement from earlier versions. The free movement of the sample was improved by minimizing the sliding friction with the new rail and slide.

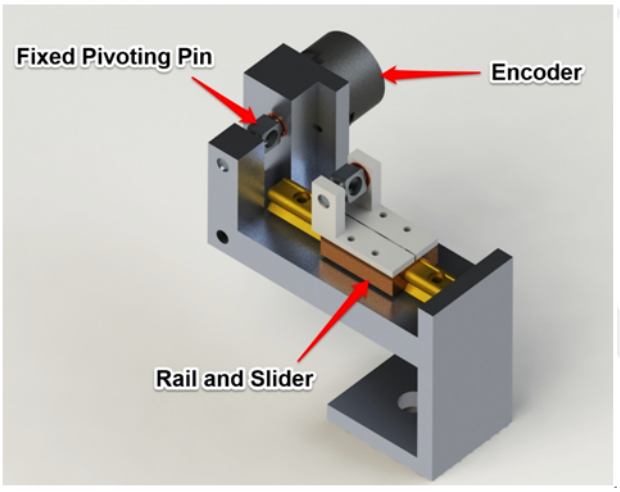


Figure 62: Three-dimensional depiction of force setup [188]

Besides, the cyclic responses of the NiTi samples were examined in the human-body-simulating fluids, the simulated body fluid (SBF), and Ringer solutions since the mechanical stability of implanted materials in body-like mediums are still important for successful and long-term implementation. Both fluids were used for comparison purposes at room and body temperatures to validate experimental findings and the reliability of NiTi before clinical use. SBF solution was prepared according to the procedure described by Kokubo with given reagents in Table 11 [60]. The reagents to prepare the SBF solution to dissolve one by one using a magnetic stirrer. The Ringer solution was prepared by dissolving the reagents by the given amounts as summarized in Table 12.

Table 11: Reagents for preparing 1000 ml of simulated body fluid (SBF) [60]

Reagent	**Amount**
NaCl	7.996 g
NaHCO3	0.350 g
KCl	0.224 g
K2HPO4.3H2O	0.228 g
MgCl2.6H2O	0.305 g
1M HCl	40 ml
CaCl2	0.278 g
Na2SO4	0.071 g
(CH2OH)3CNH2	6.057 g

Table 12: Ringer physiological solution

Reagent	**Composition** (g/L)
NaCl	7.2
KCl	0.37
CaCl2	0.17

These experiments were utilized by using a setup as shown in Figure 63. The experimental setup consists of a motor, sealed reservoir, encoder, and rail mechanisms. In this system, the required torque for the cyclic movements with determined angles was provided through an electric motor. The advantage of using the step motor was the capability to rapidly control the NiTi actuation. The step motor electrically controlled and actuated the rail system according to the angle feedback from the encoder. The reservoir was manufactured with plexiglass material and sealed with teflon tape.

The functional characterization setup was placed in a pool. An encoder was attached to the system for closed-loop control of the motor during the bending and resetting actuation. Different types of controllers were examined in order to define the most suitable for this specified case. It was determined that the simplified experimental setup generates more robust results. The reason for choosing a P controller was to decrease the steady-state error and effort of the controller on the system in order to reach the target position. An external heater was used to set the environment temperature at the body temperature to simulate the body environment. Two thermocouples were used: one attached to the pool wall and one submerged in the SBF directly. The Arduino was used to determine the output temperature and bending angle. The number of cycles was recorded until the NiTi wire fractured. In between each cyclic test, the SBF solution was refreshed.

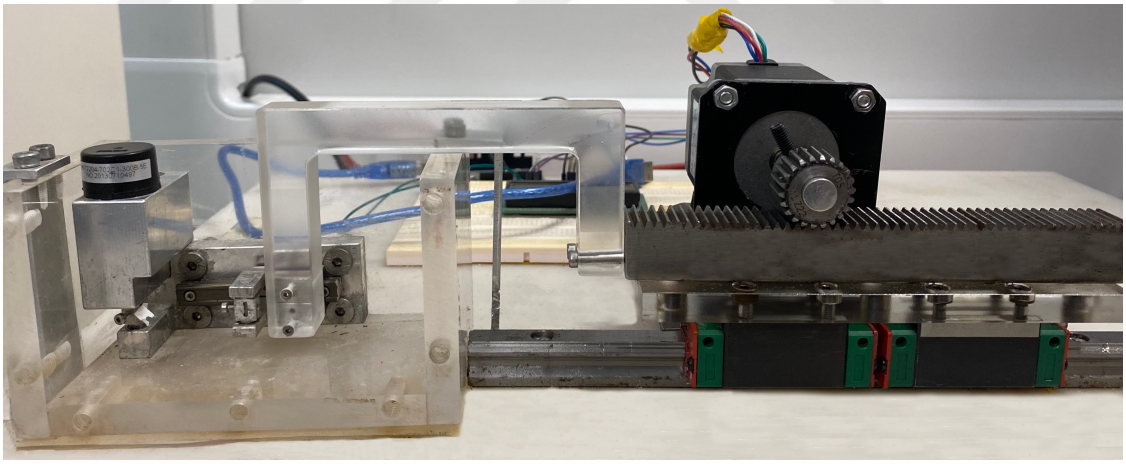


Figure 63: The experimental setup for the cyclic response tests in corrosive medium

2.2.3 Biocompatible coating procedure

Commercially available, equiatomic NiTi wires with 0.8mm diameter and 10 mm length were used as substrate material for all types of coating. Prior to coating, samples were cleaned in an ultrasonic bath using acetone, ethanol, and deionized water in the given order.

Obtaining CaP based coatings on NiTi surfaces have been utilized with dip and biomimetic coating techniques. Chemical surface treatment experiments were done with NaOH. On the other hand, deposition of the hydrogel layer has been also obtained by dip coating method. Finally, the effects of CaP and hydrogel coating on NiTi surface, mechanical properties, and biocompatibility were extensively investigated with characterization techniques. The coating types and procedures used in this dissertation were summarized in Figure 64.

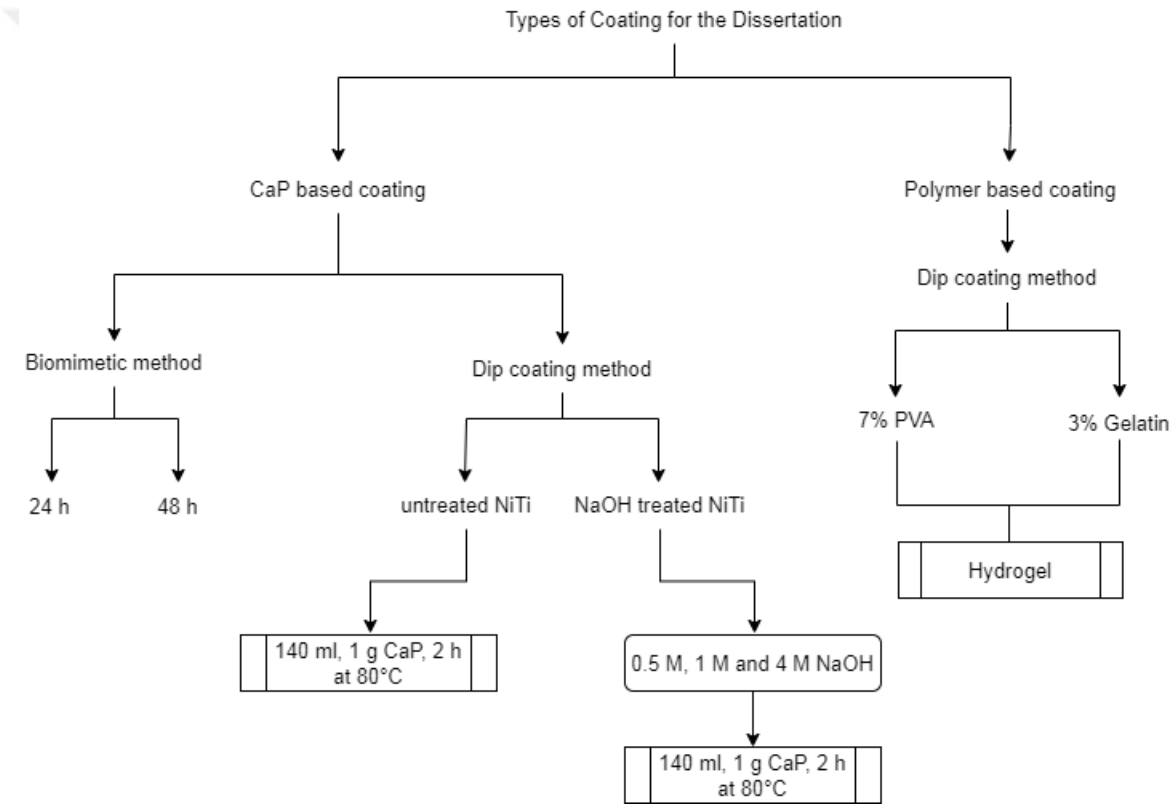


Figure 64: The types of coating for the dissertation

2.2.3.1 Biomimetic coating

The first part of the experimental studies deals with the formation of bioceramic layers via biomimetic method. NiTi samples were immersed in simulated body fluid (SBF) solution for different periods of 24 and 48 days. Before immersing, NiTi samples were firstly heat treated at 520^{o}C for 30 minutes.

Due to the heat treatment process, the oxidation layer would be present as an interface between the coating layer and the NiTi surfaces. This process also increased surface roughness that may raise the adhesion between the coating layer and the implant surface. Subsequently, NiTi samples were immersed in SBF and maintained at 37^{o}C for various durations to find the parameters of optimum coating condition. The coating was obtained by immersing the NiTi samples in the SBF solution. A holder was manufactured by using 3D printers for multiple coating purposes as shown in Figure 65. After selected immersion periods, samples were removed from the SBF solution and washed with distilled water. All samples were dried at room temperature for further analysis.



Figure 65: Manufactured holder for biomimetic method

2.2.3.2 Dip coating

The second part focuses on obtaining CaP based bioceramic coatings by dip coating method. In this method, the first step is to prepare the coating solution. As one of the most common coating materials with the best implant-bone tissue bonding feature, commercially obtained HA powders were selected as the main suspension material in this study. These HA powders also provide long term fixation and stability [190, 191]. Dip coating suspension was prepared with different parameters for 140 ml.

The summary of parameters were given in Table 13. All suspensions were prepared by adding the selected amount of CaP into distilled water followed by vigorous stirring on a magnetic stirrer to obtain a homogeneous solution.

Table 13: Selected parameters for depositing CaP based biocompatible layer on NiTi

Sample Name	**Amount of CaP**	**Temperature**	**Duration**
Sample 1	1g	40^{o}C	1 h
Sample 2	1g	60^{o}C	2 h
Sample 3	1g	80^{o}C	1 h
Sample 4	1g	80^{o}C	2 h
Sample 5	1g	80^{o}C	4 h
Sample 6	3g	80^{o}C	2 h
Sample 7	5g	80^{o}C	2 h

The cleaning steps for NiTi substrates were undertaken before the coating process as mentioned in previous sections. NiTi samples were immersed into the dip coating suspension using an in-house built electronic setup that has dipping apparatus shown as Figure 66. The setup consists of a DC motor and a holder for multiple sample coating purposes. All samples were kept in the coating suspension at selected temperatures for the specified duration and a constant withdrawn speed of 6 mm/s as suggested in the literature. The suspension was stirred continuously during the coating process. The coated samples were sintered at 520^{o}C for 30 minutes to increase their density and enhance the bonding strength in a laboratory furnace in the open atmosphere. The temperature was at an acceptable level and did not cause deterioration of the mechanical properties of the NiTi substrates, as experimentally derived in the previous chapter.

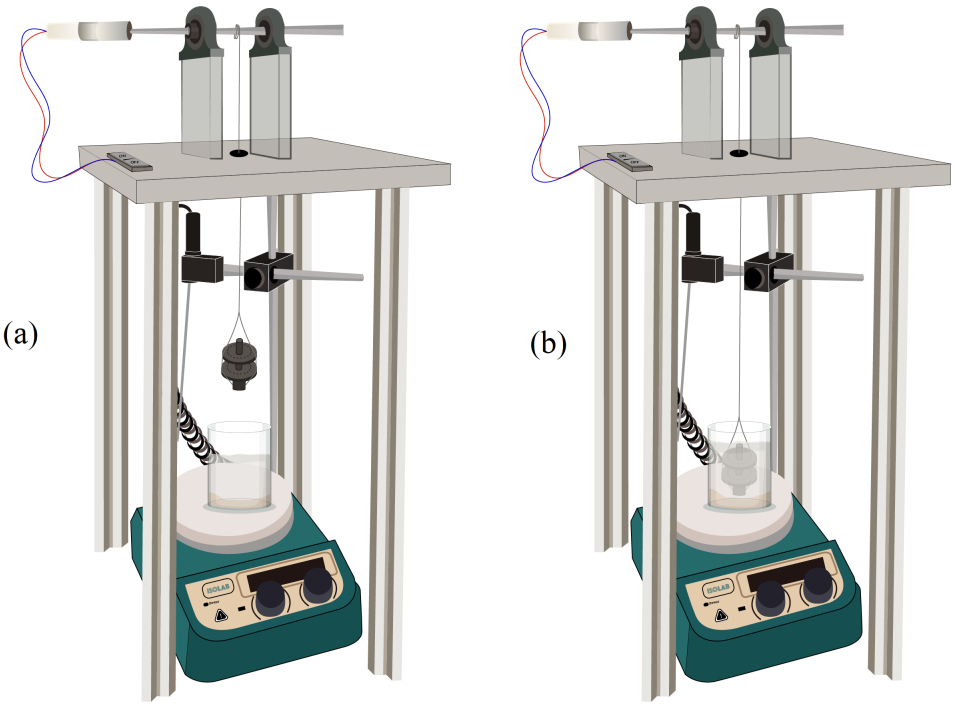


Figure 66: Dip coating setup with dipping apparatus: (a) preparation process; (b) coating process

Several researchers have utilized different surface treatment methods on NiTi substrates to enhance their necessary properties. NaOH treatment is a well-known method that has been applied to various materials. In this study, NiTi substrates were treated with 0.5 M, 1 M, and 4 M NaOH solutions at 60^{o}C for 24 hours, followed by drying at 40^{o}C for 24 hours. The dip coating method was chosen due to its desirable outcomes, including its non-destructive characteristics, fairly simple procedure, and the provision of a more quantitative coating layer.

Substrates were named according to their NaOH treatment condition as XNaOH-C, where X represents the concentration of NaOH solution and C indicates the application of the subsequent coating process. For instance, 0.5NaOH-C refers to the sample which is treated with 0.5 M NaOH solution followed by HA coating and heat treatment. Sample naming is summarized in Table 14.

Table 14: Sample naming convention based on NaOH surface treatment and HA coating conditions

$Samplename$	$Concent.of NaOH solution$	$HAcoating$
As-received	-	-
C	-	+
0.5NaOH-C	0.5 M	+
1NaOH-C	1 M	+
4NaOH-C	4 M	+

2.2.3.3 Hydrogel coating

The presence of a hydrogel layer may decrease the potential of Ni release from the implant surface and prevent inflammatory reactions by acting as a cushion. It is believed that hydrogel coated NiTi wires can be used in applications where the wires are in contact with abrasive physiological environments. The heat treatment of wire shaped NiTi substrates was conducted at 520^oC for 30 min using a set of fixtures in a furnace for shape setting. The process was finalized by water quenching. Before coating, samples were cleaned with acetone, ethanol, and distilled water in ultrasonic bath, respectively, and air-dried at ambient temperature.

In this study, the hydrogel layer was prepared by blending PVA and gelatin. A solution was prepared by dissolving PVA and gelatin type A in deionized water. Gelatin was selected due to its high similarity with human body and is one of the most frequently used agents for medical applications. Different amounts of PVA and gelatin were utilized in order to find optimum conditions. These selected amounts of agents were illustrated in Figure 67.

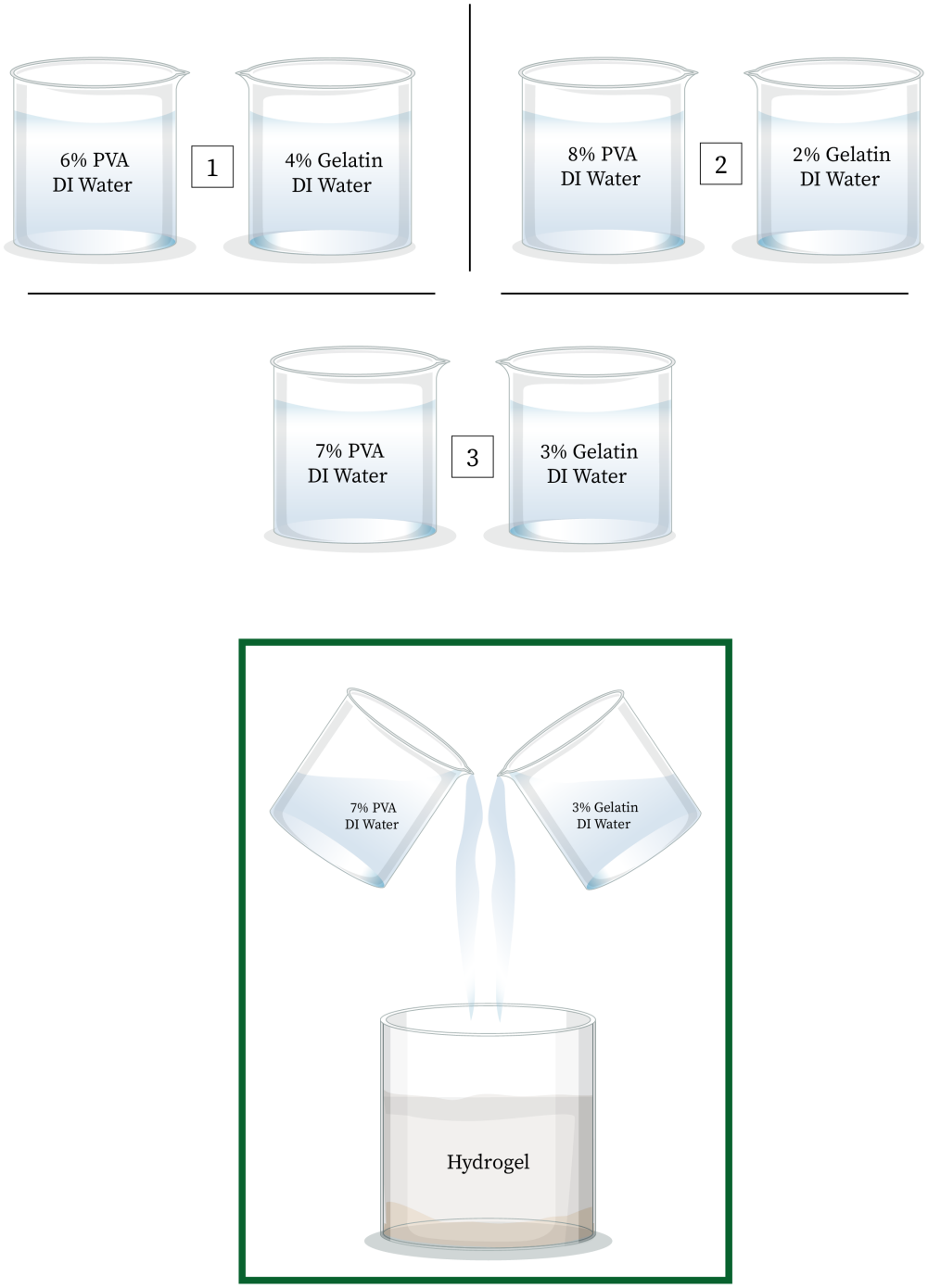


Figure 67: Different amounts of agents of hydrogel suspension

The preparation procedure was also designated by utilizing different parameters as summarized in Figure 68. In the first scenario, PVA (7% w/v) was constantly stirred for 4 hours at 60^{o}C and then left at room temperature overnight. In another beaker, gelatin type A (3% w/v) was dissolved in deionized water for 4 hours at 60^{o}C followed by mixing both solutions. In the second scenario, PVA (7% w/v) and gelatin type A (3% w/v) were constantly stirred for 2 hours at 60^{o}C in different beakers. Contrary to the previous samples, in the third beaker gelatin type A (3% w/v), was initially dissolved in DI water and then PVA (7% w/v) was added to the suspension and stirred for 4 hours in the third scenario. After all, PVA (7% w/v) and gelatin type A (3% w/v) were stirred for 2 hours at 40^{o}C separately before mixing as illustrated in scenario 4.

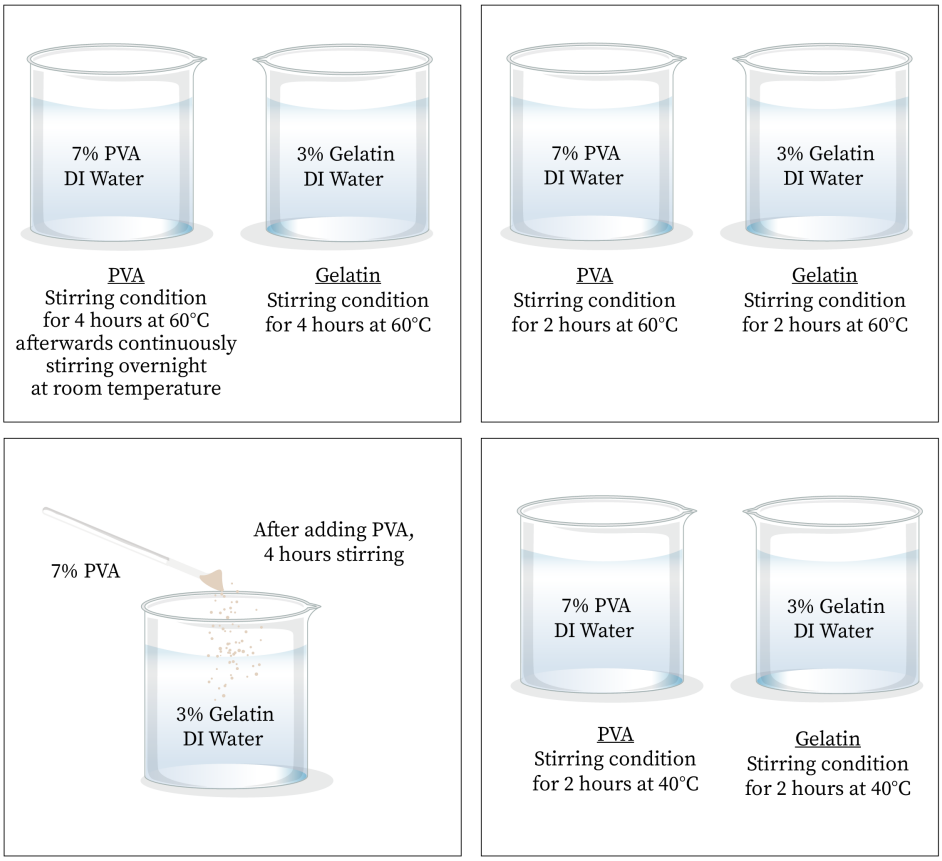


Figure 68: Different preparation parameters for hydrogel suspension

Heat-treated NiTi samples were immersed into a PVA-based solution for 30 min and then removed and kept at -20^{o}C overnight. The frozen system was then thawed at room temperature the next day, which results in a physical gel formation via polymer entanglement and hydrogen bond formation (freeze-thawing) for the PVA component. In order to ensure the stability of the gelatin component, an additional enzymatic crosslinking step was carried out. Microbial transglutaminase (TGA) is a monomeric, bacteria derived enzyme that can create crosslinks between the lysine and glutamine between proteins. It is formed of 11 alpha helices and 3 beta-strands with a molecular weight of approximately 38 kDa depending on the source microorganism. After thawing, microbial TGA with 20% w/v was used to crosslink the gelatin component of the hydrogel, which can be classified as interpenetrating networks (IPN) type.

The gelatin component of the coating is degradable enzymatically; the crosslinking process with TGA controls the degradation as it adds crosslinks between lysine and glutamine groups which are not recognized by the collagenase enzymes. In physiological conditions, the degradation of PVA occurs via erosion; as the freeze/thawing process only introduces entanglements, the non-entangled chains will be removed slowly. Samples were kept in TGA solution for 18 h at room temperature. Subsequently, the coated samples were rinsed in deionized water to obtain stable coating layers which are completely wettable in the hydrated state.

2.2.4 Surface Characterization

In this section, surface characterizations were utilized for heat treated NiTi, CaP, and hydrogel based coated NiTi, NaOH treated NiTi with optical (OM) and scanning electron microscope (SEM). Moreover, the amount of Ni ions on the surface of NiTi was investigated with X-ray photoelectron spectroscopy after NaOH treatment. Contact angle and hardness measurements were also explained in this subsection.

2.2.4.1 Heat treated NiTi samples

It has been established in the years that NiTi SMA behavior depends on stress and temperature since it is intimately associated with the crystallographic phase of NiTi alloys. The surface morphology of the heat treated NiTi samples was examined using the Olympus inverted light microscope with varied magnifications up to 100X. Moreover, a scanning electron microscope was utilized to analyze the microstructural evolution of NiTi surfaces at higher magnifications. All specimens were ground with SiC papers followed by standard polishing techniques. Samples were etched in a solution of HF, HNO_3, and acetic acid with a ratio of 1:4:5.

2.2.4.2 CaP based coated NiTi samples

Following the coating process, the structural integrity of the HA layer was investigated via microstructural observations. The surface morphology of the CaP based coated and uncoated NiTi samples were studied by optical microscopy and scanning electron microscopy (SEM, Zeiss Ultra Plus Field Emission). X-ray photoelectron spectroscopy (XPS, Thermo K-Alpha) measurements were carried out to evaluate the chemical composition of the sample surfaces as a function of NaOH treatments with varying concentrations.

2.2.4.3 Hydrogel coated NiTi samples

Surface observations of uncoated and coated samples were powered by confocal microscopy, digital microscopy, and scanning electron microscopy (SEM). For light microscopy of the coated samples, a specific dyeing process (Chondrex treatment with Sirius red kit dye) was applied. SEM analysis was performed in a ZEISS instrument operating at an accelerating voltage of 10 kV.

2.2.4.4 Contact angle measurement

The contact angle measurements were taken by the sessile drop method with a Theta Lite optical tensiometer using distilled water. Uncoated, CaP based, and hydrogel-coated samples were positioned under the syringe tip. All measurements were performed, using five drops for each sample via a light microscope system at room temperature. The drop images were captured by a digital camera attached to the system. The average of four consecutive measurements was calculated for each sample. Contact angles were determined from the images, using analyzing software.

2.2.4.5 Hardness measurement

The hardness measurements were performed to investigate the effect of heat treatment on the NiTi properties. The indenter was loaded under 1 kg load for 10 seconds. The average hardness value was obtained from readings from five experiments for each specimen.

2.2.5 Corrosion behavior

The focus of this part is to evaluate the corrosion behavior of NiTi alloys through heat treatments, surface treatment, and coating applications in simulated body fluids. Dip coating and biomimetic methods were utilized to investigate the effect of coating technique on the corrosion behavior of NiTi. Moreover, the influence of coating material was also examined with CaP and PVA-based hydrogel coated NiTi substrates. All results of the coated samples were compared with those from the uncoated NiTi.

Most corrosion studies of NiTi alloys were performed in the simulated body fluid since it acts as a physiological environment and mimic the human body conditions. Immersion of the metallic based implant material into this kind of solution leads to corrosion and attributed release of ions from the implant surface. This reaction may result in implant instability and failure of in-vivo studies, making understanding the corrosion behavior of the NiTi alloy highly crucial for medical-based applications.

Initially, the corrosion properties of the heat-treated NiTi samples were observed through potentiodynamic polarization measurements in order to investigate the effect of heat treatment. The corrosion current density (I_corr) and the corrosion rate of the tested NiTi sample were calculated with the Tafel fit method [192]. The experiments started with a scan rate of 1mV/s. All electrochemical corrosion tests were carried out at 37^{o}C and pH 7.4 in order to mimic the body environment. The measurements were taken in a three-electrode electrochemical cell. A saturated calomel electrode and a platinum wire were used as a reference and auxiliary electrodes, respectively. The NiTi samples were placed in a Teflon holder on which a 10x10mm area was exposed to the electrolyte solution as presented in Figure 69.

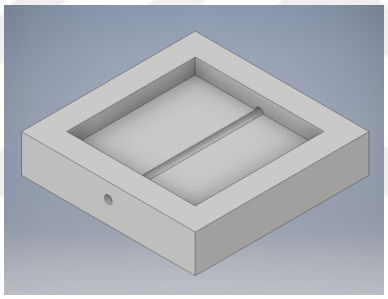


Figure 69: Design of teflon sample holder for potentiodynamic corrosion experiments

2.2.5.1 Mathematical modeling of corrosion

In conjunction with experimental efforts, corrosion modeling was carried out, using the cellular automata (CA) approach, to simulate the corrosion behavior of the uncoated and coated NiTi alloys. The computational modeling of multi-pit corrosion in medical implants based on cellular automata is divided into two sub-models; corrosion initialization and corrosion progress. In addition, the results from the experiments, where the NiTi alloy was used as an example, were utilized to run in-silico simulations for these models. The simulations were then followed by tests to investigate the effects of various environmental parameters. The materials and experimental techniques used during the present study will be described in this section.

The state of each cell has been represented by a predefined interval in the range of 0-255 units, where the uncorroded cell has a value of 0 and the corroded cell has a value of 255. This means that the corrosion result is depicted with an image of the material surface, where certain rules were prescribed to follow the cells where corrosion was initialized and would progress in time as given in Figure 70. The image used to model the corrosion of the material was 200 x 200 pixels. In this study, the material of interest was represented as a two-dimensional square lattice in the cell. In this case, each cell would be a pixel in the image, and each of these cells can be in a different state or different pixel value at any given time. The evolution of each cell and the updating of their internal states occur synchronously and are governed by a defined set of equations.

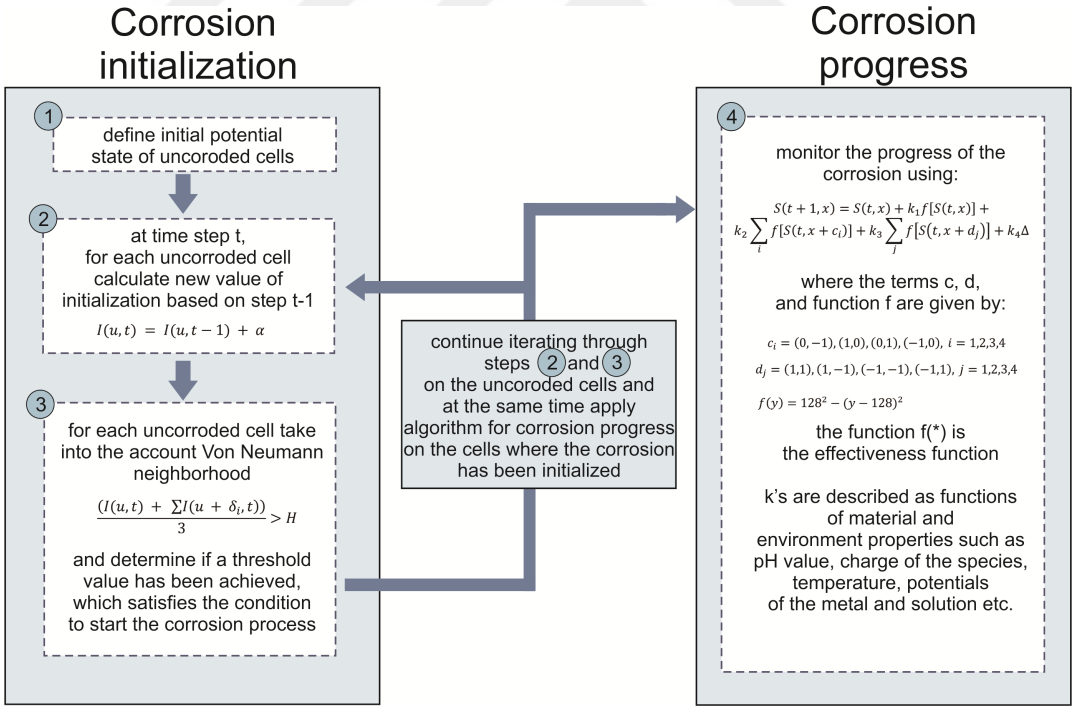


Figure 70: Flowchart of the corrosion modeling [193]

At the beginning of the simulation (t=0), the assumption is that there is no corrosion of the material, meaning the first step is the black image and all the states of the pixels are 0.

After that, corrosion initialization is started, each cell x is associated with an initial potential state I(u,t), where a is an increment of the pixel value (state potential):

$$I(u,t) = I(u,t-1) + a \tag{1}$$

For each uncorroded cell u, the potential initialization state was set according to the Von Neumann neighborhood algorithm presented below:

$$I(u,t) + \sum I(u+\delta_i, t), i = 1,2,3,4 \tag{2}$$

The parameter δ_i represents the four Von Neumann neighborhoods including up, down, right, and left. If that sum which is divided by 3 becomes larger than a certain threshold, then corrosion is initialized in cell u and the corrosion state, S(u,t), (pixel value) of that cell is set to a small positive number.

For the succeeding time steps, the corrosion initialization sub-model is applied on all the other uncorroded cells again, and simultaneously corrosion progress sub-model is applied on cells where corrosion was initialized using the equation below, where c, d (i varies between 1 to 4) and f function are given as follows;

$$S(t+1,x) = S(t,x) + k_1 f[S(t,x)] + k_2 \sum_i f[S(t,x+c_i] + k_3 \sum_j f[S(t,x+d_j] + k_4 \triangle \tag{3}$$

where;

- c_i=(0,-1), (1,0), (-1,0) and d_j= (1,1), (1,-1), (-1,-1), (-1,1)
- f(y)= 128^2 - $(y-128)^2$
- $\triangle$= standard random variable with mean of 0 and variance of 1

Figure 71 shows implemented Moore neighborhood to describe the influence of the surrounding cells on the cell of interest. In this case, c_i represents the cells down, up, right, and left from the cell of interest, while d_j represents the cells diagonally up-right, up-left, down-left, and down-right from the cell of interest.

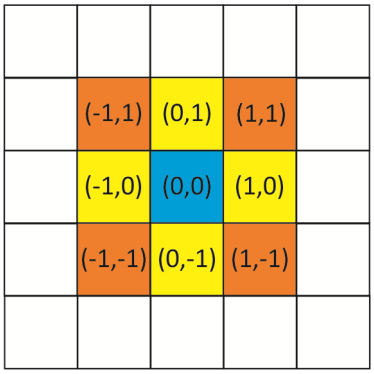


Figure 71: Area of image denoting Moore neighborhood

Additionally, other chemical parameters, which affect the corrosion mechanisms, are involved with continuous mathematical models are presented below;

$$k_1 = \lambda \times (pH - 7)^2 \times (step(4, 8.5)) \times (e^(\phi_m - \phi_s)) \times (1/T) \times (C) \times (D) \times (z) \quad (4)$$

where;

- λ: the discount factor that ranges from 1 to 3
- pH: pH value of the solution
- step (4,8.5): function with the value of 0 for the ranges between 4 and 8.5, otherwise 1
- ϕ_m: potential of the metal
- ϕ_s: potential of the solution
- T: absolute temperature
- C: concentration of the reaction species
- D: diffusivity of the reaction species
- z: charge of the reaction species

Outputs of the simulation of the corrosion model are given in the form of images for every time step. In order to quantitatively describe the outputs, the second part of the proposed methodology includes the analysis of in-silico obtained corrosion images. The calculation software can be used to compare the results obtained experimentally and from simulations. Upon finishing the simulation, resulting images were utilized to quantitatively estimate the corrosion progression over time by calculating the following statistical measures as follows:

- Mean corrosion: the average gray value of the grayscale's image histogram probability.
- Standard deviation: describes the spread of the data set and is related to image contrast.
- Skew: asymmetry of the mean value in the distribution.
- Percentage of the corroded material: sum of the corroded pixels (all non-zero values) divided by the number of pixels and multiplied by 100.
- Energy: indicates how the pixel intensities are distributed in the region under consideration. Concerning the corrosion image, this feature indicates the degree of corrosion at the pit level.
- Power: indicates the texture property in an image and, in this case, the level of corrosion itself. The higher the power value, the higher the texture change.
- Contrast: the difference between the maximum and minimum pixel intensity in an image.
- Wavelet features: calculated throughout the processes of singular values decomposition (SVD); only the first two eigenvalues are reported.

2.2.6 Cytotoxicity experiments

The biological responses of the uncoated and CaP coated samples were evaluated via cell culture assessments. In order to determine the cell viability of the NiTi samples, an indirect toxicity assessment was conducted using mouse L929 fibroblast cells. As-received, C and 0.5NaOH-C samples were evaluated for their cytotoxicity responses. All samples were eluted in a specific cell culture medium involving DMEM + 10% FBS at 37^{o}C for 72 h. A routine subculture was used to maintain the cell line. The samples were placed in a multi well tissue plate and L929 fibroblast cells were seeded with 10.000 of cells/ml for each well. The cell attachment process was initiated by keeping all samples in a CO_2 incubator at 37^{o}C for 24 h. Then, the MTT metabolic activity test was performed and the results were obtained by photometric reading at 570 nm. DMSO solution was used as a positive control while the DMEM medium was used as a negative control. The results were calculated by considering the negative control as 100% alive.

On the other hand, cell culture tests were conducted to investigate the influence of hydrogel coating on the biocompatibility of NiTi wires. The cytotoxicity tests (direct or indirect according to ISO 10993–5) are carried out with a list of suggested cell lines [194]. This standard proposes that Balb/3T3 is one of the suggested lines for cytotoxicity experiments and this was the reason this cell line was selected. Balb/3T3 is a stable mouse fibroblastic cell line widely used in biomaterials research. In line with the suggested procedures, direct contact cell culture experiments were performed according to ISO 10993–5 in this research. Balb/3T3 cells (ATCC ref CCL-163) were used. Cells were cultivated in a well (120 000 cells per well) in Dulbecco's Modified Eagle Medium (DMEM) with 10% fetal bovine serum (FBS) + 1% penicillin/streptomycin. Materials were put in contact with the cell layer for 24 h, and viability was estimated through an MTT assay. As a negative control, polyethylene terephthalate (PET) was used.

As a positive control, a polyelectrolyte multilayer coating made of polyarginine and hyaluronic acid loaded with sodium azide was used. The percentage of viability was estimated with reference to the culture on TCPS (Tissue Culture Polystyrene) as a control. A similar cultivation approach was followed for the 2D cell culture experiments. Following cell cultivation and UV treatment, 50,000 cells were deposited on top of the coated and non-coated samples. Cells were used at passage 13 and incubation took place at 37^{o}C and 5% CO_2 for 7 days. To observe cellular morphology and distribution, Balb/3T3 was fixed with paraformaldehyde 4% in phosphate-buffered saline (PBS) for 15 min. Cells were incubated in a Triton X-100 solution (0.1% in PBS) for 5 min. This was followed by two rinsing steps with PBS and incubation for 30 min with the bovine serum albumin (BSA) solution (1% v/v in PBS). After, DAPI/Phalloidin (F-Actin) stainings were performed. First, samples were incubated for 30 min with phalloidin at a dilution of 1/40 in the BSA solution (1% v/v in PBS), and two rinsing steps in PBS were performed for cytoskeleton staining. Second, the nuclei were labeled with DAPI (1 mg mL1; Promokine) at a dilution of 1/100 in PBS, and two rinsing steps were performed in PBS. All cell culture experiments were done in triplicates with at least two independent experiments. The imaging of the samples was carried out using a Zeiss LSM 710 confocal microscope system with randomly selected samples at multiple zones to avoid bias. For imaging, the following excitation/emission wavelengths were used (Phalloidin: 568 nm/600 nm and DAPI:358 nm/461 nm).

2.3 Research Equipment

All heat treatments and sintering processes were performed in the furnace pictured in Figure 72. The samples were placed in the furnace, and heated at a rate of 10^{o}C/min to achieve the desired temperature and were held for the selected duration.



Figure 72: Furnace for heat treatment

In this study, DSC analysis of NiTi samples were carried out to determine phase transformation temperatures. Phase transformation temperatures of austenite start (A_s) and austenite finish (A_f) were analyzed by DSC (Setaram, Model:DSC131) as shown in Figure 73 with a liquid nitrogen-cooling accessory.



Figure 73: Differential scanning calorimetry (DSC) to measure phase transformation temperatures

In characterization experiments, test samples were activated with joule heating by using the programmable power supply (TTI, Model:CPX 200). Displacement, bending angle, and temperature data were collected and recorded with the Data Acquisition System (DAQ) with different modules (National Instruments, Model: NI SCXI 1000) as shown in Figure 74.



Figure 74: DAQ systems and power supply

Magnetic stirrer with a hot plate (Isolab, Model:3L) and analytical balance were used in solution preparation and coating process as shown in Figure 75. The magnetic stirrer has a support stand with a thermometer with a temperature range of RT to 280^{o}C and adjustable stirrer speed in six different levels. The analytical balance is used to weigh NiTi samples and reagents for liquid solutions with 0.001 readability.

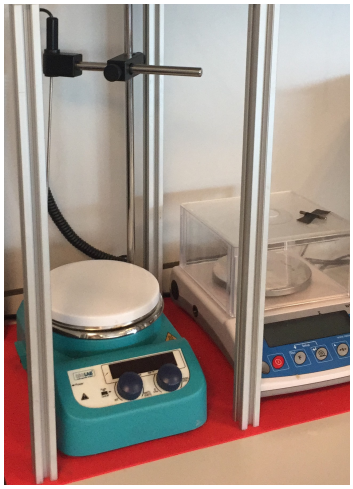


Figure 75: Magnetic stirrer and analytic balance

All electrochemical corrosion tests were carried out using a potentiostat (Gamry, Model:Interface 1000) through its software via computer at 37^{o}C and pH 7.4 in order to mimic the body environment as given in Figure 76.

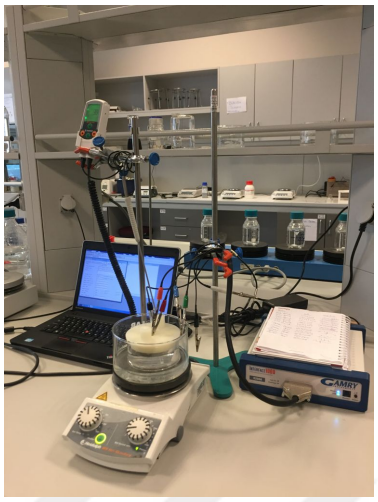


Figure 76: Experimental setup for electrochemical corrosion measurements

Surface characterization of uncoated and coated samples was conducted by using SEM, EDS, confocal and digital microscopes. Figure 77 shows confocal microscope (ZEIZZ, Smartproof 5) and digital microscope (ZEIZZ, Smartzoom 5) are utilized for measuring coating thickness and 3D surface characterization.

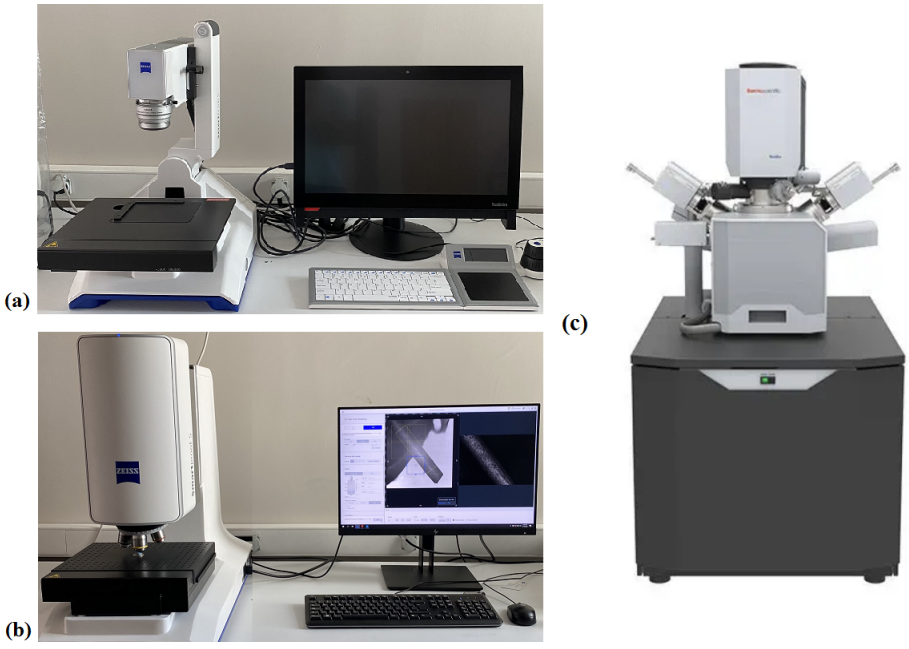


Figure 77: Equipment for surface characterization (a) confocal microscope; (b) digital microscope; (c) scanning electron microscope (SEM)

CHAPTER III

RESULTS AND DISCUSSION

This chapter is divided into two main sections. Prior to coating, functional characterization experiments were utilized to evaluate the effect of heat treatment parameters. The first section presents results related to the effect of temperature and duration parameters on the functional behavior of heat treated NiTi. These evaluations were utilized via displacement, force, repeatability, cyclic and corrosion experiments. As well as functional behavior, heat treatment effects on microstructural properties were also investigated. The second section is about the deposition of the CaP and hydrogel based coatings and is further divided into sections 3.2.1 and 3.2.2. Section 3.2.1 deals with comparing biomimetic and dip coating methods. These methods were comprehensively investigated and evaluated with experimental results and discussions. Finally, Section 3.2.2 describes the results of the effect of the hydrogel layer on NiTi surfaces. These effects were evaluated via optical microscope, SEM and EDS analysis, contact angle, hardness measurement, and bending and cytotoxicity experiments.

3.1 Effects of Heat Treatment on the Functional Behavior of NiTi Shape Memory Alloy

As it is mentioned in the previous chapters, heat treatment is one of the most known processes that affect the functional properties of NiTi SMA. Studies have repeatedly shown that the effect of heat treatment parameters is significant [195, 196]. In this section, these effects were evaluated and discussed in order to have an understanding of the functional behavior of NiTi samples that heat treated with selected temperature and duration parameters.

3.1.1 Determining transformation temperatures

In this work, two complementary techniques are successfully employed for determining the transformation temperatures of near equiatomic NiTi alloys. Results of the austenite start (A_s) and austenite finish (A_f) temperatures with heat treatment conditions are summarized in Table 15.

Table 15: Transformation temperatures of heat treated NiTi samples measured by DSC

Conditions	**Austenite Start**	**Austenite Finish**
460^{o}C for 30 minutes	32^{o}C	43^{o}C
460^{o}C for 60 minutes	36^{o}C	49^{o}C
520^{o}C for 30 minutes	37^{o}C	48^{o}C
520^{o}C for 60 minutes	42^{o}C	58^{o}C
600^{o}C for 30 minutes	47^{o}C	63^{o}C
600^{o}C for 60 minutes	49^{o}C	66^{o}C

These results are determined by using the DSC method. Results show that austenite transformation temperatures are affected by heat treatment conditions. As it is observable from the table, an increase in the annealing temperature and duration postpones austenite transformation, as was previously observed for various NiTi compositions. Both A_s and A_f temperatures tend to increase with the increase of heat treatment temperatures for a duration of 30 minutes. The DSC graph of the sample that was heat treated at 520^{o}C for 30 minutes is shown in Figure 78. As given in Table 15, A_s and A_f temperatures were found as 37^{o}C and 48^{o}C, respectively. M_s and M_f temperatures were determined as 5^{o}C and -5^{o}C. On the other hand, the transformation temperatures were determined from the temperature displacement graph as given in Figure 79. In the experiment, the NiTi actuation was monitored, while NiTi displacement was plotted with real-time temperature data. The displacement

of the LVDT core is given in millimeters. This test was performed with only one sample that was treated at 520^{o}C for 30 minutes for validation. The austenite start (A_s) and austenite finish (A_f) temperatures of the NiTi wire were determined by the intersection of the tangent lines and were found to be 35^{o}C and 47^{o}C, respectively.

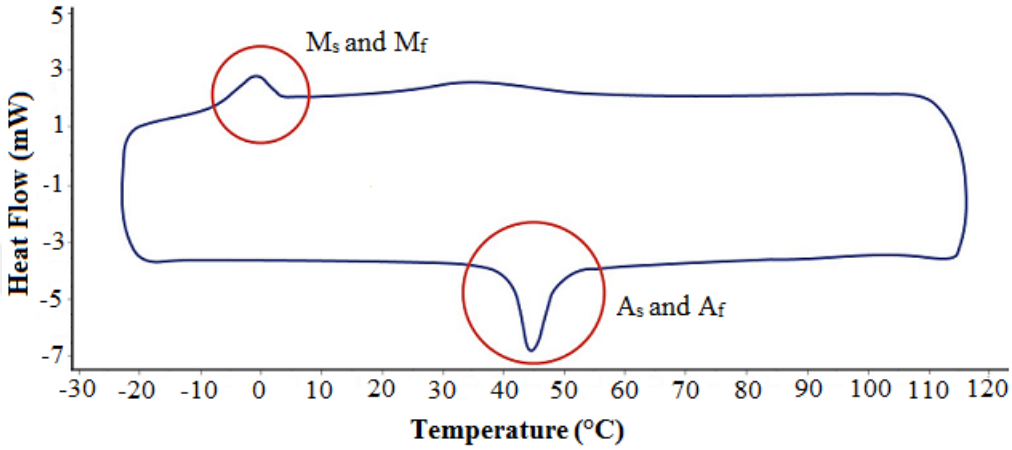


Figure 78: DSC heating and cooling curves: the austenite and martensite transformation temperatures of NiTi samples treated at 520^{o}C for 30 minutes

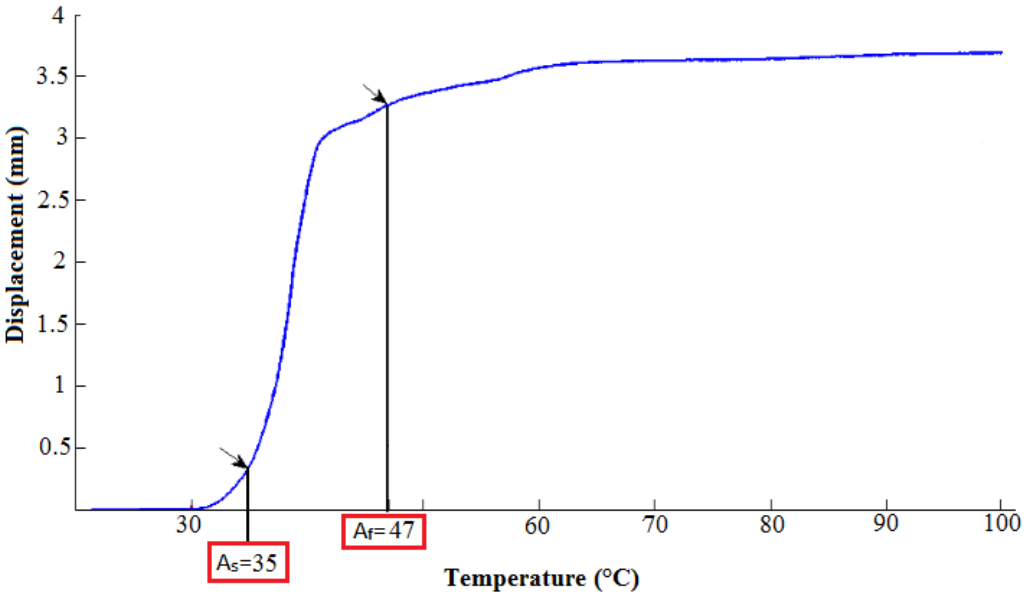


Figure 79: Temperature-displacement graph to determine austenite transformations temperatures

3.1.2 Displacement and repeatability experiments

Initial attempts [20, 21] have revealed that mechanical properties of shape memory alloys highly depend on heat treatment parameters. This section primarily presents the relationship between displacement behavior and temperature for all selected conditions via free bending test. All heat treatment parameters for the shape-setting process have been obtained experimentally. Initial efforts have been made with variable temperatures for 30 and 60 minutes as given in Figure 80. It is worth noting that all NiTi samples show significant displacement except the sample treated at 600^oC for 60 minutes. The total displacement performance of this sample was found insufficient, because the heat treatment around the recrystallization temperature, 600^oC, leads to a reduction in both yield strength and ultimate tensile strength [27]. Therefore, the maximum critical temperature for the present study should be defined as up to 600^oC.

After all, the same experiments were repeated at temperatures of 460 and 520^oC for a different duration. The results indicated that there is consistency in both experiments. The findings clearly indicate that for both temperature ranges, samples were treated with 30 min. duration show better displacement performance than other samples. Among duration parameters, the samples were treated for 30 min. duration possesses desirable properties and is selected as a duration condition. These observations are strengthened by the findings of temperature measurements. The temperature may play an important role in the instruments used for medical purposes. In order to address this concern, it is crucial to determine the maximum temperature during actuation. The first measurement was conducted with the sample treated at 520^oC and the maximum surface temperature was found between 80 to 90^oC. On the contrary, decreasing the heat treatment temperature resulted in higher surface temperatures around 100-120^oC. These uncertainties about the temperature make the use of NiTi difficult without thermal insulation for in-vivo studies since an observational verification of these predictions remains challenging.

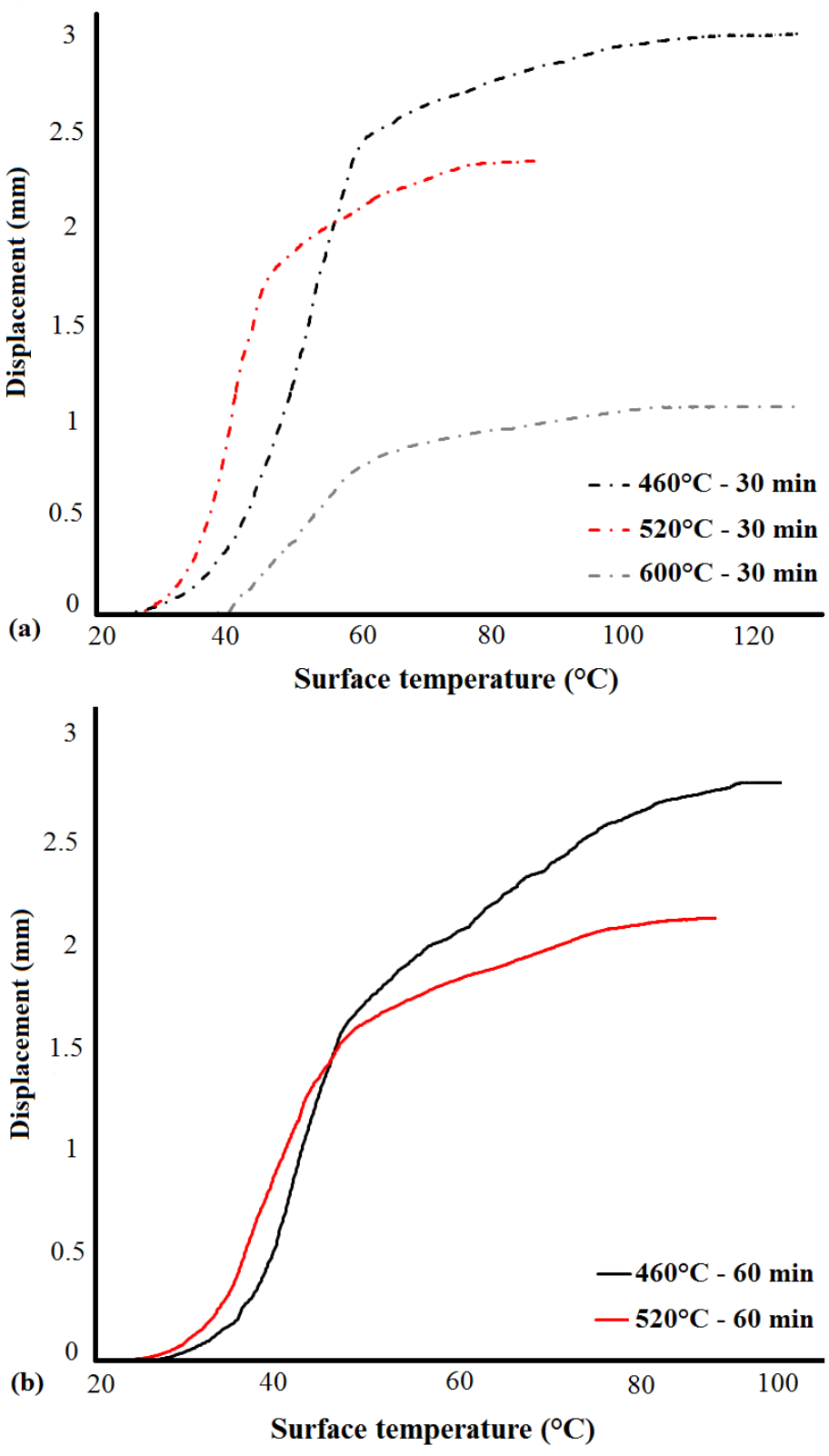


Figure 80: The displacement behavior of NiTi samples for the constant duration (a) 30 minutes and (b) 60 minutes

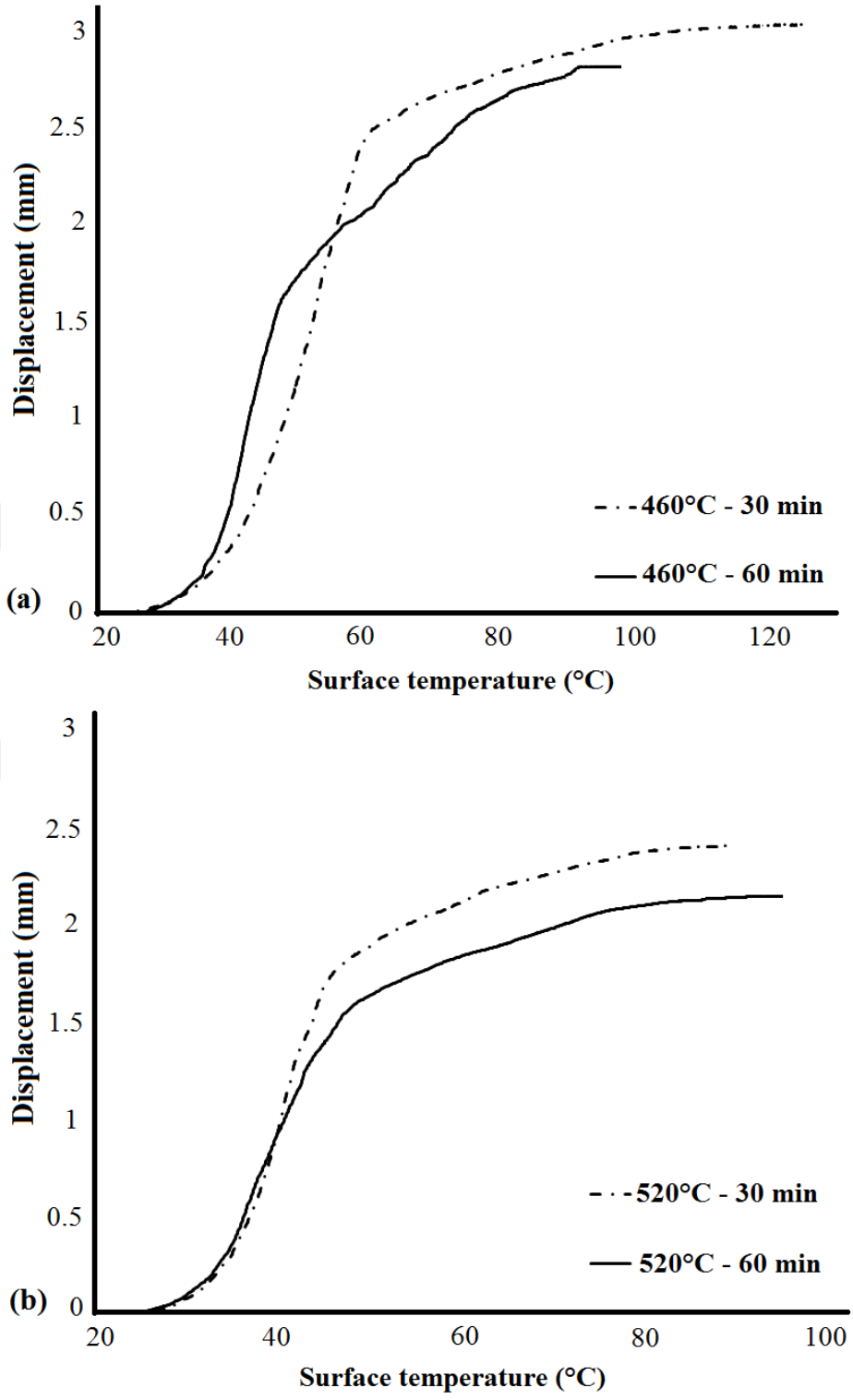


Figure 81: The displacement behavior of heat treated NiTi samples for different conditions (a) 460^{o}C for 30 and 60 minutes; (b) 520^{o}C for 30 and 60 minutes

Repeatability of implantable materials has become a hot topic in the medical industry field, particularly for orthopedical purposes. There have been many efforts to characterize the repeatability of NiTi alloy as a function of heat treatment parameters. In order to evaluate the repeatability, experiments were performed for selected parameters for five cycles as displayed in Figure 82. These results confirm the findings in Figure 80 and Figure 81 that increasing the heat treatment temperature decreases the maximum reached temperature. The increase of maximum reached temperature with decreasing annealing temperature proves the transformation temperature effect.

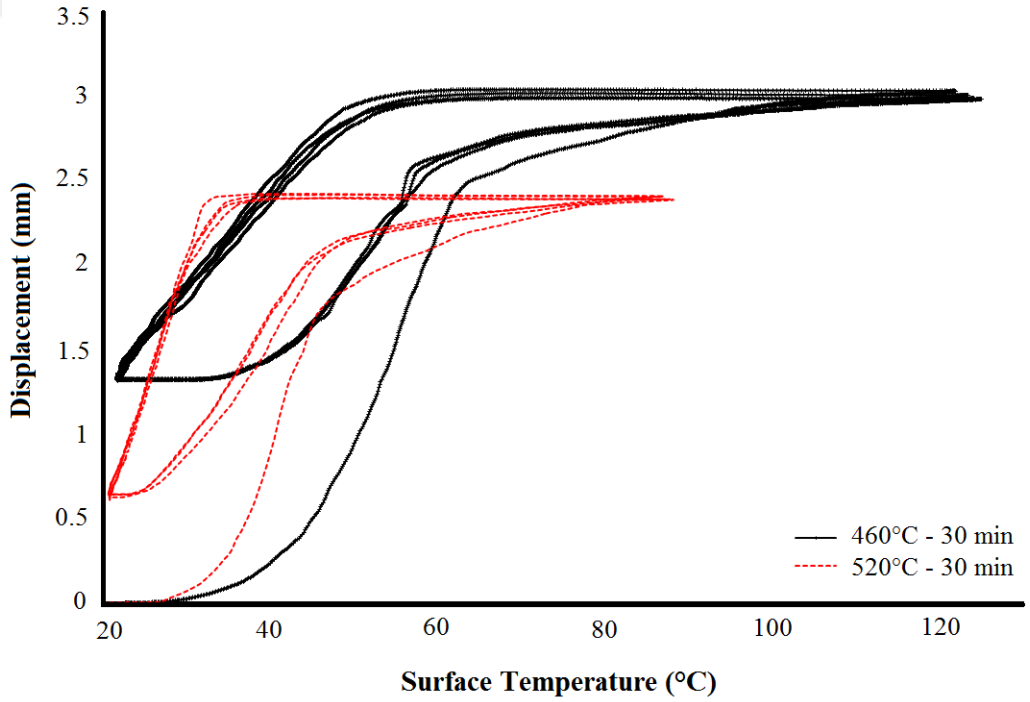


Figure 82: The repeatability behavior of heat treated NiTi samples for different conditions

The continuous repeatability of 460^{o}C and 520^{o}C samples are shown in Figure 83. The performance of the sample treated at 520^{o}C for 30 minutes was more stable than the other sample. Moreover, the sample treated at 520^{o}C reached 50 cycles without any deterioration, while the sample heat treated at 460^{o}C showed unstable behavior.

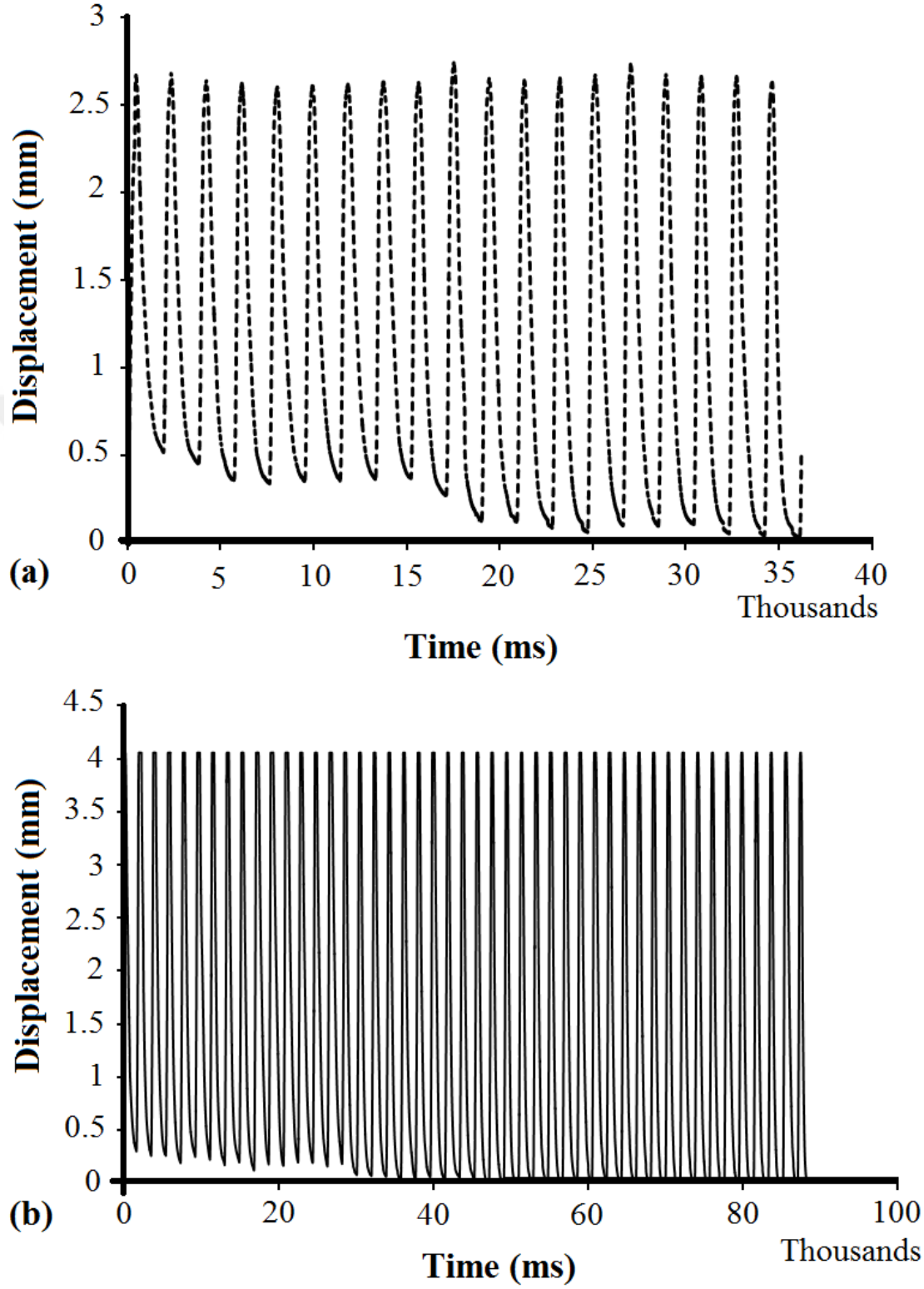


Figure 83: Repeatability of heat treated NiTi samples: 460^{o}C (above) and 520^{o}C (below) for 30 min.

Repeatability experiments were conducted for the sample treated at 520^{o}C for 50 cycles as demonstrated in Figure 84. Each cycle constituted an actuation between a bending angle of 0 to 60 degrees. It is worth mentioning that the experiment shares similar results to displacement-based tests.

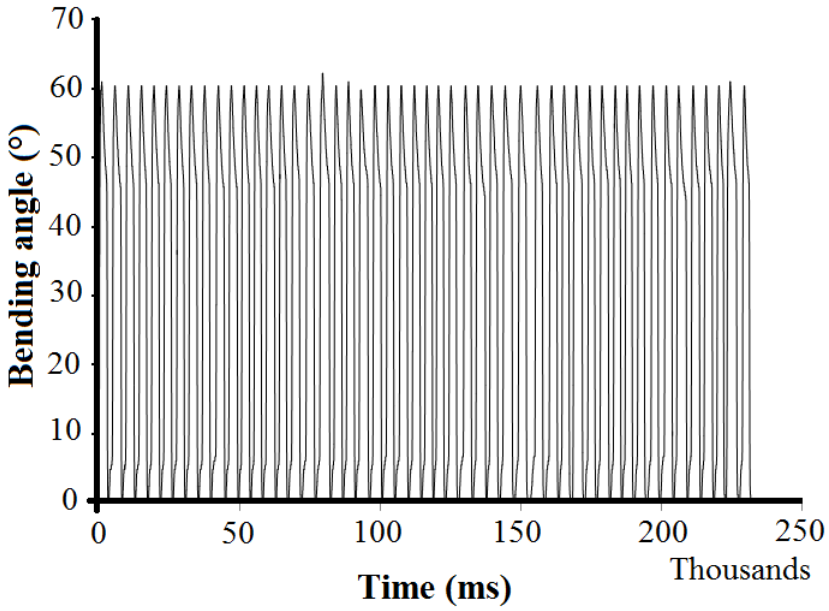


Figure 84: Repeatability of 520^{o}C for 30 minute treated NiTi samples

3.1.3 Force experiments

As it is reported in previous studies [197, 198], NiTi wires became very attractive since they have lower elastic modulus, higher elastic range, and light continuous forces in particular for orthodontic treatments. For many purposes, it is important to know the effect of heat treatment on the exhibited force. In the majority of the characterization investigations, force experiments were conducted for all heat treatment conditions to provide comprehensive examinations. Force results are summarized in Figure 85 as a function of treatment parameters. Results indicate that an increase in the treatment temperature leads to a decrease in the sustained actuation force levels. It can be seen that the sample heat treated at 520^{o}C exhibits lower forces than the sample treated at 460^{o}C.

On the other hand, except at 600^{o}C, an increase in the treatment duration results in higher actuation force levels peaking above around 470 gf after 60 min annealing at 460^{o}C. It is reported that increased duration supports the formation of Ti_3Ni_4 precipitates, which are effective in strengthening by impeding dislocation motion thus improving the shape memory behavior [199]. The discrepancy at the highest temperature could be attributed to the activation of softening mechanisms such as recrystallization at temperatures above 500°C, which apparently is the dominating factor in dictating the resulting functional response herein [200].

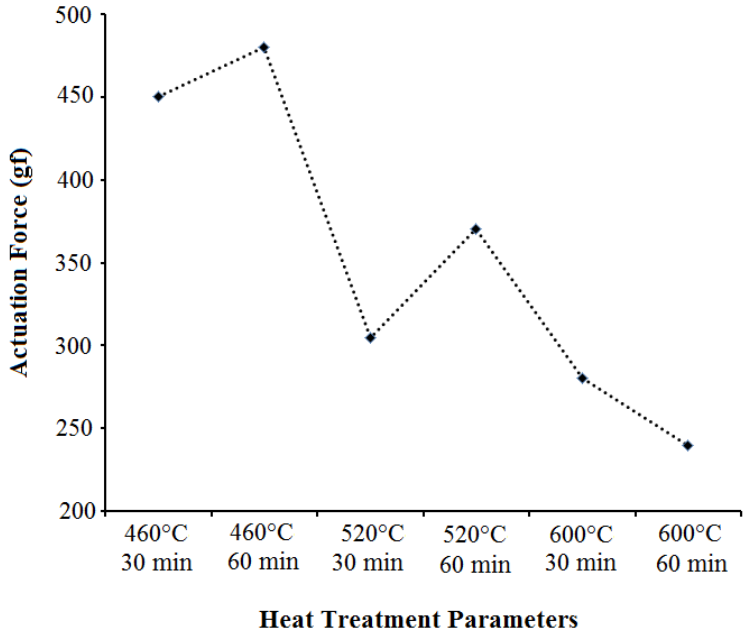


Figure 85: Actuation forces of NiTi as a function of heat treatment conditions

Figure 86 shows the force measurement of the sample heat treated at 520^{o}C for 30 minute heating and cooling thermomechanical cycle. These findings are roughly comparable with the previous studies. Braucli et al. reported that the increase of austenite finish temperature can lead to decreased force levels [201]. This observation is in good agreement with the presented findings since the measured A_f of the sample treated at 460^{o}C is higher than the sample treated at 520^{o}C.

Along the same lines, the force experiment also confirms the same result that the decreased force level is caused by the rise of the annealing temperature. This observation may be related to the formation of precipitates that can increase material strength via the interactions with dislocations, and thus eliminate their motions [201].

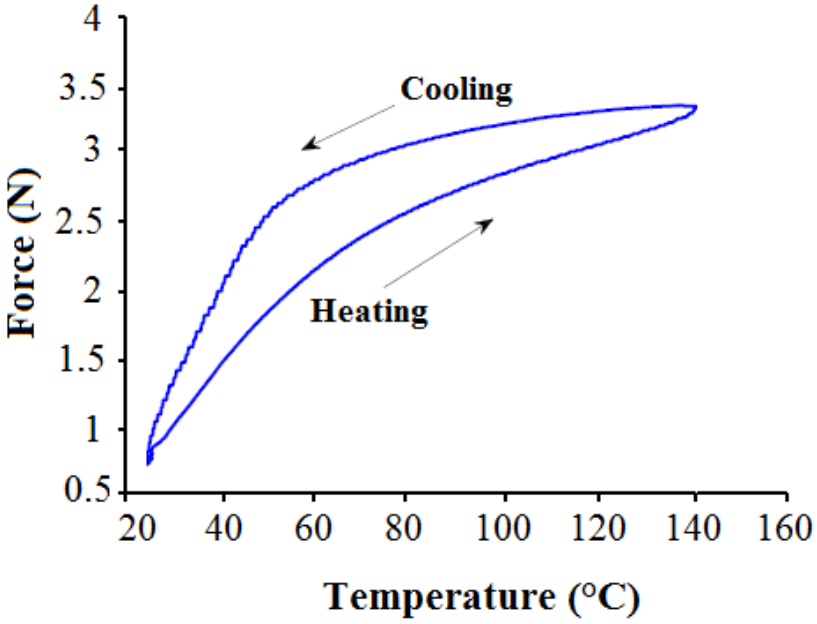


Figure 86: Force-temperature relation for the sample treated at 520^{o}C for 30 minutes

3.1.4 Cyclic experiments

The cyclic experiments were carried out in a custom-built setup at body temperature in SBF and at a constant bending angle of 15^o. Four different types of controllers; P, PI, PID, and PD; were tested on the experimental setup. The main equations that are crucial to improve the position control of the controllers are as follows:

$$u(t) = K_p e(t) + K_i \int e(t^{'}) d(t^{'}) + K_d \frac{de(t)}{dt} (5)$$

Where K_p, K_i, and K_d are non-negative coefficients for the proportional, integral, and derivative terms, respectively. These parameters are widely used in examining the performance of each controller.

These control terms can be tuned to obtain the appropriate control. The tuning conditions highly depend on each K_p, K_i, and K_d parameter. It is possible to set the unused parameters to zero. The system's response to the proportional controller has been examined for different K_p values in a custom made setup. First, the system has an oscillation as represented in Figure 87. Then, the K_p value was set as 5, 10, 15, 20, 30, and 50. It was seen that the system response becomes more stable and reaches nearly the target angle where K_p equals 10, as seen in Figure 87. On the other hand, the system's response was analyzed by using PI, PD, and PID controllers.

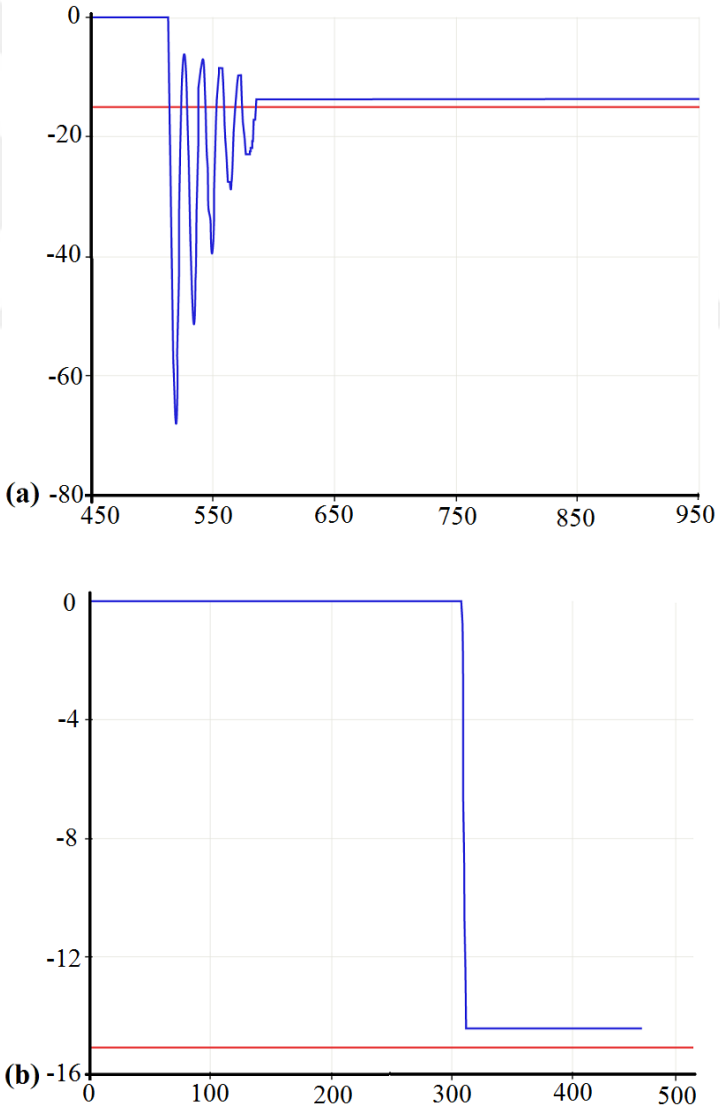


Figure 87: Response of the proportional controller (a)before and (b)after tuning

Adding derivative, integral, or derivative-integral values to the proportional controller makes the system unstable as shown in Figure 88. From a mechanical point of view, this may be attributed to the experimental setup and some of its drawbacks, such as external forces and torque due to the connection between the DC motor and the rail system. PI, PD, and PID controllers could not generate the desired position.

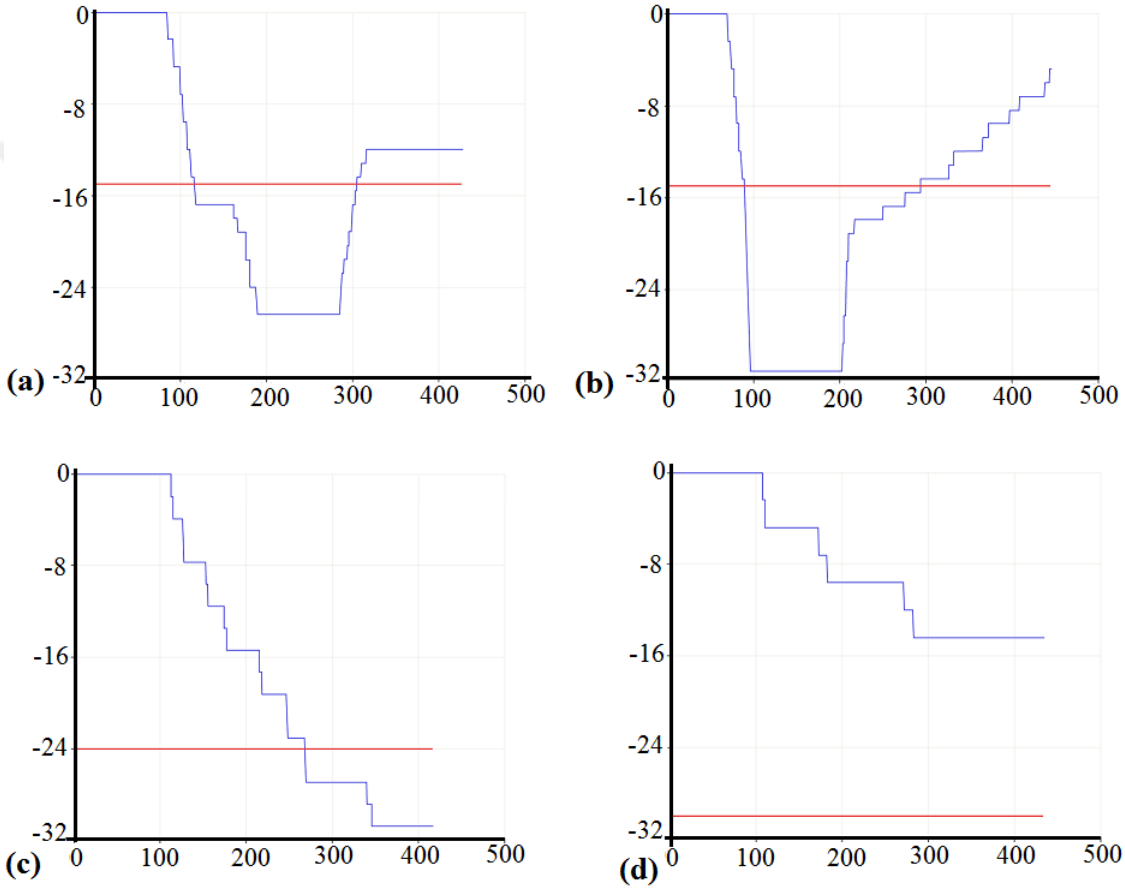


Figure 88: Response of (a) PI; (b) PD; (c) PID with different K_p, K_i, and K_d values; (d) PID with different K_p, K_i, and K_d values controllers

After obtaining the selected controller, cycle tests were utilized for all heat treated samples. There are some efforts on the cyclic life of NiTi shape memory alloys. However, there is no study that compares the cyclic behavior of NiTi shape memory alloys in different body-like media and at different frequencies.

It was reported that implantable materials were subjected to high stresses and cyclic loading in a harsh body environment resulting in the failure of the implant [202, 203]. The fatigue life determination of the NiTi samples was obtained for different frequencies in two different body-like mediums. All experiments were conducted at 1,4 and 10 Hz in the different body like mediums. These conditions were selected according to the literature survey. The cyclic experimental series started with the test that was conducted at 1, 4, and 10 Hz in simulated body fluid and Ringer solution. Figure 90 presents the number of cycles of the NiTi samples before fracturing as a function of heat treatment parameters. Among the heat treatment conditions, the substrate that was heat treated at 600^{o}C for 60 min has the highest number of cycles before the fracture occurred. Furthermore, the total number of cycles increased as the heat treatment temperature increased. These findings confirmed the work done by Vojtech reported on the improvement of cyclic life with the increase of heat treatment temperature [25].

The duration also has the same effect as the treatment temperature, which enhanced the cyclic life of the NiTi sample. It was found that there is no clear correlation between dry condition, SBF, and Ringer solutions and the total number of cycles. The lowest number of cycles was nearly the same for the sample that was heat treated at 460^{o}C for 30 and 60 min whereas the highest number of cycles was found in the sample that was heat treated at 600^{o}C for 30 and 60 min. The biggest difference was found in the NiTi sample that was treated at 600^{o}C for 30 min. To further confirm the correlation between the total number of cycles and the frequencies in the experiment, another test was performed where the body-like fluid was kept constant while the bending of the NiTi sample was recorded at 1 Hz, which is the given value in the literature for simple walking. Figure 90 is a sample representation of the results of the corrosion based cyclic experiments in which the total number of cycles increased for all conditions.

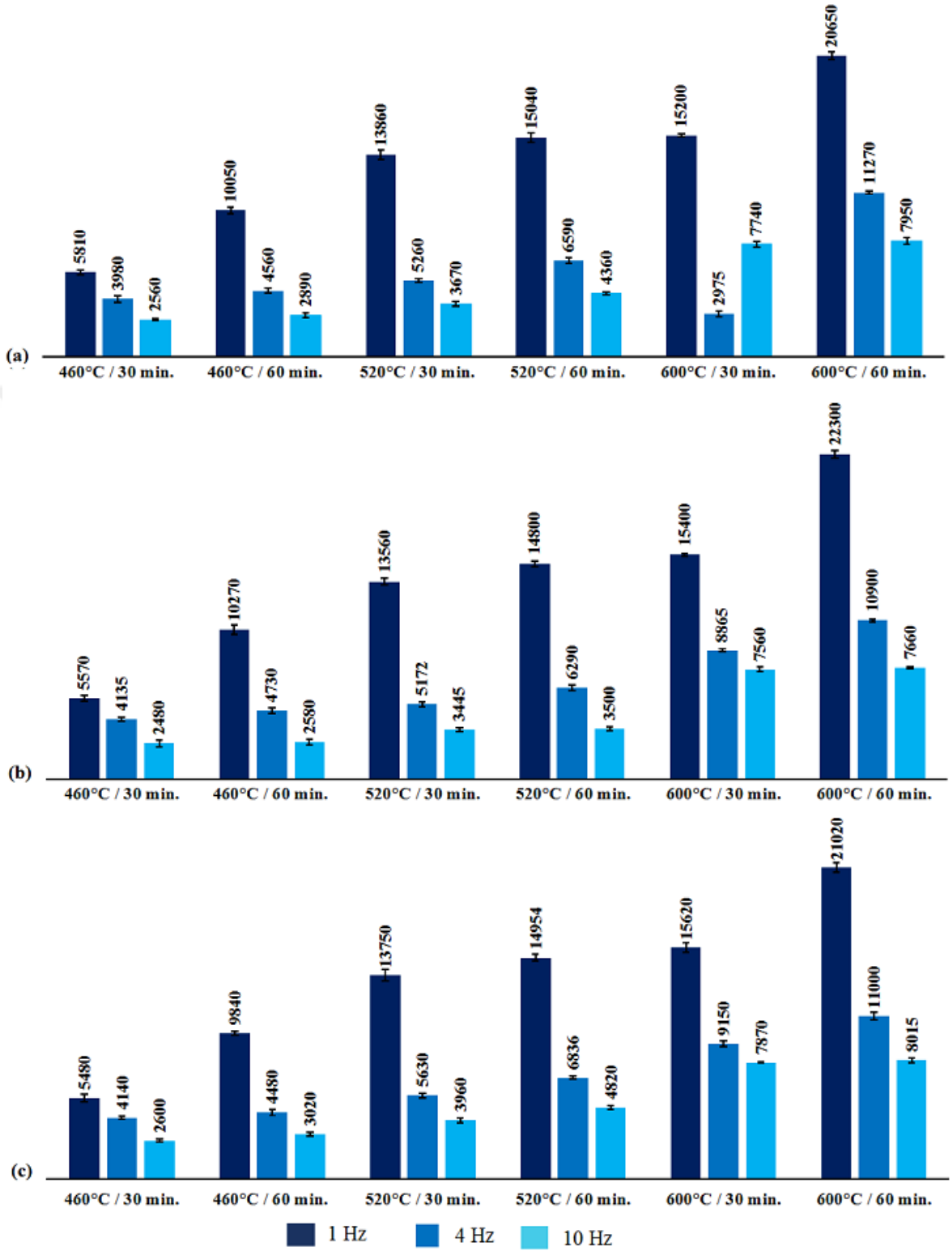


Figure 89: Effect of heat treatment on the total number of cycles before failure in different conditions (a) dry; (b) simulated body fluids, (c) Ringer solution

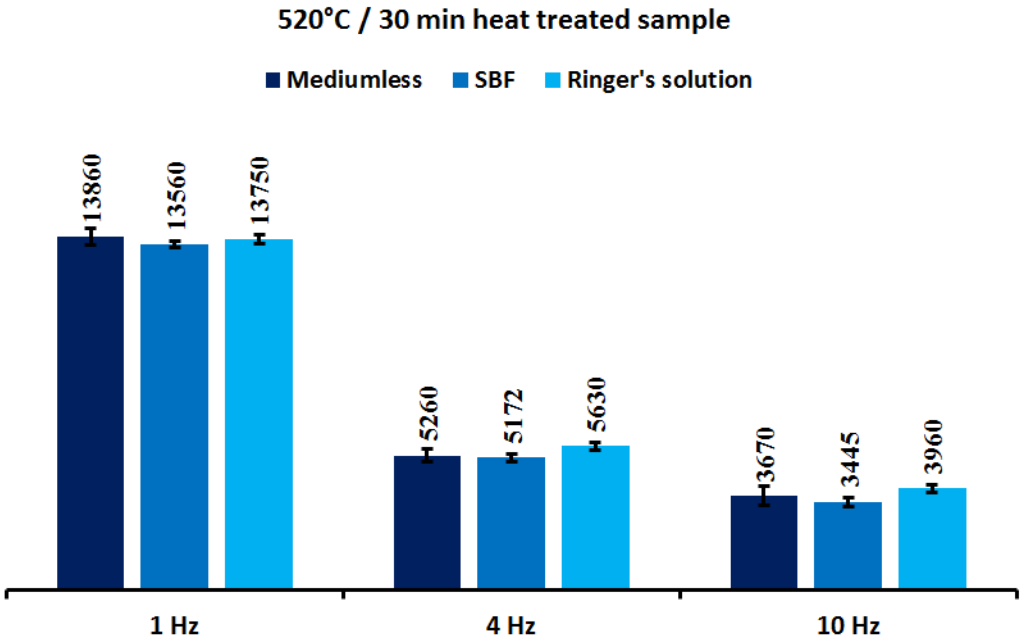


Figure 90: Effect of testing medium on the total number of cycles before failure in (a) dry; (b) simulated body fluids, (c) Ringer solution

3.1.5 Investigation on the hardness of NiTi

A preliminary study of the effect of heat treatment conditions with respect to the hardness properties was performed using microhardness apparatus with a 1 kg load. The indentation imprint's diagonal length measurement was obtained to compare the hardness of the heat treated NiTi shape memory alloys. These results show that an increase in treatment temperature leads to a reduction in hardness as shown in Figure 91. The substrate that was heat treated at 460^{o}C showed the highest hardness than that of the others. The findings confirm a significant drop in hardness for heat treatment at 600^{o}C. The discrepancy at the highest temperature could be attributed to the activation of softening mechanisms. Such softening mechanisms activate due to the recrystallization process at temperatures above 520^{o}C. The effect of duration is similar that the hardness of NiTi substrate increases with a 60-minute duration

raise due to the refinement in the precipitate size [22] except for the sample that was treated at 600^{o}C. The behavior between 30 and 60 minutes at 460^{o}C is in agreement with the results at 520^{o}C. It is reported that longer duration results in the formation of strengthening Ti_3Ni_4 precipitates. However, at 600^{o}C the duration effect does not act as expected, as reported by Mitwally et al [22]. The results obtained are in line with observations in the literature and the cyclic experiments that were summarized in the previous section.

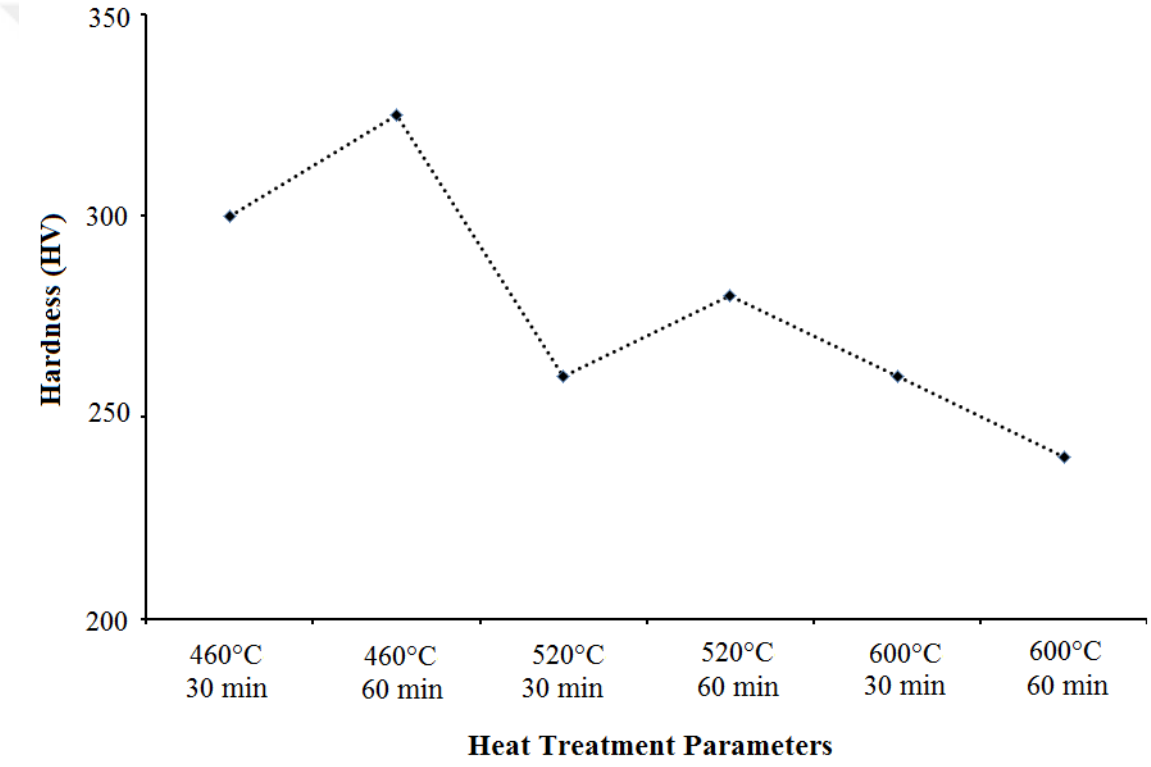


Figure 91: The variation of the hardness of NiTi samples as a function of heat treatment parameters

3.1.6 Corrosion properties

Corrosion is likely to have been seen as a problem for thousands of years, long before any effective preventive methods were discovered. Researchers focus on controlling the possible reactions between living tissues and implant material surfaces in order

to prevent harmful effects by increasing the life quality. The effects of the heat treatment conditions on the corrosion performance of NiTi alloy were evaluated through electrochemical methods in simulated body fluid solution at a pH level of 7.4 and at room temperature. The potentiodynamic tests were utilized in order to investigate the corrosion properties of the NiTi samples. The corrosion current density and corrosion rates were calculated via Tafel fit method.

Figure 92 demonstrates the potentiodynamic polarization curves. All samples were weighed before and after the potentiodynamic tests. Material loss for each parameter is summarized in Table 16. These findings are confirmed by the corrosion rates. All measurements were performed in duplicate and the average values were recorded. The highest material loss is found for the sample that was treated at 520^oC for 30 min while the minimum material loss occurred in heat treatment at 600^oC. These results are consistent with the studies in the literature.

Table 16: Total material loss after potentiodynamic test

Sample	**Material loss (gr)**
460^oC-30min	0.01543
520^oC-30min	0.02388
600^oC-30min	0.00815
460^oC-60min	0.00745
520^oC-60min	0.01829
600^oC-60min	0.00525

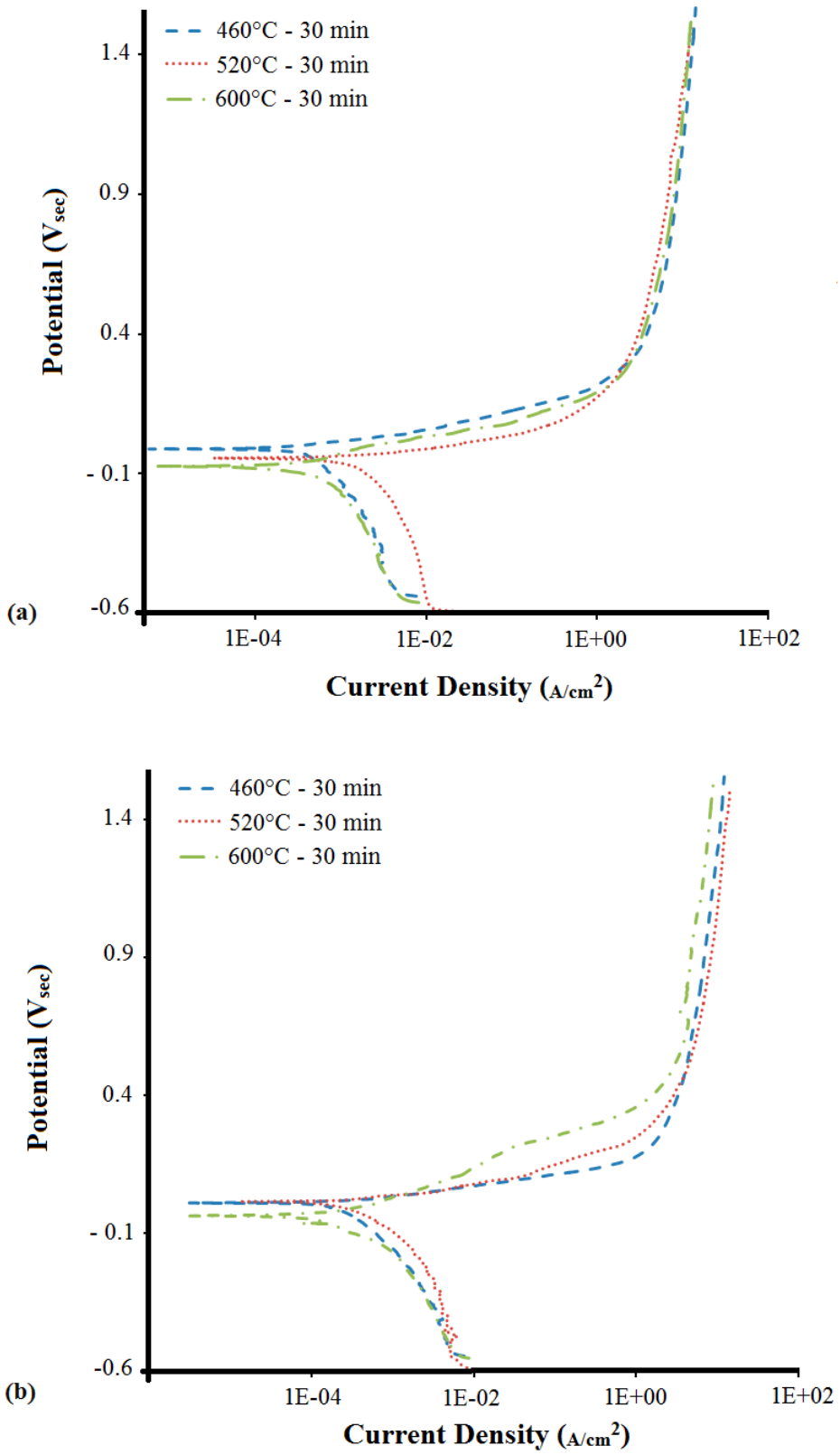


Figure 92: Potentiodynamic polarization curves of the heat-treated samples at 460^{o}C, 520^{o}C, 600^{o}C (a) 30 min and (b) 60 min, and the results of corrosion experiments

On the other hand, the increase in duration improved the corrosion resistance at constant temperature except for the sample that was heat-treated at 600^{o}C. The current densities of the 60 min-treated samples were significantly lower than those of 30 min-treated ones, pointing to an enhancement of the corrosion resistance. This change can be explained by the deposition of a stable passive oxide film. It was reported that the growth of the oxide layer on NiTi is slow when the duration is less than 2 hours [204]. Among all samples, the sample that was heat-treated at 600^{o}C for 30 min showed the lowest corrosion resistance that was obtained due to the passive layer in Kokubo based SBF which may also have resulted in better biocompatibility.

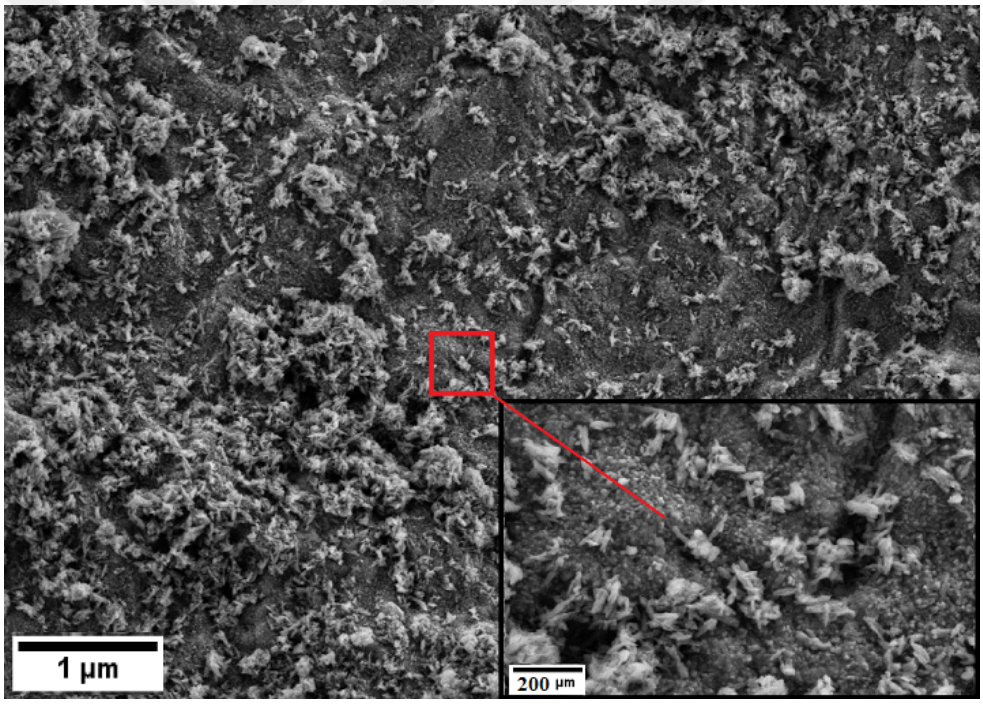


Figure 93: Surface morphology of heat treated at 520^{o}C for 30 min. NiTi sample

The surface morphology of the NiTi sample that was treated at 520^{o}C for 30 min. is shown in Figure 93. SEM images of the NiTi surface developed with heat treatment revealed flake-like structure based oxide layer as reported in previous studies [82, 205]. These structures were agglomerated in different areas and may act as a barrier resulting in enhanced corrosion behavior.

In the literature [160, 161], it is reported that pitting corrosion is one of the major reasons that lead to the failure of the implant. Figure 94 presents the microstructure of the heat-treated NiTi sample after the potentiodynamic corrosion experiment where a scanning electron microscope was used. The pits on the surface were highly observable and they may also contribute to the decrease in the cyclic life of the sample. In order to prove that the cyclic test was performed at the same frequencies in simulated body fluid. Results show the cyclic response of heat treated sample was significantly decreased after the corrosion test as shown in Figure 95 which was definitely expected.

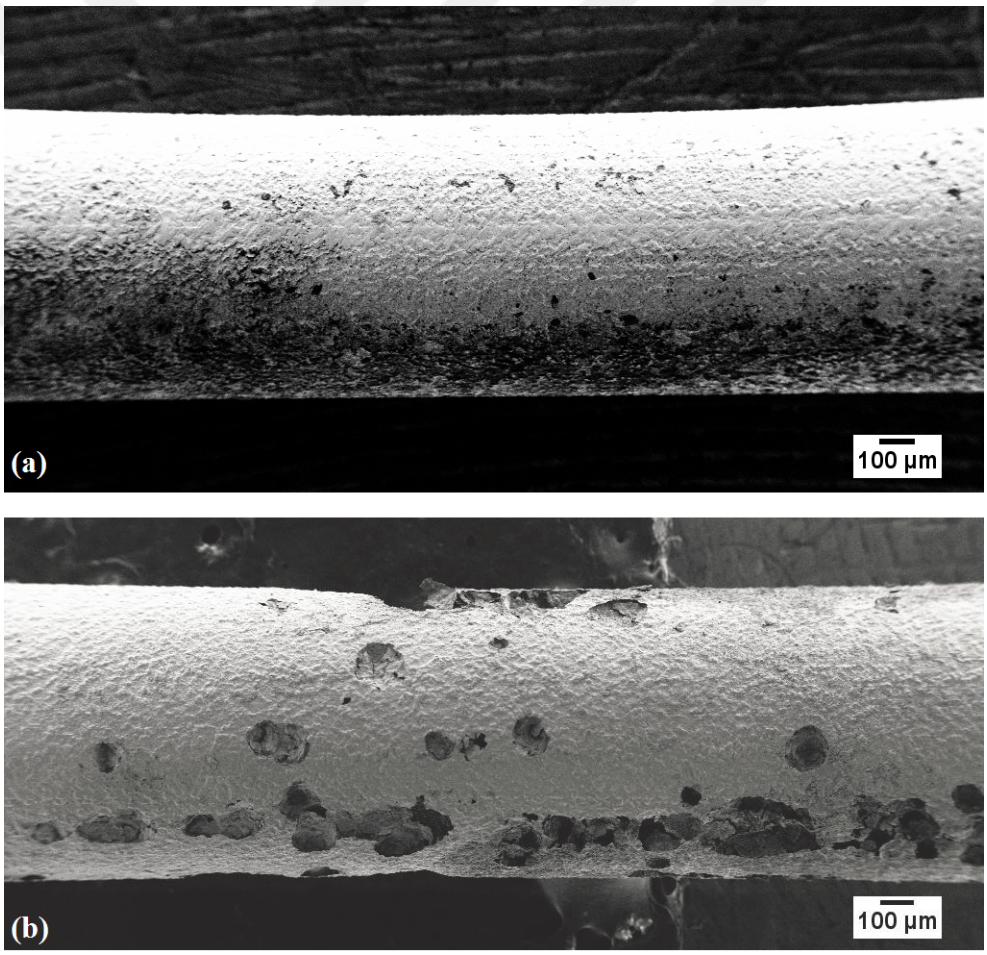


Figure 94: SEM surface micrographs of NiTi treated at 520^{o}C for 30 min. (a) before and (b) after potentiodynamic polarization experiment

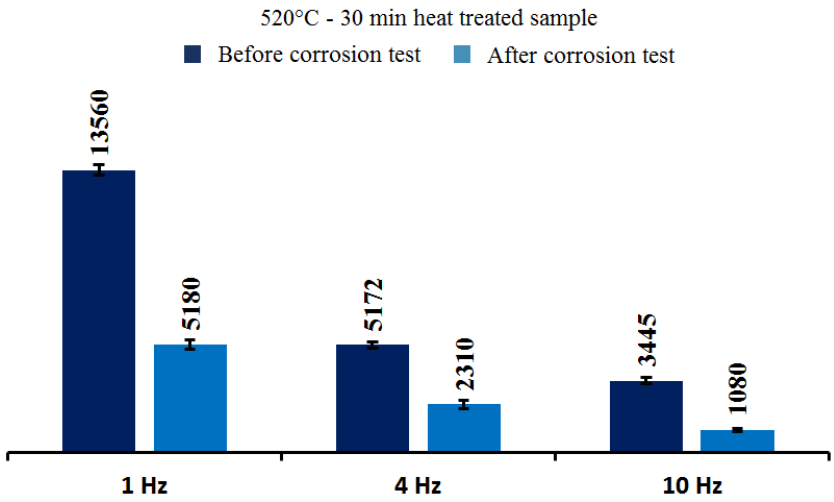


Figure 95: Effect of corrosion on the total number of cycles of the sample treated 520^{o}C for 30 min.

Besides corrosion experiments, in silico modeling of corrosion and image analysis of the corrosion process were developed with mathematical expressions for as-received NiTi SMA. The adopted values for parameters used in this simulation are summarized in Table 17. The results of the corrosion simulation are shown as generated images with different time steps.

Table 17: Selected parameters for corrosion modeling

Parameters	**Value**
pH	7.4
ϕ_m	0.23 V
ϕ_s	0.2 V
T	310.15 K
C	0.2 M/dm^3
D	0.3 m^2/s
z	0.2 Faraday

First, the influence of the pH value was investigated between the range of 7.4 to 10, with an increment of 0.2. Figure 96 shows the calculated metrics and mean corrosion for variation of pH. The results show that the increase in the pH value in the range of 7 to 10, increases the slope of faster the corrosion. For example, for step 5, high mean corrosion has already been achieved with pH=7.6. These results were also confirmed by experiments. As expected, greater corrosion is achieved at later steps. These results are also in accordance with the study conducted by Capoi [206] that shows the increment of pH value resulted in increased corrosion.

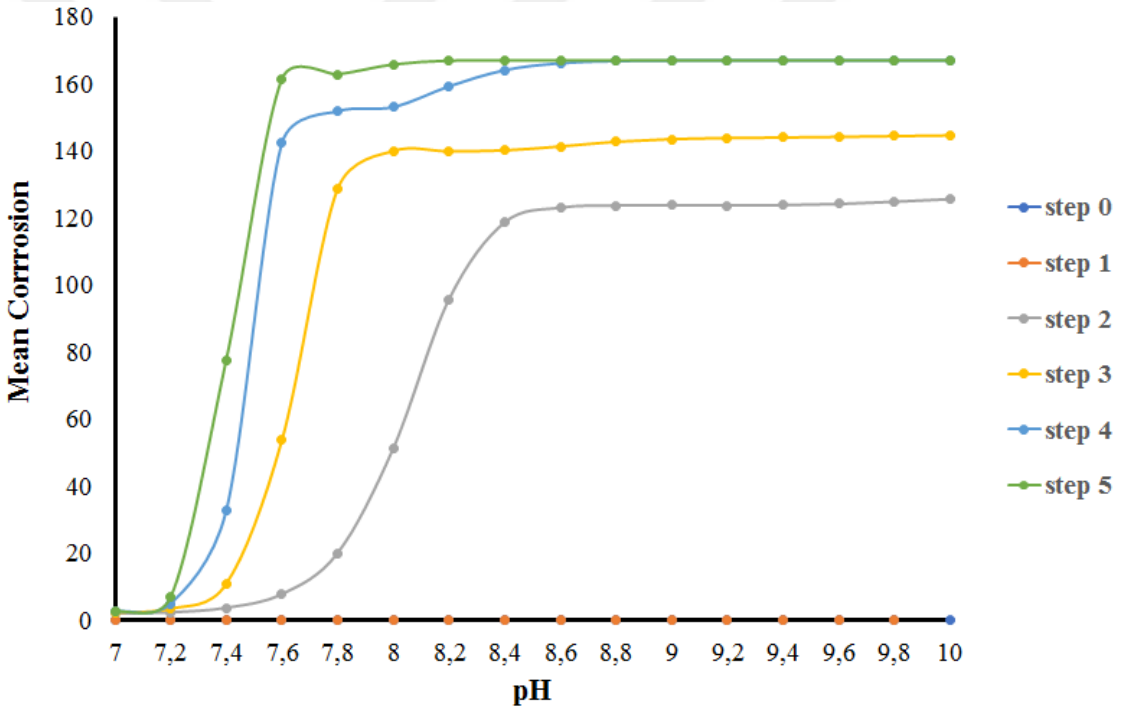


Figure 96: Relation between mean corrosion and pH of as-received NiTi sample

The effect of temperature was also investigated between the range of 24^{o}C to 40^{o}C. The results were given in the following Figure 97. It was found that the effect of investigated temperature range on corrosion rate is minimal at low temperatures between body to room temperature. These results are in line with the experimental studies from the literature, such as considered by Ahmad [207].

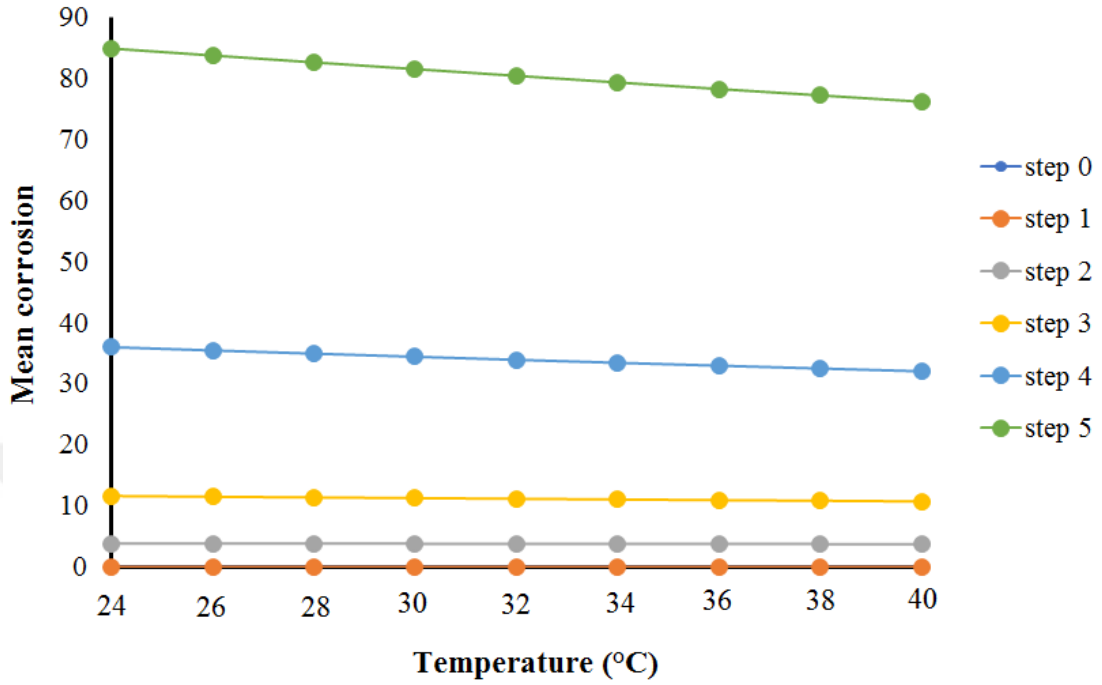


Figure 97: Relation of mean corrosion and temperature as-received NiTi sample

The influence of the concentration of the reaction species was also investigated. The parameter of C varies between the range from 0.1 to 0.5, with a step of 0.1. The influence of the concentration of the reaction species C is similar to the results obtained during the investigation of the influence of pH value, but with a higher impact than that of the pH as presented in Figure 98. As an example, consider that the mean corrosion converges towards the maximal value of 160 even for the smaller ranges (0.1 to 0.5) of this parameter. In comparison, the maximal mean corrosion can only reach the value of 80 in a situation with a corresponding range change in the pH value (7-7.5). Again, the same conclusion is reached in Trepanier [208] that with the increase in concentration species, both the mass transport rate and the chemical reaction rate are going to be influenced.

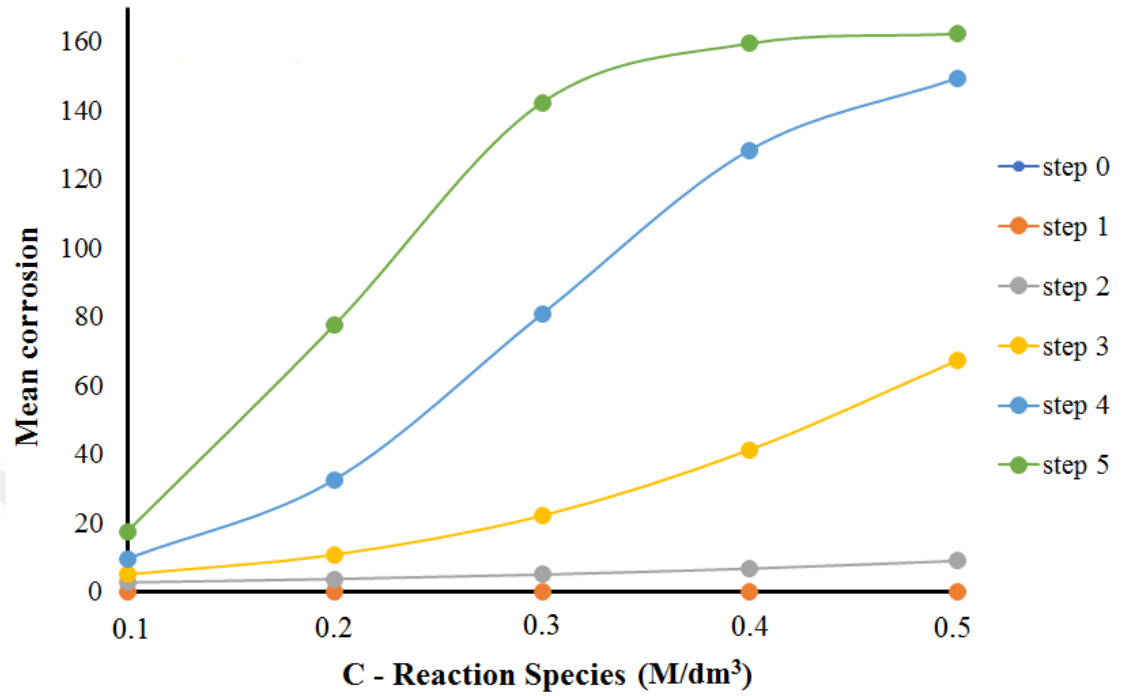


Figure 98: Relation of mean corrosion and concentration of the reaction species as-received NiTi sample

Moreover, the influence of diffusivity of the reaction species (D) was investigated. In this simulation, D is varied in the range of 0.1 to 0.5, with a step of 0.1. Mean corrosion for the variation of this parameter is presented in Figure 99. The diffusivity of the reaction species D tends to have an effect similar to the reaction species C, however with a smaller impact, as a variation in this parameter leads to slopes that are not as steep and maximal values that are smaller. The trend is similar to the variation of the reaction species C, but the effects on the level of corrosion are smaller.

Finally, the influence of the charge of the reaction species z was evaluated in the range between 0.1 to 0.5, with a step of 0.1. The mean corrosion for the variation of this parameter is presented in Figure 100. The charge of the reaction species z has mostly the same effect on the mean corrosion as the reaction species C, indicating a high level of influence which means very high level of corrosion is achieved with a small increase of parameter reaction species z.

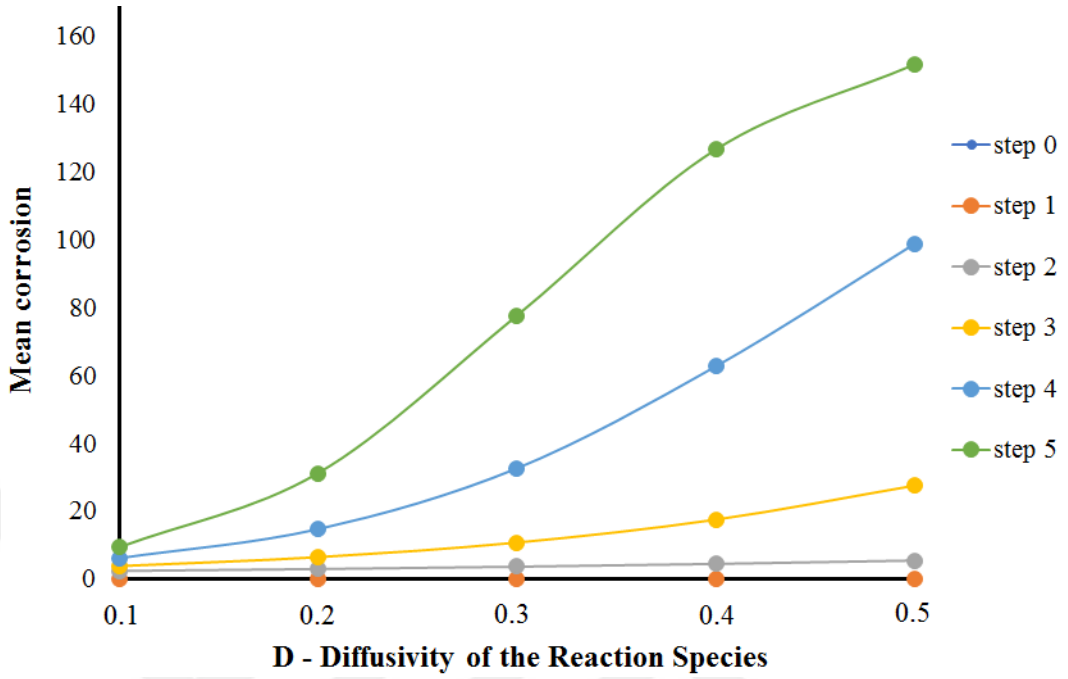


Figure 99: Relation between mean corrosion and diffusivity of the reaction species as-received NiTi sample

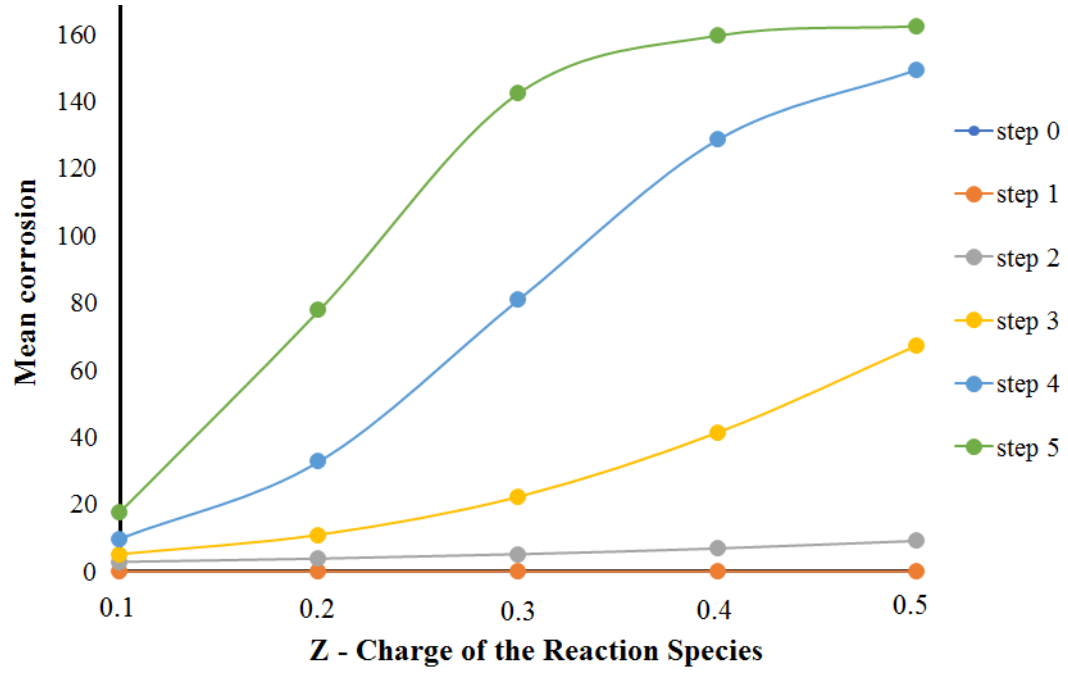


Figure 100: Relation between mean corrosion and charge of the reaction species as-received NiTi sample

Numerical simulation results of corrosion investigation are difficult to confirm experimentally. The potential difference, the concentration of the reaction species, diffusivity of the reaction species, the charge of the reaction species, and the changes throughout the corrosion process were not monitored due to the nature of the electrochemical process. Also, a large number of experiments to test the effect of the variations in pH and temperature are time consuming to perform. In such circumstances, the presented simulation findings should be useful to better understand the spatial influence of various factors on the material surface. As the values for modeling factors including pH, potential difference, temperature, concentration of the reaction species, diffusivity of the reaction species, and charge of the reaction species in the experiment were not all available. So that it was not possible to fully compare the experiment and simulations. However, the values for mean corrosion show the same order of magnitude is achieved in simulations and experiments, indicating that the methodology used in the simulations is adequate. Besides these efforts, corrosion experiments were performed in simulated body solution with two different temperature including room and body temperature to investigate and compare the effect of temperature on corrosion process. Additionally, pH is an another parameter that may monitored with experimental electrochemical experiments. Furthermore, two different pH values 7.4 and 9 were selected as control parameters for corrosion experiments to validate the effect of pH on corrosion process of simulation results. It was found that there is no significant difference found for different temperatures (corrosion rates for RT: 11.68 and BT:11.84) and , which is in accordance with the simulation results as well, thus these measurements agreed with the simulation results. Moreover, it was found that the corrosion became faster with the increase of pH from 7.4 to 9. These results were given in Figure 101 with electrochemical curves. Corrosion rates for pH of 7.4 and 9 were found 11.68 and 14.29, respectively. It may concluded that all experiment results have same trend with the simulation for selected pH and temperature parameters.

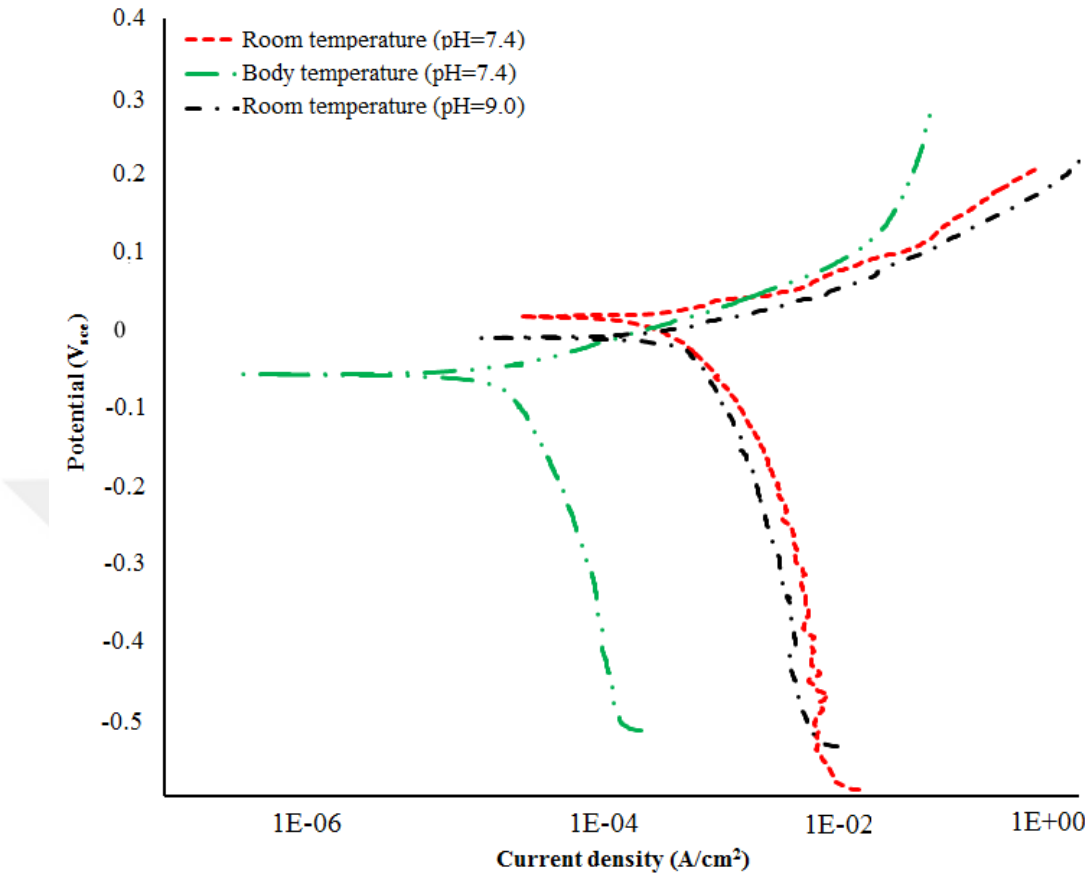


Figure 101: Electrochemical curves of NiTi samples for different temperature and pH values

Besides experimental results, review of the literature regarding comparison of the numerical results with other experiments in the literature also showed a good comparison of the proposed methodology with both numerical simulation and their experimental results. Pidaparti [209] et al. showed that the material loss curve has the same trend as the mean corrosion in presented study. They also showed that the extent of corrosion has a trend of sigmoidal function with a steepness coefficient larger than 1, meaning that it increases up to a certain number of cycles, until the whole surface is completely corroded. The same trend and curve shape are observed in this study.

Additional review of the literature has shown that a higher pH value leads to faster corrosion over time. The factor of pH is important for the corrosion resistance of a material because hydrogen ions can interact with the material and modify the surface which can affect it's corrosion resistance [208]. The influence of pH in simulations is discussed regarding the Figure 96 showing that greater corrosion is achieved over time. This is in correspondence with the findings from Capoi [206] showing that the corrosion rate is higher for the first hours of immersion, and after several days the value becomes stationary. Temperature effects on corrosion have shown both in literature and simulations that there is no major effect on corrosion in the investigated ranges as referred in Trepanier et al. [208]. Figure 3.1.6 also shows the corrosion states at six different time steps. Black pixels indicate the uncorroded cells and white pixels indicate fully corroded cells.

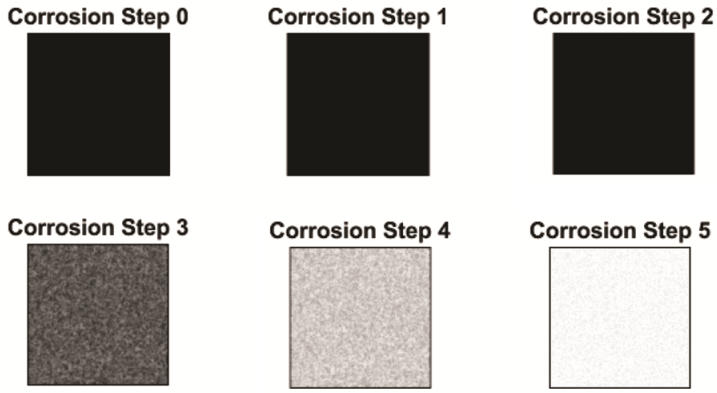


Figure 102: Corrosion state S(u,t) at time steps t=0, 1, 2, 3, 4, 5 respectively

The relation between mean corrosion values and the percentage of corroded area on the surface was summarized in Table 18. In previous section, it was mentioned that mean corrosion value was varied between 0-255. In this table, these mean corrosion values were converted to percentage values in order to clarify the effect of pH on the corrosion process with selected range that vary from 7 to 10 for 0, 19.2, 38.4, 57.6, 76.8 and 96 hours.

Table 18: Relation between mean corrosion and percentage of corrosion

Parameters	0 h		19.2 h		38.4 h		57.6 h		76.8 h		96 h	
	Mean Corrosion	Corrosion (%)	Mean Corrosion	Corrosion (%)	Mean Corrosion	Corrosion (%)	Mean Corrosion	Corrosion (%)	Mean Corrosion	Corrosion (%)	Mean Corrosion	Corrosion (%)
ph 7	0	0	0	0	2.057	0.806	2.365	0.927	2.616	1.026	2.616	1.026
pH 7.2	0	0	0	0	2.397	0.9401	3.473	1.362	5.044	1.978	6.902	2.706
pH 7.4	0	0	0	0	3.761	1.474	10.885	4.268	32.703	12.825	77.696	30.469
pH 7.6	0	0	0	0	7.833	3.071	53.731	21.071	142.320	55.811	161.417	63.300
pH 7.8	0	0	0	0	20.063	7.868	128.648	50.450	151.786	59.524	162.841	63.859
pH 8	0	0	0	0	51.326	20.128	139.967	54.889	153.074	60.029	165.784	65.013
pH 8.2	0	0	0	0	95.714	37.535	139.905	54.864	159.253	62.452	166.934	65.464
pH 8.4	0	0	0	0	118.677	46.540	140.149	54.960	164.075	64.343	166.974	65.48
pH 8.6	0	0	0	0	123.078	48.265	141.350	55.431	166.163	65.162	166.974	65.48
pH 8.8	0	0	0	0	123.729	48.521	142.725	55.970	166.802	65.412	166.974	65.48
pH 9	0	0	0	0	123.771	48.537	143.512	56.279	166.948	65.469	166.974	65.48
pH 9.2	0	0	0	0	123.740	48.525	143.831	56.404	166.971	65.478	166.974	65.48
pH 9.4	0	0	0	0	123.834	48.562	144.010	56.474	166.973	65.479	166.974	65.48
pH 9.6	0	0	0	0	124.174	48.695	144.193	56.546	166.974	65.48	166.974	65.48
pH 9.8	0	0	0	0	124.835	48.955	144.393	56.624	166.974	65.48	166.974	65.48
pH 10	0	0	0	0	125.623	49.264	144.607	56.708	166.974	65.48	166.974	65.48

3.1.7 Investigation on surface characteristics

Contact angle measurements were performed to examine the surface wettability properties of heat treated NiTi. The results of measurements are summarized in Table 19. Uncoated NiTi wire samples have an average contact angle of 111^o, which is significantly higher than heat treated NiTi samples. It can be clearly seen that all contact angles tend to decrease with heat treatments.

The hydrophilicity of surfaces was increased with an increase in both temperature and duration. The more hydrophilic surface may be attributed to lower surface energy and biocompatibility which may increase the acceptability of the suggested implant in the human body.

Table 19: Average contact angle values of heat treated NiTi samples

Sample	**Contact Angle Values (degree)**
As-received	111.15
460^oC - 30 min	102.69
460^oC - 60 min	99.12
520^oC - 30 min	96.62
520^oC - 60 min	93.43
600^oC - 30 min	93.28
600^oC - 60 min	89.77

The effects of heat treatment on the microstructural level have been widely investigated for especially austenitic compositions of NiTi alloys [210, 211]. The increase of A_s and A_f transformation temperature is one of the most important macroscopic effects [212]. The impacts of heat treatment temperature and duration on the microstructure of NiTi are initially analysed with optical microscopy as demonstrated in Figure 103. The martensitic needles become apparent due to the treatment process.

It can be seen that as the heat treatment temperature rises, the martensitic needles become coarser. At the same temperature, longer heat treatments result in needle enlargement as well. Another implication of duration is the formation of precipitates as evidenced in Figure 103. The increased tendency of precipitation with longer heat treatment has been shown in a number of works.

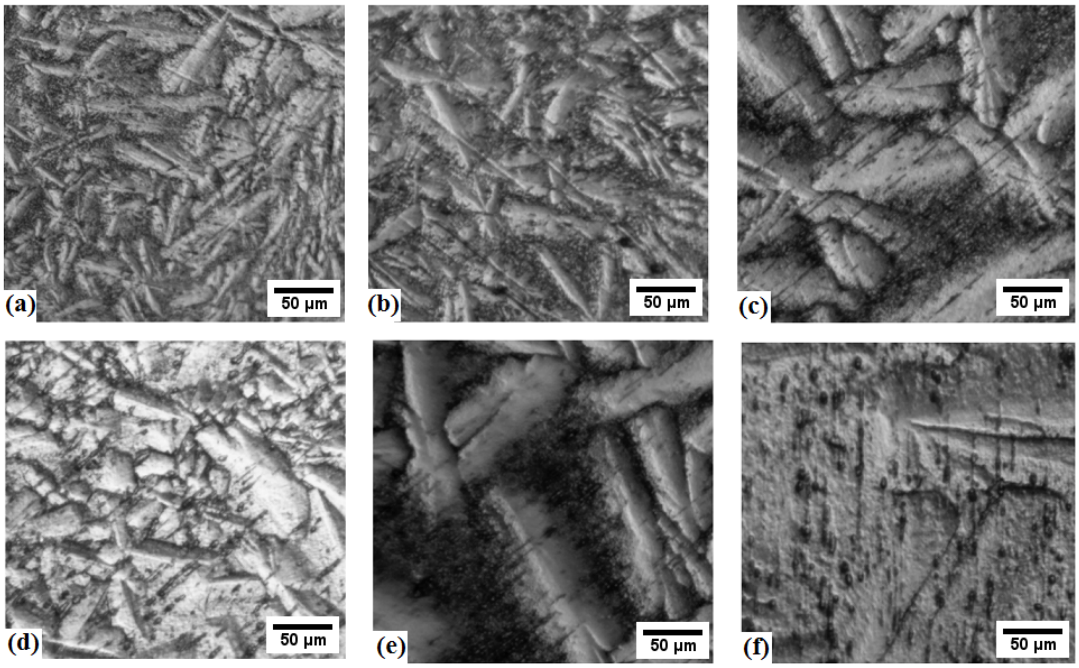


Figure 103: Optical micrographs of NiTi samples with different heat treatment parameters (a) 460^{o}C for 30 min; (b) 520^{o}C for 30 min; (c) 600^{o}C for 30 min; (d) 460^{o}C for 60 min; (e) 520^{o}C for 60 min; (d) 600^{o}C for 60 min

Further investigations of the surface morphologies of the NiTi SMA were investigated with SEM analyses. Figure 104 a shows the microstructure of as-received NiTi and the heat treated NiTi at the same magnifications. This finding clearly demonstrated the heat treatment conditions' effect on the surface morphology of NiTi substrates. As it was previously reported, heat treatment is one of the most widely used methods resulting in the presence of TiO_2 layer on the surface. In the SEM images, the annealed NiTi exhibited a different surface morphology due to the

presence of TiO_2. Further investigations at a high magnification clearly showed these structures as shown in Figure 104 b. These structures were agglomerated in different areas and may act as a barrier and limit the risk of Ni release from the implant surface [213, 214].

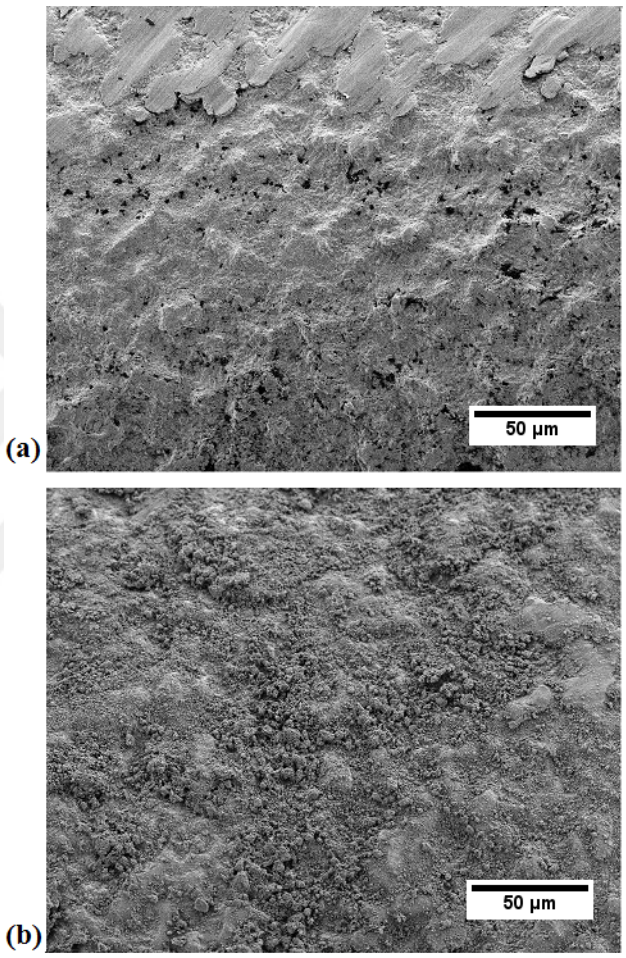


Figure 104: SEM images of NiTi samples: (a)as-received NiTi; (b)heat treated sample at 520^{o}C for 30 min

These characterization studies have been undertaken to explore the role of heat treatment parameters on the mechanical behavior of NiTi shape memory alloys. Based on all these results, the optimum shape setting parameters were chosen as 520^{o}C and 30 minutes. These parameters were found to be very sufficient in providing the necessary mechanical behavior of NiTi shape memory alloys for this dissertation.

3.2 Effect of biocompatible coating on the functional behavior of NiTi Shape Memory Alloy

NiTi alloys have been utilized as biomedical instrument for several years. Since Ni release is arguably the most fundamental concern, controlling Ni ions release from the surface is an important parameter to take into account for medical instruments as they can have long term in-vivo implications. The formation of ceramic and polymer based layer on the NiTi surface or modifying NiTi surface may resulted in enhanced biocompatibility and better mechanical properties. The aim of this section is to investigate the formation of CaP and hydrogel layer on NiTi wires to produce a barrier againts possible Ni release and the effect of chemically surface treatment methods on necessary properties of NiTi for medical purposes.

3.2.1 CaP coated NiTi Shape Memory Alloy

This subsection deals with the influence of coating method on the surface characteristics of NiTi. In this manner, biomimetic and dip coating methods were utilized with selected parameters. On the other hand, effect of NaOH pretreatment was also investigated prior to dip coating process. In this section, all samples were heat treated at 520^{o}C for 30 minutes after CaP coating.

3.2.1.1 Effect of Coating Method on the Surface Characteristics of NiTi Shape Memory Alloy

First of all, the coating layer was confirmed visually with an optical microscope with lower magnification for biomimetically coated NiTi surfaces. Optical microscope images of uncoated and coated NiTi surfaces are shown in Figure 106. The surface of biomimetically coated NiTi under optical microscopy appeared not to be changed significantly. The formation of the layer becomes observable after as given in 24 h Figure 106 b. With the increase of duration time, the density of the layer tends to increase since the formation of the coating layer was affected by the immersion time.

After immersing in the SBF for 48 hours, some CaP based particles initiate on the surface, but the surface was not covered (Figure 105 c). In order to validate the deposition process, the half of NiTi surface was immersed in SBF solution. The boundary between immersed and non immersed parts is obvious as seen in Figure 105 d, by the red line. The scratch marks were still present on the NiTi surface which means the surface was not fully covered. Besides visual investigations, the total weight change was recorded as a function of immersion periods for 6, 24, 48, and 72 hours. For 6 hours of immersion, there was no change in the weight of the NiTi samples. The weight change was significant between 24 and 48 hours, as observable in optical micrographs. After 48 and 72 hours, both immersed samples were weighed, and found that increasing the duration to 72 hours did not enhance the deposition of the CaP layer on the NiTi surface.

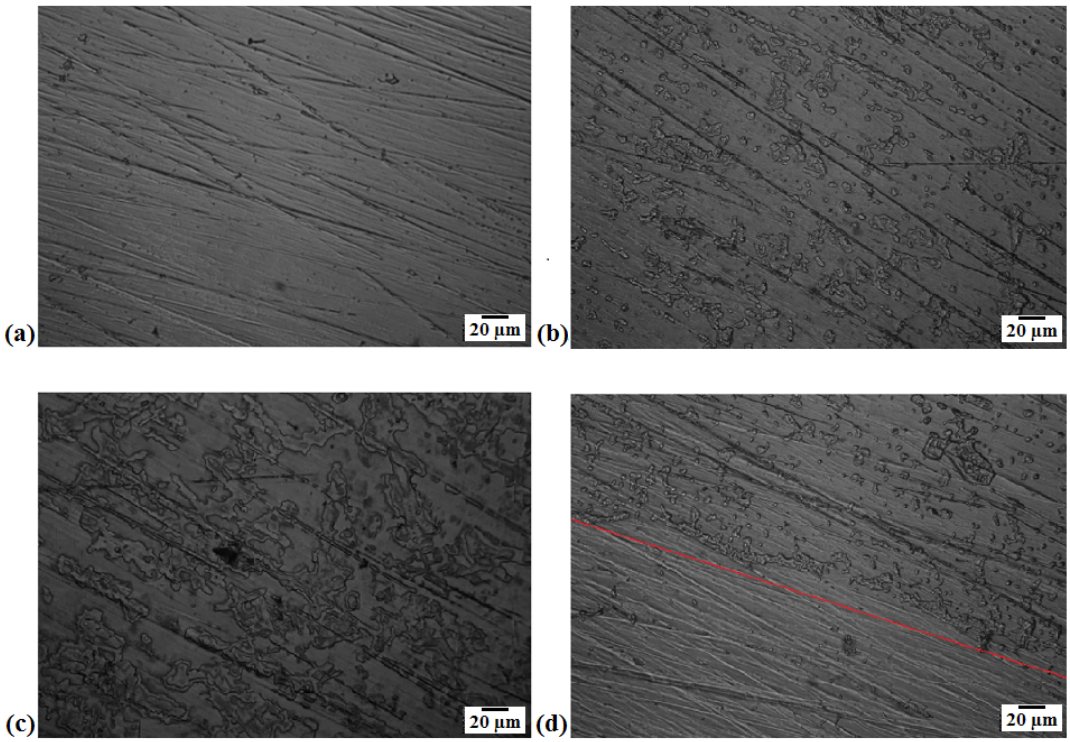


Figure 105: Initial experiments with optical microscopy at 20x magnification (a) as-received NiTi; (b) 24 h; (c) 48 h and (d) half immersion for 48 h

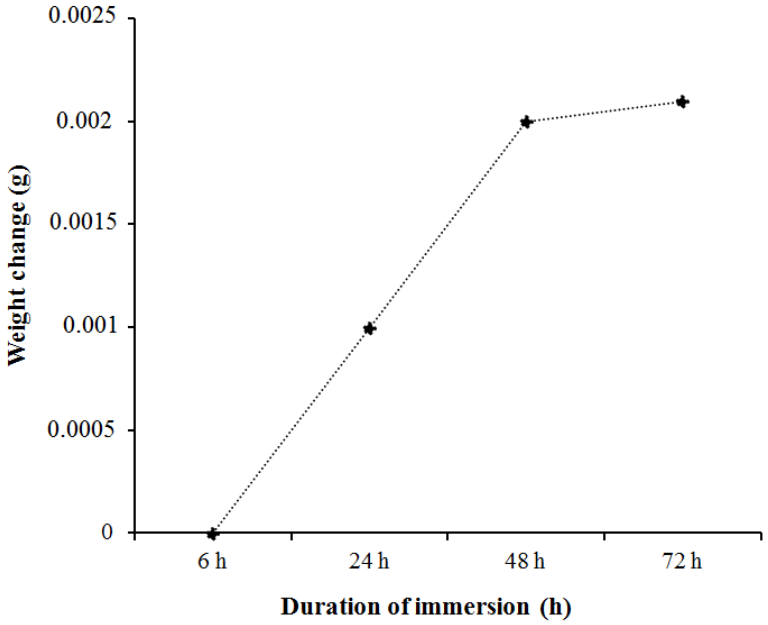


Figure 106: Total weight change as a function of immersion periods

Besides the biomimetic method, the dip coating method is utilized to deposit CaP based layer on NiTi surfaces as it is reported as one of the most efficient known coating methods due to its simplicity. So that other attempts were given for the dip coating methods that could provide a more quantitative CaP based layer on the wire shape NiTi surfaces. The half of NiTi sample was scratched in order to reveal the boundary between coated and uncoated sides as shown in Figure 107.

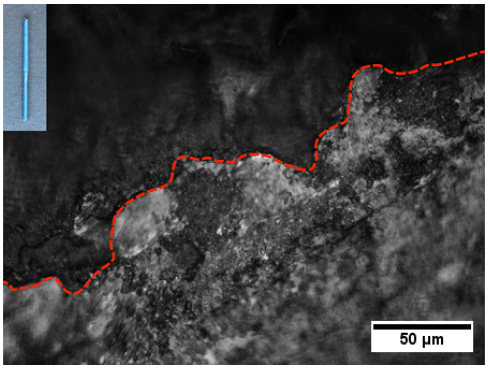


Figure 107: Optical image of initial experiments on dip coating method at 20x of as-received NiTi

Scanning electron microscopy (SEM) image of the NiTi wire sample prior to any form of coating is shown in Figure 108 a. SEM observations of the coated surfaces using two different coating methods show that the dip coating method results in a homogenous coating layer without any significant surface cracks even after the sintering stage (Figure 108 b). It was highly observable that the NiTi surface is covered by a film layer. Even if a relatively lower sintering temperature had to be chosen because of the limitations due to the shape setting characteristics of the NiTi wire substrate, the coated calcium phosphate tribasic layer resulted in a successful coating layer. Previous studies show that HA coatings are generally sintered between 800 to 1300^{o}C [215, 216]. However, this temperature range is not applicable for shape memory alloys since destroyed the shape memory effect. In order to overcome these difficulties, the sintering temperature was selected according to the results of NiTi's functional characterization experiments.

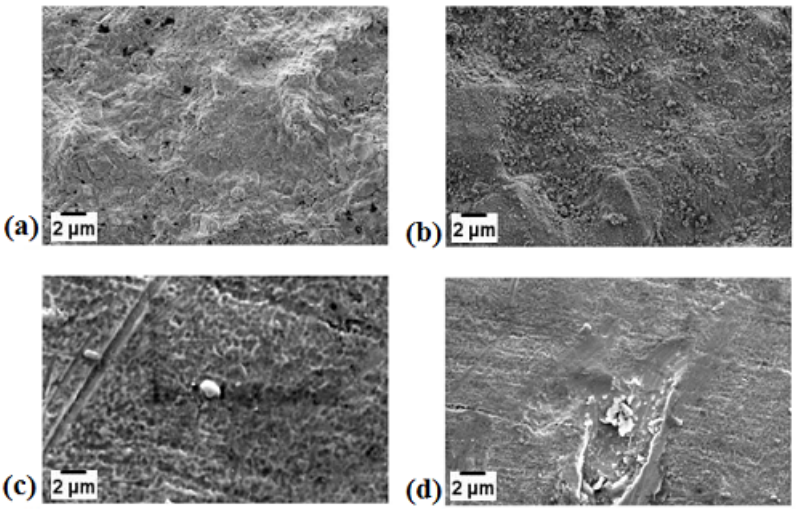


Figure 108: SEM images of (a) NiTi wire sample prior to any form of coating, (b) calcium phosphate tribasic coating on NiTi wire sample after dip coating and subsequent sintering, (c) biomimetic calcium phosphate coating on NiTi wire sample after 24 h, and (d) biomimetic calcium phosphate coating on NiTi wire sample after 48 h

On the other hand, samples coated via the biomimetic coating method reveal surface irregularities and minor cracks. NiTi samples have had different biomimetic deposition times. The biomimetic coating layer was observed to become more uniform after 48 h as compared to the coating layer obtained after 24 hrs. of immersion (Figure 108-c and d). Even after 48 h, the scratched marks due to mechanical polishing were observable on the surface. However, these marks disappeared after obtaining the dip coating method, indicating the formation of a thicker layer. Compared with the coating formed by biomimetic technique, the coating grown with dip coating has a higher degree of crystallinity. This growth may be attributed to the high Ca and P concentration that resulted in faster deposition on the NiTi surface. The CaP based layer shows a denser surface than the other surface that is coated with biomimetic technique. The thick layer may reduce the possibility of Ni release from the surface. These findings were validated with confocal microscopy analysis.

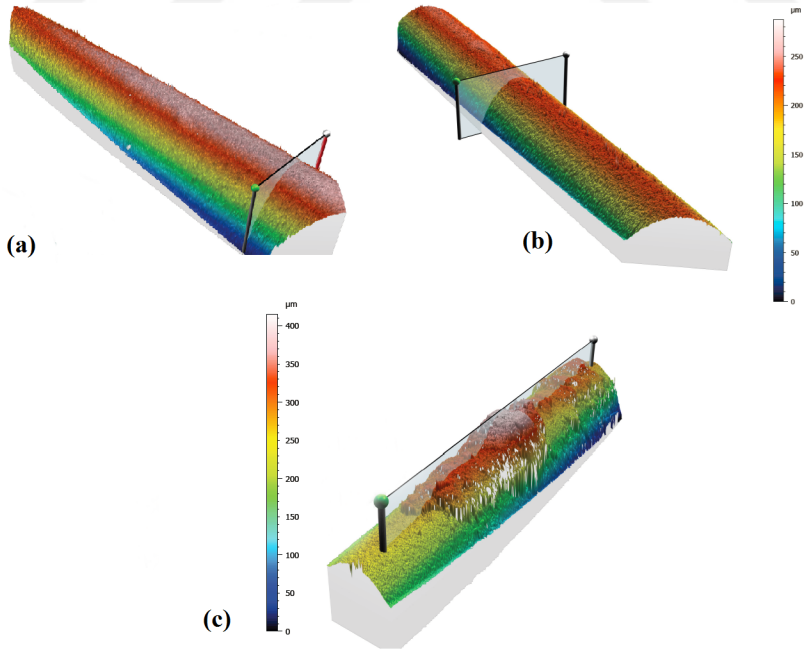


Figure 109: The thickness of the coatings on NiTi (a) biomimetic method (24h); (b) biomimetic method (48h); (c) dip coating method

The 3d view of the coated NiTi surfaces was given in Figure 109. Surface roughness tends to increase with the increase of duration for the biomimetic method as seen in Figure 109 a and b. However, CaP coating layer was more observable after obtaining the dip coating method as shown in Figure 109 c. These findings were in line with SEM results (Figure 108). The thickness of the coating was found approximately 50 microns for the sample that was coated with the dip coating method. After obtaining the dip coating method, the coating was found uniform since the surface roughness was not significantly changed as evaluated in Figure 110.

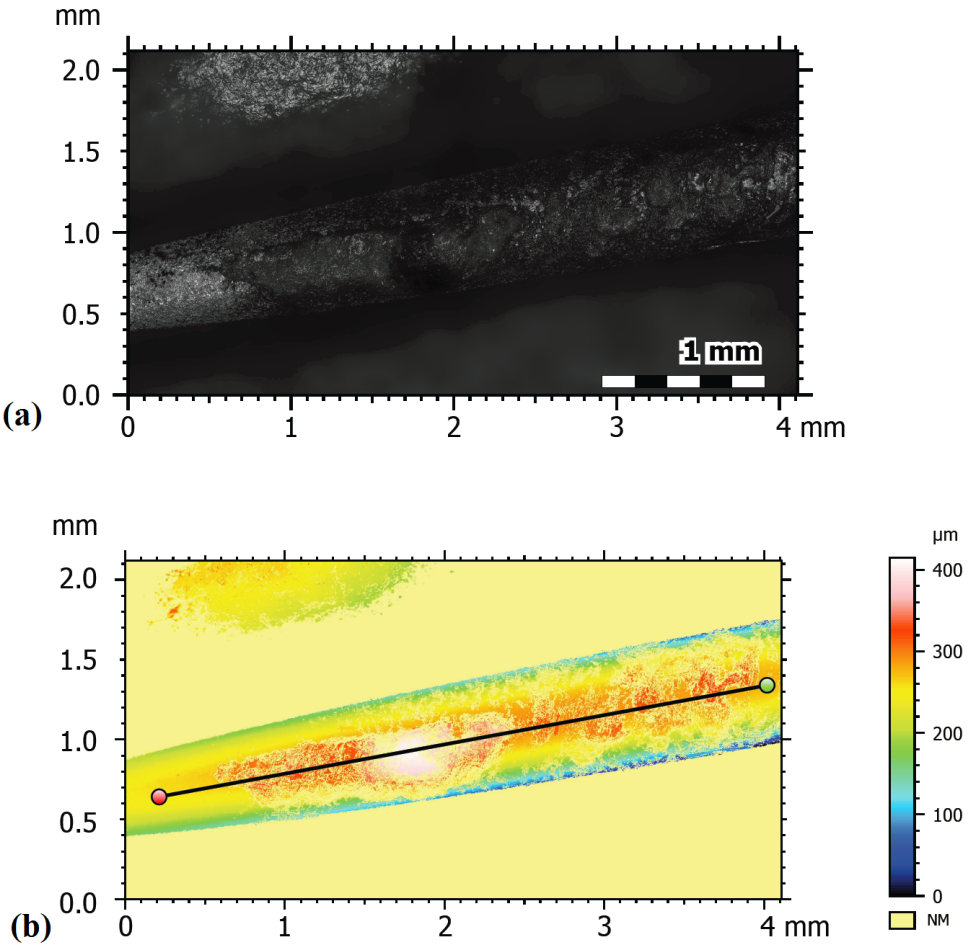


Figure 110: Confocal analysis of CaP coated NiTi via dip coating method (a) true color view of the image; (b) pseudo color view of the coated surface

Different parameters were obtained to produce CaP coating on the NiTi surfaces as shown in Figure 111. SEM analyses were utilized for as-received and coated samples. NiTi samples were named according to their coating parameters as previously summarized in Table 13. Deposition of the CaP layer was observed with sample 4 as given in Figure 111 e. The deposition of CaP layer on the surface was not fully achieved with the selected parameters for sample 1, sample 2, and sample 3. It was concluded that these parameters were not suitable for dip coating. On the other hand, the amount of CaP in the suspension varied between 1 g to 5 g. However, SEM images showed that the amount of CaP has no effect on the surface morphologies of coated NiTi samples since all surfaces have similar surface characteristics.

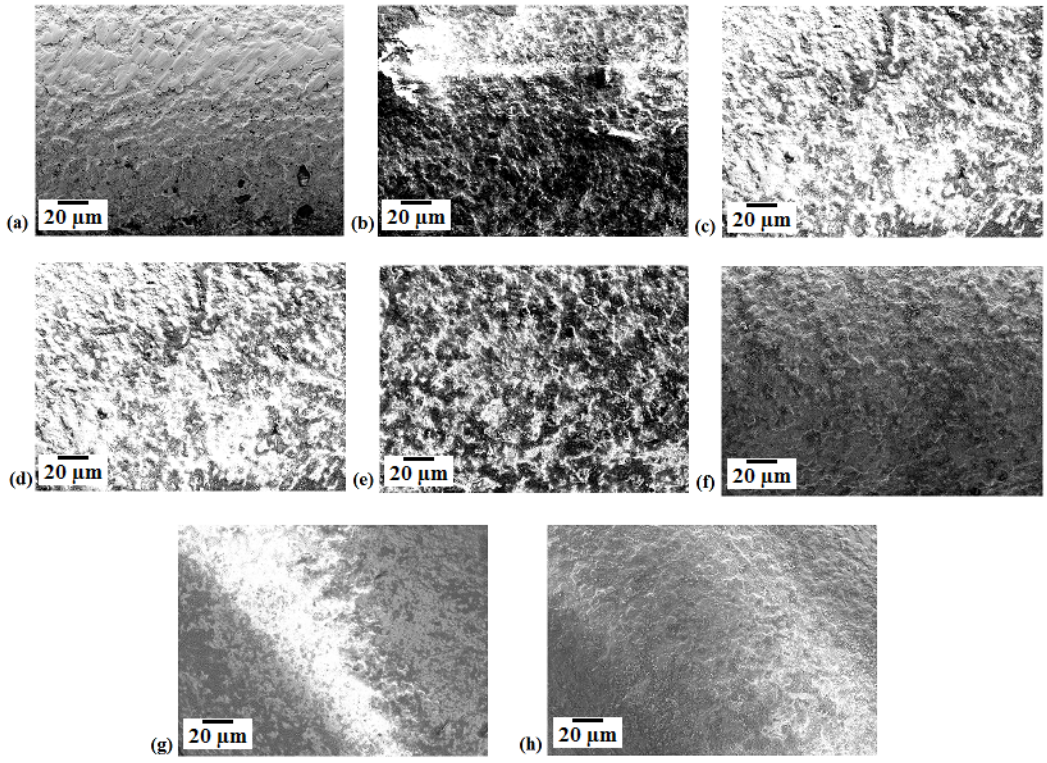


Figure 111: SEM micrograph of CaP coated NiTi surface with different parameters via dip coating method (a) as-received; (b) sample 1; (c) sample 2; (d) sample 3; (e) sample 4; (f) sample 5; (g) sample 6; (h) sample 7

Effects of the different coating parameters on the surface morphologies were determined by precision weighing. The weight change of the samples after the coating process was recorded with respect to coating parameters as given in Figure 112. The weight of the deposition of CaP layer was increased with the rise of temperature from 40 to 80^{o}C. It was seen that no weight change was observed for Sample 4, Sample 5, Sample 6, and Sample 7 with constant temperature and immersion periods that means the amounts of CaP have no effect on the weight of CaP coated NiTi samples. These results are consistent with the SEM analyses.

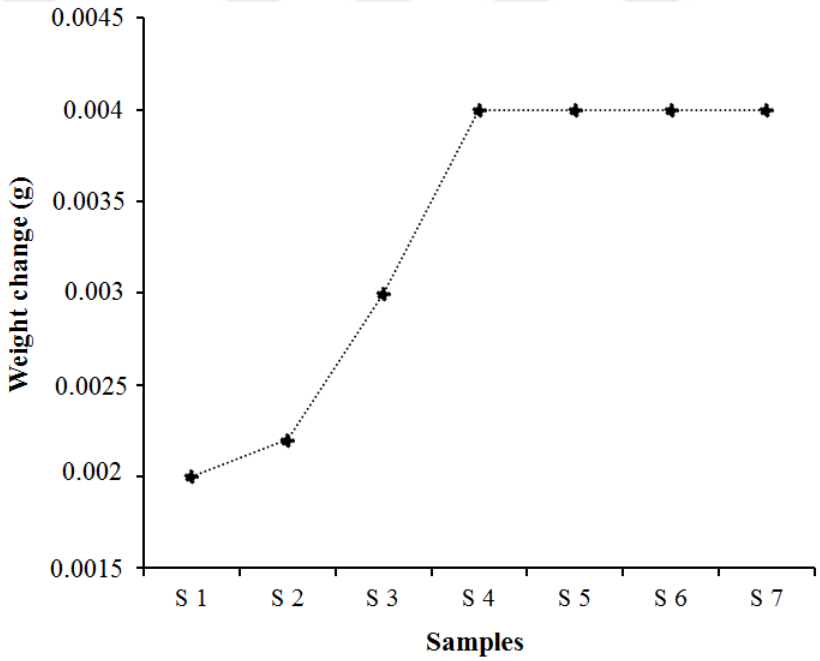


Figure 112: Weight change of the CaP coated NiTi samples as a function of different coating parameters

Figure 113 is the high magnification image of the previous figure that claims the nanoscale character of CaP based coatings. It can be seen from the figure that many small spherical particles were formed on the NiTi surface. Therefore, the samples that are coated with the dip coating method were found to be more useful than those coated with the biomimetic technique.



Figure 113: SEM image of CaP coated NiTi surface with dip coating method

Contact angle measurements were also conducted via the sessile droplet method in order to gain a better insight into the surface wettability properties of the coating layers. These results are given in Table 20. Uncoated NiTi wire samples have an average contact angle of 111^o, which is significantly higher than coated NiTi samples. For both of the coating methods, the contact angle values decrease below the value of the uncoated sample. Contact angles below 90^o are a sign of a hydrophilic surface with improved surface adhesion and biocompatibility. Although biomimetic coating results in relatively low contact angle values after 24 h, they increase following immersion for 48 h. which is crucial to obtain a successful coating layer as validated by the SEM observations. However, the dip coating method and subsequent sintering results in a contact angle of 75^o denoting a hydrophilic surface coupled with a homogeneous coating layer without significant surface irregularities. The more hydrophilic surface may be attributed to lower surface energy.

Table 20: Average contact angle values of CaP coated NiTi samples

Sample	**Contact Angle Values (degree)**
As-received	111.15
Dip coated NiTi	75.81
Biomimetic coated NiTi (24h)	84.51
Biomimetic coated NiTi (48h)	83.73

The difference between the coating layers may be attributed to the methods used to produce the coating layers as well as the geometry of the wire shaped substrate. Although biomimetic coating is known to be a successful coating technique that can be used to obtain calcium phosphate layers on NiTi surfaces, the specific geometry of the wire shaped samples utilized in this study is thought to result in the observed unfavorable surface properties. According to these results, the dip coating method was found more promising in this dissertation. After selecting the coating method, the following experiments were obtained for further characterization.

The mechanical stability of the coated layer and shape memory of the sample was examined with the basic bending experiment. The bending experiments show that the properties of shape memory were not altered by the biomimetic or dip coating process. It was found that the CaP based layer was withstand between 0-15^o bending which is necessary considering their use in the human body. However, above 15^o, the coating layer was ruptured as reported in previous studies [91]. These findings were validated with EDS analyses. Results show that concentration of Ni and Ti elements tends to increase with the increase of bending angle of 15^o as given in Figure 114 that may be attributed to the damaged surface. The percentage weight of Ca was found as similar to Sample 1 and Sample 2.

Sample Name	Bending Angle	Results
Sample 1	0	withstand
Sample 2	15	withstand
Sample 3	30	ruptured

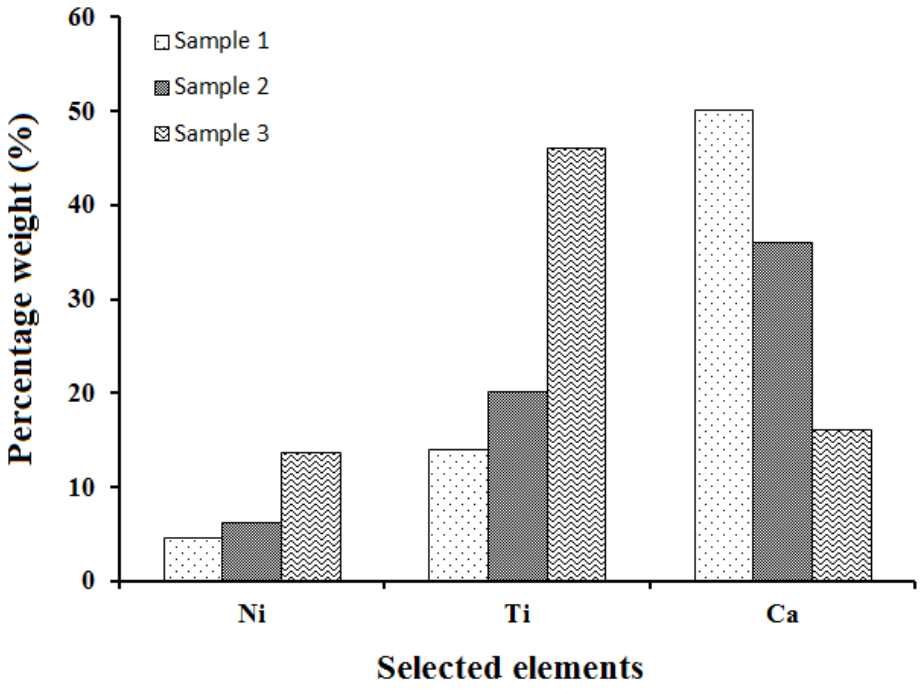


Figure 114: Elemental analysis of NiTi samples after bending test

After the coating process, cyclic experiments were performed with CaP coated NiTi samples. Figure 12 displays the total number of cycles of CaP coated NiTi for the three different frequencies. In order to evaluate the relation between cyclic performance and environmental conditions, three mediums were carried out for each frequency. Results reveal that coated layer has a comparatively small effect on the cyclic performance of NiTi samples since these findings agreed with the results of uncoated NiTi samples.

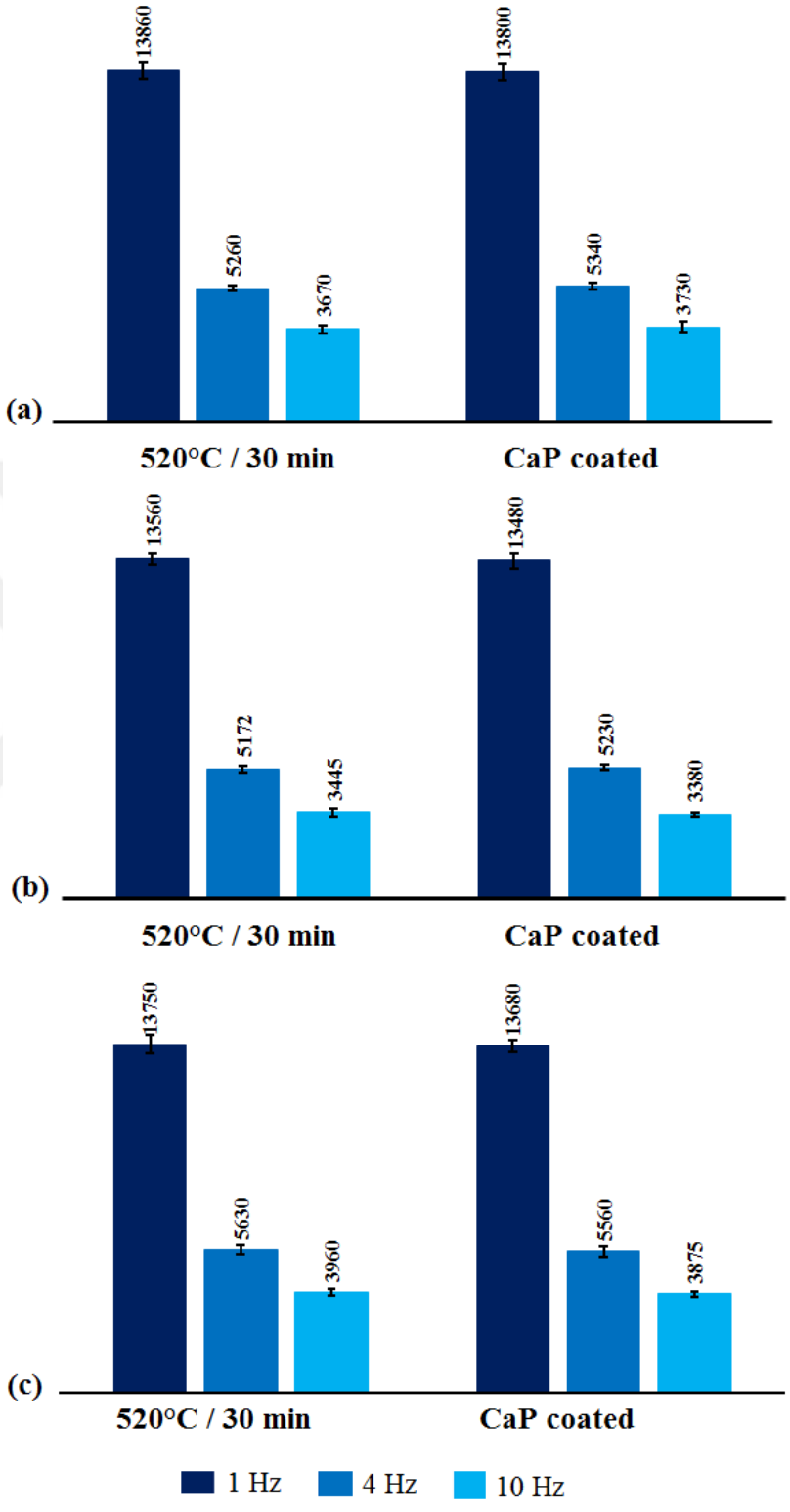


Figure 115: Cyclic behavior of uncoated NiTi and CaP coated NiTi (a) dry condition; (b) SBF solution; (c) Ringer solution

The presence of CaP layer on the NiTi does not impact the cyclic behavior significantly at all frequencies in all conditions. The maximum number of cycles was found around 13800 for both uncoated and coated NiTi samples at 1 Hz and showed a similar trend with the increase of frequency to 10 Hz. It's clear that the fatigue life deteriorated with an increase in frequency from 1 Hz to 10 Hz. This behavior may be attributed to the rapid crack initiation and propagation on the NiTi surfaces at higher frequencies. Independent of environmental conditions, the maximum number of cycles was similar for all conditions. The differences in cycle numbers before fraction are not significant for both uncoated and coated NiTi. This behavior may be attributed based on the similar mechanical properties of both samples since the presence of CaP layer does not alter the YS and UTS of the NiTi. With respect to the reached number of cycles to failure at 1 Hz, the cyclic performance of NiTi is approximately four times higher than the experiments performed at 10 Hz. Microstructural studies of fracture surfaces could be employed for further characterization. Therefore, initial SEM analyses were utilized to investigate the fracture surface as shown in Figure 116 in order to simulate NiTi response in dry condition at 4 Hz. However such characterization is beyond the scope of current work and may be detailed in follow-up research.

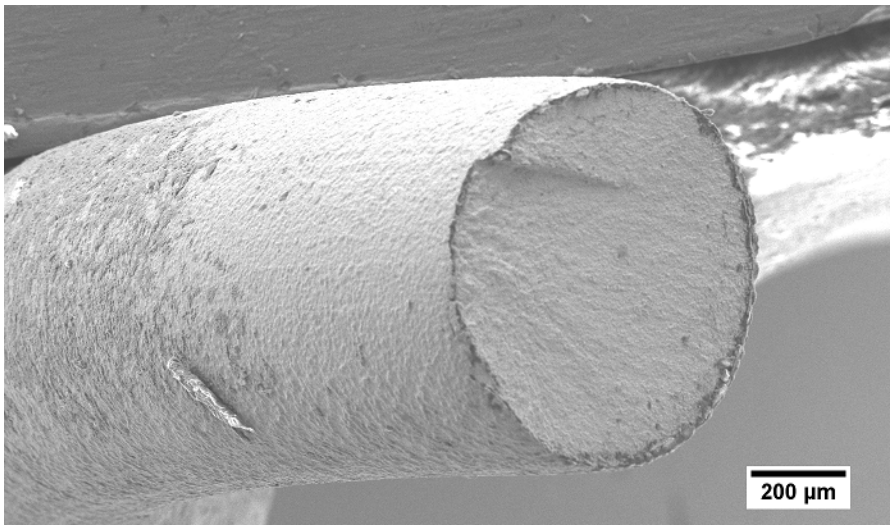


Figure 116: Fracture surface of CaP coated NiTi tested in dry condition at 4 Hz

Calcium phosphate coating plays a significant role in improving the corrosion resistance of the NiTi wire samples irrespective of the coating technique as shown in Table 21. The biomimetic coating method results in a substantial decrease in the corrosion rate standing at 11.68 mpy for the as-received sample. Increasing the immersion time from 24 to 48 h decreases the corrosion rate of the NiTi substrates from 6.15 to 2.28 mpy. However, the dip coating method results in a very low corrosion rate of 0.001 mpy denoting a successful protective layer of the coated surface.

Table 21: Corrosion rate values of the NiTi samples as a function of coating method

Sample	**Corrosion rate (mpy)**
As-received	11.68
Dip coated NiTi	0.001
Biomimetic coated NiTi (24h)	6.15
Biomimetic coated NiTi (48h)	2.28

Besides electrochemical measurements, material loss for each coating method was calculated and summarized in Table 22. These findings substantiate the effectiveness of the coating process to improve the corrosion resistance of the surfaces for both biomimetic and dip coating methods. All the measurements were repeated thrice for consistency and the average values were recorded. The highest material loss is found for the as-received sample as expected while coating resulted in decreasing the material loss of NiTi. The weight loss dramatically decreased on the sample that was coated via the dip coating method due to the formation of a more dense CaP layer. All these findings are consistent with electrochemical measurements. These results confirm that a proper coating method is highly recommended to obtain better corrosion properties.

Table 22: Total material loss as a function of coating method

Sample	Material loss (g)
As-received	0.04863
Dip coated NiTi	0.00335
Biomimetic coated NiTi (24h)	0.0297
Biomimetic coated NiTi (48h)	0.0351

In order to examine the biocompatibility of coated and uncoated NiTi, in vitro cytotoxicity assays were carried out. MTT cell growth assays showed that CaP coated sample had the maximum cell viability compared to the as-received and negative material. The possible mechanism underlying this finding is the formation of CaP and oxidation layer as observable in Figure 104 since the biocompatibility of NiTi may be attributed to the oxidation that is produced naturally caused by the heat treatment process.

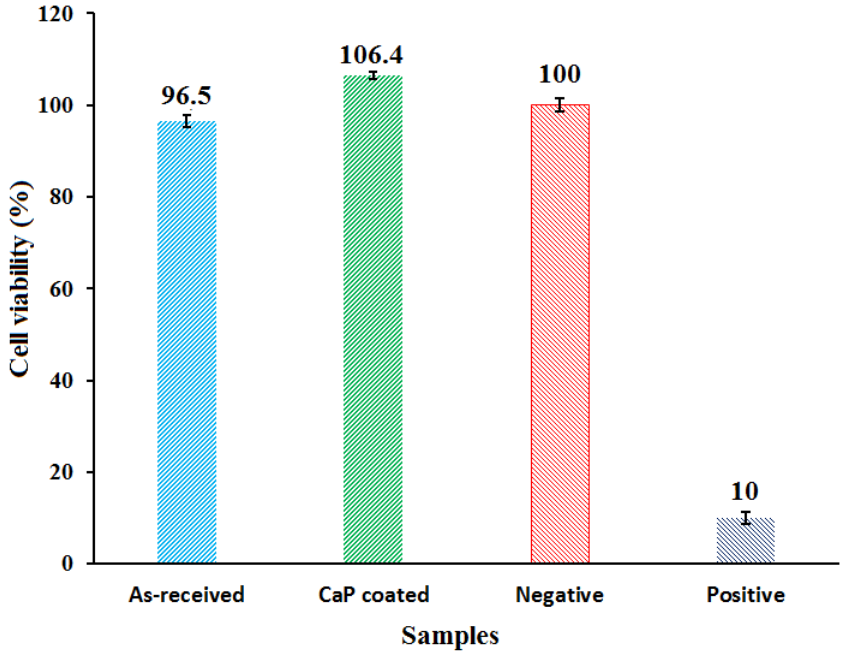


Figure 117: Cytotoxicity analyses of as received and CaP coated NiTi

3.2.1.2 Evaluation of NaOH pre-treatment on the surface characteristics of CaP coated NiTi alloy

Several researchers have utilized different surface treatment methods on NiTi substrates to improve the stability of the coating layer and to enhance its attachment on the substrate. NaOH treatment is a well-known method that has been applied to various substrate coating couples in order to modify the substrate surface for improved coating quality [217].

These experimental series investigate the effect of NaOH pre-treatment on the CaP based coating of NiTi wires and demonstrate for the first time that the effect of surface pre-treatment of wire form NiTi with NaOH prior to HA coating is noticeable even for low concentrations and adversely affects the corrosion performance and the ensuing biocompatibility. It should be noted that all NiTi samples were heat treated at 520^{o}C for 30 minutes after dip coating process.

Surface morphologies of the as-received and coated (with and without NaOH pre-treatment) samples are shown in Figure 118-a and e. Morphology of the as-received material contains surface irregularities with an initial roughness (Figure 118-a). Formation of a HA layer was observed after dip coating followed by the subsequent heat treatment as evidenced by the disappearance of the grain substructure. The combination of coating and heat treatment resulted in the coalescence of HA particles and the formation of a well-densified layer (Figure 118-b). Previous works report that nanosized HA particles accomplish a dense coating layer even at low sintering temperatures which is in agreement with the observations of the current study [218, 219]. The uniform coating on sample C can be observed in view of the lower magnification SEM micrographs (Figure 118-b inset) while the other surfaces which belong to NaOH pre-treated samples have inhomogeneous surface topography pointing to the reduced coating quality with increasing NaOH concentration. The non-uniform distribution of HA particles is visible as shown in Figure 118-c and e.

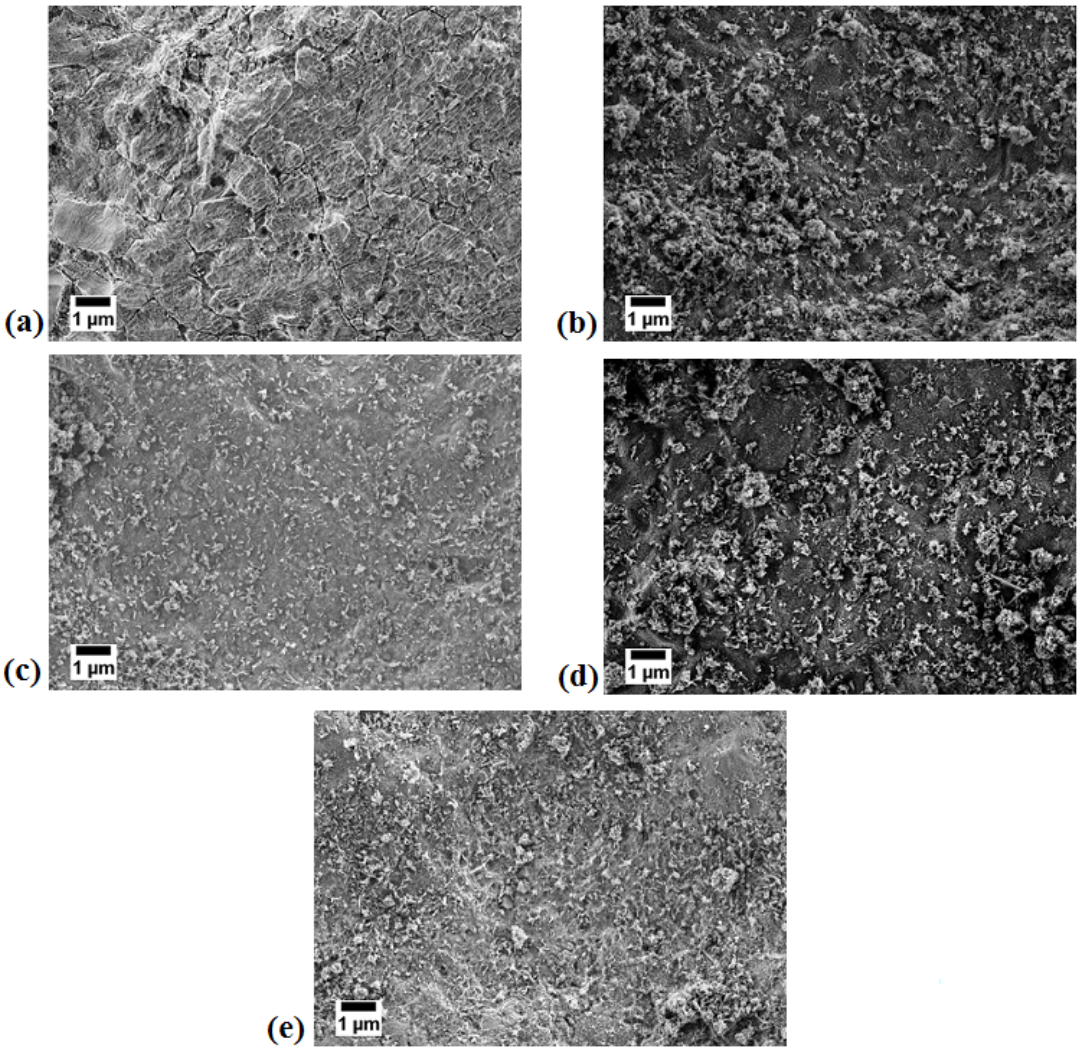


Figure 118: SEM micrographs of NiTi samples with different surface conditions; (a) as-received, (b) heat treated and CaP coated, (c) 0.5NaOH treated and CaP coated, (d) 1NaOH treated and CaP coated, (e) 4NaOH treated and CaP coated

The Ca/Ni and Ni/Ti coefficients as a function of different surface treatment conditions were obtained using XPS measurements as shown in Figure 119, Figure 120 and Figure 121 to evaluate the effect of NaOH pre-treatment on the surface characteristics of the samples. Results indicated that the Ca/Ni ratio decreased with the increasing concentration of NaOH treatment denoting elevated Ni levels on the

surface of the samples. The Ca/Ni ratio was the most favorable (26.56) for sample C having no surface treatment. Moreover, increasing the concentration of the NaOH solution intensified the Ni/Ti ratio in the treated samples. These findings are in agreement with Chrzanowski et al. [220] reporting increased nickel content in the surface top layer with NaOH treatment which would pose the potential risk of decreasing the biocompatibility due to the heightened risk of Ni release. With increasing NaOH concentration Ni/Ti ratio was observed to escalate, indicating that the obtained surfaces are rich in Ni. The increase in the Ni/Ti ratio may be attributed to the formation of a thin film in oxide form rich in Ni on the substrate surface as a result of NaOH treatment [220]. However, Ni was also traced for the sample without NaOH treatment although to a much lesser extent as compared to its counterparts with NaOH treatment.

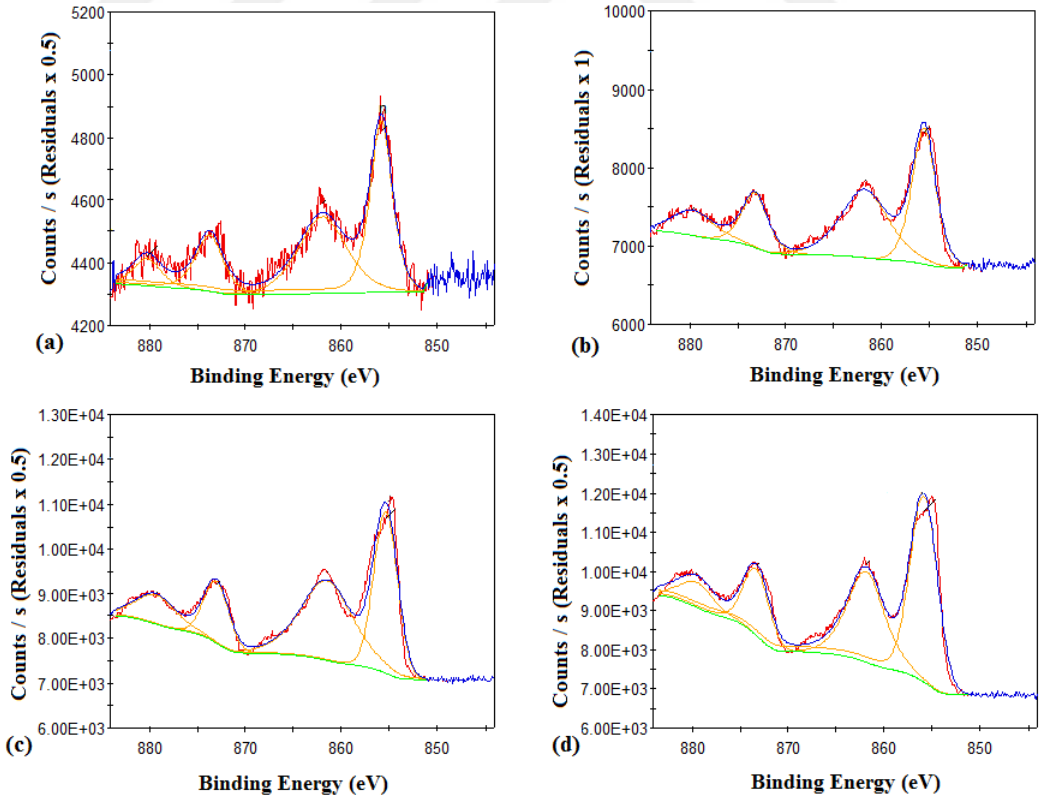


Figure 119: XPS measurements of Ni elements for the following samples (a) C; (b) 0.5NaOH-C; (c) 1NaOH-C; (d) 4NaOH-C

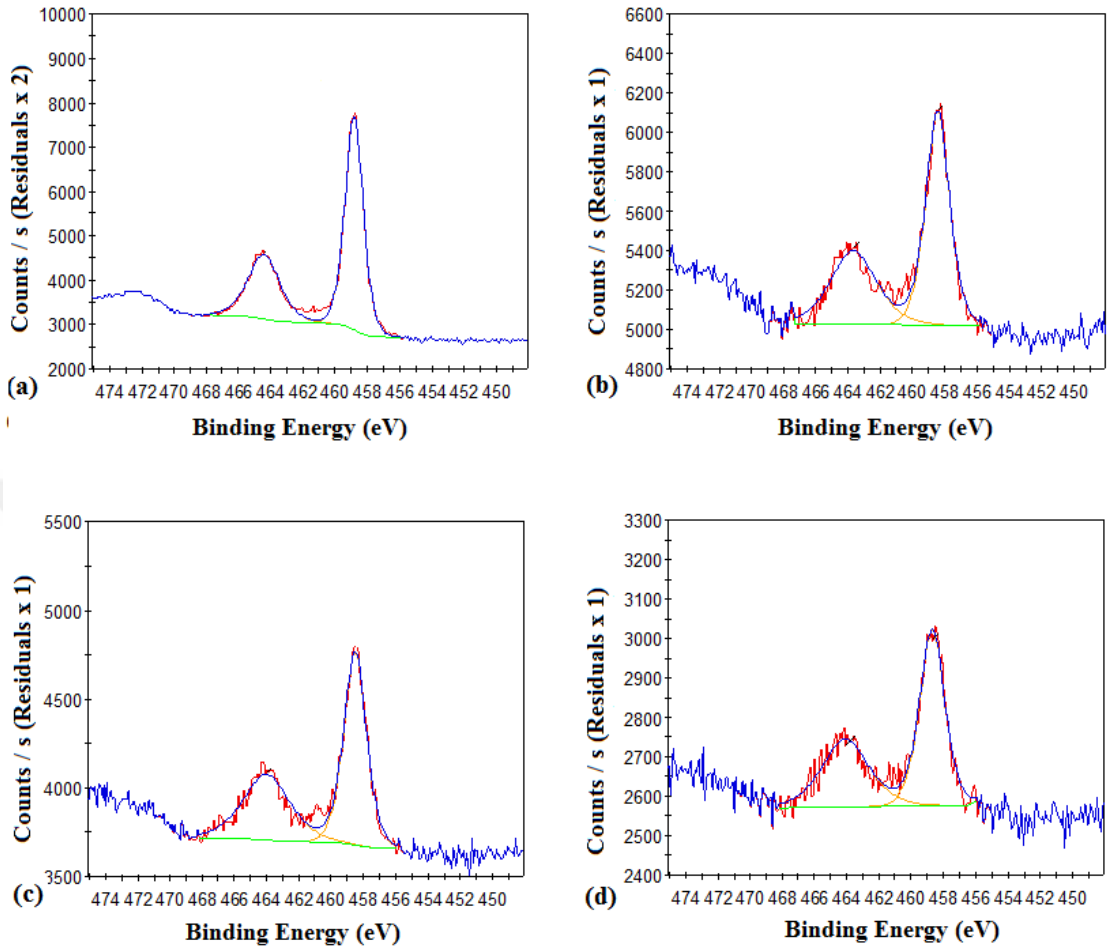


Figure 120: XPS measurements of Ti elements for the following samples (a) C; (b) 0.5NaOH-C; (c) 1NaOH-C; (d) 4NaOH-C

The increase in Ni/Ti ratio on the sample surfaces may also be associated with the heat treatment applied for sintering purposes. Several research efforts underline similar observations. For instance, a significant increase in Ni concentration was reported after a heat treatment at 500^{o}C for 15 min [67]. Wu et al. also revealed the effect of heat treatment on the Ni release from NiTi surfaces exhibiting that the released concentration increased significantly between 450^{o}C and 550^{o}C [221]. However, sintering is a crucial step that may not be omitted in order to obtain a sufficiently strong bond between the HA coating and the NiTi substrate for real-life applications.

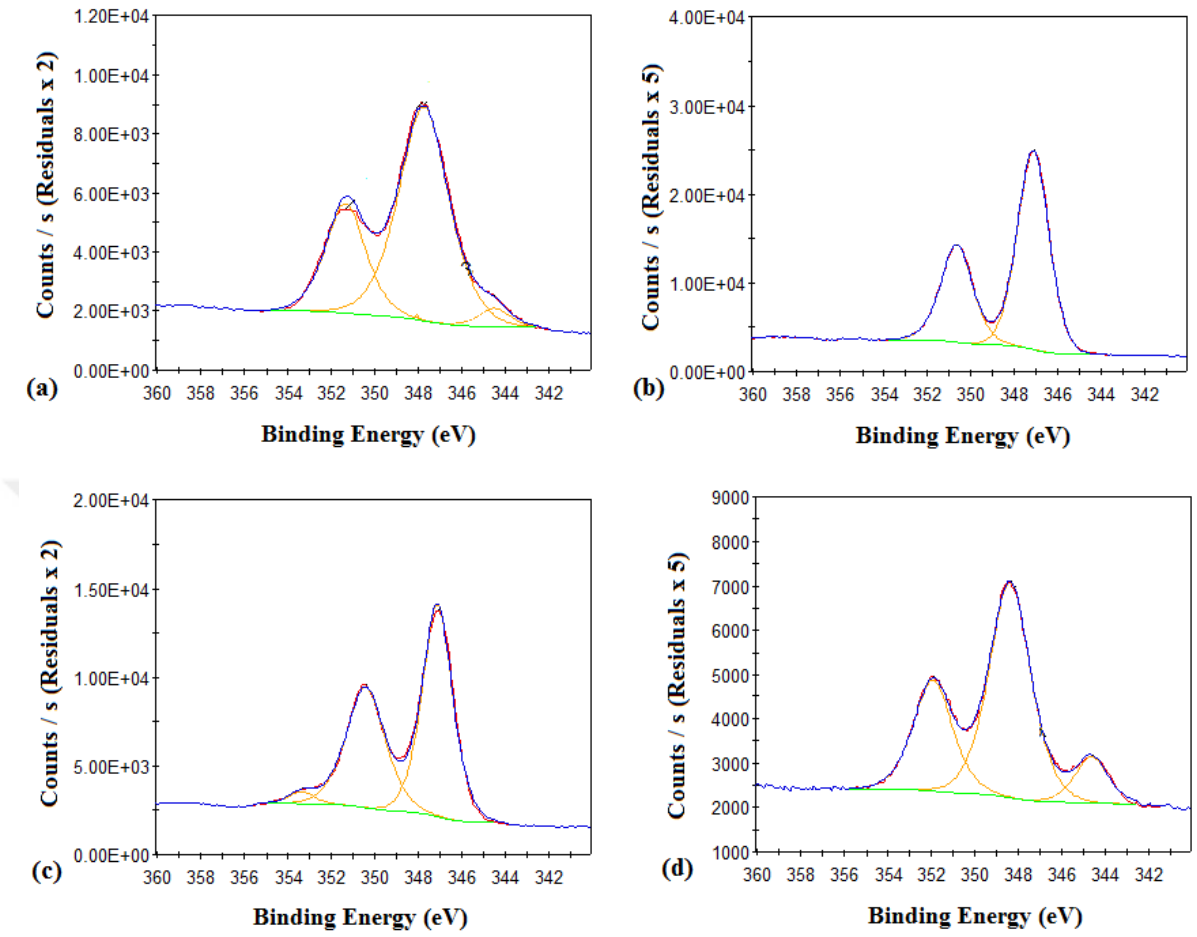


Figure 121: XPS measurements of Ca elements for the following samples (a) C; (b) 0.5NaOH-C; (c) 1NaOH-C; (d) 4NaOH-C

Results obtained in this study indicate that NaOH treatment and sintering may have a combined effect on the increased Ni/Ti ratio. Surface irregularities and cracks occurring on the NaOH treated samples could also affect the Ni/Ti ratio. The 4NaOH-C has the highest Ni/Ti ratio (9.84) and the lowest Ca/Ni (1.63) as shown in Figure which obviously is not suitable for biomedical applications since a Ni/Ti high ratio is undesirable due to the risk of Ni release and its detrimental biological effects [140]. It can be asserted that among the conditions studied, C displays the most suitable characteristics for biomedical applications by displaying the highest Ca/Ni and the lowest Ni/Ti ratios.

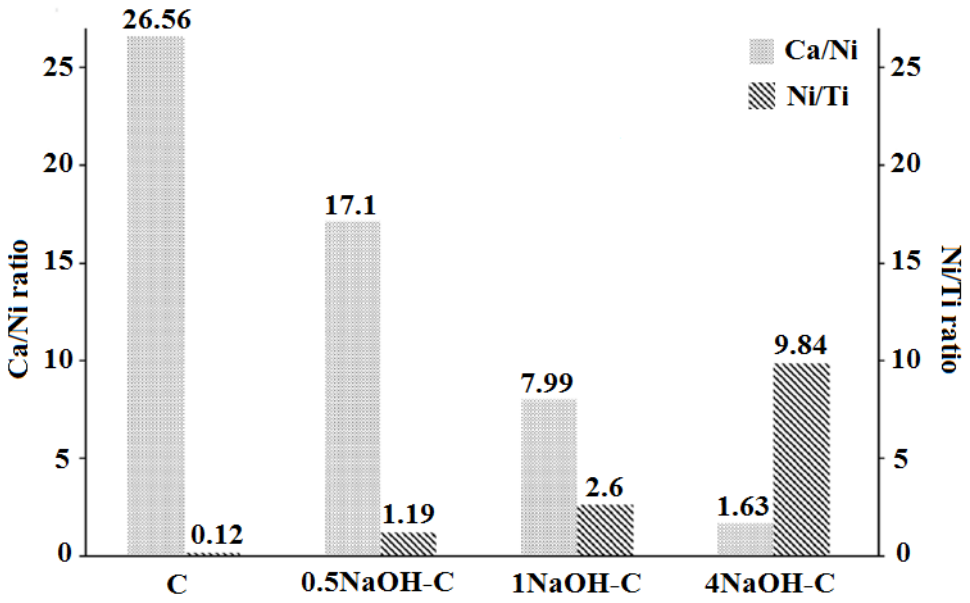


Figure 122: Ca/Ni and Ni/Ti ratio of NaOH treated samples with selected conditions

Contact angle measurements were conducted to assess the wettability characteristics of selected surfaces (Figure 123), for which the contact angle values are given in Table 23. As-received NiTi was used as a reference having the highest contact angle. HA coating clearly had a positive effect on decreasing the contact angle thus increasing wettability. However, as can be seen in Table 16, NaOH treatment resulted in a variation of the contact angle where the contact angle increases as the NaOH concentration increases. The contact angle values were significantly higher for both NaOH treated samples when compared with that of the HA coated sample without prior surface treatment. Sample C has the lowest contact angle value and the surface shows hydrophilic characteristics. Several studies have confirmed that hydrophilic surfaces which have contact angles smaller than 90^o are more suitable for biomedical applications [222]. The low contact angle mostly addresses favorable properties which improve cell attachment onto the surface including good adhesion, high wettability, and high surface energy [223]. Results of the contact angle measurements suggest

that the surface obtained with HA coating without any prior NaOH treatment has good adhesion properties and thus might have higher biocompatibility which is clearly evidenced by the findings of cell viability tests as elaborated in the following.

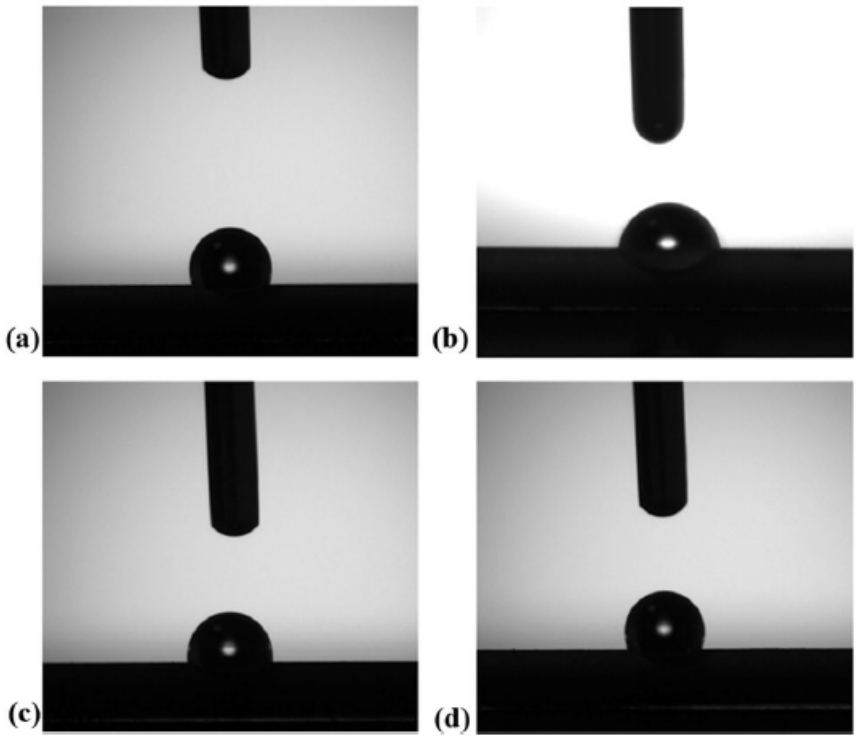


Figure 123: Images of contact angle measurements; (a) as-received, (b) C, (c) 0.5NaOH-C, (d) 1NaOH-C

Table 23: Contact angle measurements

Sample	**Contact Angle Values (degree)**
As-received	111.15
C	75.81
0.5NaOH-C	97.83
1NaOH-C	109.26

The influence of NaOH treatment on the cyclic behavior of NiTi alloys was investigated by performing cycle experiments. Cyclic experiments were conducted at 1, 4, and 10 Hz up to 15^o bending angle in dry condition, simulated body fluid, and Ringer solution as previously performed. Figure 124 presents the number of cycles of the NiTi samples before fracturing as a function of NaOH treatment parameters. The total number of cycles decreased with the increased concentration of NaOH solution as expected. Moreover, these series also showed that there is no clear correlation between dry condition, SBF, and Ringer solutions and the total number of cycles.

The total number of cycles was found to decrease with initiating NaOH treatment. Prior to NaOH treatment, the total number of cycles was found more promising. Moreover, the increase in NaOH concentration lead deterioration of the mechanical properties which resulted in decreased cyclic life. Besides these findings, Figure 125 shows the fracture surface of the sample that was treated with NaOH prior to bioceramic coating in dry condition at 4 Hz.

Further analyses were conducted to investigate the effect of NaOH treatment on the corrosion properties of NiTi. Corrosion experiments were performed in SBF solution at 37^oC, according to which the effect of NaOH treatment on corrosion behavior was found significant. It was determined that sample C possessed the best corrosion resistance while 4 NaOH-C has the highest corrosion current density and corrosion rate. Results of the corrosion test denote to pitting corrosion of the NaOH treated samples where corrosion rates increase with increasing NaOH concentration. The polarization curves are shown in Figure 126. The results showed that the corrosion performance degraded with the increased concentration of NaOH solution. After electochemical corrosion experiments, SEM analyses were conducted for C and 0.5NaOH-C samples with different magnifications. Additionally, the effect of NaOH treatment prior to coating process on the weight loss of NiTi was recorded and summarized in Table 24.

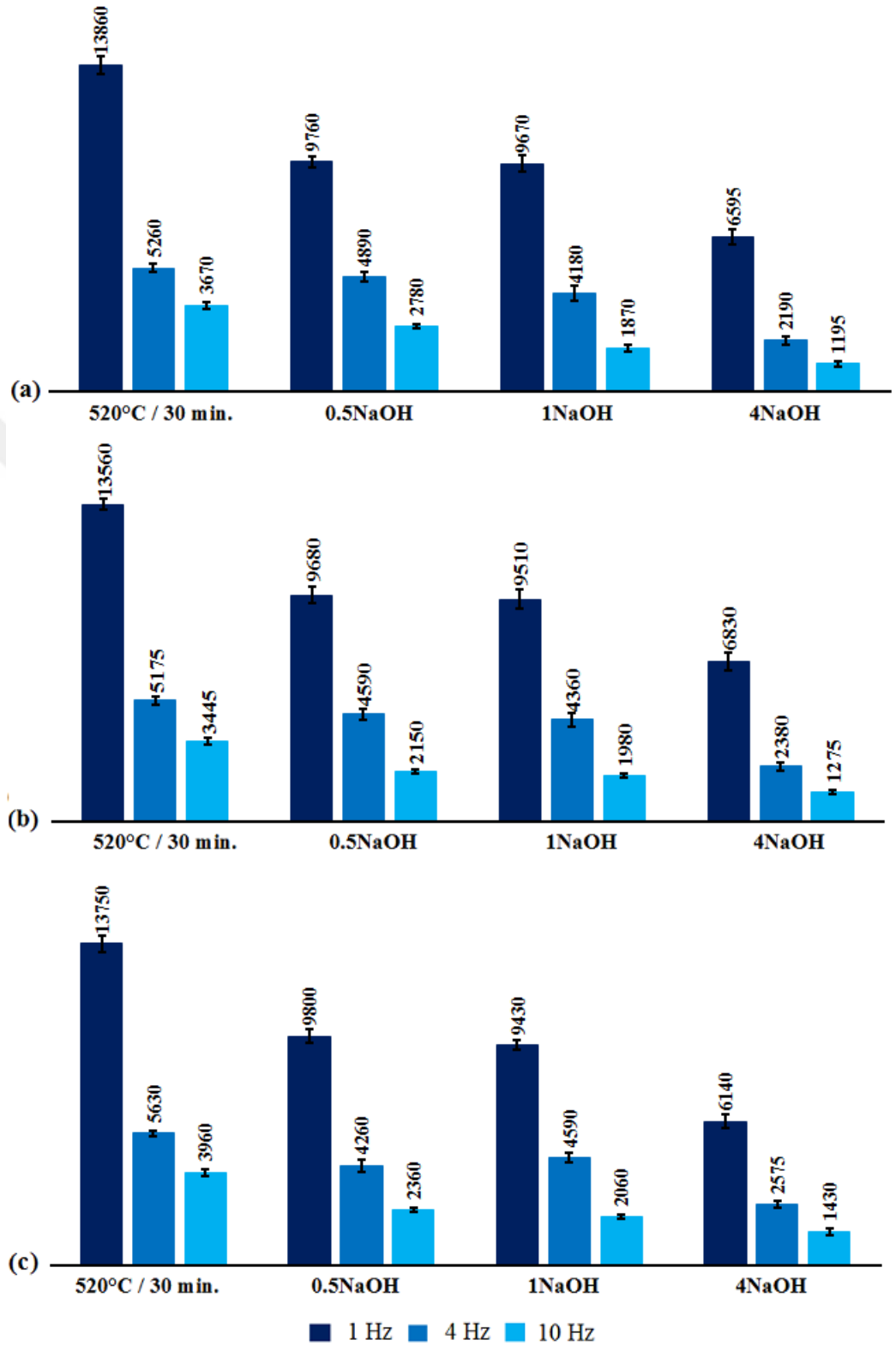


Figure 124: Cyclic behavior of untreated and NaOH treated NiTi samples (a) dry condition; (b) SBF solution; (c) Ringer solution



Figure 125: Fracture surface of the sample that treated with NaOH prior to bioceramic coating in dry condition at 4 Hz

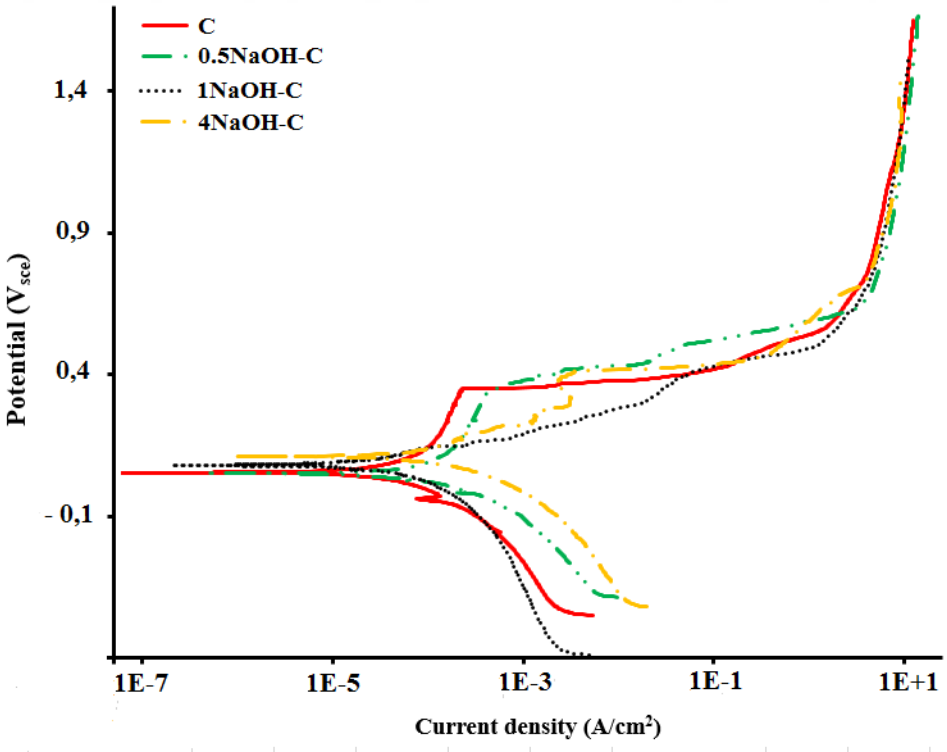


Figure 126: Polarization curves of NiTi samples with different surface conditions

Table 24: Total material loss of NaOH treated NiTi after electrochemical measurements

Sample	Material loss (g)
As-received	0.04863
C	0.00335
0.5NaOH-C	0.00549
1NaOH-C	0.00785

In Figure 127, the surface morphology of NiTi samples subjected to SBF solution can be traced. It is notable that the application of 0.5 M NaOH treatment reveals cracks on the coating layer (Figure 127 b and d) while sample C has crack-free morphology pointing to a more stable coating structure against corrosion.

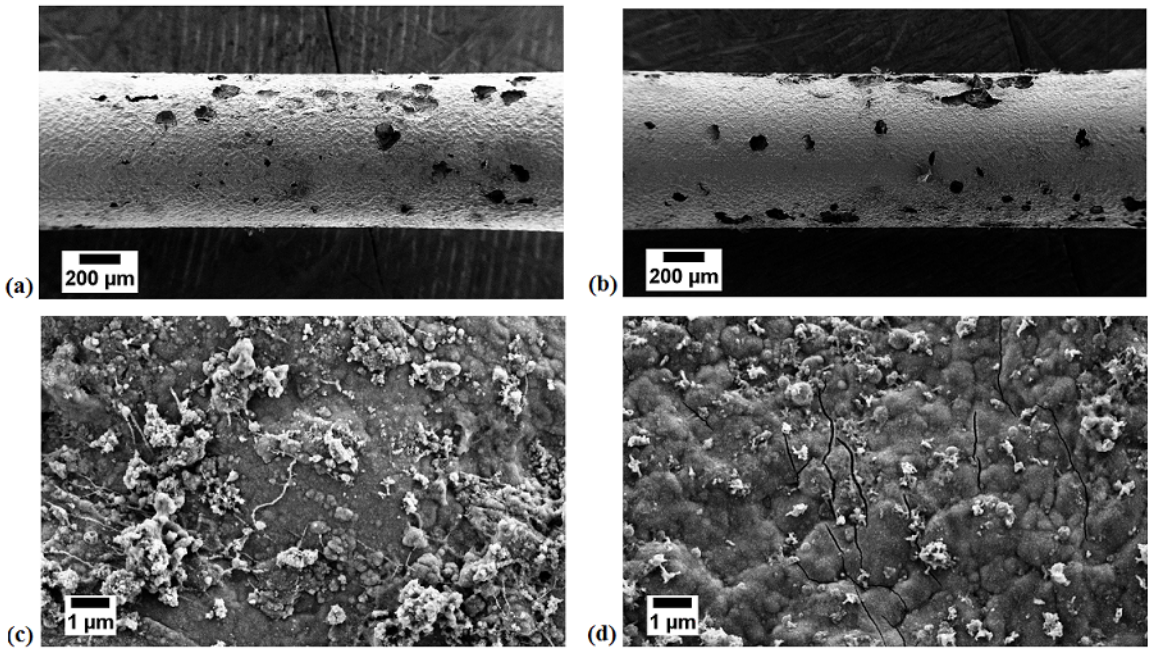


Figure 127: SEM micrographs of NiTi samples following corrosion experiments in different magnifications (a) sample C; (b) sample 0.5NaOH-C; (c) sample C (higher magnification); (d) sample 0.5NaOH-C (higher magnification)

The NaOH treated sample had a higher pit density on the surface and the surface pits can easily be discerned at high magnification as observed in Figure 127 b. This observation is in parallel with the potentiodynamic polarization test results and may be attributed to the mismatch of the thermal expansion coefficients of the HA coating layer and the underlying oxide layer rich in Ni which forms due to the NaOH treatment. Moreover, comparison Figure 127 c and d show that NaOH treatment leads to a variation in the surface morphology of the samples possibly due to an intermediate oxide layer between the NiTi surface and the HA coating.

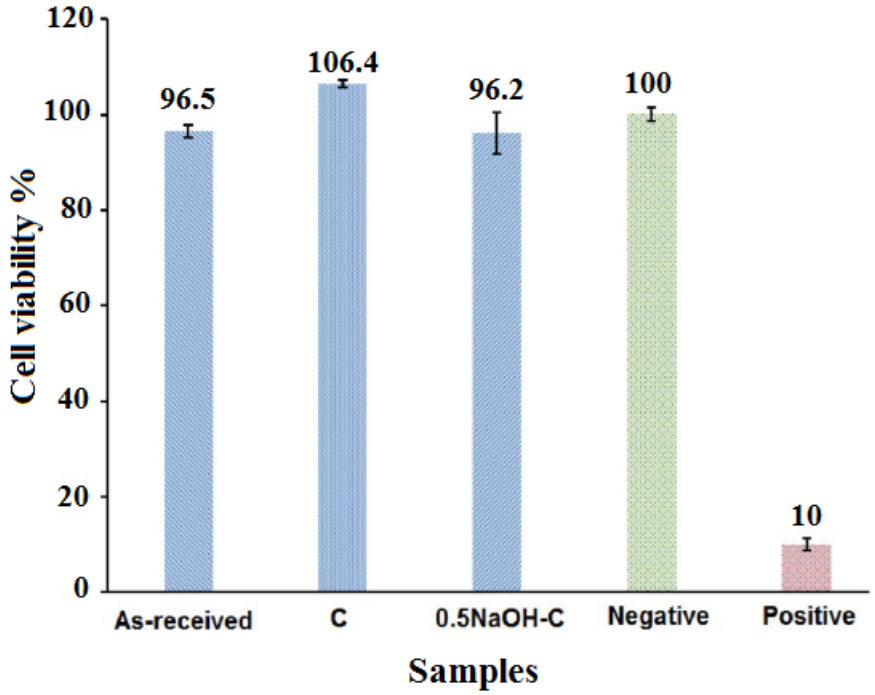


Figure 128: Cell viability test results of as-received, C and 0.5NaOH-C NiTi samples

Cell culture assessments were obtained using mouse L929 fibroblast cells. After 1-day incubation, the cell viability on the samples was determined via photometric reading. Figure 128 shows that no remarkable toxicity is observed for all samples. The results indicated that L929 fibroblast cells successfully grow on all NiTi surfaces after 24 h following seeding.

As-received sample had relatively lower cell viability compared to the negative. A similar result was obtained for 0.5 NaOH-C sample which had a lower cell viability compared to the negative and a similar value compared to the as-received sample indicating that the sample with NaOH pre-treatment followed by HA coating had no significant improvement on the cell viability as compared to the as-received state. On the other hand, sample C without prior NaOH treatment had cell viability almost 10% higher than the sample with NaOH pretreatment. It can be asserted that this result is promising in favor of the non-treated sample and corroborates the SEM observations as previously shown in Figure 118. These observations indicating that the samples without NaOH treatment result in a more successful subsequent HA coating layer. Accordingly, findings obtained in this section via a blend of surface characterizations and biological analysis have the potential to shed light on the utilization of HA coated NiTi as a prospective implant material.

3.2.2 Hydrogel coated NiTi Shape Memory Alloy

NiTi SMA implants should be covered by a biocompatible layer for shielding from aggressive body fluids, protecting surrounding body tissues against toxic products, and decreasing the risk of Ni ions diffused out of the metal. As mentioned in the previous section, ceramic coatings are very brittle and cannot normally withstand plastic deformation of the substrate without cracking [224, 225]. During operation medical instruments may encounter soft tissues and hard surfaces like ceramic coated implants may damage the surrounding tissues. Compared to the ceramic-based coating, hydrogel coating may provide a soft and flexible structure makes the hydrogel an attractive option for medical applications. This layer can withstand many cycles of stress as well as strain loadings, and may serve as a bioinert surface that expedites direct bonding to the living tissue that may prevent implantation failure and revision surgery [226].

All these properties make the hydrogel a valuable coating material. However, the difficulty of observing the optical and mechanical characterization of this coating material constitutes a major challenge. Several investigations have proved the significant benefits of hydrogel in experimental and clinical studies. Nevertheless, the main drawback of a hydrogel is their poor mechanical properties. However, if applied as a surface coating on a bulk implant body, their mechanical instability is a lesser concern. This subsection mainly focused to demonstrate the viability of a novel coating approach of PVA based hydrogel for NiTi wire substrate. It should be mentioned that all NiTi samples were treated at 520^oC for 30 minutes before coating process. Moreover, according to previous experiments as shown in Figure 67 and 68, the results of experiments for different amounts and preparation steps were summarized in Table 25 and Table 26.

Table 25: Selection of ideal amounts of PVA and gelatin

Amounts	*Results*
6% PVA and 4% Gelatin	Hardened
8% PVA and 2% Gelatin	Hydrous
7% PVA and 3% Gelatin	Ideal

Table 26: Results of preparation steps

Scenario	*Results*
Scenario 1	Failed
Scenario 2	Failed
Scenario 3	Failed
Scenario 4	Succeed

Figure 129 shows the formation of a hydrogel that is observed via light microscopy and SEM analysis with further support. The reddish gel-like zones on the surface of the coated samples indicate the presence of the hydrogel layer albeit their absence on the bare samples as shown in Figure 129 a and b. This is with the virtue of Chondrex treatment (Sirius red kit dye) of the former, leading to binding and eventually color dyeing. This observation was also confirmed by further SEM characterizations. It is clear that the surface morphology varies significantly following the generation of a hydrogel layer on the bare NiTi substrate as in Figure 129 c and d. Due to the strengths and limitations of the SEM approaches for hydrogel, further investigations focused on conducting an alternative method to verify the presence of the hydrogel layer on the surface.

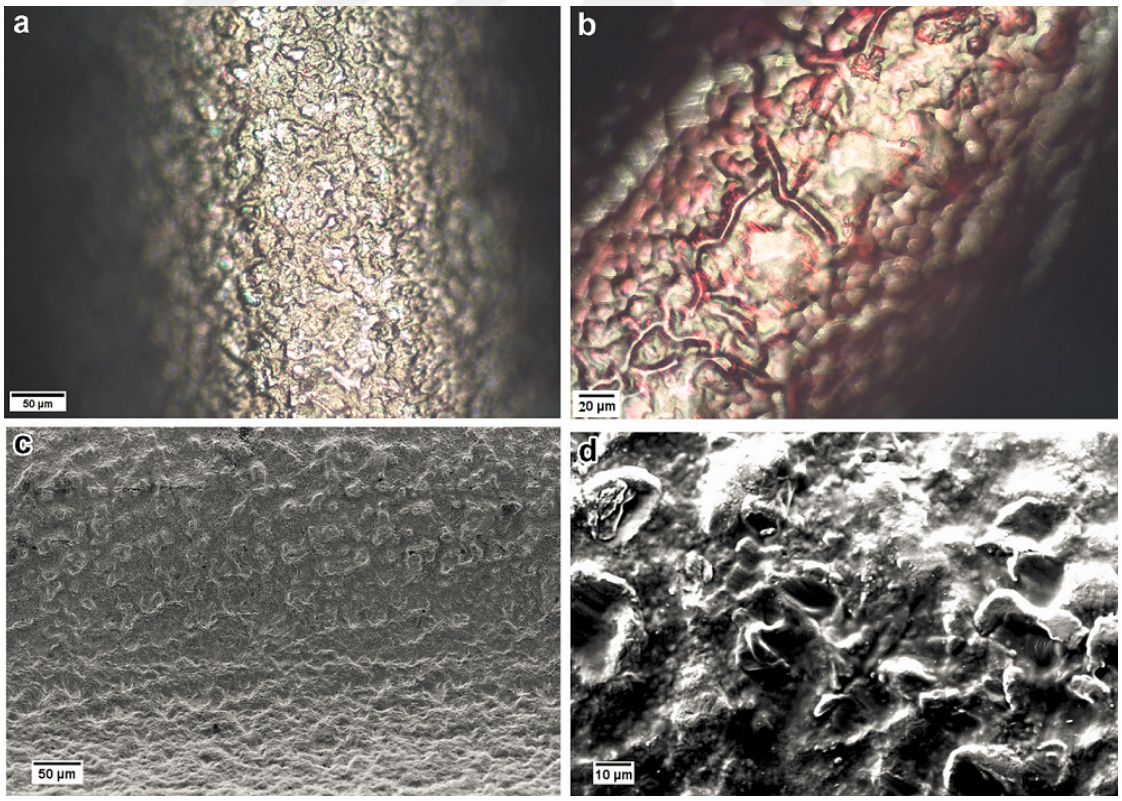


Figure 129: Surface images of the NiTi substrate; (a) and (c) before, (b) and (d) after coating with a hydrogel layer

Figure 130 shows the initial attempts at image processing experiments that provide the surface morphology of coated NiTi samples. In this figure, part (a) represents the original images that obtained with optical microscopes and part (b) represents the images after the image processing steps. With this method, the RGB images were converted to grayscale versions. Prior to SEM analyses, these primitive findings show that the method may found not be fully promising, and further investigations were needed to solidify the significance of the presence of hydrogel on NiTi surfaces as reported following parts.

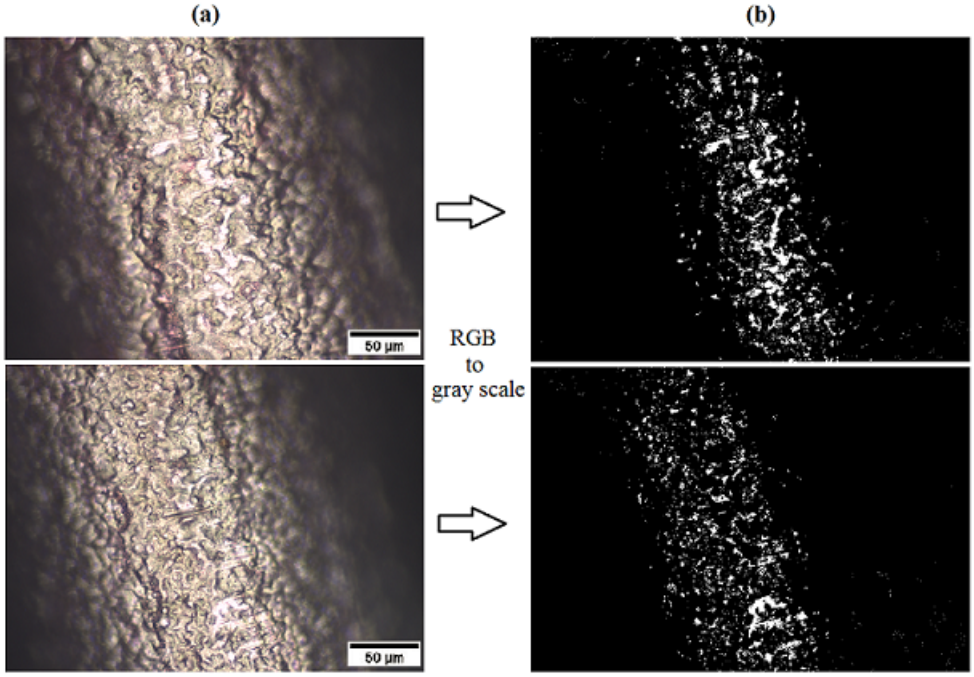


Figure 130: OM images (a) RGB images of hydrogel coated NiTi samples; (b) converted grayscale images of hydrogel coated NiTi samples

The subsequent experiments concentrated on obtaining visual observation to provide insights into the amount of coating on the surface for long time application. Initially, the density of the white area is minimum assuming that the NiTi sample was fully coated as shown previously in Figure 130.

All coated samples were immersed in Tris solution for the differing duration to evaluate the stability of the hydrogel coating on the NiTi surfaces. Figure 131 shows the surface morphology of hydrogel-coated NiTi after immersion for different periods and shows that with the increase in the duration, the density of the white area has increased.

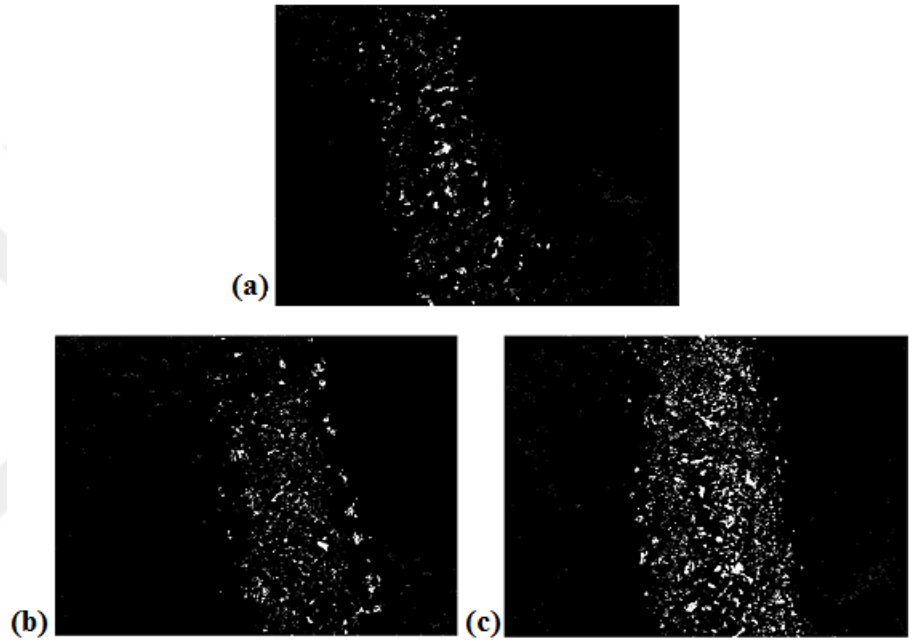


Figure 131: After immersing NiTi samples in SBF solution: (a) 7 days; (b) 14 days; and (c) 28 days

Hydrogels have been attracting considerable attention in the biomedical field due to their favorable properties. Despite these properties, hydrogels exhibit poor mechanical strength. In order to compensate for these weak mechanical properties, hydrogels may need to be bounded to metallic or ceramic surfaces. Several ongoing efforts to characterize the mechanical behavior of hydrogel coating are underway. However, the viscoelastic, hydrophilic, and soft nature of the hydrogel layer, along with the cylindrical geometry of the substrate render the utilization of mechanical measurement methods unreliable.

Moreover, cross-sectional measurements of thickness via SEM are also highly challenging due to the freeze-drying procedure of the samples to be observed, as this leads to shrinkage and modification of the layer dimensions. Still, mechanical measurements and light microscopy on chondrex treated coated samples reveal a hydrogel layer thickness of about 30 microns since this value stands close to what is already reported in the literature [227].



Figure 132: SEM image of hydrogel coating on the NiTi surface

Figure 132 shows the hydrogel layer on the NiTi surface that observed with SEM. Prior to submerged into hydrogel solution, NiTi samples were anchored to the coating apparatus that normally constitute a boundary between immersed and non-immersed NiTi sample. This boundary was obviously visible as given in Figure 132. The hydrogel was successfully coated on immersed surface whereas non-immersed part of NiTi was not coated. These observations lead to facilitate the determination of the thickness of hydrogel layer. The measurement the thickness of hydrogel highly challenging since hydrogels have high water content.

After coating process that obtained in atmospheric condition, shrinking mechanism may rapidly occurred and resulting in reduced coating thickness comparing to moist body condition. However due to limitation of resources, the thickness measurement were obtained confocal analyses as shown in Figure 133 in atmospheric environment. The thickness of coating was found between 30 to 50 micron for the sample that coated with dip coating method. Even so, this range was quite normal for the coatings applied by dip coating process [228]. As it is already mentioned, prior to hydrogel coating, all samples were heat treated at 520^{o}C for 30 minutes.

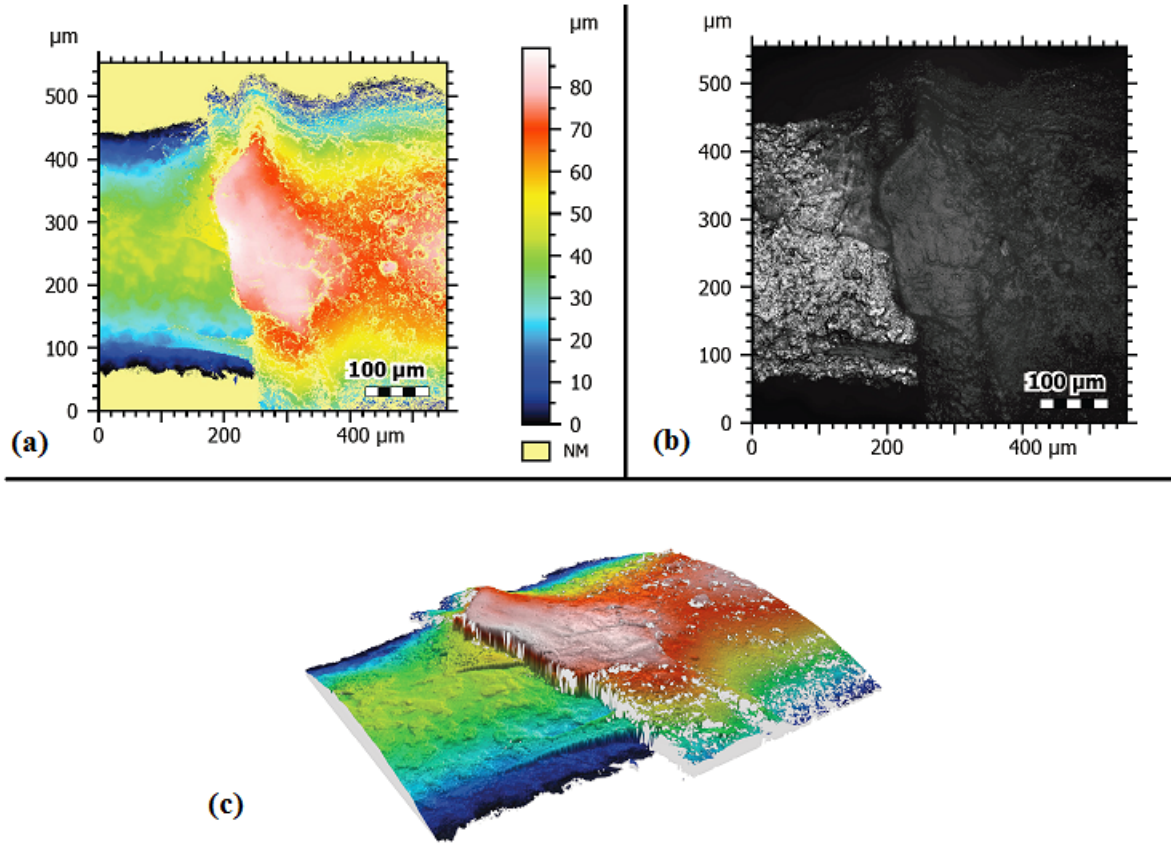


Figure 133: Confocal images of hydrogel coated surface (a) pseudo color view; (b) true color view of the image; (c) 3D view of the surface

The coating quality of the NiTi SMAs depends on the uniformity of the deposited layer on the surface which is significantly affected by coating methods. The uniformity of the hydrogel layer on the NiTi surface was also evaluated with SEM and digital microscopy as shown in Figure 134. The uniformity of the hydrogel layer was observed with 3D imaging and color mapping via confocal microscopy and SEM analyses. The hydrogel coating on NiTi wire was appear to be dense and homogeneous in selected area as given in Figure 134 a and b. According to the calculated average thickness and surface roughness values, the hydrogel coating was found as uniform along the NiTi wire (Figure 134 c). Finally, coatings with a uniform thickness was also observable via SEM analyses (Figure 134 d).

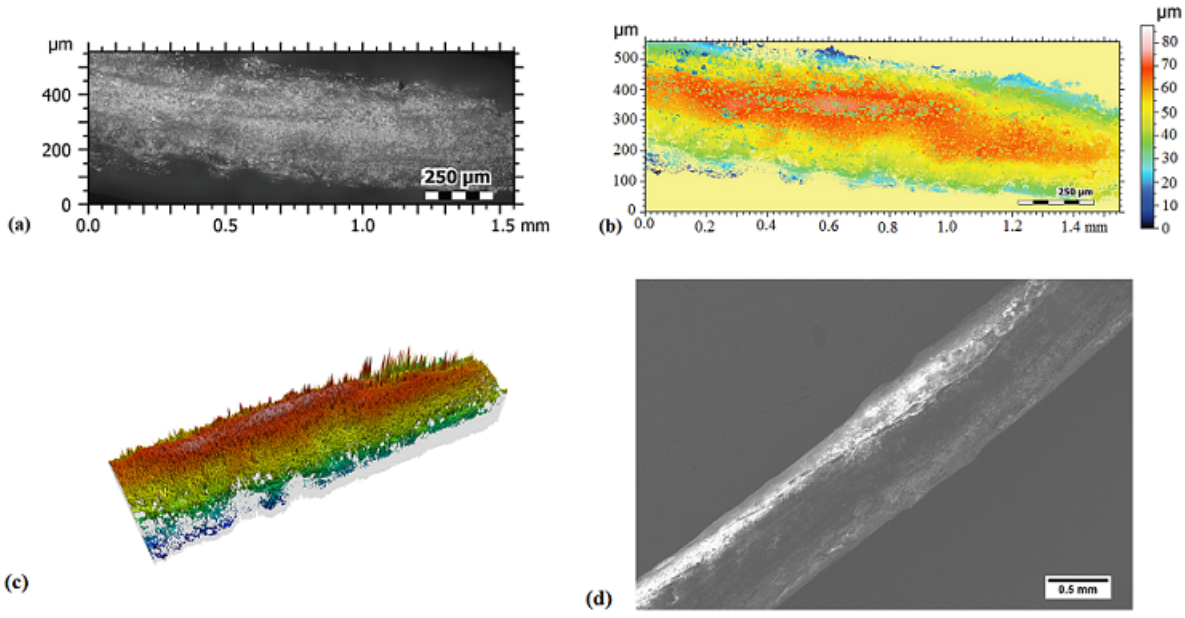


Figure 134: Confocal images of hydrogel coated NiTi (a) pseudo color view of the surface; (b) true color view of the image; (c) 3D view of the surface; (d) SEM images of hydrogel coated NiTi

Another important aspect that must be considered is decreasing the potential of Ni release which is one of the major aims of this dissertation. The effect of obtaining hydrogel layer on the NiTi surface was also evaluated with EDS analyses. Figure 133

depicts the elemental mapping analyses with related results. Mapping measurements were conducted in the selected area on the basis of presence and non presence of hydrogel layer visually for sampling through arrow direction. Results were compared based on selected elements including C, N, O, Ni and Ti.

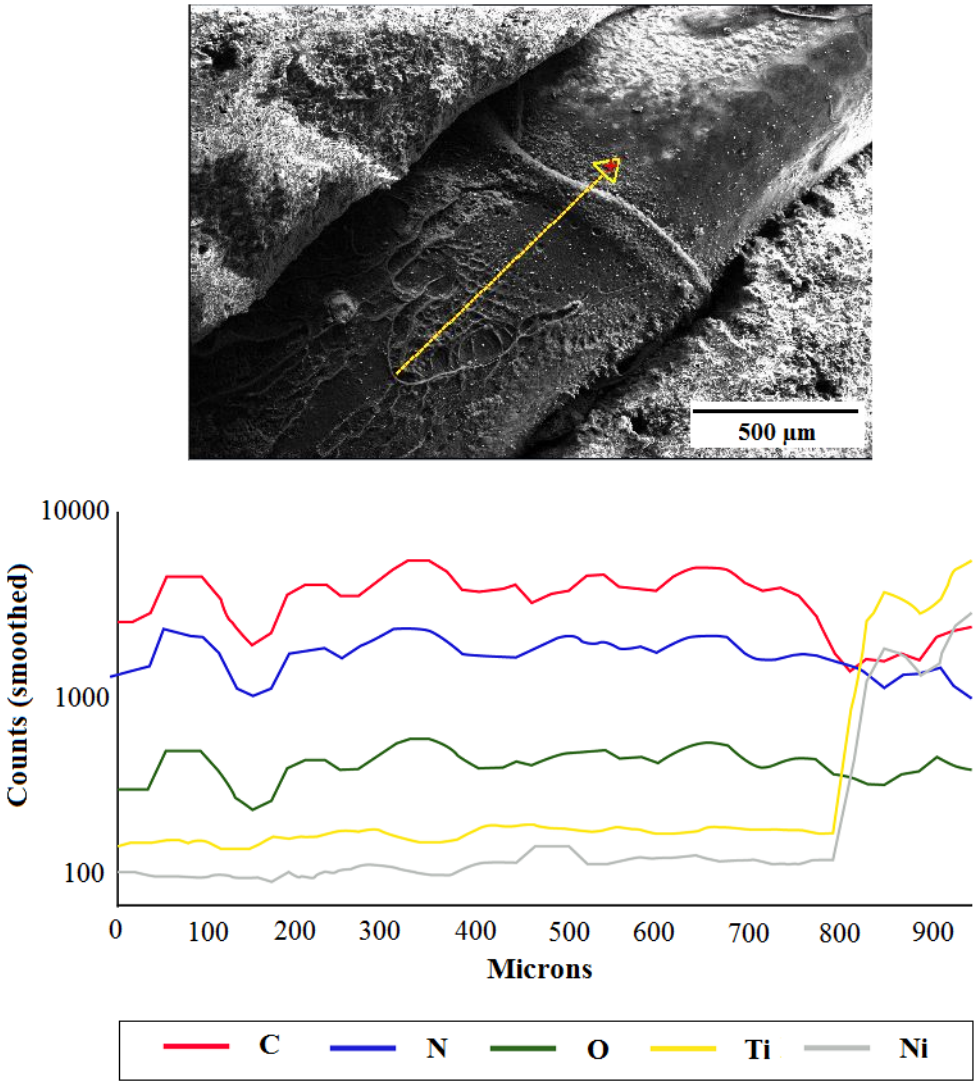


Figure 135: Elemental analyses of hydrogel coated NiTi sample for selected elements

The back of the arrow was placed on the coated section where as the tip was on uncoated part of NiTi. The results of measurements state that the concentration of Ni and Ti tends to more stable through arrow mostly. However at the tip of arrow, Ni

and Ti were significantly increased as expected. Same measurement was utilized with another hydrogel coated sample. In the coated area, the amounts of Ni and Ti were traced in much lesser extent. These findings appear to be related to the succession of the hydrogel coating process.

Hardness experiments have been conducted to test the presence of hydrogel coating on NiTi substrate. Although indentation tests on soft layers may lead to inaccurate results, it still serves as a good indicator for initial experiments. Figure 136 presents the microhardness measurements of both the uncoated and coated samples. After the formation of the hydrogel layer, the hardness significantly decreased, indicating to the presence of a softer layer on the harder NiTi substrate.

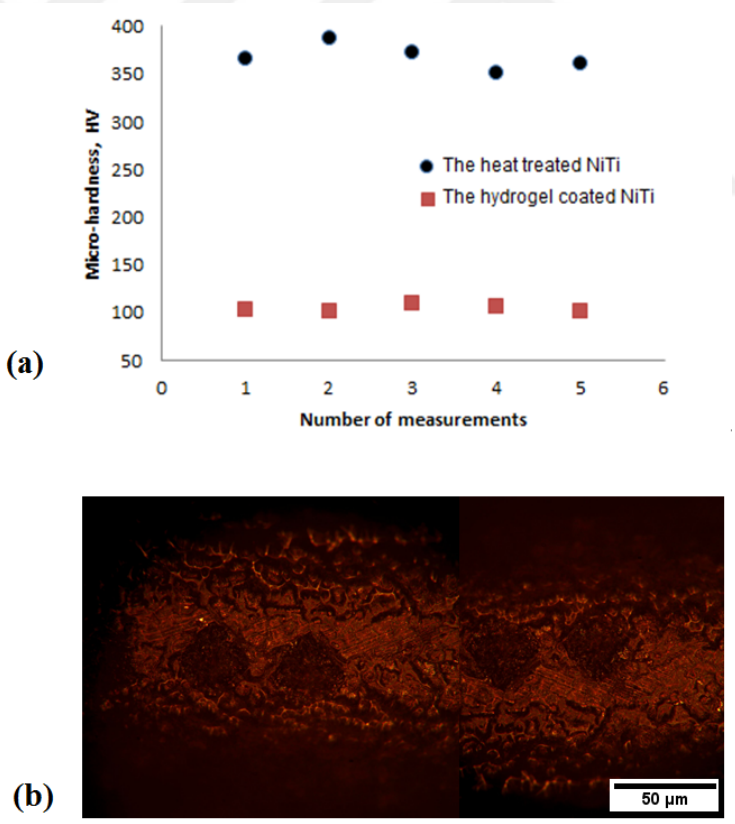


Figure 136: Hardness measurement: (a) experimental results of uncoated NiTi and hydrogel-coated NiTi; (b) hydrogel coated surface after hardness test

Contact angle measurements were conducted to assess the wettability characteristics of uncoated NiTi and hydrogel-coated NiTi samples as shown in Figure 137. The contact angle value of the uncoated NiTi surface was found to reach 111.15 ± 2^o. However, after coating with the hydrogel layer, the coated surface became hydrophilic with the value of 72.6 ± 3^o. Moreover, studies also claim that most of the metal substrate polymer-based coatings can be applied to make the surface hydrophilic. The findings presented herein show agreement with the previous literature and are highly prominent especially in the field of medical applications since hydrophilic surfaces are crucial for antibacterial features.

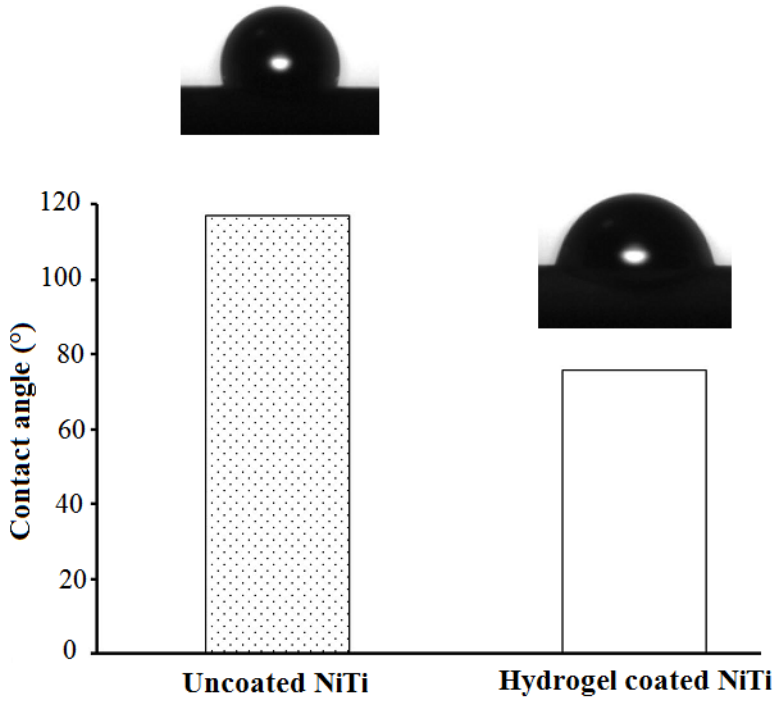


Figure 137: Contact angle of water droplets on uncoated and hydrogel-coated NiTi surfaces with the respective variation in contact angles

Figure 138 demonstrates the free bending behavior of the uncoated and coated NiTi samples as a function of surface temperature. It was seen that both samples reached the maximum bending angle, which is 140^o, as determined by the shape

setting process. As shape memory is a bulk property, it is reasonable that a thin hydrogel coating does not interfere in an adverse manner. Functional tests indicated that the hydrogel coating layer has no negative effect on the bending characteristic of NiTi wire which demonstrates that NiTi preserves its shape memory capacity. However, the surface temperature decreases significantly with the presence of hydrogel layer. Besides free bending experiment, withstand performance of hydrogel coated layer was also investigated with cycle tests. This test was conducted at constant bending angle of 15^o at 1 Hz in SBF for 500 and 1000 cycles. The hydrogel layer on the surface was withstand after 500 cycles without any delaceration. On the other hand, the hydrogel layer was ruptured after 1000 cycles. The surfaces were imaged with digital microscopy as shown in Figure 139.

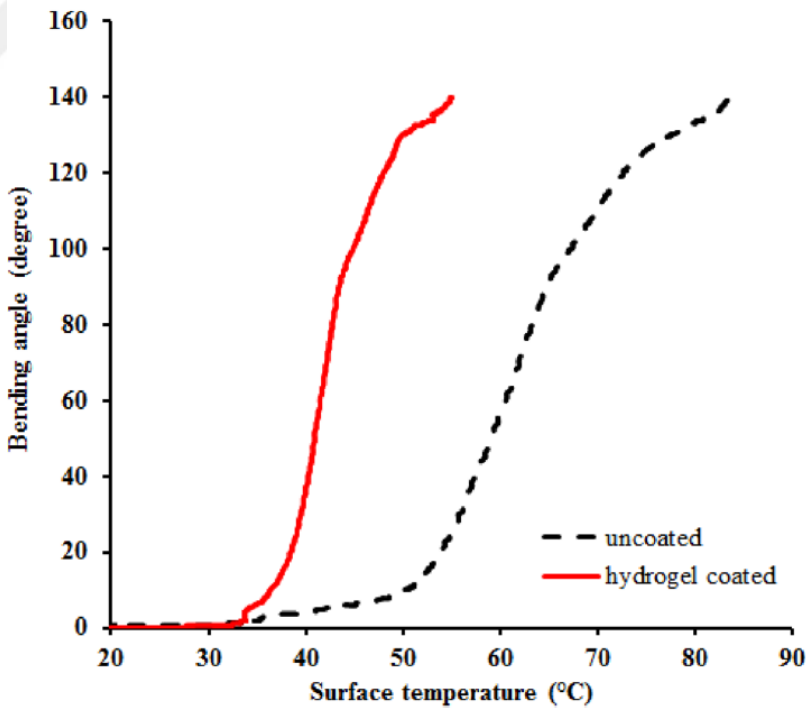


Figure 138: Bending behavior of uncoated and hydrogel-coated NiTi samples

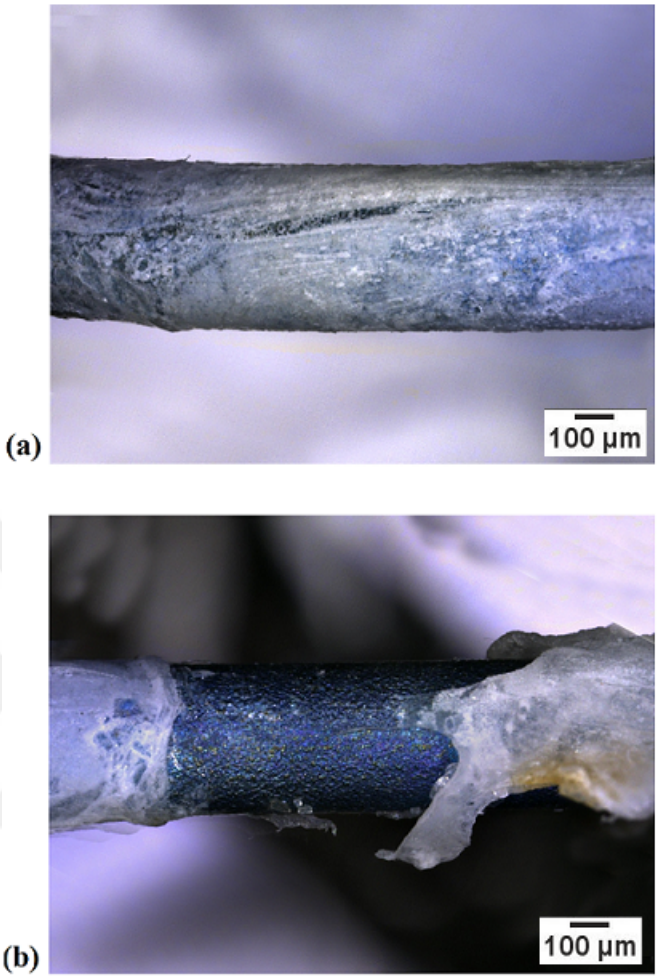


Figure 139: Hydrogel coated NiTi sample after cyclic experiment in dry condition (a) 500 cycle; (b)1000 cycle

Cyclic experiments of hydrogel coated NiTi sample were performed to explore the effect of hydrogel layer on the cyclic behavior. From the Figure 140, a steady decrease in the maximum number of cycles can be clearly observed for the uncoated and coated NiTi samples with the increase of frequency level. The comparison of the cyclic performance of uncoated NiTi and hydrogel coated NiTi revealed that hydrogel layer has a comparatively small effect on the fatigue life of NiTi samples for all environmental condition.

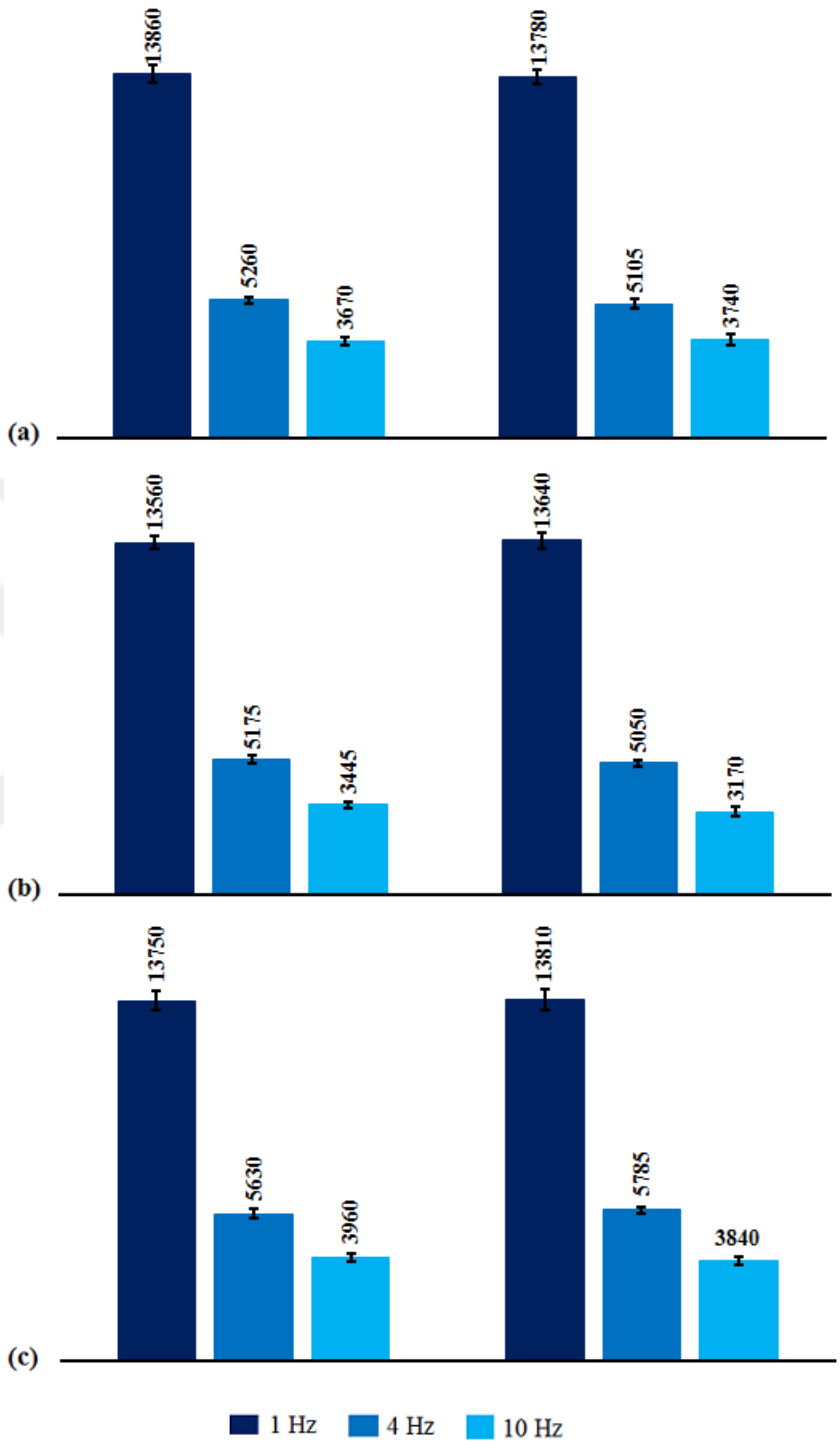


Figure 140: Cyclic behavior of hydrogel coated NiTi sample in (a) dry condition; (b) SBF solution; (c) Ringer solution at different frequencies

Furthermore, results reveal that the effect of environmental condition as compared to the frequency level of the experiments is considerably lower. The maximum number of cycles was found above 13850 for both uncoated and hydrogel coated NiTi samples at 1 Hz. Obviously, as discussed before, as the level of frequency increases, an overall decrease of number of cycles and, thus, deteriorated cyclic performance is observable that leads to rapid failure of the NiTi sample. According to all experiments, such number of cycles already be similar to each other. Lastly, the one of the fracture surface of hydrogel coated NiTi sample was given in Figure 141 for the sample that tested in dry condition at 4 Hz.

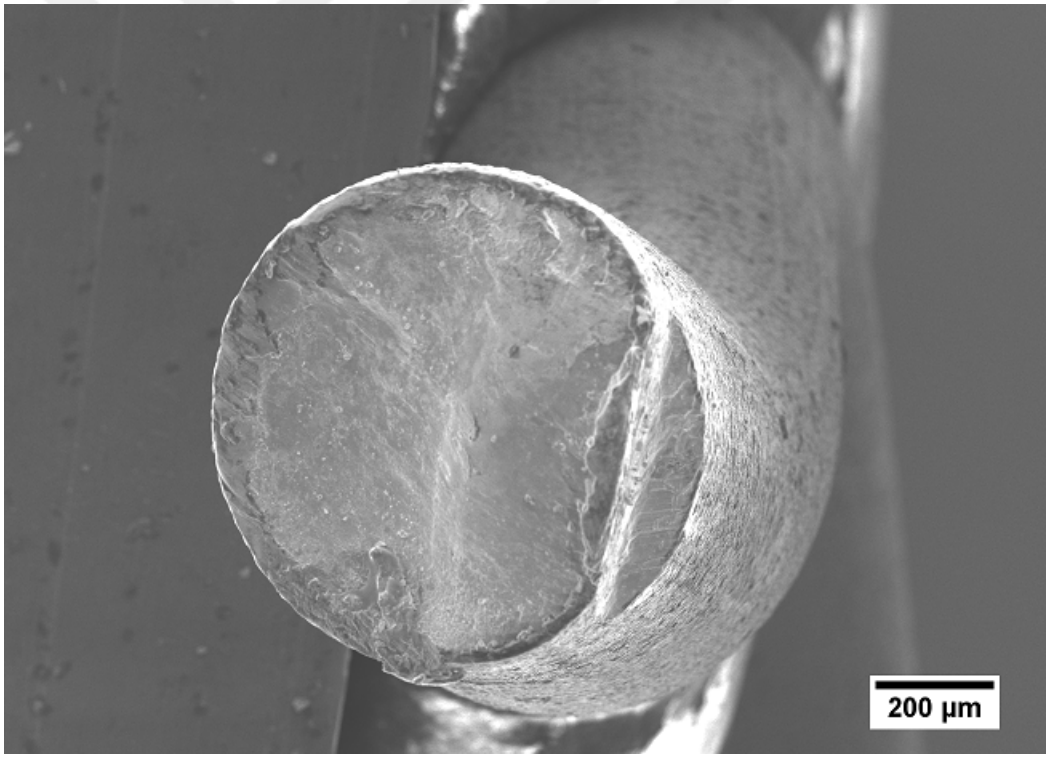


Figure 141: Fracture surface of hydrogel coated NiTi sample that tested in dry condition at 4 Hz

Hydrogel stability on the sample surface after immersion in simulated body fluid (SBF) at 37^{o}C was shown through corrosion experiments. The potentiodynamic polarization curves of the samples observed in SBF are given in Figure 142. It is

evident that the hydrogel-coated sample exhibits much nobler corrosion potential than the uncoated counterpart. Enhancement of corrosion resistance for coated surfaces could be attributed to the effectiveness of the hydrogel layer as a physical and chemical barrier protecting the NiTi substrate. These findings are in line with the previous studies. Indeed, hydrogels were recently demonstrated to be viable hydrogel coatings was used as a physical barrier for the prevention of corrosion [229, 230].

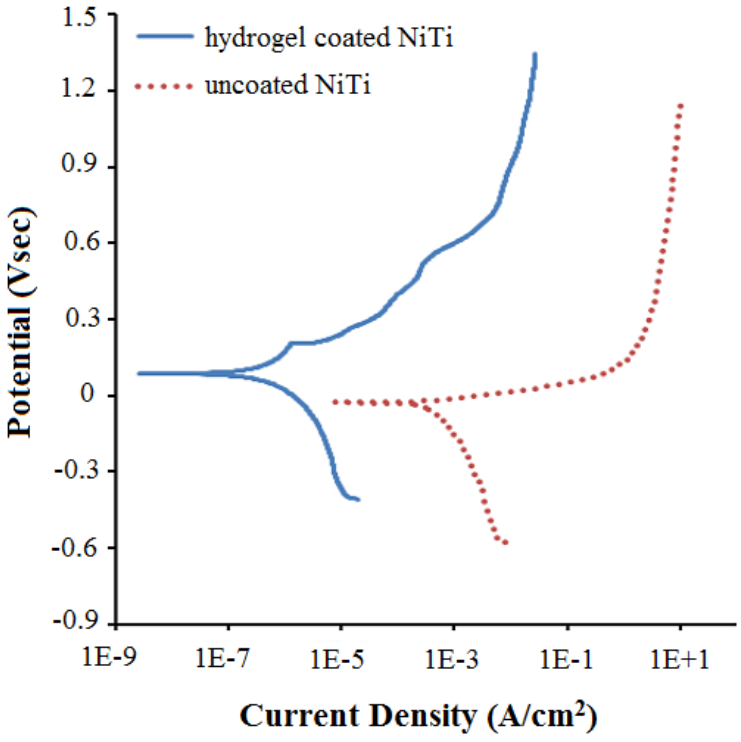


Figure 142: Potentiodynamic polarization curves of uncoated NiTi and hydrogel coated NiTi at 37^{o}C

The surface morphology of the hydrogel coated layer was characterized after corrosion experiment. Figure 143 shows the corroded surface of hydrogel coated NiTi sample. As seen in the both image, hydrogel layer was completely deteriorated. The surface pits can easily be discerned with digital microscopy as observed in Figure 143 b. Besides surface morphology analyses, the weight loss also measured after electrochemical experiment and summarized in Table 27.

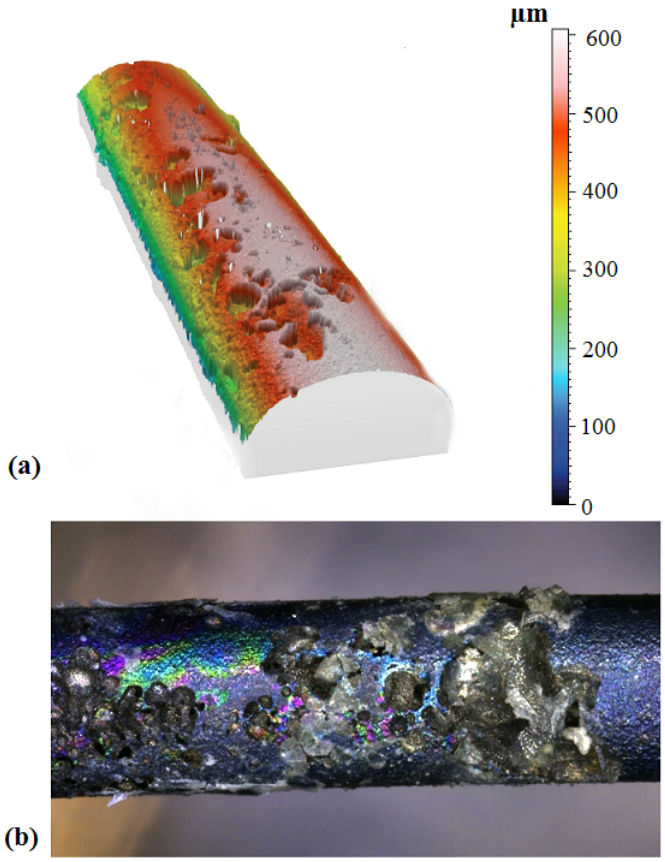


Figure 143: Corroded surface of hydrogel coated NiTi sample after corrosion experiment (a) color-map analysis; (b)digital microscope image at magnification of 105x

Table 27: Total material loss of hydrogel coated NiTi after electrochemical measurements

Sample	**Material loss (g)**
As-received	0.04863
Hydrogel coated	0.00658

The biocompatibility levels of the uncoated and hydrogel-coated NiTi were determined through direct contact cytotoxicity experiments. Even though PVA is biocompatible, due to its superhydrophilicity, it does not adsorb proteins, and it has

a bioinert surface. The 24 hours experiments were conducted to show that by the addition of gelatin, it is possible to obtain a hydrogel structure that could act as a barrier for corrosion, and possible release of nickel ions without deteriorating the cell attachment capability of the substrate surface. Samples were cultured with an almost confluent layer (80%) of Balb/3T3 cells, and the viability was estimated as in Figure 144. It was found that none of the configurations tested exhibited cytotoxicity since viability up to 70% was maintained for all cases, which is the limit set by ISO 10993. The average viability of the hydrogel-coated sample was slightly higher with a substantially lower variation.

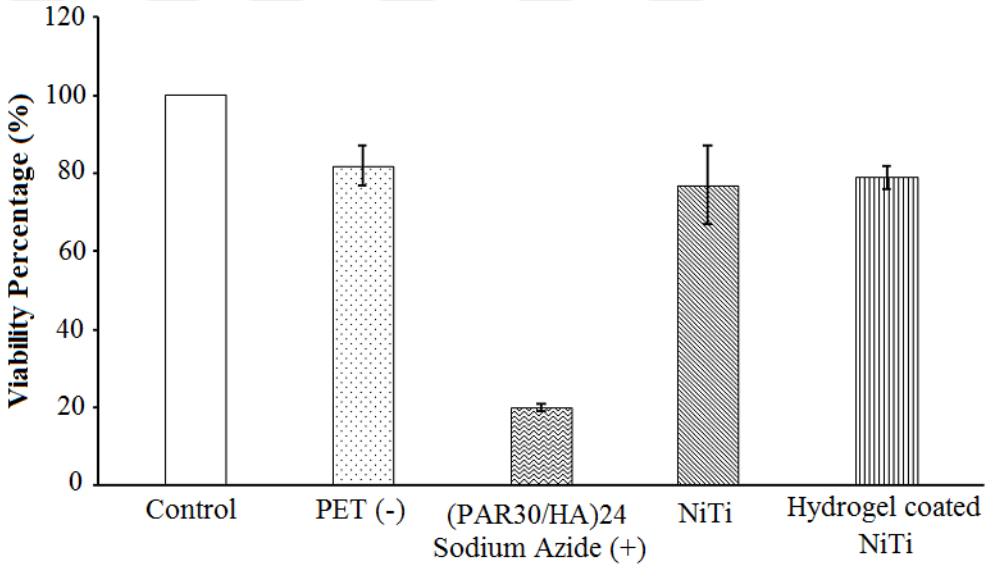


Figure 144: Viability of Balb/3T3 cells estimated after 24 h of contact with different materials

The cellular organization and colonization of Balb/3T3 cells after 7 days were demonstrated in Figure 145 a. For all configurations, decent surface coverage was found on the sample with well spread F-Actin filaments, pointing to the suitability of both samples for cell viability. 24 h after seeding, the cell numbers were similar for all three conditions, showing that there is no difference between the conditions prior to the introduction of the samples.

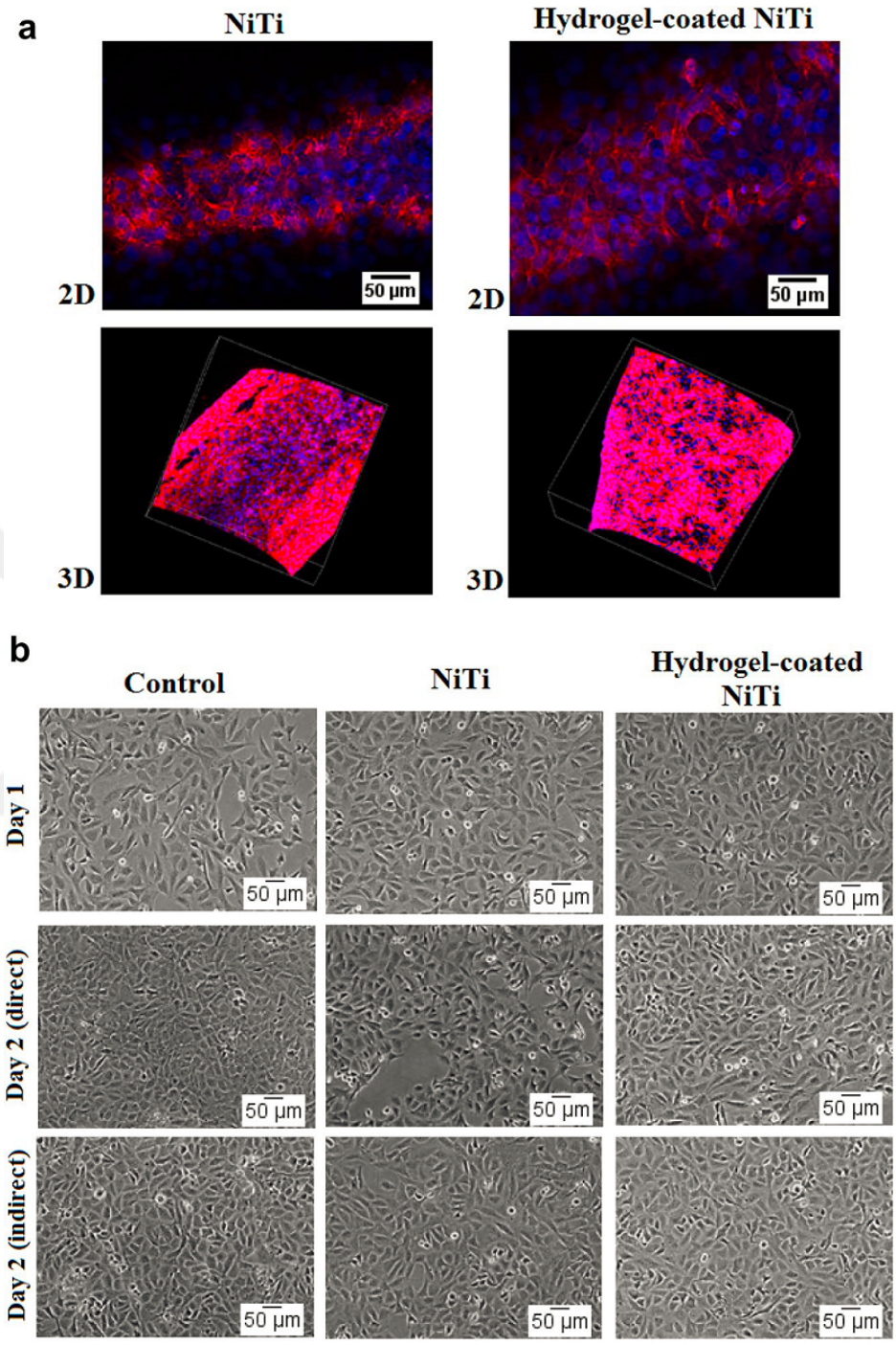


Figure 145: A DAPI/F-Actin stainings performed on Balb/3T3 cells after 7 days of culture on uncoated and hydrogel-coated samples (top) and confocal microscopy 3D reconstructions (bottom) scale bar = 100 m; b Balb/3T3 cells after direct (top) and indirect (bottom) cytotoxicity tests (magnification 10X)

Figure 145 b shows the confocal images to disclose that the presence of hydrogel does not induce cellular clustering. It was observed that after an additional 24 h of direct or indirect exposure to the coated and uncoated NiTi samples, the cellular viability was quantified by biochemical assays, and the results were verified by the microscopic analysis. Typically, cells prefer gelatin-rich zones which would be problematic on the wire surface in the case of a non-homogenous distribution of gelatin in the coating. Bioactivity levels of the coated and uncoated samples were above the cytotoxicity limit of 70% cell viability and can be considered non-cytotoxic. According to cytotoxicity results, it may be concluded that there is no Ni release from hydrogel coated NiTi surface since Ni ion release may resulted in severe cell death [165].

For PVA/Gelatin hydrogels, the degradation of the PVA component takes place through erosion and leaching of the PVA polymer chains; as there are no covalent bonds, the structure is not completely non-degradable. The level of degradation depends on the application; but for an orthopedic implant, this will be in the span of months. The gelatin component is amenable to enzymatic degradation by collagenases, but with a decreased rate due to the transglutaminase crosslinking. In contrast, this process will occur in a period spanning from days to several weeks. As the degradation timeline is within the resolution of the inflammation timeline, the presence of connective and local functional tissues is expected after the complete degradation of the hydrogel [231]. This will create a new extracellular matrix-based boundary against Ni release which is facilitated by the inflammatory environment of the initial wound if there was no coating layer present on the metallic substrate. Though, the lack of a hydrogel layer would result in the exposure of epithelial to temperatures over 80^{o}C, which potentially leads to irreversible tissue damage.

Regarding the long-term behavior of the proposed coating, a potential scenario can be perceived based on a few notable works. A literature review provides information on the potential behavior of hydrogel-coated NiTi samples for long-term application.

NiTi shape memory alloys have been utilized for various orthopedic applications including load bearing plates for bone fracture treatment, fixations for long bone shafts, correctors for spinal treatments, spinal spacers, and orthopedic staples.

Ruperez et al. reported that the highest Ni ion release from NiTi immersed in SBF occurs within the first hour [232]. In this study, before applying the hydrogel coating, NiTi wires were heat-treated with selected parameters for the shape setting process. This treatment additionally leads to the formation of an oxide layer on the substrate surface [157]. Subsequently, the sample was coated with PVA-based hydrogel. Since oxide layers are able to confining the diffusion of Ni ions [221], a dual coating composed of oxide and hydrogel layers may prove to be an effective barrier. They can also minimize the risk of Ni release from the implant surface for even long-period utilizations. This is particularly relevant for load-bearing applications where the implant components need to be dynamic and thus are prone to wear. Consequent release of harmful ions and the generation of wear-related debris are of critical importance in such applications. Thus, the improved tissue/implant interface enabled by the proposed coating in this work can contribute to evading these adverse effects without preventing implant integration.

3.3 Effect of biocompatible coating on the mathematical modeling of corrosion

The corrosion modeling was introduced in depth with main structure and results. In order to investigate the effect of biocompatible coating on the mathematical modeling of corrosion, the potential difference of metal was changed in the model. The influence of potential difference was investigated. The potential difference was varied in the range of 0.1 to 1V, with a step of 0.1V. It was not necessary to investigate a separate influence for each parameter, as only the potential difference is present in the governing equations for corrosion. The mean corrosion and entropy for the variation in this parameter are presented in Figure 146.

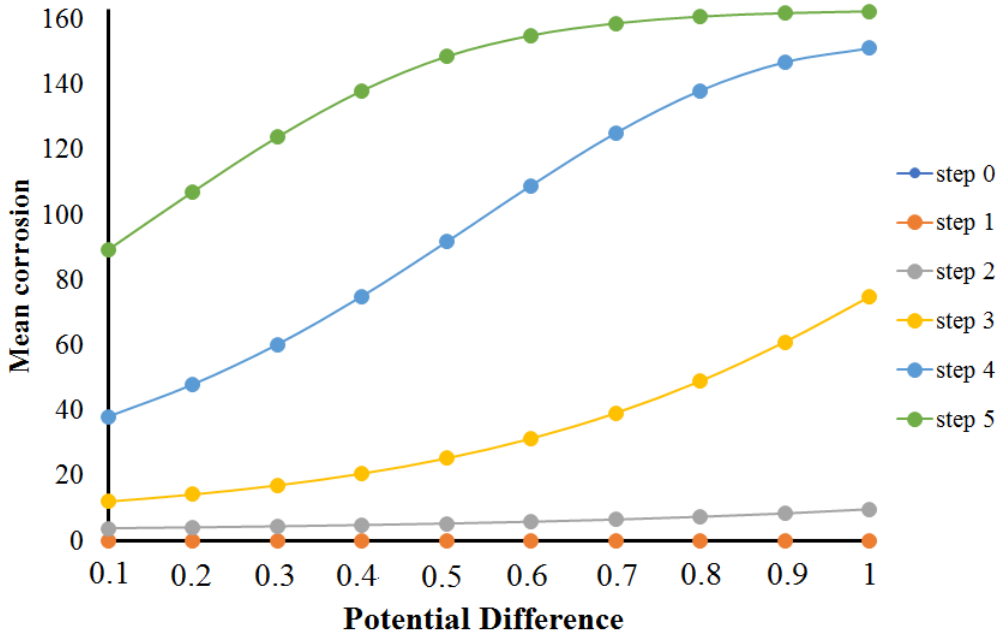


Figure 146: Relation between mean corrosion and potential difference

In theory, the potential difference should be minimum when coating process applied due to change of potential of the metal. The results show that with the increase in difference potential difference in the range of 0.1 to 1, it was noticeable that a slow increase in the mean corrosion in accordance with [208] and [207]. The explanation for a such trend change is that higher potential difference increases both the chemical reaction rate and the mass transport rate, which in turn increases the corrosion rate. The slopes are less steep than they are when there is variation in the pH value. It should be noted that the potential differences highly depend on the selected metal and solution. In this dissertation, the potential of the metal was selected for NiTi (as-received) before any kind of surface modification process including heat treatment, NaOH treatment, or coating and the selected solution was simulated body fluid. The potential difference may vary on the selection of metal or environmental conditions. Due to these reasons, all surface treatment and modification processes may effect the mean corrosion as a function of the potential difference parameter in the mathematical model.

Besides modeling, the number of steps were significantly affected with the initiation of both biocompatible layer as shown in Figure 147. The increase step addresses enhanced corrosion resistance. Number of black pixels were tend to decreased with the increase of number of step. Finally at step 24, the sampling area became white that indicate fully corroded cells.

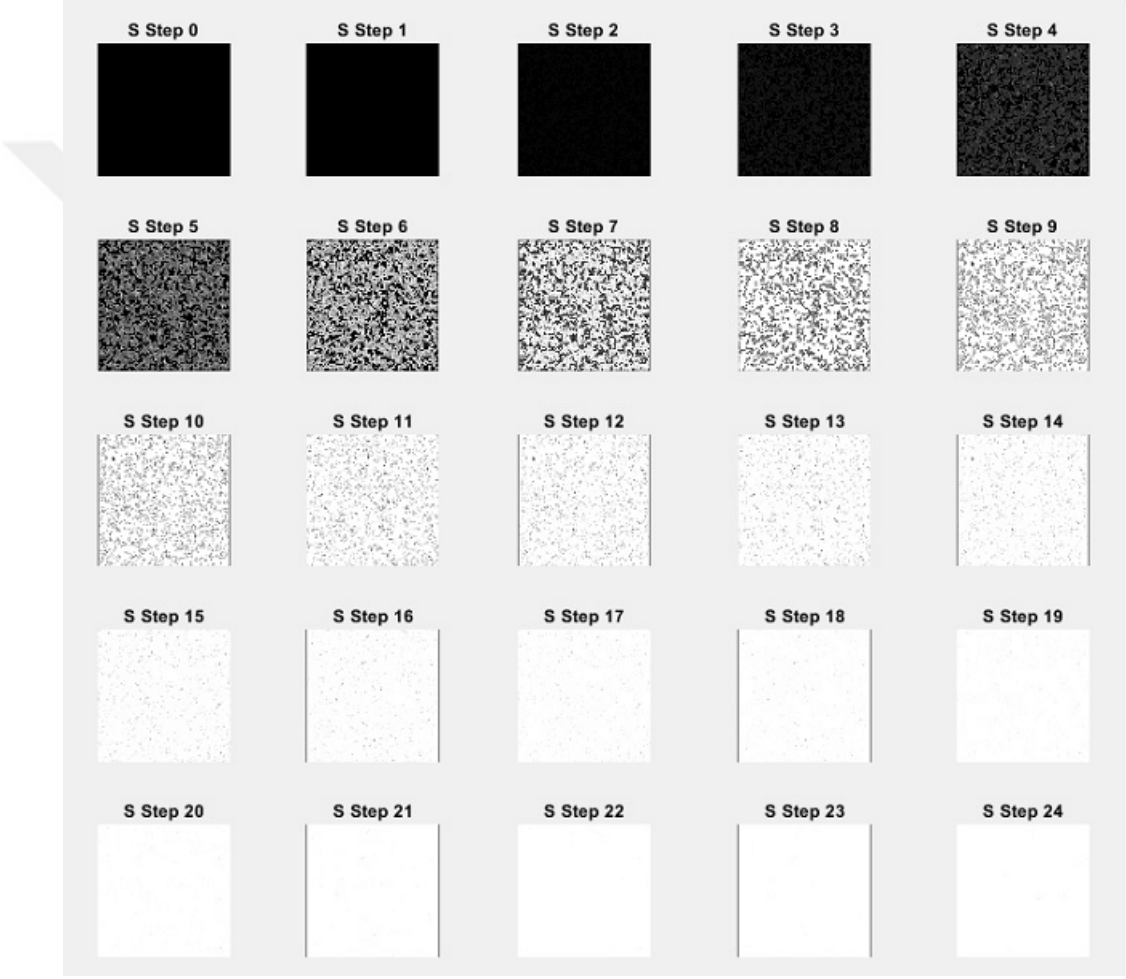


Figure 147: Evolution of black and white pixels as a function of step

CHAPTER IV

CONCLUSIONS

The aim of this dissertation is firstly to identify the influence of heat treatment conditions on the functional behavior of NiTi shape memory alloys. Heat treatment temperature strongly affects the mechanical properties of NiTi shape memory alloy including transformation temperatures, cyclic behavior, force level, hardness, and corrosion resistance. For the constant duration, with an increase of heat treatment temperature, the austenite start (A_s) and the austenite finish (A_f) temperatures increase. On the other hand, increasing the heat treatment duration from 30 minutes to 60 minutes was found to increase austenite start and finish temperatures for constant heat treatment temperatures. To the best of our knowledge, cyclic actuation under bending in wire form has not been previously considered. Among the heat treated NiTi shape memory alloys, the sample treated with 520^oC for 30 min shows the best cyclic performance. With the given bending configuration, the sample can be successfully achieved up to 50 actuation cycles. The corrosion resistance tends to decrease with increasing heat treatment temperature for a constant duration, whereas increasing the duration at a constant temperature enhances the corrosion performance. NiTi sample that was treated at 600^oC for 30 min demonstrated the lowest corrosion rate compared to other conditions. On the other hand, increasing the duration resulted in a decrease in the corrosion rate. At 600^oC, the reverse effect was found with the increase of heat treatment duration. The NiTi substrate heat treated at 520^oC for 30 min possesses the most essential mechanical properties compared to other heat treated NiTi samples. Thus, the substrate treated at 520^oC for 30 min was selected as an adjusted parameter for the shape setting process in this dissertation.

Furthermore, to fill the gap in the literature due to the limitations of the previously discussed investigations, this dissertation concentrated on biocompatible coatings on NiTi samples. CaP and hydrogel based coatings on NiTi wire samples were obtained to combine the mechanically superior NiTi shape memory alloys with the excellent biocompatibility of the coating layer to achieve implants with the most attractive medical performance. Firstly, the effect of the coating method on NiTi surfaces was evaluated through biomimetic and dip coating methods. SEM observations showed a successful coating layer obtained by the dip coating method as compared to the biomimetic technique. The initiation of the dip coating method resulted in the formation of well-densified CaP based layer on the NiTi surfaces. The coalescence of HA particles was observable on the surface. Compared with the biomimetic method, dip coating is found to be more suitable with wire shape surfaces. Therefore, contact angle measurements suggest that the dip coating method is more appropriate in obtaining contact angle values lower than 90° along with a homogeneous coating layer.

The application of NaOH surface treatment strongly and negatively affects coating quality and corrosion resistance. The coated sample without prior surface treatment showed the best corrosion performance. In contrast, elevation in the Ni amount was recorded on the treated sample surfaces with the increase of NaOH concentration, clearly indicating that corrosion resistance and coating quality deteriorate with NaOH modification. NaOH treatment considerably decreased the surface wettability such that the surface without NaOH treatment prior to HA coating has better wettability characteristics. Cytotoxicity experiments demonstrated the absence of significant toxicity for all samples irrespective of the NaOH pre-treatment. However, HA coated samples without prior NaOH treatment resulted in more promising cell viability counts.

On the other hand, PVA/Gelatin hydrogel was utilized for this dissertation as a coating materials since it is more than 90% hydrated, and thus, the metallic substrate forms a hydrated connection with the surrounding physiological fluids, which helps to dissipate heat. In particular, their resemblance to living tissue is a highly preferred feature for biomedical applications. With the deposition of the hydrogel layer on the NiTi surface, the surface became hydrophilic. It was well revealed that hydrophilic surfaces are more suitable than hydrophobic surfaces for biomedical requirements. Bending experiments show, for the first time, that the coating layer was able to withstand the bending movement as hydrogels display soft and flexible behavior. On the other hand, it has the added benefit of reduced actuation temperature. MTT test shows similar results for CaP and hydrogel coated, and uncoated NiTi samples in terms of spreading in comparison with the uncoated substrate. Both coatings could lead to better bioactivity and cell attachment which makes NiTi alloy more promising for the medical field.

Coating a metallic surface had a significant influence on the corrosion behavior of NiTi. Presented efforts have shown that both CaP based and hydrogel coating leads to a significant enhancement of the corrosion resistance. Obtained results were compared with the relevant values of bioceramic and hydrogel coated NiTi wire samples, and the comparison proved that CaP based coated NiTi sample had the lowest corrosion rate compared to the uncoated NiTi and hydrogel coated NiTi. In order to estimate the corrosion damage on the implants with given conditions, simulation studies were also utilized. Initial works have been done on modeling the corrosion behavior of the NiTi alloy. It was found that increase of pH leads to increase of corrosion and the higher potential difference increases both the chemical reaction rate and the mass transport rate, which in turn increases the corrosion rate. Preliminary results from in-silico models show that the developed model accurately captures the corrosion progress development in response to changes of different environmental parameters.

Most fatigue environments in the body involve irregular cyclic motion against highly compliant tissue. Extensive experiment series is being done to better understand the cyclic and corrosion contributions to fatigue lifetime. The cyclic behavior of heat treated and coated NiTi samples was investigated in different corrosive environments. Cyclic experiments were conducted at 1 Hz, 4 Hz, and 10 Hz in dry conditions, SBF, and Ringer solutions. All findings were consistent for all uncoated and coated NiTi samples. It was found that the number of cycles decreased with the increase in frequency. Coating materials and environmental conditions do not have any noticeable effects on the cyclic behavior of NiTi.

Suggestions for Future work

1. Concentration of solution, different surface modifications, immersion periods, and temperature were selected as coating parameters in this dissertation. Dip coating and biomimetic methods were utilized in order to prove state of art in particular for wire form shape memory alloys. Controlling coating thickness is beyond the scope of the dissertation. However, to follow up on the current work, controlling coating thickness for both CaP and hydrogel coating may be investigated in more detail.

2. In order to investigate coating characteristics, it is important to measure coating thickness. The measurement of the thickness of hydrogel is highly challenging since hydrogels have high water content. After the coating process is obtained in atmospheric conditions, the shrinking mechanism may rapidly occur and resulting in reduced coating thickness compared to moist body conditions. Therefore, extended investigations on the measurement of coating thickness in wet conditions may be a topic of interest for future works.

3. The mathematical modeling of corrosion mechanisms is an important issue for clinical applications. Therefore, preliminary results from in-silico models show that the developed model accurately captures the corrosion progress development in response to changes in different environmental parameters. Furthermore, detailed investigations may be examined in the follow-up works.

4. To further investigation of the corrosion-related cyclic behavior may be conducted as future works. A detailed microstructural study of the NiTi samples before and after fatigue experiments may benefit the knowledge in the literature. Consequently, further research on the effects of test frequency, the environment of experiments, and heat treatment parameters on the cyclic performance of NiTi SMAs can be conducted.

REFERENCES

[1] K. Otsuka and C. M. Wayman, *Shape memory materials*. Cambridge University Press, 1999.

[2] A. Ölander, "An electrochemical investigation of solid cadmium-gold alloys," *Journal of the American Chemical Society*, vol. 54, no. 10, pp. 3819–3833, 1932.

[3] A. Mehta, V. Imbeni, R. Ritchie, and T. Duerig, "On the electronic and mechanical instabilities in ni50. 9ti49. 1," *Materials Science and Engineering: A*, vol. 378, no. 1-2, pp. 130–137, 2004.

[4] S. Thompson, "An overview of nickel-titanium alloys used in dentistry," *International Endodontic Journal*, vol. 33, no. 4, pp. 297–310, 2000.

[5] T. W. Duerig, K. Melton, and D. Stöckel, *Engineering aspects of shape memory alloys*. Butterworth-heinemann, 2013.

[6] J. Mohd Jani, M. Leary, A. Subic, and M. A. Gibson, "A review of shape memory alloy research, applications and opportunities," *Materials Design (1980-2015)*, vol. 56, pp. 1078–1113, 2014.

[7] D. C. Lagoudas, *Shape memory alloys: modeling and engineering applications*. Springer, 2008.

[8] G. F. Andreasen and T. B. Hilleman, "An evaluation of 55 cobalt substituted nitinol wire for use in orthodontics," *The Journal of the American Dental Association*, vol. 82, no. 6, pp. 1373–1375, 1971.

[9] D. Wever, J. Elstrodt, A. Veldhuizen, *et al.*, "Scoliosis correction with shape-memory metal: results of an experimental study," *European Spine Journal*, vol. 11, no. 2, pp. 100–106, 2002.

[10] M. H. Wu, L. Schetky, *et al.*, "Industrial applications for shape memory alloys," in *Proceedings of the International Conference on Shape Memory and Superelastic Technologies*, vol. 171, 2000.

[11] D. J. Hartl and D. C. Lagoudas, "Aerospace applications of shape memory alloys," *Proceedings of the Institution of Mechanical Engineers, Part G: Journal of Aerospace Engineering*, vol. 221, no. 4, pp. 535–552, 2007.

[12] Y. Liu, J. Van Humbeeck, R. Stalmans, and L. Delaey, "Some aspects of the properties of niti shape memory alloy," *Journal of Alloys and Compounds*, vol. 247, no. 1-2, pp. 115–121, 1997.

[13] G. M. Simsek and G. G. Yapici, "Influence of heat treatment parameters on the functional behavior and corrosion performance of a shape memory wire actuator," in *Materials Science Forum*, vol. 986, pp. 55–60, Trans Tech Publ, 2020.

[14] J. Khalil-Allafi and B. Amin-Ahmadi, "The effect of chemical composition on enthalpy and entropy changes of martensitic transformations in binary niti shape memory alloys," *Journal of Alloys and Compounds*, vol. 487, no. 1-2, pp. 363–366, 2009.

[15] M. Paryab, "The effect of heat treatment on the microstructural and superelastic behavior of niti alloy with 58.5 wt.% ni," *Journal of Environmental Friendly Materials*, vol. 3, no. 1, pp. 23–27, 2019.

[16] R. R. Adharapurapu, *Phase transformations in nickel-rich nickel-titanium alloys: influence of strain-rate, temperature, thermomechanical treatment and nickel composition on the shape memory and superelastic characteristics*. University of California, San Diego, 2007.

[17] J. Frenzel, E. P. George, A. Dlouhy, C. Somsen, M.-X. Wagner, and G. Eggeler, "Influence of ni on martensitic phase transformations in niti shape memory alloys," *Acta Materialia*, vol. 58, no. 9, pp. 3444–3458, 2010.

[18] T. B. Massalski, J. Murray, L. Bennett, and H. Baker, "Binary alloy phase diagrams. vol. i and ii," *American Society for Metals, 1986,*, p. 2224, 1986.

[19] A. R. Pelton, S. M. Russell, and J. DiCello, "The physical metallurgy of nitinol for medical applications," *Jom*, vol. 55, no. 5, pp. 33–37, 2003.

[20] A. Nespoli, E. Villa, and F. Passaretti, "Functional properties and morphology of niti articulated actuation elements during thermo-mechanical cyclic tests," *Metals and Materials International*, vol. 21, no. 3, pp. 504–510, 2015.

[21] S. Miyazaki, T. Imai, Y. Igo, and K. Otsuka, "Effect of cyclic deformation on the pseudoelasticity characteristics of ti-ni alloys," *Metallurgical transactions A*, vol. 17, no. 1, pp. 115–120, 1986.

[22] M. E. Mitwally and M. Farag, "Effect of cold work and annealing on the structure and characteristics of niti alloy," *Materials Science and Engineering: A*, vol. 519, no. 1-2, pp. 155–166, 2009.

[23] H. Sadiq, M.-B. Wong, R. Al-Mahaidi, and X. Zhao, "The effects of heat treatment on the recovery stresses of shape memory alloys," *Smart Materials and Structures*, vol. 19, no. 3, p. 035021, 2010.

[24] S. H. Yoon and D. J. Yeo, "Phase transformations of nitinol shape memory alloy by varying with annealing heat treatment conditions," in *Smart Materials III*, vol. 5648, pp. 208–215, SPIE, 2004.

[25] D. Vojtěch, "Influence of heat treatment of shape memory niti alloy on its mechanical properties," in *International Conference Metals*, pp. 18–20, 2010.

[26] M. Nishida, C. Wayman, R. Kainuma, and T. Honma, "Further electron microscopy studies of the ti11 ni14 phase in an aged ti 52at% ni shape memory alloy," *Scripta Metallurgica*, vol. 20, no. 6, pp. 899–904, 1986.

[27] G. Tadayyon, M. Mazinani, Y. Guo, S. M. Zebarjad, S. A. Tofail, and M. J. Biggs, "Study of the microstructure evolution of heat treated ti-rich niti shape memory alloy," *Materials Characterization*, vol. 112, pp. 11–19, 2016.

[28] F. Butera, "Shape memory actuators," *Advanced Materials and Processes*, vol. 166, no. 3, pp. 37–40, 2008.

[29] D. Stoeckel, "Shape memory actuators for automotive applications," *Materials & Design*, vol. 11, no. 6, pp. 302–307, 1990.

[30] C. Bil, K. Massey, and E. J. Abdullah, "Wing morphing control with shape memory alloy actuators," *Journal of Intelligent Material Systems and Structures*, vol. 24, no. 7, pp. 879–898, 2013.

[31] L. McDonald Schetky, "Shape memory alloy applications in space systems," *Materials Design*, vol. 12, no. 1, pp. 29–32, 1991.

[32] M. M. Kheirikhah, S. Rabiee, and M. E. Edalat, "A review of shape memory alloy actuators in robotics," *RoboCup 2010: Robot Soccer World Cup XIV*, pp. 206–217, 2011.

[33] L. Machado and M. Savi, "Medical applications of shape memory alloys," *Brazilian Journal of Medical and Biological Research*, vol. 36, pp. 683–691, 2003.

[34] V. Gyunter, V. Itin, L. Monasevich, and Y. I. Paskal, "Shape memory effects and their application in medicine," *Nauka Novosibirsk*, 1992.

[35] L. Castleman, S. Motzkin, F. Alicandri, V. Bonawit, and A. Johnson, "Biocompatibility of nitinol alloy as an implant material," *Journal of biomedical materials research*, vol. 10, no. 5, pp. 695–731, 1976.

[36] Y. Haga, "Active catheter using polymer links," *Minimally Invasive Therapy & Allied Technologies*, vol. 6, p. 56, 1997.

[37] G. Lim, K. Park, M. Sugihara, K. Minami, and M. Esashi, "Future of active catheters," *Sensors and Actuators A: Physical*, vol. 56, no. 1-2, pp. 113–121, 1996.

[38] K. Yanagihara, H. Mizuno, H. Wada, and S. Hitomi, "Tracheal stenosis treated with self-expanding nitinol stent," *The Annals of Thoracic Surgery*, vol. 63, no. 6, pp. 1786–1789, 1997.

[39] I. Vinograd, B. Klin, T. Brosh, M. Weinberg, Y. Flomenblit, and Z. Nevo, "A new intratracheal stent made from nitinol, an alloy with "shape memory effect"," *The Journal of Thoracic and Cardiovascular Surgery*, vol. 107, no. 5, pp. 1255–1261, 1994.

[40] G. Airoldi, G. Riva, and M. Vanelli, "Superelasticity and shape memory effect in niti orthodontic wires," *Journal de Physique IV*, vol. 5, no. C8, pp. C8–1205, 1995.

[41] V. R. M. A. Fernandesa D.J., Eliasa C.N., "Mechanical performance of nickel-titanium archwires," *Materials Research*, vol. 6, no. 18, pp. 1264–1277, 2015.

[42] S. Kapila and R. Sachdeva, "Mechanical properties and clinical applications of orthodontic wires," *American Journal of Orthodontics and Dentofacial Orthopedics*, vol. 96, no. 2, pp. 100–109, 1989.

[43] S. Miyazaki, "Thermal and stress cycling effects and fatigue properties of ni-ti alloys," *Engineering Aspects of Shape Memory Alloys*, vol. 394, 1990.

[44] J. O'Leary, J. Nicholson, and R. Gatturna, "The use of ni–ti in the homer mammalok," *Butterworth-Heinemann, Engineering Aspects of Shape Memory Alloys(UK), 1990,*, pp. 477–482, 1990.

[45] D. S. Levi, N. Kusnezov, and G. P. Carman, "Smart materials applications for pediatric cardiovascular devices," *Pediatric Research*, vol. 63, no. 5, pp. 552–558, 2008.

[46] M. Simon, R. Kaplow, E. Salzman, and D. Freiman, "A vena cava filter using thermal shape memory alloy: Experimental aspects," *Radiology*, vol. 125, no. 1, pp. 89–94, 1977.

[47] K. Kuribayashi, K. Tsuchiya, Z. You, D. Tomus, M. Umemoto, T. Ito, and M. Sasaki, "Self-deployable origami stent grafts as a biomedical application of ni-rich tini shape memory alloy foil," *Materials Science and Engineering: A*, vol. 419, no. 1-2, pp. 131–137, 2006.

[48] M. Schmerling, M. Wilkov, A. Sanders, and J. Woosley, "Using the shape recovery of nitinol in the harrington rod treatment of scoliosis," *Journal of Biomedical Materials Research*, vol. 10, no. 6, pp. 879–892, 1976.

[49] Z. Laster, A. MacBean, P. Ayliffe, and L. Newlands, "Fixation of a frontozygomatic fracture with a shape-memory staple," *British Journal of Oral and Maxillofacial Surgery*, vol. 39, no. 4, pp. 324–325, 2001.

[50] G. Lim, K. Minami, K. Yamamoto, M. Sugihara, M. Uchiyama, and M. Esashi, "Multi-link active catheter snake-like motion," *Robotica*, vol. 14, no. 5, pp. 499–506, 1996.

[51] S. Maeda, K. Abe, K. Yamamoto, O. Tohyama, and H. Ito, "Active endoscope with sma (shape memory alloy) coil springs," in *Proceedings of Ninth International Workshop on Micro Electromechanical Systems*, pp. 290–295, IEEE, 1996.

[52] J. Peirs, D. Reynaerts, and H. Van Brussel, "Design of a shape memory actuated endoscopic tip," *Sensors and Actuators A: physical*, vol. 70, no. 1-2, pp. 135–140, 1998.

[53] Y. Haga, Y. Tanahashi, and M. Esashi, "Small diameter active catheter using shape memory alloy," in *Proceedings MEMS 98. IEEE. Eleventh Annual International Workshop on Micro Electro Mechanical Systems. An Investigation of Micro Structures, Sensors, Actuators, Machines and Systems (Cat. No. 98CH36176*, pp. 419–424, IEEE, 1998.

[54] H. Y. M. T. Esashi, M., "U.s. patent no. 6,936,015," 2005.

[55] K. C. Dee, D. A. Puleo, and R. Bizios, *An introduction to tissue-biomaterial interactions*. John Wiley & Sons, 2003.

[56] D. E. Cutright, S. N. Bhaskar, B. Perez, R. M. Johnson, and G. S. Cowan Jr, "Tissue reaction to nitinol wire alloy," *Oral Surgery, Oral Medicine, Oral Pathology*, vol. 35, no. 4, pp. 578–584, 1973.

[57] A. Kapanen, J. Ryhänen, A. Danilov, and J. Tuukkanen, "Effect of nickel–titanium shape memory metal alloy on bone formation," *Biomaterials*, vol. 22, no. 18, pp. 2475–2480, 2001.

[58] C. Trepanier, T. Leung, M. Tabrizian, L. Yahia, J.-G. Bienvenu, J.-F. Tanguay, D. Piron, and L. Bilodeau, "Preliminary investigation of the effects of surface treatments on biological response to shape memory niti stents," *Journal of Biomedical Materials Research: An Official Journal of The Society for Biomaterials, The Japanese Society for Biomaterials, and The Australian Society for Biomaterials*, vol. 48, no. 2, pp. 165–171, 1999.

[59] W. Chrzanowski, E. A. Abou Neel, D. A. Armitage, and J. C. Knowles, "Effect of surface treatment on the bioactivity of nickel–titanium," *Acta Biomaterialia*, vol. 4, no. 6, pp. 1969–1984, 2008.

[60] T. Kokubo, F. Miyaji, H.-M. Kim, and T. Nakamura, "Spontaneous formation of bonelike apatite layer on chemically treated titanium metals," *Journal of the American Ceramic Society*, vol. 79, no. 4, pp. 1127–1129, 1996.

[61] T. Miyazaki, H.-M. Kim, T. Kokubo, C. Ohtsuki, H. Kato, and T. Nakamura, "Mechanism of bonelike apatite formation on bioactive tantalum metal in a simulated body fluid," *Biomaterials*, vol. 23, no. 3, pp. 827–832, 2002.

[62] W. A. Daoud, J. H. Xin, and Y.-H. Zhang, "Surface functionalization of cellulose fibers with titanium dioxide nanoparticles and their combined bactericidal activities," *Surface Science*, vol. 599, no. 1-3, pp. 69–75, 2005.

[63] M. Pohl, T. Glogowski, S. Kühn, C. Hessing, and F. Unterumsberger, "Formation of titanium oxide coatings on niti shape memory alloys by selective oxidation," *Materials Science and Engineering: A*, vol. 481, pp. 123–126, 2008.

[64] Y. Yu, T. Sun, and Y. Wang, "Bioactive titanium oxide coatings fabricated on niti sma via thermal treatment for medical applications," *Procedia Engineering*, vol. 141, pp. 115–120, 2016.

[65] Z. Yang, X. Wei, P. Cao, and W. Gao, "Surface modification of nitinol by chemical and electrochemical etching," *Modern Physics Letters B*, vol. 27, no. 19, p. 1341012, 2013.

[66] B. Katona, E. Bognár, B. Berta, P. Nagy, and K. Hirschberg, "Chemical etching of nitinol stents," *Acta of Bioengineering and Biomechanics*, vol. 15, no. 4, 2013.

[67] S. A. Shabalovskaya, "Surface, corrosion and biocompatibility aspects of nitinol as an implant material," *Biomedical Materials and Engineering*, vol. 12, no. 1, pp. 69–109, 2002.

[68] K. Ozeki, T. Yuhta, H. Aoki, and Y. Fukui, "Inhibition of ni release from niti alloy by hydroxyapatite, alumina, and titanium sputtered coatings," *Biomedical Materials and Engineering*, vol. 13, no. 3, pp. 271–279, 2003.

[69] H. Maleki-Ghaleh, V. Khalili, J. Khalil-Allafi, and M. Javidi, "Hydroxyapatite coating on niti shape memory alloy by electrophoretic deposition process," *Surface and Coatings Technology*, vol. 208, pp. 57–63, 2012.

[70] O. Albayrak, O. El-Atwani, and S. Altintas, "Hydroxyapatite coating on titanium substrate by electrophoretic deposition method: effects of titanium dioxide inner layer on adhesion strength and hydroxyapatite decomposition," *Surface and Coatings Technology*, vol. 202, no. 11, pp. 2482–2487, 2008.

[71] D.-Y. Lin and X.-X. Wang, "Preparation of hydroxyapatite coating on smooth implant surface by electrodeposition," *Ceramics International*, vol. 37, no. 1, pp. 403–406, 2011.

[72] A. Stoch, W. Jastrze, E. Długoń, W. Lejda, B. Trybalska, G. Stoch, A. Adamczyk, *et al.*, "Sol–gel derived hydroxyapatite coatings on titanium and its alloy ti6al4v," *Journal of Molecular Structure*, vol. 744, pp. 633–640, 2005.

[73] E. Sachlos, J. Czernuszka, *et al.*, "Making tissue engineering scaffolds work. review: the application of solid freeform fabrication technology to the production of tissue engineering scaffolds," *Eur Cell Mater*, vol. 5, no. 29, pp. 39–40, 2003.

[74] E. Verron, I. Khairoun, J. Guicheux, and J.-M. Bouler, "Calcium phosphate biomaterials as bone drug delivery systems: a review," *Drug Discovery Today*, vol. 15, no. 13-14, pp. 547–552, 2010.

[75] K. Dudek, M. Dulski, T. Goryczka, and A. Gerle, "Structural changes of hydroxyapatite coating electrophoretically deposited on niti shape memory alloy," *Ceramics International*, vol. 44, no. 10, pp. 11292–11300, 2018.

[76] J. Katić, M. Metikoš-Huković, and R. Babić, "Synthesis and characterization of calcium phosphate coatings on nitinol," *Journal of Applied Electrochemistry*, vol. 44, no. 1, pp. 87–96, 2014.

[77] T. Sun, N. Xue, C. Liu, C. Wang, and J. He, "Bioactive (si, o, n)/(ti, o, n)/ti composite coating on niti shape memory alloy for enhanced wear and corrosion performance," *Applied Surface Science*, vol. 356, pp. 599–609, 2015.

[78] C. F. Dunne, K. Roche, B. Twomey, and K. T. Stanton, "Deposition of hydroxyapatite onto shape memory niti wire," *Materials Letters*, vol. 176, pp. 185–188, 2016.

[79] T. Kokubo, S. Ito, Z. Huang, T. Hayashi, S. Sakka, T. Kitsugi, and T. Yamamuro, "Ca, p-rich layer formed on high-strength bioactive glass-ceramic a-w," *Journal of Biomedical Materials Research*, vol. 24, no. 3, pp. 331–343, 1990.

[80] Y.-M. Lim, Y.-J. Park, Y.-H. Yun, and K.-S. Hwang, "Functionally graded ti/hap coatings on ti–6al–4v obtained by chemical solution deposition," *Ceramics International*, vol. 28, no. 1, pp. 37–41, 2002.

[81] S. Bharati, M. K. Sinha, and D. Basu, "Hydroxyapatite coating by biomimetic method on titanium alloy using concentrated sbf," *Bulletin of Materials Science*, vol. 28, no. 6, pp. 617–621, 2005.

[82] Y. Gu, B. Tay, C. Lim, and M. Yong, "Biomimetic deposition of apatite coating on surface-modified niti alloy," *Biomaterials*, vol. 26, no. 34, pp. 6916–6923, 2005.

[83] M. Chen, X. Yang, Y. Liu, S. Zhu, Z. Cui, and H. C. Man, "Study on the formation of an apatite layer on niti shape memory alloy using a chemical treatment method," *Surface and Coatings Technology*, vol. 173, no. 2-3, pp. 229–234, 2003.

[84] M. Chen, X. Yang, R. Hu, Z. Cui, and H. C. Man, "Bioactive niti shape memory alloy used as bone bonding implants," *Materials Science and Engineering: C*, vol. 24, no. 4, pp. 497–502, 2004.

[85] T. Sun and M. Wang, "Mechanical performance of apatite/tio2 composite coatings formed on ti and niti shape memory alloy," *Applied Surface Science*, vol. 255, no. 2, pp. 404–408, 2008.

[86] Y. Cai, X. Yang, Z. Cui, M. Chen, K. Hu, and C. Li, "Biofunctionalization of niti shape memory alloy promoting osseointegration by chemical treatment," in *Hydroxyapatite Coatings for Biomedical Applications*, pp. 289–359, CRC Press, 2013.

[87] C. J. Brinker and A. J. Hurd, "Fundamentals of sol-gel dip-coating," *Journal de Physique III*, vol. 4, no. 7, pp. 1231–1242, 1994.

[88] B. Mavis and A. C. Taş, "Dip coating of calcium hydroxyapatite on ti-6al-4v substrates," *Journal of the American Ceramic Society*, vol. 83, no. 4, pp. 989–991, 2000.

[89] T. Li, J. Lee, T. Kobayashi, and H. Aoki, "Hydroxyapatite coating by dipping method, and bone bonding strength," *Journal of Materials Science: Materials in Medicine*, vol. 7, no. 6, pp. 355–357, 1996.

[90] J. Choi, D. Bogdanski, M. Köller, S. A. Esenwein, D. Müller, G. Muhr, and M. Epple, "Calcium phosphate coating of nickel–titanium shape-memory alloys. coating procedure and adherence of leukocytes and platelets," *Biomaterials*, vol. 24, no. 21, pp. 3689–3696, 2003.

[91] C. Benaqqa, J. Chevalier, M. Saädaoui, and G. Fantozzi, "Slow crack growth behaviour of hydroxyapatite ceramics," *Biomaterials*, vol. 26, no. 31, pp. 6106–6112, 2005.

[92] A. Z. Tareq, M. S. Hussein, and A. M. Mustafa, "Synthesis and characterization of pva-gelatin hydrogel membranes for controlled delivery of captopril," *Int. Res. J. Pure Appl. Chem*, vol. 12, no. 4, pp. 1–10, 2016.

[93] W. O. Herrmann and H. Wolfram, "Process for the preparation of polymerized vinyl alcohol and its derivatives," June 5 1928. US Patent 1,672,156.

[94] V. Goodship and D. Jacobs, *Polyvinyl alcohol: materials, processing and applications*, vol. 16. Smithers rapra technology, 2009.

[95] E. A. Kamoun, X. Chen, M. S. M. Eldin, and E.-R. S. Kenawy, "Crosslinked poly (vinyl alcohol) hydrogels for wound dressing applications: A review of remarkably blended polymers," *Arabian Journal of chemistry*, vol. 8, no. 1, pp. 1–14, 2015.

[96] R. W. Korsmeyer and N. A. Peppas, "Effect of the morphology of hydrophilic polymeric matrices on the diffusion and release of water soluble drugs," *Journal of Membrane Science*, vol. 9, no. 3, pp. 211–227, 1981.

[97] A. Aina, A. Morris, M. Gupta, N. Billa, N. Madhvani, R. Sharma, S. Doughty, V. Shah, and Y. Boukari, "Dissolution behavior of poly vinyl alcohol in water and its effect on the physical morphologies of plga scaffolds," *Pharmaceutical and Biosciences Journal*, pp. 01–06, 2014.

[98] E.-E. Hago and X. Li, "Interpenetrating polymer network hydrogels based on gelatin and pva by biocompatible approaches: synthesis and characterization," *Advances in Materials Science and Engineering*, vol. 2013, 2013.

[99] M. G. Cascone, S. Maltinti, N. Barbani, and M. Laus, "Effect of chitosan and dextran on the properties of poly (vinyl alcohol) hydrogels," *Journal of Materials Science: Materials in Medicine*, vol. 10, no. 7, pp. 431–435, 1999.

[100] K. M. El Salmawi, "Gamma radiation-induced crosslinked pva/chitosan blends for wound dressing," *Journal of Macromolecular Science, Part A*, vol. 44, no. 5, pp. 541–545, 2007.

[101] S. Levi, V. Rac, V. Manojlovi, V. Raki, B. Bugarski, T. Flock, K. E. Krzyczmonik, and V. Nedovi, "Limonene encapsulation in alginate/poly (vinyl alcohol)," *Procedia Food Science*, vol. 1, pp. 1816–1820, 2011.

[102] J. O. Kim, J. K. Park, J. H. Kim, S. G. Jin, C. S. Yong, D. X. Li, J. Y. Choi, J. S. Woo, B. K. Yoo, W. S. Lyoo, *et al.*, "Development of polyvinyl alcohol–sodium alginate gel-matrix-based wound dressing system containing nitrofurazone," *International Journal of Pharmaceutics*, vol. 359, no. 1-2, pp. 79–86, 2008.

[103] E.-R. Kenawy, E. A. Kamoun, M. S. M. Eldin, and M. A. El-Meligy, "Physically crosslinked poly (vinyl alcohol)-hydroxyethyl starch blend hydrogel membranes: Synthesis and characterization for biomedical applications," *Arabian Journal of Chemistry*, vol. 7, no. 3, pp. 372–380, 2014.

[104] O. Wichterle and D. Lim, "Hydrophilic gels for biological use," *Nature*, vol. 185, no. 4706, pp. 117–118, 1960.

[105] A. S. Hoffman, "Hydrogels for biomedical applications," *Advanced Drug Delivery Reviews*, vol. 64, pp. 18–23, 2012.

[106] S. R. Lustig, J. M. Caruthers, and N. A. Peppas, "Dynamic mechanical properties of polymer-fluid systems: characterization of poly (2-hydroxyethyl methacrylate) and poly (2-hydroxyethyl methacrylate-co-methyl methacrylate) hydrogels," *Polymer*, vol. 32, no. 18, pp. 3340–3353, 1991.

[107] N. Lavrov, T. Kryzhanovskaya, and P. Vondrachek, "Properties of hydrogels of 2-hydroxyethyl methacrylate modified by silicone rubber," *Journal of Applied Chemistry of the USSR*, vol. 64, no. 11, 1991.

[108] A. Moussaid, S. J. Candau, and J. G. Joosten, "Structural and dynamic properties of partially charged poly (acrylic acid) gels: nonergodicity and inhomogeneities," *Macromolecules*, vol. 27, no. 8, pp. 2102–2110, 1994.

[109] Y. Cohen, O. Ramon, I. Kopelman, and S. Mizrahi, "Characterization of inhomogeneous polyacrylamide hydrogels," *Journal of Polymer Science Part B: Polymer Physics*, vol. 30, no. 9, pp. 1055–1067, 1992.

[110] J. P. Baker, H. W. Blanch, and J. M. Prausnitz, "Equilibrium swelling properties of weakly lonizable 2-hydroxyethyl methacrylate (hema)-based hydrogels," *Journal of Applied Polymer Science*, vol. 52, no. 6, pp. 783–788, 1994.

[111] M. Nagura, T. Hamano, and H. Ishikawa, "Structure of poly (vinyl alcohol) hydrogel prepared by repeated freezing and melting," *Polymer*, vol. 30, no. 4, pp. 762–765, 1989.

[112] O. Ariga, M. Kato, T. Sano, Y. Nakazawa, and Y. Sano, "Mechanical and kinetic properties of pva hydrogel immobilizing β-galactosidase," *Journal of Fermentation and Bioengineering*, vol. 76, no. 3, pp. 203–206, 1993.

[113] P. J. Flory and J. Rehner Jr, "Statistical mechanics of cross-linked polymer networks i. rubberlike elasticity," *The Journal of Chemical Physics*, vol. 11, no. 11, pp. 512–520, 1943.

[114] A. Buyanov, L. Revel'skaya, G. Petropavlovskii, M. Lebedeva, S. Zakharov, L. Nud'ga, and L. Kozhevnikova, "Elastic behavior of equilibrium-swollen polyelectrolyte hydrogels based onacrylamide and sodium acrylate," *Journal of Applied Chemistry of the USSR*, vol. 65, no. 1, pp. 150–157, 1992.

[115] N. A. Peppas and L. Brannon-Peppas, "Hydrogels at critical conditions. part 1. thermodynamics and swelling behavior," *Journal of Membrane Science*, vol. 48, no. 2-3, pp. 281–290, 1990.

[116] J. L. Holloway, A. M. Lowman, and G. R. Palmese, "Mechanical evaluation of poly (vinyl alcohol)-based fibrous composites as biomaterials for meniscal tissue replacement," *Acta Biomaterialia*, vol. 6, no. 12, pp. 4716–4724, 2010.

[117] K. Ishihara, K. Fukazawa, V. Sharma, S. Liang, A. Shows, D. C. Dunbar, Y. Zheng, J. Ge, S. Zhang, Y. Hong, *et al.*, "Antifouling silicone hydrogel contact lenses with a bioinspired 2-methacryloyloxyethyl phosphorylcholine polymer surface," *ACS omega*, vol. 6, no. 10, pp. 7058–7067, 2021.

[118] M. Suzuki, "An artificial muscle by pva hydrogel can generate high power close to living skeletal muscles," in *Images of the Twenty-First Century. Proceedings of the Annual International Engineering in Medicine and Biology Society,*, pp. 916–917, IEEE, 1989.

[119] M. Bassil, J. Davenas, and M. E. Tahchi, "Electrochemical properties and actuation mechanisms of polyacrylamide hydrogel for artificial muscle application," *Sensors and Actuators B: Chemical*, vol. 134, no. 2, pp. 496–501, 2008.

[120] J. Silver and J. H. Miller, "Regeneration beyond the glial scar," *Nature Reviews Neuroscience*, vol. 5, no. 2, pp. 146–156, 2004.

[121] S. A. Busch and J. Silver, "The role of extracellular matrix in cns regeneration," *Current Opinion in Neurobiology*, vol. 17, no. 1, pp. 120–127, 2007.

[122] M. Qi, Y. Gu, N. Sakata, D. Kim, Y. Shirouzu, C. Yamamoto, A. Hiura, S. Sumi, and K. Inoue, "Pva hydrogel sheet macroencapsulation for the bioartificial pancreas," *Biomaterials*, vol. 25, no. 27, pp. 5885–5892, 2004.

[123] A. Hejčl, P. Lesnỳ, M. Přádnỳ, J. Michalek, P. Jendelova, J. Štulík, and E. Sykova, "Biocompatible hydrogels in spinal cord injury repair," *Physiol. Res*, vol. 57, no. 3, pp. S121–S132, 2008.

[124] A. Jain, Y.-T. Kim, R. J. McKeon, and R. V. Bellamkonda, "In situ gelling hydrogels for conformal repair of spinal cord defects, and local delivery of bdnf after spinal cord injury," *Biomaterials*, vol. 27, no. 3, pp. 497–504, 2006.

[125] S. Herber, J. Bomer, W. Olthuis, P. Bergveld, and A. v. d. Berg, "A miniaturized carbon dioxide gas sensor based on sensing of ph-sensitive hydrogel swelling with a pressure sensor," *Biomedical Microdevices*, vol. 7, no. 3, pp. 197–204, 2005.

[126] P. S. Murphy and G. R. Evans, "Advances in wound healing: a review of current wound healing products," *Plastic Surgery International*, vol. 2012, 2012.

[127] G. Fundueanu, M. Constantin, and P. Ascenzi, "Poly (vinyl alcohol) microspheres with ph-and thermosensitive properties as temperature-controlled drug delivery," *Acta Biomaterialia*, vol. 6, no. 10, pp. 3899–3907, 2010.

[128] R. F. Donnelly, C. M. Cassidy, R. G. Loughlin, A. Brown, M. M. Tunney, M. G. Jenkins, and P. A. McCarron, "Delivery of methylene blue and meso-tetra (n-methyl-4-pyridyl) porphine tetra tosylate from cross-linked poly (vinyl alcohol) hydrogels: a potential means of photodynamic therapy of infected wounds," *Journal of Photochemistry and Photobiology B: Biology*, vol. 96, no. 3, pp. 223–231, 2009.

[129] T.-H. Nguyen, R. Ventura, Y.-K. Min, and B.-T. Lee, "Genipin cross-linked polyvinyl alcohol-gelatin hydrogel for bone regeneration," *Journal of Biomedical Science and Engineering*, vol. 9, no. 9, pp. 419–429, 2016.

[130] K. Pal, A. K. Banthia, and D. K. Majumdar, "Preparation and characterization of polyvinyl alcohol-gelatin hydrogel membranes for biomedical applications," *Aaps Pharmscitech*, vol. 8, no. 1, pp. E142–E146, 2007.

[131] S. Pawde and K. Deshmukh, "Characterization of polyvinyl alcohol/gelatin blend hydrogel films for biomedical applications," *Journal of Applied Polymer Science*, vol. 109, no. 5, pp. 3431–3437, 2008.

[132] L. Fan, H. Yang, J. Yang, M. Peng, and J. Hu, "Preparation and characterization of chitosan/gelatin/pva hydrogel for wound dressings," *Carbohydrate Polymers*, vol. 146, pp. 427–434, 2016.

[133] N. E. Vrana, Y. Liu, G. B. McGuinness, and P. A. Cahill, "Characterization of poly (vinyl alcohol)/chitosan hydrogels as vascular tissue engineering scaffolds," in *Macromolecular Symposia*, vol. 269, pp. 106–110, Wiley Online Library, 2008.

[134] M. Trzaskowski, B. Butruk, and T. Ciach, "Hydrogel coatings for artificial heart implants," *Challenges of Modern Technology*, vol. 2, no. 1, 2011.

[135] L. Drago, W. Boot, K. Dimas, K. Malizos, G. M. Hänsch, J. Stuyck, D. Gawlitta, and C. L. Romanò, "Does implant coating with antibacterial-loaded hydrogel reduce bacterial colonization and biofilm formation in vitro?," *Clinical Orthopaedics and Related Research®*, vol. 472, no. 11, pp. 3311–3323, 2014.

[136] D. Zang, H. Yi, Z. Gu, L. Chen, D. Han, X. Guo, S. Wang, M. Liu, and L. Jiang, "Interfacial engineering of hierarchically porous niti/hydrogels nanocomposites with exceptional antibiofouling surfaces," *Advanced Materials*, vol. 29, no. 2, p. 1602869, 2017.

[137] K. Chen, X. Yang, D. Zhang, L. Xu, X. Zhang, and Q. Wang, "Biotribology behavior and fluid load support of pva/ha composite hydrogel as artificial cartilage," *Wear*, vol. 376, pp. 329–336, 2017.

[138] K. Chen, J. Liu, X. Yang, and D. Zhang, "Preparation, optimization and property of pva-ha/paa composite hydrogel," *Materials Science and Engineering: C*, vol. 78, pp. 520–529, 2017.

[139] K.-T. Oh, C.-J. Hwang, Y.-S. Park, and K.-N. Kim, "In vitro corrosion resistance of orthodontic super stainless steel wire: The effects of stress relieving heat-treatment," *Journal of the Electrochemical Society*, vol. 149, no. 9, p. B414, 2002.

[140] H.-H. Huang, Y.-H. Chiu, T.-H. Lee, S.-C. Wu, H.-W. Yang, K.-H. Su, and C.-C. Hsu, "Ion release from niti orthodontic wires in artificial saliva with various acidities," *Biomaterials*, vol. 24, no. 20, pp. 3585–3592, 2003.

[141] N. Schiff, B. Grosgogeat, M. Lissac, and F. Dalard, "Influence of fluoridated mouthwashes on corrosion resistance of orthodontics wires," *Biomaterials*, vol. 25, no. 19, pp. 4535–4542, 2004.

[142] L. El Medawar, P. Rocher, J.-C. Hornez, M. Traisnel, J. Breme, and H. Hildebrand, "Electrochemical and cytocompatibility assessment of nitinol memory shape alloy for orthodontic use," *Biomolecular Engineering*, vol. 19, no. 2-6, pp. 153–160, 2002.

[143] M. Niinomi, "Recent titanium r&d for biomedical applications in japan," *Jom*, vol. 51, no. 6, pp. 32–34, 1999.

[144] Y. Okazaki and E. Gotoh, "Comparison of metal release from various metallic biomaterials in vitro," *Biomaterials*, vol. 26, no. 1, pp. 11–21, 2005.

[145] B. Aksakal, Ö. Yildirim, and H. Gul, "Metallurgical failure analysis of various implant materials used in orthopedic applications," *Journal of Failure Analysis and Prevention*, vol. 4, no. 3, pp. 17–23, 2004.

[146] J. Ryhänen, E. Niemi, W. Serlo, E. Niemelä, P. Sandvik, H. Pernu, and T. Salo, "Biocompatibility of nickel-titanium shape memory metal and its corrosion behavior in human cell cultures," *Journal of Biomedical Materials Research: An Official Journal of The Society for Biomaterials and The Japanese Society for Biomaterials*, vol. 35, no. 4, pp. 451–457, 1997.

[147] D. Stöckel, "Status and trends in shape memory technology," in *Actuator*, vol. 92, pp. 79–84, Citeseer, 1992.

[148] Q. Meng, Y. Liu, H. Yang, B. S. Shariat, and T.-h. Nam, "Functionally graded niti strips prepared by laser surface anneal," *Acta Materialia*, vol. 60, no. 4, pp. 1658–1668, 2012.

[149] O. Cisse, O. Savadogo, M. Wu, and L. Yahia, "Effect of surface treatment of niti alloy on its corrosion behavior in hanks' solution," *Journal of Biomedical Materials Research: An Official Journal of The Society for Biomaterials, The Japanese Society for Biomaterials, and The Australian Society for Biomaterials and the Korean Society for Biomaterials*, vol. 61, no. 3, pp. 339–345, 2002.

[150] T. Hu, Y. Xin, S. Wu, C. Chu, J. Lu, L. Guan, H. Chen, T. F. Hung, K. Yeung, and P. K. Chu, "Corrosion behavior on orthopedic niti alloy with nanocrystalline/amorphous surface," *Materials Chemistry and Physics*, vol. 126, no. 1-2, pp. 102–107, 2011.

[151] X. Sun, Z. Kang, X. Zhang, H. Jiang, R. Guan, and X. Zhang, "A comparative study on the corrosion behavior of porous and dense niti shape memory alloys in nacl solution," *Electrochimica Acta*, vol. 56, no. 18, pp. 6389–6396, 2011.

[152] X. Zhang *et al.*, "A study of shape memory alloy for medicine in shape memory alloy 86 proceeding of the international symposium of shape memory alloys," *China. Academic Publishers*, p. 123, 1986.

[153] J. Khalil-Allafi, B. Amin-Ahmadi, and M. Zare, "Biocompatibility and corrosion behavior of the shape memory niti alloy in the physiological environments simulated with body fluids for medical applications," *Materials Science and Engineering: C*, vol. 30, no. 8, pp. 1112–1117, 2010.

[154] L. Jinlong, L. Tongxiang, W. Chen, and D. Limin, "Surface corrosion enhancement of passive films on niti shape memory alloy in different solutions," *Materials Science and Engineering: C*, vol. 63, pp. 192–197, 2016.

[155] N. Figueira, T. Silva, M. Carmezim, and J. Fernandes, "Corrosion behaviour of niti alloy," *Electrochimica Acta*, vol. 54, no. 3, pp. 921–926, 2009.

[156] J. Espinos, A. Fernandez, and A. Gonzalez-Elipe, "Oxidation and diffusion processes in nickel-titanium oxide systems," *Surface Science*, vol. 295, no. 3, pp. 402–410, 1993.

[157] M. Chembath, J. Balaraju, and M. Sujata, "Effect of anodization and annealing on corrosion and biocompatibility of niti alloy," *Surface and Coatings Technology*, vol. 302, pp. 302–309, 2016.

[158] R. Vandenkerckhove, M. Chandrasekaran, P. Vermaut, R. Portier, and L. Delaey, "Corrosion behaviour of a superelastic ni–ti alloy," *Materials Science and Engineering: A*, vol. 378, no. 1-2, pp. 532–536, 2004.

[159] D. Starosvetsky and I. Gotman, "Corrosion behavior of titanium nitride coated ni–ti shape memory surgical alloy," *Biomaterials*, vol. 22, no. 13, pp. 1853–1859, 2001.

[160] I. Milošev and B. Kapun, "The corrosion resistance of nitinol alloy in simulated physiological solutions: Part 1: The effect of surface preparation," *Materials Science and Engineering: C*, vol. 32, no. 5, pp. 1087–1096, 2012.

[161] I. Milošev and B. Kapun, "The corrosion resistance of nitinol alloy in simulated physiological solutions part 2: The effect of surface treatment," *Materials Science and Engineering: C*, vol. 32, no. 5, pp. 1068–1077, 2012.

[162] M. Chembath, J. Balaraju, and M. Sujata, "Surface characteristics, corrosion and bioactivity of chemically treated biomedical grade niti alloy," *Materials Science and Engineering: C*, vol. 56, pp. 417–425, 2015.

[163] L. Tan, R. Dodd, and W. Crone, "Corrosion and wear-corrosion behavior of niti modified by plasma source ion implantation," *Biomaterials*, vol. 24, no. 22, pp. 3931–3939, 2003.

[164] J. Briceño, A. Romeu, E. Espinar, J. Llamas, and F. Gil, "Influence of the microstructure on electrochemical corrosion and nickel release in niti orthodontic archwires," *Materials Science and Engineering: C*, vol. 33, no. 8, pp. 4989–4993, 2013.

[165] G. Rondelli and B. Vicentini, "Localized corrosion behaviour in simulated human body fluids of commercial ni-ti orthodontic wires," *Biomaterials*, vol. 20, no. 8, pp. 785–792, 1999.

[166] X. Li, J. Wang, E.-h. Han, and W. Ke, "Influence of fluoride and chloride on corrosion behavior of niti orthodontic wires," *Acta Biomaterialia*, vol. 3, no. 5, pp. 807–815, 2007.

[167] R. M. Pidaparti, "Structural corrosion health assessment using computational intelligence methods," *Structural Health Monitoring*, vol. 6, no. 3, pp. 245–259, 2007.

[168] B. Chopard and M. Droz, "Cellular automata modeling of physical systems," *Cambridge University Press*, 2005.

[169] T. Toffoli and N. Margolus, *Cellular automata machines: a new environment for modeling*. MIT press, 1987.

[170] S. Chen, K. Diemer, G. D. Doolen, K. Eggert, C. Fu, S. Gutman, and B. J. Travis, "Lattice gas automata for flow through porous media," *Physica D: Nonlinear Phenomena*, vol. 47, no. 1-2, pp. 72–84, 1991.

[171] J. Wells, D. Janecky, and B. Travis, "A lattice gas automata model for heterogeneous chemical reactions at mineral surfaces and in pore networks," *Physica D: Nonlinear Phenomena*, vol. 47, no. 1-2, pp. 115–123, 1991.

[172] P. Bak, K. Chen, and C. Tang, "A forest-fire model and some thoughts on turbulence," *Physics Letters A*, vol. 147, no. 5-6, pp. 297–300, 1990.

[173] R. Pidaparti, M. J. Palakal, and L. Fong, "Cellular automata approach to aircraft corrosion pit growth.," in *FLAIRS Conference*, pp. 93–98, 2004.

[174] R. M. Pidaparti, L. Fang, and M. J. Palakal, "Computational simulation of multi-pit corrosion process in materials," *Computational Materials Science*, vol. 41, no. 3, pp. 255–265, 2008.

[175] M. Sivakumar, K. S. Kumar Dhanadurai, S. Rajeswari, and V. Thulasiraman, "Failures in stainless steel orthopaedic implant devices: A survey," *Journal of Materials Science Letters*, vol. 14, no. 5, pp. 351–354, 1995.

[176] S. Bhaumik, K. Ramaiah, and C. Saikrishna, "Nickel–titanium shape memory alloy wires for thermal actuators," in *Micro and Smart Devices and Systems*, pp. 181–198, Springer, 2014.

[177] T. Chaturvedi, "An overview of the corrosion aspect of dental implants (titanium and its alloys)," *Indian Journal of Dental Research*, vol. 20, no. 1, p. 91, 2009.

[178] D. Jones, "Principles and prevention of corrosion," *Macmillan Publishing Company(USA), 1992,*, p. 568, 1992.

[179] J. Yu, Z. Zhao, and L. Li, "Corrosion fatigue resistances of surgical implant stainless steels and titanium alloy," *Corrosion Science*, vol. 35, no. 1-4, pp. 587–597, 1993.

[180] H. H. Uhlig *et al.*, "Corrosion handbook," 1948.

[181] Y. Okazaki and E. Gotoh, "Implant applications of highly corrosion-resistant ti-15zr-4nb-4ta alloy," *Materials Transactions*, vol. 43, no. 12, pp. 2943–2948, 2002.

[182] S. Teoh, "Fatigue of biomaterials: a review," *International Journal of Fatigue*, vol. 22, no. 10, pp. 825–837, 2000.

[183] A. Pardo, E. Ilic, K. Thorwarth, M. Stiefel, and R. Hauert, "Corrosion fatigue in dlc-coated articulating implants: an accelerated methodology to predict realistic interface lifetime," *Science and Technology of Advanced Materials*, vol. 20, no. 1, pp. 173–186, 2019.

[184] C.-W. Chan, "A study on the corrosion fatigue behaviour of laser-welded shape memory niti wires in a simulated body fluid," *Surface and Coatings Technology*, vol. 320, pp. 574–578, 2017.

[185] H. Funakubo, *Shape Memory Alloys*. Gordon and Breach, 1984.

[186] K. S. Kasprzak, F. Sunderman, and K. Salnikow, "Nickel carcinogenesis," *Mutation Research/Fundamental and Molecular Mechanisms of Mutagenesis*, vol. 533, no. 1, pp. 67–97, 2003.

[187] *Standart Test Method for Determination of Transformation Temperature of Nickel Titanium Shape Memory Alloys by Bend and Free Recovery*. ASTM, F2082/F2082M-16, 1984.

[188] A. Vahidyeganeh, *Development of Antagonistically Actuated Active Joints with Shape Memory Alloys*. 2017.

[189] M. Ho and J. P. Desai, "Characterization of sma actuator for applications in robotic neurosurgery," in *Annual International Conference of the IEEE Engineering in Medicine and Biology Society*, pp. 6856–6859, IEEE, 2009.

[190] S. Dorozhkin, "Calcium orthophosphates in nature, biology and medicine. materials 2 (2): 399–498," 2009.

[191] A. Y. Malysheva and B. Beletskii, "Biocompatibility of apatite-containing implant materials," *Inorganic Materials*, vol. 37, no. 2, pp. 180–183, 2001.

[192] F. Mansfeld, "The polarization resistance technique for measuring corrosion currents," in *Advances in Corrosion Science and Technology*, pp. 163–262, Springer, 1976.

[193] T. Šušteršič, G. M. Simsek, G. G. Yapici, M. Nikolić, R. Vulović, N. Filipovic, and N. E. Vrana, "An in-silico corrosion model for biomedical applications for coupling with in-vitro biocompatibility tests for estimation of long-term effects," *Frontiers in Bioengineering and Biotechnology*, p. 768, 2021.

[194] I. Iso, "10993–5: 2009 biological evaluation of medical devices—part 5: tests for in vitro cytotoxicity," *International Organization for Standardization, Geneva*, 2009.

[195] W. B. Cross, A. H. Kariotis, and F. J. Stimler, "Nitinol characterization study," tech. rep., NASA, 1969.

[196] X. Huang and Y. Liu, "Effect of annealing on the transformation behavior and superelasticity of niti shape memory alloy," *Scripta Materialia*, vol. 45, no. 2, pp. 153–160, 2001.

[197] W. A. Brantley and T. Eliades, "Orthodontic materials: scientific and clinical aspects," *American Journal of Orthodontics and Dentofacial Orthopedics*, vol. 119, no. 6, pp. 672–673, 2001.

[198] D. W. Berzins and H. W. Roberts, "Phase transformation changes in thermocycled nickel–titanium orthodontic wires," *Dental Materials*, vol. 26, no. 7, pp. 666–674, 2010.

[199] G.-B. Cho, Y.-H. Kim, S.-G. Hur, C.-A. Yu, and T.-H. Nam, "Transformation behavior and mechanical properties of a nanostructured ti- 50.0 ni (at.%) alloy," *Metals and Materials International*, vol. 12, no. 2, pp. 181–187, 2006.

[200] K. Nurveren, A. Akdoğan, and W. Huang, "Evolution of transformation characteristics with heating/cooling rate in niti shape memory alloys," *Journal of Materials Processing Technology*, vol. 196, no. 1-3, pp. 129–134, 2008.

[201] L. M. Brauchli, H. Keller, C. Senn, and A. Wichelhaus, "Influence of bending mode on the mechanical properties of nickel-titanium archwires and correlation to differential scanning calorimetry measurements," *American Journal of Orthodontics and Dentofacial Orthopedics*, vol. 139, no. 5, pp. e449–e454, 2011.

[202] U. Kamachi Mudali and B. Raj, "Corrosion science and technology: mechanism, mitigation and monitoring," *CRC Press*, 2008.

[203] B. Kasemo and J. Lausmaa, "Surface science aspects on inorganic biomaterials," *CRC Crit. Rev. Clin. Neurobiol.;(United States)*, vol. 4, 1986.

[204] A. Mahmud, Z. Wu, J. Zhang, Y. Liu, and H. Yang, "Surface oxidation of niti and its effects on thermal and mechanical properties," *Intermetallics*, vol. 103, pp. 52–62, 2018.

[205] M. Uchida, H.-M. Kim, T. Kokubo, S. Fujibayashi, and T. Nakamura, "Structural dependence of apatite formation on titania gels in a simulated body fluid," *Journal of Biomedical Materials Research Part A: An Official Journal of The Society for Biomaterials, The Japanese Society for Biomaterials, and The Australian Society for Biomaterials and the Korean Society for Biomaterials*, vol. 64, no. 1, pp. 164–170, 2003.

[206] M. Capoşi, M. Prodana, and D. Ioniţă, "Effect of temperature and ph on the metal release from tini," *Sci. Bull*, vol. 73, pp. 27–36, 2011.

[207] Z. Ahmad, *Principles of corrosion engineering and corrosion control*. Elsevier, 2006.

[208] C. Trépanier and A. R. Pelton, "Effect of temperature and ph on the corrosion resistance of passivated nitinol and stainless steel," in *SMST-2004: Proceedings of the International Conference on Shape Memory and Superelastic Technologies*, p. 361, ASM International, 2006.

[209] R. M. Pidaparti, A. Puri, M. J. Palakal, and A. Kashyap, "Two-dimensional corrosion pit initiation and growth simulation model," *J. Computers, Materials, Continua*, vol. 2, pp. 65–76, 2005.

[210] P. Surbled, C. Clerc, B. Le Pioufle, M. Ataka, and H. Fujita, "Effect of the composition and thermal annealing on the transformation temperatures of sputtered tini shape memory alloy thin films," *Thin Solid Films*, vol. 401, no. 1-2, pp. 52–59, 2001.

[211] Y. Zhang, Z. Li, C. Esling, J. Muller, X. Zhao, and L. Zuo, "A general method to determine twinning elements," *Journal of Applied Crystallography*, vol. 43, no. 6, pp. 1426–1430, 2010.

[212] J. Van Humbeeck, "Non-medical applications of shape memory alloys," *Materials Science and Engineering: A*, vol. 273, pp. 134–148, 1999.

[213] M. H. Elahinia, M. Hashemi, M. Tabesh, and S. B. Bhaduri, "Manufacturing and processing of niti implants: A review," *Progress in Materials Science*, vol. 57, no. 5, pp. 911–946, 2012.

[214] L.-H. Li, Y.-M. Kong, H.-W. Kim, Y.-W. Kim, H.-E. Kim, S.-J. Heo, and J.-Y. Koak, "Improved biological performance of ti implants due to surface modification by micro-arc oxidation," *Biomaterials*, vol. 25, no. 14, pp. 2867–2875, 2004.

[215] A. Boccaccini, S. Keim, R. Ma, Y. Li, and I. Zhitomirsky, "Electrophoretic deposition of biomaterials," *Journal of the Royal Society Interface*, vol. 7, no. suppl_5, pp. S581–S613, 2010.

[216] B. Ferrari and R. Moreno, "A review: Epd kinetics," *J Eur Ceram So c*, vol. 30, pp. 1069–1078, 2010.

[217] X. Liu, P. K. Chu, and C. Ding, "Surface modification of titanium, titanium alloys, and related materials for biomedical applications," *Materials Science and Engineering: R: Reports*, vol. 47, no. 3-4, pp. 49–121, 2004.

[218] A. Carradò, "Nano-crystalline pulsed laser deposition hydroxyapatite thin films on ti substrate for biomedical application," *Journal of Coatings Technology and Research*, vol. 8, no. 6, pp. 749–755, 2011.

[219] T. Sridhar, U. K. Mudali, and M. Subbaiyan, "Sintering atmosphere and temperature effects on hydroxyapatite coated type 316l stainless steel," *Corrosion Science*, vol. 45, no. 10, pp. 2337–2359, 2003.

[220] W. Chrzanowski, E. A. A. Neel, D. A. Armitage, K. Lee, W. Walke, and J. C. Knowles, "Nanomechanical evaluation of nickel–titanium surface properties after alkali and electrochemical treatments," *Journal of the Royal Society Interface*, vol. 5, no. 26, pp. 1009–1022, 2008.

[221] S. Wu, X. Liu, Y. Chan, J. Ho, C. Chung, P. K. Chu, C. Chu, K. Yeung, W. Lu, K. Cheung, *et al.*, "Nickel release behavior, cytocompatibility, and superelasticity of oxidized porous single-phase niti," *Journal of Biomedical Materials Research Part A*, vol. 81, no. 4, pp. 948–955, 2007.

[222] M. Sandhyarani, T. Prasadrao, and N. Rameshbabu, "Role of electrolyte composition on structural, morphological and in-vitro biological properties of plasma electrolytic oxidation films formed on zirconium," *Applied Surface Science*, vol. 317, pp. 198–209, 2014.

[223] Y. Han, D. Chen, J. Sun, Y. Zhang, and K. Xu, "Uv-enhanced bioactivity and cell response of micro-arc oxidized titania coatings," *Acta Biomaterialia*, vol. 4, no. 5, pp. 1518–1529, 2008.

[224] G. McKay, R. Macnair, C. MacDonald, and M. Grant, "Interactions of orthopaedic metals with an immortalized rat osteoblast cell line," *Biomaterials*, vol. 17, no. 13, pp. 1339–1344, 1996.

[225] D. Wever, A. Veldhuizen, J. De Vries, H. Busscher, D. Uges, and J. Van Horn, "Electrochemical and surface characterization of a nickel–titanium alloy," *Biomaterials*, vol. 19, no. 7-9, pp. 761–769, 1998.

[226] F. Macionczyk, B. Gerold, and R. Thull, "Repassivating tantalum/tantalum oxide surface modification on stainless steel implants," *Surface and Coatings Technology*, vol. 142, pp. 1084–1087, 2001.

[227] J. Liu, S. Qu, Z. Suo, and W. Yang, "Functional hydrogel coatings," *National Science Review*, vol. 8, no. 2, p. nwaa254, 2021.

[228] M. Wei, "Electrophoresis of hydroxyapatite on metal substrates.," 1999.

[229] J. Wen, J. Lei, J. Chen, J. Gou, Y. Li, and L. Li, "An intelligent coating based on ph-sensitive hybrid hydrogel for corrosion protection of mild steel," *Chemical Engineering Journal*, vol. 392, p. 123742, 2020.

[230] M. Saveleva, A. Vladescu, C. Cotrut, L. Van der Meeren, M. Surmeneva, R. Surmenev, B. Parakhonskiy, and A. G. Skirtach, "The effect of hybrid coatings based on hydrogel, biopolymer and inorganic components on the corrosion behavior of titanium bone implants," *Journal of Materials Chemistry B*, vol. 7, no. 43, pp. 6778–6788, 2019.

[231] J. Barthes, P. Lagarrigue, V. Riabov, G. Lutzweiler, J. Kirsch, C. Muller, E.-J. Courtial, C. Marquette, F. Projetti, J. Kzhyskowska, *et al.*, "Biofunctionalization of 3d-printed silicone implants with immunomodulatory hydrogels for

controlling the innate immune response: An in vivo model of tracheal defect repair," *Biomaterials*, vol. 268, p. 120549, 2021.

[232] E. Rupérez, J. M. Manero, L.-A. Bravo-González, E. Espinar, and F. J. Gil, "Development of biomimetic niti alloy: influence of thermo-chemical treatment on the physical, mechanical and biological behavior," *Materials*, vol. 9, no. 6, p. 402, 2016.

VITA

Görkem Muttalip Şimşek has Bachelor of Science degree in Mechanical Engineering. He then gained his M.Sc. from the Mechanical Engineering Department at Mersin University in 2014. His master's study is titled "Formation of bioceramic film layer on Ti6Al4V substrate by hydrothermal crystallization method" and supported by Mersin University under the advisory of Assoc. Professor Önder Albayrak. In 2014, he has started his Ph.D. with Professor Dr. Güney Güven Yapıcı at the Özyeğin University. During his Ph.D., he was working as a Research and Teaching Assistant in the Engineering Faculty for almost five years.

His dissertation research concentrated on the characterization of mechanical properties of Nickel Titanium shape memory alloys through biocompatible coating. He graduated from Özyeğin University with a doctorate degree in Mechanical Engineering in April 2023. He is currently working at the Turkish Aerospace Industry Academy as a chief engineer.